Vol. 125 Nos. 1-6

March-April 1959

PROCEEDINGS OF THE ACADEMY OF SCIENCES

OF THE USSR

(DOKLADY AKADEMII NAUK SSSR)

Physical Chemistry Section

A publication of the Academy of Sciences of the USSR

IN ENGLISH TRANSLATION

Year and issue of first translation:
Vol. 112, Nos. 1-6 Jan.-Feb. 1957

Annual subscription	*$160.00*
Single issue	*35.00*

Copyright 1960

CONSULTANTS BUREAU ENTERPRISES, INC.
227 West 17th Street, New York, N. Y.

A complete copy of any paper in this issue may be purchased from the publisher for $5.00

Note: The sale of photostatic copies of any portion of this copyright translalion is expressly prohibited by the copyright owners.

Printed in the United States of America

PROCEEDINGS OF THE ACADEMY OF SCIENCES OF THE USSR

Physical Chemistry Section

Volume 125, Numbers 1-6 March-April 1959

CONTENTS

	PAGE	RUSS. ISSUE	RUSS. PAGE
Chemiluminescence in Thermal Decomposition Reactions. R. F. Vasil'ev, O. N. Karpukhin and V. Ya. Shlyapintokh	213	1	106
Pulsating and Spinning Detonation of Gaseous Mixtures in Tubes. Yu. N. Denisov and Ya. K. Troshin	217	1	110
Crystal Structure of Normal Paraffins n-$C_{30}H_{62}$ and n-$C_{32}H_{66}$ at High Pressure. S. S. Kabalkina	221	1	114
Deformation in Crystalline Polyethyleneterephthalate Films. P. V. Kozlov, V. A. Kabanov and A. A. Frolova	227	1	118
Adiabatic Combustion – A New Method of Investigation and Its Application to Hydrogen–Chlorine Mixtures. A. A. Kuliev and A. I. Rozlovskii	231	1	122
Structure of the Liquid AuSn Alloy. A. S. Lashko	235	1	126
The Theory of Thermal Chain Flame Propagation with Two Active Centers Having Different Diffusion Coefficients. L. A. Lovachev	239	1	129
The Formation of Hexachloroethane by γ-Irradiation of Carbon Tetrachloride. B. I. Losev, M. A. Troyanskaya and É. A. Bylyna	245	1	133
Design of a New Cell for the Measurement of Pressures of Saturated Metal Vapors. Yu. N. Lyubitov and V. M. Polyanskii	247	1	135
The Effect of Ionizing Radiation on the Electrochemical Activity of Metals Covered with Semiconducting Oxide Films. I. L. Rozenfel'd and E. K. Oshe	251	1	139
Quantum Mechanical Effects and the Temperature Dependence of the Rate of the Electrolytic Evolution of Hydrogen and Deuterium. St. G. Khristov	255	1	143
The Effect of Negative Groups on the Electrochemical Reduction of the Carbon – Halogen Bond in Organic Compounds. The Polarographic Behavior of the Halogenated Nitroalkanes. S. G. Mairanovskii, A. A. Fainzil'berg, S. S. Novikov and V. A. Klimova	261	2	351
The Selective Penetration of Dissolved Elements from a Liquid Phase into a Crack. B. A. Movchan and I. Ya. Dzykovich	265	2	354
The Asymmetry in the Distribution of the Coordination Numbers of the Molecules of Water. V. K. Prokhorenko, O. Ya. Samoilov and I. Z. Fisher	269	2	356
Theory of Shock-Induced Detonations. L. G. Bolkhovitinov	273	3	570
An Investigation of the Thermal Dehydration of Crystalline, and Amorphous, Silica by the Method of Mass Spectrographic Analysis. A. V. Bondarenko	277	3	573

CONTENTS (continued)

	PAGE	RUSS. PAGE	RUSS. ISSUE
The Role of Oxygen in Radiolytic Discoloration of Aqueous Solutions of Indigo Carmine. A. A. Zansokhova, V. D. Orekhov and M. A. Proskurnin	281	3	577
Separation Coefficients for the Chlorine Isotopes in the Reversible Vaporization of HCl. K. I. Matveev, O. V. Uvarov and N. M. Zhavoronkov	285	3	580
A Contribution to the Theory of Radiation Chemistry. L. S. Polak and A. Ya. Temkin	289	3	584
The Infrared Spectra of Nitric Oxide Adsorbed on Ferric and Chromic Oxides. L. M. Roev and A. N. Terenin	293	3	588
Adsorption of Penicillin on Polymeric Adsorbents. G. V. Samsonov, V. V. Vedeneeva and A. A. Selezneva	297	3	591
Kinetic Polarographic Currents from the Delayed Discharge of Thiocyanate Complexes of Nickel. Ya. I. Tur'yan and G. F. Serova	301	3	595
The Diminution of the Melting Point of Water in the Capillaries of a Porous Body. V. A. Bakaev, V. F. Kiselev and K. G. Krasil'nikov	305	4	831
A Method for the Determination of the Phase State in Binary Systems. I. B. Borovskii and I. D. Marchukova	309	4	835
Sensitized Radiolytic Oxidation of Leuco Methylene Blue in Aqueous Solutions. A. N. Zansokhova and V. D. Orekhov	313	4	838
The Theory of Single Electron Quantum Mechanical Systems which Include a Large Subsystem. Jaroslav Koutecký and Antonin Fingerland	317	4	841
The General Principles of the Coprecipitation of Microadditives During Crystal Growth. I. V. Melikhov, M. S. Merkulova and G. Éval'd	323	4	845
The Effect of Conjugation Between an Anthracene Ring and a Double Bond in an Alkene Substituent on the Fluorescence and Absorption Spectra. A. S. Cherkasov	327	4	848
The Alteration of the Photoelectric Work Function of ZnO, NiO, and Cr_2O_3, by the Adsorption of Gases and Vapors. F. I. Vilesov and A. N. Terenin	331	5	1053
Suppressed Catalytic Activity of Polyvalent Metals in Rubber. A. S. Kuz'minskii, V. D. Zaitseva and N. N. Lezhnev	335	5	1057
Joule Effect Associated with the Flow and Stopping of Abnormally Viscous Substances. V. P. Pavlov and G. V. Vinogradov	339	5	1061
The Combined Action of Organic Cations and Halide Anions on the Evolution of Hydrogen on a Mercury Electrode. Tza Chuan-hsin and Z. A. Iofa	343	5	1065
The Mechanism of the Anodic Formation of the Persulfate Ion. Ts'u Yung-Ts'ao and Mi Tien-Ying	347	5	1069
The Effect of Surface Hydration on the Adsorption of Aliphatic Alcohols (from solution) on Silica. L. G. Ganichenko, V. F. Kiselev and K. G. Krasil'nikov	351	6	1277
Certain Regularities in the Properties of Solutions of Strong Electrolytes. A. I. Gorbanev, Yu. M. Kessler, Yu. M. Povarov and É. S. Sevost'yanov	355	6	1281

CONTENTS (continued)

	PAGE	RUSS. PAGE	RUSS. ISSUE
Concerning the Mechanism of the Intercrystalline Corrosion of Stainless Steels in Nitric Acid. A. I. Krasil'shchikov, L. M. Volchkova, I. K. Burtseva and V. D. Plyasunov	359	6	1285
Certain Details of the Cathodic Process on Stainless Steels in Nitric Acid Solutions. E. N. Mirolyubov, M. M. Kurtepov and N. D. Tomashov	363	6	1288
An X-ray Method of Studying the Density on the Detonation Front of Gaseous Mixtures. M. A. Rivin, Ya. B. Zel'dovich, V. A. Tsukerman, V. V. Sof'ina, and A. S. Beregovskii	367	6	1292
The Colloidal State of Dyes and Metachromatism. M. V. Savost'yanova and L. G. Matsinova	369	6	1294
The Oxidizing Properties of Atomic Hydrogen in the Radiational Oxidation of Divalent Iron Ions. V. N. Shubin and P. I. Dolin	375	6	1298
The Effect of Oxidation Products on the Oxidation Kinetics of Hexadecane. V. M. Yur'ev, A. N. Pravednikov and S. S. Medvedev	379	6	1301

CHEMILUMINESCENCE IN THERMAL DECOMPOSITION REACTIONS

R. F. Vasil'ev, O. N. Karpukhin and V. Ya. Shlyapintokh

Institute of Chemical Physics, Academy of Sciences USSR

(Presented by Academician V. N. Kondrat'ev, October 29, 1958)

In the present communication we are presenting the results of experiments in which we had detected some extremely weak luminescence originating from the decomposition of several organic compounds in hydrocarbon solvents.

Figure 1 gives a schematic representation of the set-up used by us to register the emission of light. The glass reaction vessel was located in a light-proof chamber. The vessel consisted of a thermally insulated glass jacket warmed with water. The image of the vessel was projected onto the photocathode of a photomultiplier FÉU-19, whose current was registered on a high-resistance electronic potentiometer ÉPPV-51. When the ratio of signal to noise was 1:1 the sensitivity of the registering system in the 0.05 hertz transmission band was $2 \cdot 10^{-12}$ lumens or $\sim 10^4$ photons per second in the region of maximum sensitivity of the photomultiplier (400 mμ).

We carried out the thermal decomposition of tetralin, 2,7-dimethyloctane, and isopropylbenzene hydroperoxides, of benzoyl peroxide, and azoisobutyronitrile. The three hydroperoxides were prepared by the oxidation of corresponding hydrocarbons, and they were decomposed directly without a solvent. Benzoyl peroxide and azoisobutyronitrile were recrystallized from methyl and ethyl alcohols, respectively. Chlorobenzene, which was used as the solvent for these two compounds, was purified by the usual method (see [1]).

The reaction conditions are shown in Table 1.

Experiments have shown that the light intensity increases with increasing temperature (see Fig. 2). In the cases of 2,7-dimethyloctane and tetralin hydroperoxides and benzoyl peroxide, the emitted light was intense enough to permit a determination of its temperature dependence. It is evident from Fig. 3 that all three compounds satisfy quite well the $I \sim \exp(-A/RT)$ law. The temperature coefficients A are listed in Table 1.

At any given temperature the intensity remained constant for many hours; however, each compound had limiting temperature above which the intensity did not remain constant with time but decreased exponentially. For example, for azoisobutyronitrile this limit was at 80°.

The presence of chemiluminescence indicates that there are some excited particles in the reaction zone. The spectrally sensitive regions in the photomultiplier FÉU-19 (350-600 mμ) correspond to photons with an energy of 80-45 kcal/mole. The excited molecule must obtain this amount of energy in one (or several – in cases of stepwise excitation) primary process. The only possible processes which could cause excitation in the systems used by us are the recombinations of radicals, since all of the investigated compounds dissociate into radicals; for example,

$$C_{10}H_{21}OOH \rightarrow C_{10}H_{21}\dot{O} + \dot{O}H$$
$$(CH_3)_2C(CN)N = N(CN)C(CH_3)_2 \rightarrow$$
$$\rightarrow 2(CH_3)_2\dot{C}(CN) + N_2$$

etc.

The recombination of radicals usually proceeds with the emission of several kilocalories of energy per

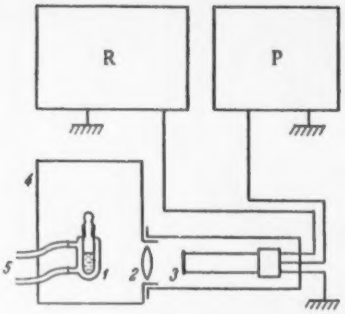

Fig. 1. Schematic representation of the experimental set-up. 1) Insulated vessel; 2) lens; 3) photomultiplier FÉU-19; 4) lightproof chamber; 5) to the thermostat. R) recitifier VS-16; P) potentiometer EPPV-51.

mole. This energy can be transferred into the excitation energy of the molecules formed by the recombination of radicals or into the excitation of a third particle, or just be dissipated as heat.

Under stationary conditions the rate of radical formation equals the rate of their destruction (recombination).

$$W_{\text{form.}} = W_{\text{recomb.}}.$$

The rate of radical formation is proportional to the rate of decomposition of the original compound

$$W_{\text{form.}} \sim W_{\text{decomp.}}.$$

On the other hand, the rate of formation of the excited particles and the number formed are proportional to the recombination rate,

$$N_{\text{excit.}} \sim W_{\text{recomb.}}$$

Therefore, the intensity of chemiluminescence, which is proportional to the number of excited particles, is proportional to the decomposition rate of the starting compound,

$$I \sim N_{\text{excit.}} \sim W_{\text{decomp.}}$$

It is well known that the decomposition kinetics of the compounds studied by us satisfy a first-order equation [3]:

$$W_{\text{decomp.}} = \frac{dC}{dt} = kC = kC_0 e^{-kt},$$

where C_0 and C_1 are the initial concentration and the concentration at time t; k is the rate constant which has the form

$$k = ae^{-E/RT},$$

(a = preexponential coefficient; E = decomposition activation energy).

Thus we will get the following time and temperature-dependent equation for the light intensity:

$$I \sim e^{-E/RT} e^{-kt}.$$

The majority of our reactions obeyed this equation quite well.

At moderate temperatures the light intensity remained constant with time due to the small value of the rate constant k (for example, for tetralin hydroperoxide at 97°, $k = 8.8 \cdot 10^{-6}$ sec^{-1}), while at elevated temperature the intensity decreased according to $I \sim e^{-kt}$.

The temperature dependence of the intensity should be determined by the factor $e^{-E/RT}$. And in fact, the temperature coefficients A obtained by us (see Table 1) are equal to the decomposition energies of the corresponding compounds. Thus, the general reaction scheme presented by us explains quite well our experimental data.

In most of the works devoted to the study of chemiluminescence in solution, the systems investigated

TABLE 1

Compound	Temperature range, in °C	Solvent	Concentration, moles/liter	A, kcal/mole	E, kcal/mole
Tetralin hydroperoxide	57-97	No solvent	1.3	26.5± 1.5	24-24.4 [2]
Benzoyl peroxide	47-84	Chlorobenzene	0.10	31.9± 1.0	27-33 [3]
Azoisobutyronitrile	35-97	Chlorobenzene	0.12	–	–
Isopropylbenzene hydroperoxide	72-96	No solvent	0.31	–	–
2,7-Dimethyloctane hydroperoxide	73-84	No solvent	0.26	29.3± 1.0	–

contained besides the reagents an especially added compound which would be easily excited by the chemical energy of the reaction (for example, luminol). As a rule the light intensity changed in the same way as the reaction rate, but it characterized primarily the added compound and not the properties of the reagents themselves.

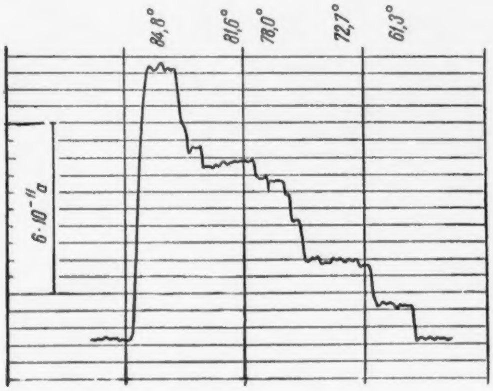

Fig. 2. Variation of emitted light intensity (photocurrent in the photomultiplier) with temperatures during the decomposition of tetralin hydroperoxide.

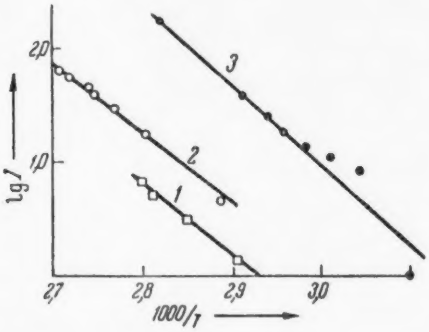

Fig. 3. Temperature dependence of emitted light intensity. 1) 2,7-Dimethyloctane hydroperoxide; 2) tetralin hydroperoxide; 3) benzoyl peroxide.

We believe that in order to investigate the chemical reaction mechanism it is of a much greater importance to study the chemiluminescence of the investigated system itself. Unfortunately very little has been done in this field with any bearing on the reactions in solution. However, the data already available indicate that light emission is observed in even the most common reactions (in which relatively simple molecules participate) at moderate temperatures. It seems that in such simple systems chemiluminescence is a very widespread phenomenon and characterizes many types of reactions.

Thus, light emission in the visible region was observed in Grignard reactions [4] and in the oxidation of several organic compounds [5]. Light emission in the ultraviolet region (200-240 $m\mu$) was observed by Audubert and co-workers [6] in such reactions as neutralization of strong acids by strong alkali, hydration and dehydration of quinine sulfate, as well as in several oxidation—reduction reactions: autooxidation of bisulfite, oxidation of organic compounds by permanganate ion, chromic acid, and bromine, anodic oxidation of Al, Mg, Ta, Si, et al. Heats of all of the above-enumerated reactions are several tens of kilocalories per mole. Therefore the emission of light in the 200-240 $m\mu$ region (energy 140-120 kcal mole) was explained by Audubert through a stepwise excitation mechanism. The low yield of the emitted light (of the order of 1 photon per 10^{14}-10^{15} primary processes) would tend to support such a view. In all of Audubert's reactions one would obviously expect some primary radiation, too; that he did not record any can be explained by the fact that there were no sensitive long-wave light detectors at that time.

We have already noted that in our experiments the spectral region of the emitted light corresponded to an energy of 45-80 kcal mole. Therefore, we can safely assume that we did observe the light emitted by particles excited in a primary process; the yield of emitted light in our experiments was of the order of 1 photon per 10^8 primary processes, i.e., much higher than in Audubert's experiments.

LITERATURE CITED

[1] V. Ya. Shlyapintokh and N. M. Émanuél', Bull. Acad. Sci. USSR, Div. Chem. Sci. 1957, 783.*

[2] D. G. Knorre, Z. K. Maizus, L. K. Obukhova and N. M. Émanuél', Progr. Chem. 26, 417 (1957).

[3] M. Szwarc, Chem. Rev. 47, 75 (1950).

[4] Wedekind, Phys. Zs. 7, 805 (1906).

[5] M. Trautz, Zs. Phys. Chem. 53, 1 (1905).

[6] P. Audubert, Trans. Farad. Soc. 35, 197 (1939).

Received September 20, 1958

---

*Original Russian pagination. See C. B. Translation.

PULSATING AND SPINNING DETONATION OF GASEOUS MIXTURES IN TUBES

Yu. N. Denisov and Ya. K. Troshin
Institute of Chemical Physics of the Academy of Sciences USSR

(Presented by Academician Ya. B. Zel'dovich, November 28, 1958)

The scant amount of available information about the intrinsic nature of detonation waves is still the major hindrance to the development of a complete detonation theory. The current theories propose either a hypothetical ensemble composed of a plane shock front and a chemical reaction front behind it [1], or by isolating a single many-headed spinning detonation limit themselves to the analysis of the breaks in the wave fronts [2, 3] or of gaseous vibrations behind the front [4, 5].

The purpose of this work was to study experimentally the structure of gaseous detonation waves in tubes. The investigation was done by a method of continuous photography of the reaction (with time) and by a "tracer" method, similar to that used by Mach in recording collisions between shock waves [6].

The tracer method of studying the detonation involves a way of fixing the "trace" left on the inside surface of a detonation tube by nonhomogeneous dynamic pressures at the forward front. The inside of the glass detonation tube was covered with a thin layer of carbon-black; the small inertia of its particles permits a rapid registering of any changes in the dynamic pressure. The high optical density of these particles makes it possible to either photograph the resulting trace so that it may be magnified by means of a projecting device on photographic paper, which gives a negative picture of the trace imprint, or to subject this trace to direct visual measurements.

It is known that the detonation structure, as photographically registered, will vary from normal to spinning depending on the initial pressure of the gaseous explosive mixture provided its composition and the tube diametes remain constant [7]. Keeping this in mind, we investigated the detonation at various initial pressures p_0 of stoichiometric mixtures of oxygen + hydrogen, methane and acetylene. At atmospheric pressure one usually observes normal detonation in these mixtures. It turned out, however, that by increasing the resolving power of the recording apparatus we were able to detect on the continuous photograph of such a detonation wave the characteristic traits of a photorecorded spinning detonation: a striated structure of after-emission and a wavy front line. At the same time the tracer method recorded diamond-shape imprints on the tube walls, which attested to the pulsating changes in the dynamic pressure at the forward detonation front caused by a many-headed high-frequency spin (Fig. 1a). As the initial pressure of the mixture was decreased the fine structure of the tracer imprints became larger * (Fig. 1b), and in the region of detonation it abruptly changed from a diamond-shaped into a spiral-shaped trace of a single-headed spin (Fig. 1c).

Analyzing the data obtained by the tracer method and continuous photography we can conclude that the spiral-shaped and diamond-shaped traces are impressed on the tube walls by breaks in the forward detonation front — transverse compression layers in which the chemical reaction is predominantly localized. The breaks which are characterized by high pressures and temperatures [2, 3] propagate towards each other along the surface of the forward detonation front, collide, re-form after the collision, separate from each other, and collide again. Only in the case of a single-headed spin does the break undergo a rotational and translation motion.

* Zel'dovich and Kompaneits theoretically predicted an increasing number of spin heads as the reaction time decreases and as one moves away from the region of detonation ([3]p. 169). However, they analyzed non-interacting breaks.

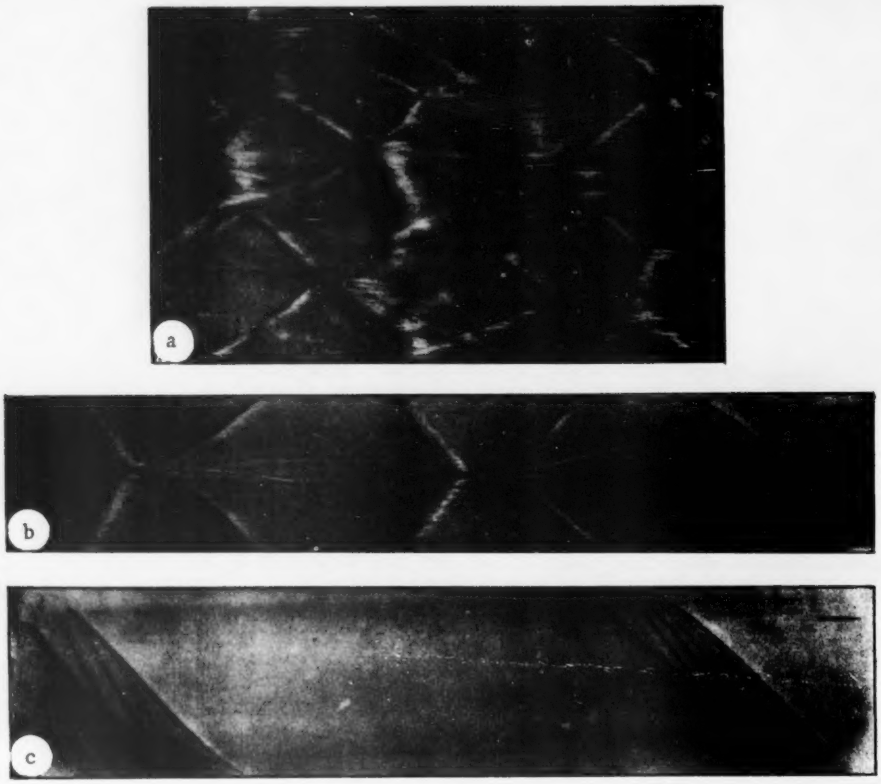

Fig. 1. Gaseous detonation trace imprints on the inside surface of a detonation tube. $2H_2$ + + O_2 mixture. a) p_0 = 300 mm, d = 16 mm, 7.5 x , traces of periodic explosions are visible; b) p_0 = 130 mm, d = 11 mm, 1.75 x ; c) p_0 = 50 mm, d = 13 mm, 1.75 x . The detonation is propagated from left to right.

Besides these breaks, during a many-headed spinning detonation the tracer method recorded high excitations (explosions) (see for example Fig. 1a), which periodically and very rapidly eveloped the space between adjacent breaks in the forward front, all this points to discrete nature of such a detonation process — its quasi-stationary state.

In Fig. 2 we have shown the dependence of certain detonation-wave parameters on the initial pressure of the mixture. The pulse scale ΔZ is based on the spacing between the wavy front line on the continuous photograph, or on the diagonal distance on the idamond-shaped trace imprint along the funnel generatrix, or else on the spacing between the spiral-shaped traces in single-headed spinning detonations. The pulse frequency ν = = $D/\Delta Z$ (where D is the detonation rate); n = number of collisions between breaks (pulses) along the circumference of the detonation tube; α = angle between the funnel generatrix and the translational motion of the break.

The curves shown in the graphs have been plotted as continuous functions, yet not all the curve points actually exist; the distance ΔZ changes stepwise for n = 1, 2,.... Other functions are similarly discrete.

The shape of the forward front (Fig. 3) was discovered by means of the tracer method, which recorded a collision between a detonation wave and a plane shock front. This gives a winding line of a collision indicating that the forward detonation front is not plane. Actually the curvature of the forward front is even greater than was recorded, since one has to consider the fact that the protruding and extruding portions of the forward front will encounter the plane shock front at different times.

The forward front of a single-headed spinning detonation (Fig. 3a) remains constant in a coordinate system which moves along with the break in this front at a constant rotational and translational velocity of the spinning detonation.

In a many-headed spinning detonation the forward front changes periodically in the coordinate system which is moving forward with the average propagation velocity of the detonation wave – convexities become concavities and vice versa (Fig. 3, b, c).

Such a periodic change in the form of the front as well as the periodic nature of the collisions between the breaks (which are propagated along the surface of the forward front) and the resulting pressure fluctuations at the points of collision provide the basis for a subdivision of the gaseous detonation in tubes into pulsating and spinning; moreover, in the second category we are only including a single-headed spinning detonation.

Let us compare the characteristic features of these two types of detonation waves–

	Spinning detonation	Pulsating detonation
I. Form of the forward front in a coordinate system moving with the front.	Remains constant; the front outline spatially resembles a narrow Moebius strip.	Changes periodically; convex planes become concave and vice versa.
II. The nature of motion on the forward front.	Translational and rotational motion.	Translational and vibrational motion.
III. Number of simultaneous collisions between breaks (pulses) along the circumference of the forward front.	0	n = 1,2...
IV. Number of breaks in the forward front.	1	2n

The pulsating detonation is a three-dimensional process and its propagation mechanism is quite different from the initial one-dimensional hypothesis of Jost and Bekker [8], which treated a single-headed spin as if it were an intermittent propagation process in a detonation wave.

As a result of the above-presented work we can safely conclude that the chemical reaction is localized in particular segments of the detonation wave front. Moreover, the break in the forward front plays here a leading role. This structural element of the pulsating detonation wave appears in a "pure" form within the limits of the propagating detonation and exists independently in a spinning detonation process.**

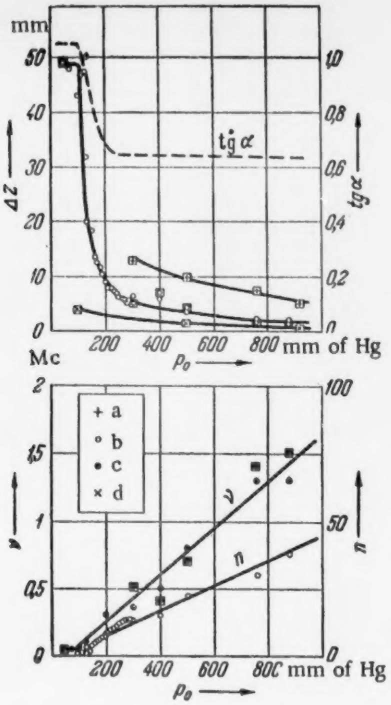

Fig. 2. The dependence of certain detonation wave parameters on the initial pressure of the mixture (d = 16 mm). a) $CH_4 + 2O_2$; b) $2H_2 + O_2$; c) $2H_2 + O_2$ (for the value of ν); d) $C_2H_2 + 2.5O_2$. The squares denote points obtained by continuous photography, the points without squares by the tracer method.

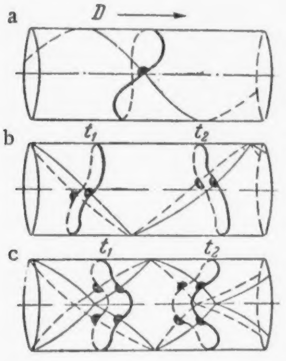

Fig. 3. The shape of the forward front of a detonation wave at times t_1 and t_2. a) Spinning; b) pulsating with n = 1*; c) pulsating with n = 2.

---

* Manson [4] theoretically predicted this type of a detonation wave, but for a single-headed spin.

** At the same time the spiral trace of the break also has some periodic internal nonhomogeneous spots (Fig. 1c), which indicates that there is a fine structure in the spinning detonation.

We have to consider it experimentally proven that the structure of a gaseous detonation wave in tubes is not just a simple combination between a flat shock front and a chemical reaction front, which combination is the basis of contemporary hydrodynamic theory of detonations [1, 3]. This combination, as has now been shown by Shchelkin [9], is unstable, and it is quite possible that it is this fact that causes the localization of the chemical reaction in separate portions of the detonation wave front.

The authors are grateful to corresponding member Acad. Sci. USSR, Prof. K. I. Shchelkin for his discussion of this work and some useful comments.

LITERATURE CITED

[1] Ya. B. Zel'dovich, Theory of Detonation Propagation in Gaseous Systems, J. Exptl. Theor. Phys. 10, 542 (1940).

[2] K. I. Shchelkin, Rapid Combustion and Spinning Detonation in Gases, War Press USSR, 1949.*

[3] Ya. B. Zel'dovich and A. S. Kompaneits, Detonation Theory, Moscow, 1955.*

[4] N. Manson, Propagation des detonations et des deflagrations dans les melanges gaseux, Paris, 1947.

[5] J. A. Fay, J. Chem. Phys. 20, No. 6 (1952).

[6] E. Mach and J. Sommer, Sitzungsberichte Akademie Wien, 75, II (1877).

[7] Ya. K. Troshin and K. I. Shchelkin, Bull. Acad. Sci. USSR, Div. Theor. Sci. No. 8, 142 (1957).

[8] W. Jost, Explosion and Combustion Processes in Gases, (IL, 1952) [Russian translation].

[9] K. I. Shchelkin, J. Exptl. Theor. Phys. 36, 600 (1959).

Received November 15, 1958

---

* In Russian.

CRYSTAL STRUCTURE OF NORMAL PARAFFINS n-$C_{30}H_{62}$ AND n-$C_{32}H_{66}$ AT HIGH PRESSURE

S. S. Kabalkina

Institute of High-Pressure Physics at the Academy of Sciences USSR

(Presented by Academician N. V. Belov, October 31, 1958)

It has been experimentally established [1, 2] that in a true crystalline state,normal paraffins can have two types of subcells: rhombic (R) and triclinic (T). Under ordinary conditions the even-numbered paraffins from n-$C_{18}H_{38}$ to n-$C_{26}H_{54}$ have a subcell T, while all the odd ones, and the even ones from n-$C_{28}H_{58}$ to n-$C_{36}H_{74}$ have a subcell R.

A. I. Kitaigorodskii did a geometrical analysis of the molecular packing in paraffins into layers and of the arrangement of these layers [3]. Normal paraffins exhibit phase polymorphism in the solid state. Thus,at temperatures near the melting point both n-$C_{18}H_{38}$ and -$C_{20}H_{42}$ have a rhombic subcell [4], while at lower temperatures a subcell T.

By means of electron diffraction methods [5] it was established that thin films of n-$C_{18}H_{38}$ and n-$C_{20}H_{42}$ also have a subcell R. One can assume that there are conditions under which the even-numbered paraffins from n-$C_{28}H_{58}$ and up, and other ones have a subcell T. No such transition was observed at lower temperatures [4].

The present work is devoted to the elucidation of the effects of high pressure on the structure of n-$C_{30}H_{62}$ and n-$C_{32}H_{66}$. The investigation was conducted under hydrostatic and quasihydrostatic pressures in a high-pressure x-ray chamber [6, 7] (Fig. 1); it was designed to permit a direct measurement of liquid pressures with a manganin manometer [8], with an accuracy of ± 100 kg/cm^2.

A paraffin sample 0.4-0.5 mm in diameter was placed inside a beryllium cone. The pressure (hydrostatic) was exerted on the sample by means of benzene through a 0.3-0.5 lithium lining, which shielded the sample from benzene.

In Fig. 2 we have presented some x-ray patterns of n-$C_{30}H_{62}$ obtained at various hydrostatic pressures using a copper source. Each pair of x-ray pictures consists of two patterns: one obtained at high pressure,another at atmospheric. The patterns under high pressures contain only the (110) and (200) lines of the R-modification (same as pictures at atmospheric pressure), which enables us to determine the values of $\underline{a}$ and $\underline{b}$ corresponding to a given $\underline{p}$. The effective radius of the chamber used in our calculations was determined for each x-ray picture from the pattern obtained at atmospheric pressure.

In Table 1 we have listed the values of $\underline{a}$, $\underline{b}$, and ab for n-$C_{30}H_{62}$ and n-$C_{32}H_{66}$ at various pressures $\underline{p}$.

A comparison shows that the ab values corresponding to the absolute zero temperature can be obtained by compressing the compounds at room temperature to 3500-4000 kg/cm^2.

According to Fig. 4 the parameter $\underline{c}$ in n-$C_{30}H_{62}$ remains constant (within ± 0.03 A) at high pressures, and consequently the compressibility along the molecular chain length is insignificant in comparison with that in the perpendicular directions. This result is in agreement with Müller's data [10] for n-$C_{23}H_{48}$ and -$C_{29}H_{60}$ (he studied their compressibility up to 1500 kg/cm^2), as well as with the results obtained from the thermal expansion of normal paraffins [11].

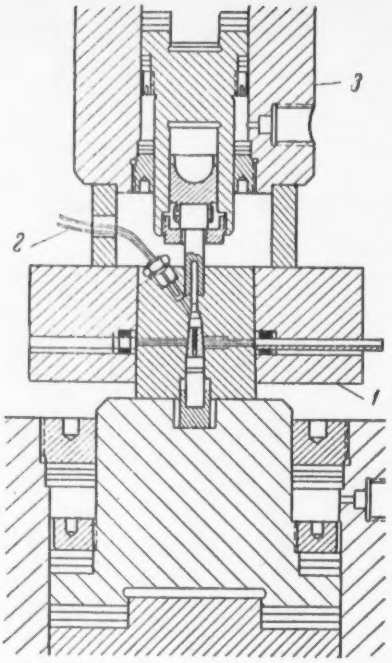

Fig. 1. High-pressure x-ray camera (1), with a manganin manometer (2) in the multiplier (3).

The data obtained make it possible to use the formula V = const ·ab (a function of pressure) for the unit cell volume of paraffins with a fair degree of accuracy.

In Fig. 3 we have plotted the $V_{(P)}$ function for $n-C_{30}H_{62}$: the oxidation gives values of ab. It has the form of two straight lines with different slopes, indicating a change in the compressibility at high pressures.

In Table 2 we have listed the coefficients of linear compressibility $\frac{1}{p}\,\frac{\Delta a}{a}$ and $\frac{1}{p}\,\frac{\Delta b}{b}$ for various values of p.

It follows from the table that the compressibility coefficients of the first line (1-7000 kg/cm^2 pressure range are much greater than those of the second (7,000-13,500 kg/cm^2 pressure range). Thus $\frac{1}{p}\,\frac{\Delta a}{a} = (6.8 \pm 0.3)\cdot 10^{-6}\ kg/cm^2$ for the first line and $\frac{1}{p}\,\frac{\Delta a}{a} = (5.4 \pm 0.3)\cdot 10^{-6}\ kg/cm^2$ for the second. The data obtained indicate that there is no sudden volume decrease in $n-C_{30}H_{62}$ at high pressures, but there is a sudden change in the compressibility coefficient, and consequently at high pressures there is a transition of the 2nd type instead of the 1st.

The absence of a transition of the 1st type was confirmed by the form of the x-ray patterns at high pressures; the pictures lack the additional lines corresponding to a triclinic cell.

Since the data for $n-C_{30}H_{62}$ and $n-C_{32}H_{66}$ (Tables 1 and 2) agree quite well, then all that was said for one holds true for the other.

TABLE 1

Parameters of $n-C_{30}H_{62}$ and $n-C_{32}H_{66}$ Subcells at High Pressures

p, kg/cm^2	a, Å	b, Å	ab, $Å^2$	p, kg/cm^2	a, Å	b, Å	ab, $Å^2$
$n-C_{30}H_{62}$				$n-C_{30}H_{62}$			
1	7,44	4,95	36,83	8700	7,08	4,75	33,63
1250	7,36	4,89	35,99	9000	7,07	4,75	33,55
3000	7,29	4,86	35,43	10500	7,00	4,71	32,97
4200	7,21	4,81	34,68	13500	6,93	4,64	32,15
5600	7,14	4,77	34,06				
5800	7,16	4,77	34,15	$n-C_{32}H_{66}$			
5900	7,14	4,77	34,06				
6000	7,11	4,78	33,98				
6100	7,14	4,76	33,99	4900	7,15	4,79	34,25
7100	7,14	4,77	34,06	5700	7,13	4,78	34.08
7300	7,08	4,75	33,63	8700	7,10	4,75	33,72
8200	7,14	4,77	34,06	13600	6,95	4,64	32,28

For $n-C_{30}H_{62}$ at T = 77°K: a = 7.19 A, b = 4.91 A, ab = = 35.30 A^2 [4]; at T = 0°K (extrapolated values): a = 7.20 A, b = 4.86 A, ab = 34.99 A^2 [9].

The graph $V_{(P)}$ (Fig. 3) makes it possible to estimate the work done in compressing n-$C_{30}H_{62}$ to p = 13,500 kg/cm^2; it was found to be $1.84 \cdot 10^{-4}$ ergs per CH_2 which constitutes about 20% of the lattice energy per CH_2 group at ordinary conditions (sublimation energy [12] $1.05 \cdot 10^{-13}$ erg/CH_2).

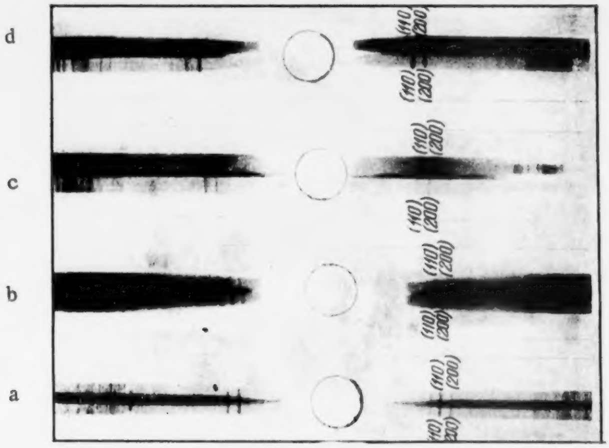

Fig. 2. X-ray patterns of n-$C_{30}H_{62}$. a) At p = 1200 kg/cm^2; b) p = 6000 kg/cm^2; c) p = 10,000 kg/cm^2; d) p = 13,500 kg/cm^2. Pressure hydrostatic, light from a copper source.

TABLE 2

Coefficients of Linear Compressibility Along the a and b Axes in n-$C_{30}H_{62}$ and n-$C_{32}H_{66}$

p, kg/cm^2	$\frac{1}{p}\frac{\Delta a}{a}\cdot 10^6, \frac{cm^2}{kg}$	$\frac{1}{p}\frac{\Delta b}{b}\cdot 10^6, \frac{cm^2}{kg}$	p, kg/cm^2	$\frac{1}{p}\frac{\Delta a}{a}\cdot 10^6, \frac{cm^2}{kg}$	$\frac{1}{p}\frac{\Delta b}{b}\cdot 10^6, \frac{cm^2}{kg}$
	n-$C_{30}H_{62}$			n-$C_{30}H_{62}$	
3000	6,7	6,3	7100	5,7	5,1
4300	7,2	6,8	8200	4,9	4,5
5600	7,2	6,7	8700	5,6	4,8
5800	6,5	6,3	9600	5,3	4,5
5900	6,8	6,3	10450	5,6	4,6
6000	7,4	5,9	13500	5,1	4,7
6150	6,5	6,4	Average	5,4±0,3	4,7±0,2
7300	6,6	5,7			
Average	6,8±0,3	6,2±0,3		n-$C_{32}O_{66}$	
			5000	7,8	6,7
			5800	7,2	6,1
			8700	5,2	4,7
			13600	4,8	4,6

In Table 3 we have compared the intermolecular distances between hydrogen atoms at pressures up to 6000 kg/cm^2 (above this pressure a phase transition occurs). The Table was compiled on the basis of a geometrical analysis by using the following parameters: interatomic C−H distance.1.13 A, C−C 1.53 A. The distance between any two neighboring unbound (to each other) carbon atoms in the chain is 2.54 A, $\varphi_b = 41.2°$, $\epsilon = 109°30'$.

The other half of this work was devoted to the investigation of the n-$C_{30}H_{62}$ and n-$C_{32}H_{66}$ crystal structure at light quasihydrostatic pressures. As a medium for the transmission of pressure we used lithium. The investigation was carried out in the same x-ray chambers, without a manganin manometer. The x-ray pictures obtained (Fig. 4) indicate beyond any doubt the existence of a reversible transition in the crystal structure of n-$C_{30}H_{62}$ and n-$C_{32}H_{66}$ at high pressures. Two new lines (d = 4.35 A and d = 2.50 A) which appear under high pressures and disappear when the pressure is reduced definitely point to a transition.

TABLE 3

The Closest H–H Intermolecular Distances in n-$C_{30}H_{62}$ at High Pressures (for the atomic subscripts see [9])

	1 kg/cm^2	3000 kg/cm^2	6000 kg/cm^2
	Intermolecular distances, A		
$H_1 - H_3$	2.48	2.40	2.32
$H_1 - H_4$	2.92	2.85	2.81
$H_2 - H_4$	2.86	2.79	2.72
$H_2 - H_5$	2.42	2.36	2.31

TABLE 4

Interplanar Distances of the Most Intense Reflections from R and T Subcells

Modification	p, kg/cm^2	Interplanar distance, A						
T-subcell								
n-$C_{20}H_{42}$	1	4,54		3,79	3,58		2,58	
R-subcell								
n-$C_{30}H_{62}$	1		4,12	3,73		2,97		2,48
n-$C_{30}H_{62}$	7000	4,35	3,96	3,56		2,87		2,41
n-$C_{32}H_{66}$	9000	4,35	3,92	3,51		2,83	2,50	2,38
n-$C_{32}H_{66}$	4500	4,45	4,02	3,61		2,92	2,55	2,43

In Table 4 we have listed the interplanar distances in n-$C_{20}H_{42}$ and n-$C_{30}H_{62}$ atmospheric pressure and in n-$C_{30}H_{62}$ and n-$C_{32}H_{66}$ at high pressures. It follows from the table that the x-ray patterns of n-$C_{30}H_{62}$ and n-$C_{32}H_{66}$ obtained at high quasihydrostatic pressures (6000–10,000 kg/cm^2) correspond to two-phase systems R + T, since they contain both the R and T-subcell lines (pressure was determined by means of the $V_{(P)}$ function in Fig. 3 for the rhombic modification). Actually, if we take the compressibility of a n-$C_{30}H_{62}$ lattice as 4% (p = 7000 kg/cm^2), then multiply by the corresponding coefficient we will get (at atmospheric pressure) d_1 = 4.53 A, d_2 = 4.12 A, d_3 = 3.71 A, d_4 = 2.99 A, d_5 = 2.51 A. Consequently, at high pressures alongside the rhombic modification one observes the appearance of the triclinic. A. I. Kitaigorodskii and Yu. V. Mnyukh [13] made similar observations in polyethylene at atmospheric pressure. Thus it is obvious that hydrostatic and quasihydrostatic pressures have different effects on the structures of n-$C_{30}H_{62}$ and n-$C_{32}H_{66}$: hydrostatic pressure produces a transition of the 2nd type while quasihydrostatic, the 1st type. The following explanation is possible: under quasihydrostatic pressures the shearing forces displace the molecular planes relative to each other and change straight layers into skew.

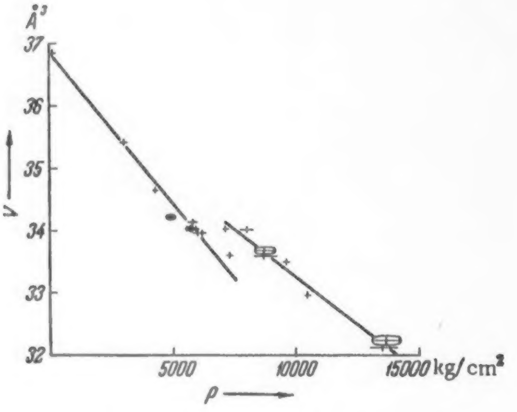

Fig. 3. Unit cell volume of n-$C_{30}H_{62}$ as a function of pressure. The ovals encircle the data for n-$C_{32}H_{66}$.

In concluding I would like to thank Prof. L. F. Vereshchagin and Prof. A. I. Kitaigorodskii for their interest in this work and discussion of results, and also L. V. Fedin for his help in working out the results.

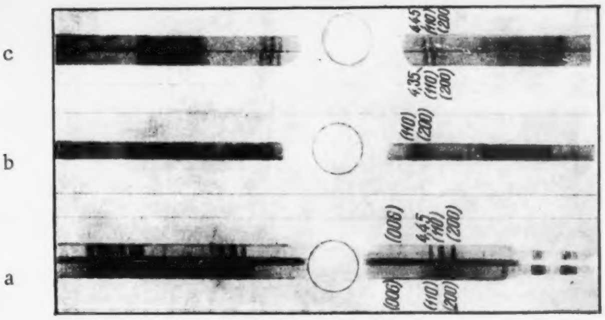

Fig. 4. X-ray patterns of n-$C_{30}H_{62}$ and n-$C_{32}H_{66}$ at high quasihydrostatic pressures. a) n-$C_{30}H_{62}$, upper picture at p = 7000 kg/cm^2, lower at p = 1 kg/cm^2, cell diameter 80 mm); b) n-$C_{32}H_{66}$ at p = 1 kg/cm^2, cell diameter 62.6 mm; c) n-$C_{32}H_{66}$, upper picture at p = = 4,500 kg/cm^2, lower at p = 9000 kg/cm^2, cell diameter 62.6 mm. Light from a copper source through a nickel filter.

LITERATURE CITED

[1] C. W. Bunn, Trans. Farad. Soc. 35, 482 (1939).

[2] A. Müller and K. Londsdale, Acta Cryst. 1, 129 (1948).

[3] A. I. Kitaigorodskii, Crystallography 2, 456, 646 (1957).

[4] A. Müller, Proc. Roy. Soc. 127, 417 (1930).

[5] A. N. Lobachev, Crystallography, (1958).

[6] L. F. Vereshchagin and I. V. Brandt, Proc. Acad. Sci. 108, No. 3 (1958).*

[7] L. F. Vereshchagin and S. S. Kabalkina, Proc. Acad. Sci. 113, No. 4 (1957).*

[8] B. S. Aleksandrov and L. F. Vereshchagin, J. Theor. Phys. 9, 843 (1939).

[9] A. I. Kitaigorodskii and Yu. V. Mnyukh, Proc. Acad. Sci. 121, No. 2 (1958).*

[10] A. Müller, Proc. Roy. Soc. 178, 227 (1941).

[11] A. Müller, Proc. Roy. Soc., A138, 514 (1932).

[12] A. R. Ubbelohde, Trans. Farad. Soc. 34, 282 (1938).

[13] A. I. Kitaigorodskii and Yu. V. Mnyukh, Proc. Acad. Sci. 121, 115 (1958).*

Received October 25, 1958

---

*Original Russian pagination. See C. B. Translation.

DEFORMATION IN CRYSTALLINE POLYETHYLENETEREPHTHALATE FILMS

P. V. Kozlov, V. A. Kabanov and A. A. Frolova
M. V. Lomonosov Moscow State University

(Presented by Academician V. A. Kargin, July 12, 1958)

It was of some interest to study the conditions under which polymeric crystals and spherulites break down and the relationships between crystallization and orientation processes which take place during deformation of crystalline polymers below their melting points (cold stretching), since the phenomenon of cold stretching is widely utilized in the preparation of fibers and films.

In this work polyethyleneterephthalate films were investigated. The choice of this material was guided by the fact that its vitrification point (~80°) and melting point (~265°) are well above the room temperature. At room temperature the relaxation processes in polyethyleneterephthalate are greatly retarded. This makes it possible to start at room temperature and by gradually raising it, detect all the intermediate stages in the crystallization and orientation processes occurring when the material is stretched.

We used for our investigation two samples with different degrees of crystallization; they were prepared by crystallizing an amorphous polyethyleneterephthalate film through heating for 30 min at 115° and 150°, respectively. The density of the first batch of samples was 1.358 g/cm^3 as determined by the gradient tube [1] method; the density of the second batch was 1.369 g/cm^3 (density of the amorphous film was 1.313 g/cm^3). After the initial heating the original transparent amorphous film became clouded, and when analyzed in polarized light it exhibited spherulitic structure. The x-ray picture (Fig. 1a) indicates an isotropic distribution of the crystals which had formed in the film. Samples of such films were stretched on a Polanyi instrument at various temperatures and rates up to double their original length. Figure 1b shows an x-ray picture of a stretched portion of a sample which was stretched at room temperature. It is evident that the polymer became more amorphous in the stretching process. Only a slightly increased intensity of the diffuse halo in the equatorial region attests to some degree of chain orientation in the amorphous structure. The spherulite picture in the polarized light also disappeared.

In several works [2, 3] V. A. Kargin and T. I. Sogolova have developed a theory that the stretching of crystalline polymers proceeds through a mechanical "melting" of those crystals which were randomly oriented relative to the external mechanical field. However, it was difficult to detect the disordered state in their polymers (an intermediate stage in the deformation) by any direct structural method, since their compounds (polyethylene, polyamides, natural rubber) were stretched above the vitrification points, and consequently any disorder in the crystals is followed by an immediate recrystallization. The vitrification point of polyethyleneterephthalate is in the 80-90° range, and consequently its crystallization rate at room temperature is almost nil, i.e., any breakup of crystals at this temperature cannot be accompanied by recrystallization, and the intermediate structures in the stretching process can easily be recorded.

As the stretching temperature was raised, the orientation of the stretched material became more perfect, but the effects of crystallization did not become noticeable until the vitrification temperature was attained all of which is in accord with the data obtained on the amorphous fibers of polyethyleneterephthalate [4]. When the crystalline films were stretched above the vitrification point, the higher the temperature, the deeper became the recrystallization processes. The nature of the corresponding x-ray pictures, where some uniform rings

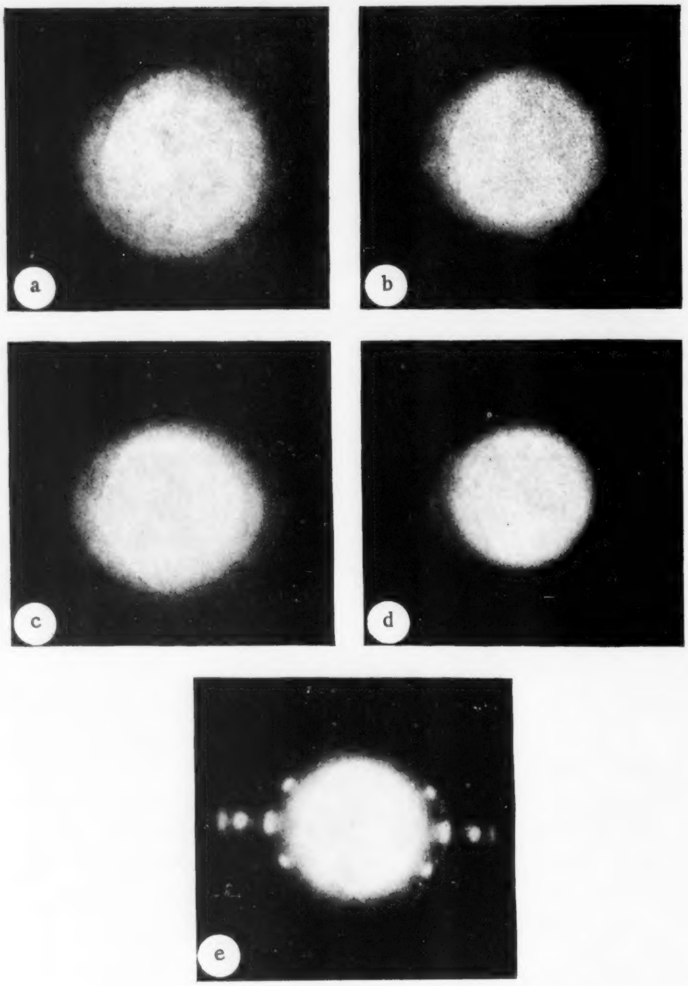

Fig. 1. X-ray pictures of a crystallized polyethyleneterephthalate film. a) Before stretching; b) after stretching at room temperature; c) stretched at 100°C at a rate of 0.017 mm/sec; d) stretched at 100°C at a rate of 0.17 mm/sec; e) stretched in cold and then heated above the vitrification point.

were superimposed on the structure, indicated that simultaneously with the formation of crystals oriented in the mechanical field, some isotropically distributed crystals were also formed (Fig. 1c). The same could be concluded from the clouding of the film and the appearance of spherulites in the stretched portions of the samples. The number of isotropically distributed crystals increased with rising temperature, which fact was also characterized by an increased intensity of the uniform rings in the x-ray pictures. At the same time the number of spherulites formed also increased. Increased stretching rate had the same effect as decreased temperature (Fig. 1c, d), by increasing the orientation and decreasing the fraction of isotropically distributed crystals. This was due to the fact that as the temperature was raised or the stretching rate decreased more chains or chain packets (per unit time) succeeded in escaping the effect of the mechanical field under the action of thermal motion and formed crystals which were more or less randomly distributed relative to the mechanical field.

In order to obtain crystals oriented strictly along the mechanical field it was essential to stretch the amorphous film in cold, then heat it in the stretched state above the vitrification point. After such a treatment the

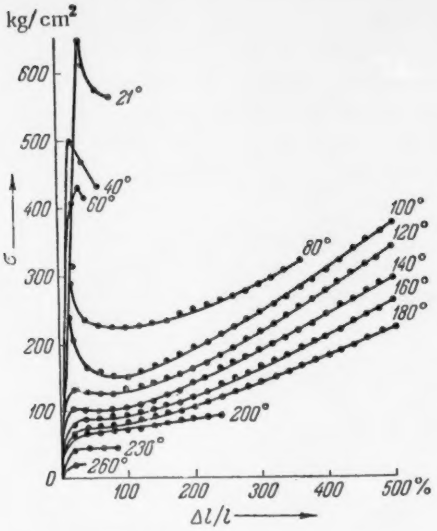

Fig. 2. Stretching curves of polyethyleneterephthalate films crystallized by heating for 30 min at 115°C. The stretching rate was 0.017 mm/sec.

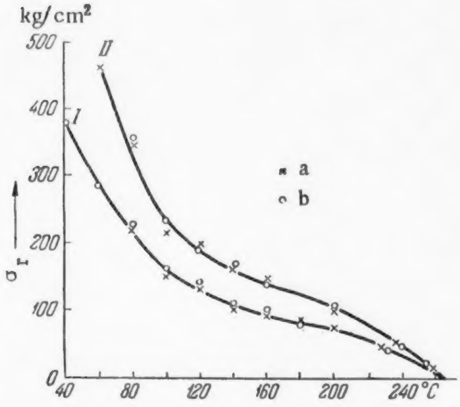

Fig. 3. The recrystallization strain σ_r as a function of temperature. 1) Films crystallized at 115°C; II) films crystallized at 150°. a) Stretching rate 0.017 mm/sec; b) stretching rate 0.17 mm/sec.

crystallization was not accompanied by continuous mechanical destruction of the structure. At the same time the chains or relatively disordered chain packets became oriented along the force field by the preliminary stretching, i.e., the structure was prepared beforehand for the formation of crystals with a parallel orientation of their crystallographic axes. No spherulites were formed in this case. The film remained transparent even after crystallization (Fig. 1e).

We have also investigated the relationship between strain and deformation in crystallized polyethyleneterephthalate films over a wide temperature range and at stretching rates differing by a factor of 10. The results of one such experiment are presented in Fig. 2. Corresponding curves at moderate temperatures exhibited overstrain maxima, indicating the relaxational nature of the deformation. Similar deformation–strain curves were obtained with amorphous polymeric glasses in the region of forced elasticity, which confirms Yu. S. Lazurkin's hypothesis [5] about a common molecular mechanism in the deformations of crystalline polymers and amorphous polymeric glasses. Why this should be so can easily be understood on the basis of polymeric packet-structure theory presented in a work of V. A. Kargin, A. I. Kitaigorodskii, and G. L. Slonimskii [6]. A packet of polymeric chains in a formation similar to a cluster in a low-molecular liquid, but existing for a much longer time due to the large relaxation periods typical of polymers. A structurally crystalline packet differs from an amorphous only in the fact that in a crystalline packet, besides a parallel chain orientation, there is an azimuthal order in the distribution of chain axes and side groups. The degree of orderliness inside an amorphous packet may exhibit a wide range of variations, and in several cases approaches that of a crystalline packet. The deformation of polymers can be regarded as a rectification and rearrangement of polymeric chain packets via a mechanism common to both the amorphous and crystalline polymers. The difference resides in the fact that to the rearrangement energy of the amorphous structure we have to add in the crystalline polymer the heat of fusion of polymeric crystals.

The nonequilibrium nature of the stretching processes, shown by the deformation – strain curves in Fig. 2, makes it hard to estimate the recrystallization strain. However, if we extend the horizontal portions of the stretching curves to their intercepts with the ordinate, then it turns out that the values of the intercepts are independent of the deformation rate, but are only connected with the degree of crystallization in the 1st sample (Fig. 3). This enabled us to treat them as recrystallization strains. The magnitudes of these strains decreased with increasing temperature, but in the temperature range which corresponded to high crystallization rates this decrease was retarded. One of us together with V. A. Kargin and I. Yu. Marchenko [8], as well as G. L. Slonimskii and V. A. Ershova [7], observed a similar retardation in certain other crystallizing polyesters, polyamides, and isotactic polystyrene. This phenomenon can be readily explained if we take into account the fact that recrystallization strain depends not only on the temperature but also on the number of crystals formed per unit time in a unit volume of the sample during recrystallization; the number will have a maximum in the temperature range corresponding to the highest crystallization rate. The increased number of crystals formed per unit volume of the polymer during stretching compensates the temperature-dependent drop in the recrystallization strain. Thus, in this work we have confirmed by a direct structural method the fact that the stretching of crystalline polymers proceeds though an amorphous stage. By using a high-vitrification-point polymer we were able to separate the amorphous stage from the recrystallization stage.

On the basis of structural and mechanical data obtained in the investigation of the processes accompanying the stretching of crystalline polyethyleneterephthalate films (recrystallization, orientation, destruction and formation of spherulites) it was possible to deduce the relaxation nature of these processes.

In concluding, the authors wish to express their deep gratitude to Acad. V. A. Kargin for his valuable advice in the course of this work and during the discussion of results.

LITERATURE CITED

[1] R. V. Bouer, R. C. Spenser and R. M. Wiley, J. Polym. Sci. 21, 249 (1946).

[2] V. A. Kargin and T. I. Sogolova, Proc. Acad. Sci. 88, 867 (1953).

[3] V. A. Kargin and T. I. Sogolova, J. Phys. Chem. 27, 1039, 1208, 1213, 1325 (1953).

[4] V. O. Gorbacheva and N. V. Mikhailov, Colloid. J. 20, 38 (1958).*

[5] Yu. S. Lazurkin, Doctoral Dissertation, Moscow, 1954.

[6] V. A. Kargin, A. I. Kitaigorodskii and G. L. Slonimskii, Colloid. J. 19, 131 (1957).*

[7] G. L. Slonimskii and V. A. Ershova, High-Molecular Compounds, 1, No. 2 (1959).

[8] V. A. Kargin, V. A. Kabanov and I. Yu. Marchenko, High-Molecular Compounds, 1, No. 1 (1959).

Received June 18, 1958

---

* Original Russian pagination. See C. B. Translation.

ADIABATIC COMBUSTION – A NEW METHOD OF INVESTIGATION AND ITS APPLICATION TO HYDROGEN–CHLORINE MIXTURES

A. A. Kuliev and A. I. Rozlovskii

Institute of Physics and Mathematics of the Academy of Sciences Azerb. SSR

(Presented by Academician Ya. B. Zel'dovich, November 21, 1958)

Ignition under adiabatic compression occurs in many practical and important combustion processes; its peculiarity rests in the absence of any distorting wall effects. Ya. T. Gershanik, Ya. B. Zel'dovich, and A. I. Rozlovskii [1] proposed a new method of adiabatically compressing burning mixtures by a rapid stream of gases. The investigated mixture was placed in glass tube sealed at one end and while at a pressure below atmospheric it was compressed by the air rushing in as the plug sealing off the tube was suddenly jerked out. In this method the terminal compression was always 1 atm; as a refinement of this method we propose a simple apparatus in which the terminal pressure could be varied at will anywhere below one atmosphere.

The compression (buffering bulb) and combustion chambers were combined by rupturing the membrane dividing them. The mixture was compressed in a tube 1.3 m long and 18.3 mm in diameter which was connected through a ground joint to a 10-liter buffering bulb. The open end of the tube was located in the middle of the bulb and terminated in a female ground joint to which were attached several flat diaphragms with holes of various sizes (D = 8-32 mm) in their middle. The joint with the diaphragm was covered by a thin rubber membrane which hugged the joint very tightly.

The bulb and the tube were evacuated simultaneously, then the tube was heated to T_0 and filled with the burning mixture to a pressure p_0 while air was slowly allowed to leak into the bulb. Under a pressure p_a (determined by the diameter of the diaphragm opening and the number of overlapping membranes) the membrane breaks and the mixture is compressed in the tube. A careful check showed that there wasn't any noticeable gas leakage from the bulb into the tube.

Mixtures of hydrogen and chlorine were selected for our investigation. Previously the mechanism as well as the fundamental kinetics of this slow reaction were established [2]. The absolute values of the critical parameters for this spontaneous combustion calculated from that data were close to the experimental values, but the effective activation energy (A = 22 kcal/mole) calculated from the experimental parameters is much lower than the value for a slow reaction (A = 35 kcal/mole). It has been established [3] that an unbranched chain mechanism with heterogeneous initiation of active centers would not be compatible with the spontaneous combustion of these mixtures [3]. In a normal combustion of hydrogen + chlorine mixtures (with an excess of chlorine), as well as in a slow reaction, the kinetics for the reaction independent of any wall effects should be determined by the equilibrium dissociation of chlorine [4]. It is essential to study the adiabatic combustion to supplement the available data about this reaction mechanism. The method of preparing hydrogen + chlorine mixtures was described in [4]. Experiments were carried out on a 70% Cl_2 + 30% H_2 mixture. The adiabatic compression temperature T_a (resulting from the isentropic nature of this compression, see [1]) was calculated from Poisson's equation.

It was noted in [1] that if the tube was opened very suddenly the pressure inside it might have for a while exceeded atmospheric; however, in our apparatus no distortions connected with such an "overcompression" took place. There was still the possibility that just before a strongly stretched compressed rubber membrane broke the rate of leakage would increase.* In order to avert the possibility of "overcompression" we initially retarded

---

*Let us note that the possibility of "overcompression" also exists in rapidly operating reciprocating engines, for example, in the apparatus described in [5].

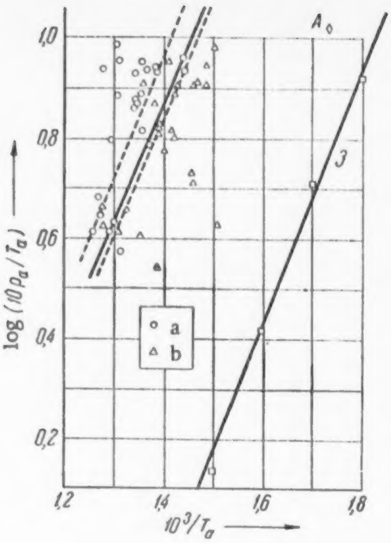

Fig. 1. The effect of terminal pressure on the critical ignition temperature. a) Combustion; b) no combustion. The dotted line limits the distribution of experimental data.

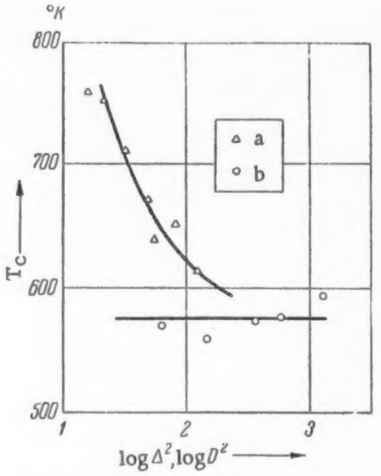

Fig. 2. The effect of the conditions under which the compressed air was introduced on the ignition temperature (p_0 = 91 mm of Hg, p_a = 600 mm). a) Retarded; b) unretarded.

the flow of air into the tube in order to also check the effects of retardation itself. For this purpose the end of the tube was closed with a rubber stopper containing a hole into which were introduced 12-mm-long glass tubes of various diameters Δ (4.0-11.3 mm).

In Fig. 1 we have presented the results of our work on the relationship between the critical ignition temperature T_c and the terminal pressure under a constant p_0 = 92 mm and Δ = 5.7 mm; the coordinates are in units of log (p_a/T_a) and $1/T_a$. The points corresponding to the appearance and disappearance of combustion are bound (with a fair degree of accuracy) by a critical line with a temperature coefficient of 2600, which is in good agreement with the corresponding experimental value [6] from the combustion of such mixtures (2700).

In Fig. 2 we have plotted T_c as a function log Δ^2 or (in experiments without retardation) log D^2 at p_a = 600 mm. Variations in D under compression by unretarded stream of air had practically no effect on the critical conditions, and consequently the "overcompression" could not have introduced any errors in this case either. In experiments with the retarding tube, T_c decreased noticeably with increasing tube cross section, approaching T_c for unretarded flow. During retardation heat losses resulted in increased ignition temperature and with increased Δ the compression approached the adiabatic form.

In Fig. 3 we have plotted the $T_c(p_0)$ function at p_a = 300 mm and Δ = 5.7 mm. It is obvious that at low p_0 there also are some deviations from the adiabatic compression conditions; these deviations decrease with increasing p_0, and are caused by the intermixing between the compressed mixture and the inflowing air, just as occurred in [1].

In order to compare the critical conditions in a heated vessel with those under adiabatic compression we converted the data given in [6] to our experimental conditions (Fig. 1, curve 3). We assumed that for a given T_c value the p_c decreased 1.33-fold during a transition from a mixture containing 50% Cl_2 to one with 70% of Cl_2, and that the effect of diameter d (of the vessel) obeys the equation $p_c d^{4/3}$ = constant derived in [2]. If we consider that the compression in unretarded experiments is adiabatic, then for p_a = 600 mm, T_c will be higher under adiabatic compression than in the heated vessel, but by no more than 35° (Point A in Fig. 1).

However, the combustion conditions (evolution of heat) are not identical in both cases. To compare the critical ignition point under adiabatic compression T_a with that in the vessel T_i it is necessary to compute the absolute values of p_a (T_a) as was done theoretically in [7]; the derivation done in [8] did not allow such a calculation.

Let us examine the combustion in a plane-parallel vessel. Relying on the principles derived in [8], we will look for the equilibrium temperature gradient along the coordinate x for a given wall-temperature T_0 when the temperature along the vessel's axis is T_a.

Taking $\theta_a = RT_a^2/A$, $(T_a - T)/\theta_a = \vartheta$, $2x/d = y$ and transposing the exponent with respect to T_a, we can

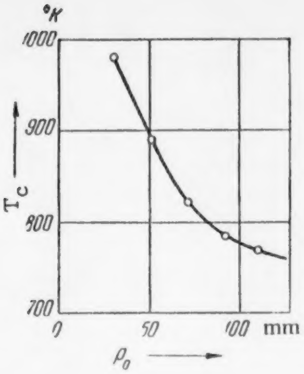

Fig. 3. Effect of the initial pressure on the critical ignition point.

convert the thermal-conductivity equation into the form

$$d^2\vartheta/dy^2 = \delta_a e^{-\vartheta}, \tag{1}$$

where $\delta_a = Qd^2 z_a e^{-A/RT_a}/4\lambda_a\theta_a$; Q = heat of reaction; z = the preexponential reaction coefficient; λ = thermal conductivity; the subscript a refers to the temperature T_a.

The solutions of equation (1) will be,

$$e^{\vartheta/2} = \operatorname{ch}\left(y\sqrt{\delta_a/2}\right), \qquad e^{\vartheta_0/2} = \operatorname{ch}\sqrt{\delta_a/2}, \tag{2}$$

where $\vartheta_0 = (T_a - T_0)/\theta_a$. Since $\vartheta_0\ 2 \gg 1$,

$$\begin{gathered} e^{\vartheta_0/2} = (e^{\vartheta_0/2 + \ln 2})/2 \approx \operatorname{ch}(\vartheta_0/2 + \ln 2) \approx \operatorname{ch}\vartheta_0/2, \\ \delta_a = \vartheta_0^2/2, \quad q\,d^2 z_a e^{-A/RT_a}/\lambda_a = 2(T_a - T_0)^2/\theta_a. \end{gathered} \tag{3}$$

Comparing Eq. (3) with the critical spontaneous-combustion condition in a heated vessel, and taking into account only the difference between T_a and T_i in the exponent, we will get

$$T_a - T_i = \theta \ln \frac{1}{\delta_i}\left(\frac{T_a - T_i}{\theta}\right)^2. \tag{4}$$

We are assuming that the δ_a/δ_i ratio is highly dependent on the shape of the vessel, and so in Eq. (4) we have to take $\delta_i = 2$ (cylindrical vessel) to correctly describe our results [7]. With $T_0 = 388$°K, $p_a = 600$ mm, $T_a = 576$°K, the effective A = 22.0 kcal/mole and $T_a - T_i = 69°$ for an unretarded flow; i.e., the calculated $T_a - T_i$ difference is even slightly in excess of the experimental.

This approximate solution, which did not consider the true nonstationary nature of the process, could be confirmed by another independent approximate method. Neglecting the temperature gradient in the cross-section of the reactor and supplementing the theory in [8] with the thermal-emission coefficient calculated theoretically in [7] for spontaneous combustion, we get a T_a 28° greater than the given one. A comparison between T_a and T_i proves that in a space away from the walls the reaction is not inhibited any more than in a heated vessel, and that the concentrations of active centers (if we take into account any possible computational and experimental errors) are about the same in both cases. It is obvious that the creation of active centers during the combustion in a heated vessel does not depend on any interaction with the walls. The questions as to the causes of anomalous combustion in chlorine + hydrogen mixtures and the chain-branching mechanism still remain unanswered.

In concluding let us note that the study of combustion under moderate temperatures by means of a comparatively slow adiabatic compression is evidently preferable to the shock-tube method which has acquired wide use after work [1] had already been published and which was connected with several difficulties [9-14]. The method whereby the mixture is heated in a shock wave created in front of a fast-traveling bullet [15] is also free of some of the shortcomings inherent in the shock-tube. By using this method for the study of combustion processes at T = 1300-1600°K and the corresponding induction periods τ of the order of $10^{-5} - 10^{-6}$ sec, we can actually supplement the data from the investigation of adiabatic combustions at moderate temperatures. As an example let us compare the T_c and τ values for oxygen mixtures with H_2 and CS_2 taken from [1] and [15]. Calculations give reasonable values of A = 15 kcal/mole for CS_2 and 20 for H_2; the latter one is fairly close to the value given in [16]; A= 25 kcal/mole. The τ (T_c) function derived in [14] for H_2 also agrees with the A = 20 kcal/mole value, although the absolute values of τ are about 20 times smaller in this case.

LITERATURE CITED

[1] Ya. T. Gershanik, Ya. B. Zel'dovich and A. I. Rozlovskii, J. Phys. Chem. 24, 85 (1950).

[2] A. I. Rozlovskii, J. Phys. Chem. 28, 51 (1954).

[3] A. I. Rozlovskii, J. Phys. Chem. 29, 3 (1955).

[4] A. I. Rozlovskii, J. Phys. Chem. 30, 2489, 2713 (1956).

[5] Yu. N. Ryabinin, J. Exptl. Theor. Phys. 23, 461 (1952).

[6] A. V. Zagulin, J. Phys. Chem. 4, 92 (1933).

[7] D. A. Frank-Kamenetskii, J. Phys. Chem. 13, 738 (1939); 32, 1182 (1958).

[8] O. M. Todes, J. Phys. Chem. 13, 868 (1939).

[9] W. C. Shepherd, III Symp. Combustion, 1949, p. 301.

[10] J. A. Fay, IV Symp. Combustion, 1953, p. 501.

[11] R. Loison and M. Giltaire, Mém. Artill. Franc., 28, 949 (1954).

[12] M. Giltaire, Explosifs, 8, 9 (1955).

[13] J. A. Fay and E. Lekawa, J. Appl. Phys. 27, 261 (1956).

[14] M. Steinberg and W. E. Kaskan, V Symp. Combustion, 1955, p. 664.

[15] Ya. B. Zel'dovich and I. Ya. Shlyapintokh, Proc. Acad. Sci. 65, 871 (1949); I. Ya. Shlyapintokh, Dissertation at the Institute of Chem. Phys. Acad. Sci. USSR, 1949.

[16] V. A. Poltorak and V. V. Voevodskii, J. Phys. Chem. 24, 299 (1950).

Received November 12, 1958

STRUCTURE OF THE LIQUID AuSn ALLOY

A. S. Lashko

Institute of Metal Physics of the Academy of Sciences USSR

(Presented by Academician G. V. Kurdiumov, November 27, 1958)

In studying the structure of liquid alloys it is interesting to know the effects of intermolecular interactions on the nature of closest packing. In papers [1-3] it was shown by x-ray diffraction analysis that in a series of binary metallic alloys of the eutectic concentration (for example Bi−Sn, Bi−Pb, Sn−Pb, Sn−Zn) the relative distribution of atoms at temperatures close to the melting point corresponded to the random closest packing of each component. In these systems, both in the solid as well as liquid state, interaction between like atoms is greater than between unlike ones.

In the present work we investigated the liquid AuSn alloy of a stoichiometric composition (50%), which in the solid state forms an intermetallic compound with a nickel arsenide structure (see Fig. 1). Previously [5] only a qualitative x-ray diffraction study was carried out. In the present work the intensity curves for the liquid AuSn alloy were obtained on the free surface of the sample by using monochromatic K_α radiation from a copper source and a high-temperature vacuum x-ray chamber. The temperature of the sample was kept about 10-15° above its melting point. The scattered x-rays were recorded on an MSTR-4 counter.

A special characteristic of the liquid alloy intensity curves (see Fig. 2) is the presence of two maxima on top of the first peak; the location of these maxima can be denoted by the functions:

$$s_1 = 2{,}79\text{Å}^{-1} \text{and } s_2 = 2{,}40\text{ Å}^{-1}, \text{where } s = \frac{4\pi}{\lambda}\sin\vartheta;$$

λ = wavelength of the x-rays, 2ϑ = scattering angle.

If we assume that there are two types of atomic packing in the liquid alloy, and that the superposition of their intensity distributions results in the observed splitting of the first peak on the curve, then the radii of the principal coordination spheres of these distributions can be calculated from the formula [4],

$$R = \frac{7{,}7}{s_{\max}},$$

i.e.,

$$R_1 = 7{,}7/2{,}79 = 2{,}76\text{ Å and } R_2 = 7{,}7/2{,}40 = 3{,}20\text{ Å}.$$

In the crystalline state the first three coordinations are characterized by the following atomic distribution. The nearest neighbors of a Au atom are 2 Au atoms at a distance of 2.75 A and 6 Sn atoms at a distance of 2.84 A. A Sn atom has 6 neighboring Sn atoms at a distance of 3.71 A. The fact that the coordination sphere radius (R_1 = 2.76 A) calculated from the intensity curve of the liquid alloy, and the radius (r_1 = 2.75 A) calculated from the atomic distribution in the crystal lattice are in good agreement with each other may indicate that the liquid alloy is ordered in a manner similar to that in the crystalline state. The coordination sphere radius R_2 = 3.20 A, calculated from the location

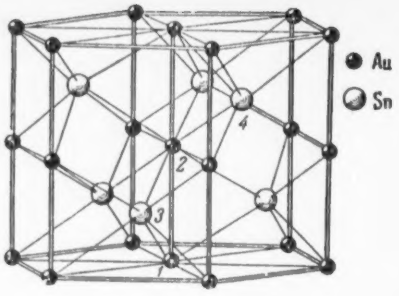

Fig. 1. AuSn lattice.

of the S = 2.40A^{-1} maximum on the intensity curve, is in good agreement with the average coordination-sphere radius for the statistical distribution r_s, provided we use in our calculations the radii of the first three coordination spheres of the crystalline AuSn:

$$r_s = \frac{2{,}75\cdot 2+2{,}84\cdot 6+3{,}71\cdot 6}{14} = 3{,}20\,\text{Å}\,.$$

Thus, alongside the ordered distribution there must also be some randomly distributed atoms in the liquid alloy. The coordination numbers for these distributions can be determined from the atomic distribution curve. The atomic distribution curve was calculated from the following formula [3],

$$4\pi r^2\{n_1K_1^2\rho_1(1)+n_1K_1K_2\rho_2(1)+n_2K_2^2\rho_2(2)+n_2K_2K_1\rho_1(2)\} =$$
$$= 4\pi r^2(n_1K_1+n_2K_2)^2\rho_0+\frac{2r}{\pi}\int_0^{s_0}(i_e-1)\,s\sin sr\,ds;$$

where $i_e - 1 = I_e - \sum n_i f_i^2 \sum n_i f_i^2$; $\rho_j(i)$ is the radial distribution function for the j-th type of atoms with reference to an i-th atom located at the origin:

$$K_i^2 = \left(\frac{f_i^2}{n_1f_1^2+n_2f_2^2}\right)_{\text{av}};$$

ρ_0 = the average atomic density of the sample; n_1, n_2 = atom-fractions; f_1, f_2 = scattering factors for the first and second type of atoms, respectively; I_e = intensity of scattered x-rays in electronic units.

The atomic distribution curve (see Fig. 3) has a nice maximum at 2.95 A. The area under this maximum is 8. The coordination numbers were computed from the following equations:

a) for an ordered distribution

$$\frac{N_1}{N}\{K_1^2Z_1(1)+K_2^2Z_2(2)+2K_1K_2Z_2(1)\} = A;$$

b) for a random statistical distribution,

$$\left(\frac{n_1}{n}\right)^2(K_1+K_2)^2Z = A;$$

$Z_2(2)$ the same for the second type of atoms; $Z_2(1)$ is the number of type-two atoms in the first coordination sphere of type-one atoms; A is the area under the maximum on the atomic distribution curve (Fig. 3); Z is the coordination number.

If we assume that half the Au and Sn atoms are statistically distributed, while the remaining atoms have a closest packing similar to that in crystalline AuSn, then the coordination number for the statistical distribution will be 10. The location of the maximum on the atomic distribution curve can now be taken as the mean between the radii of the coordination spheres in the ordered and statistical distributions.

$$\frac{2{,}76+3{,}20}{2} = 2{,}98\,\text{Å}.$$

This value is in good agreement with the 2.95A value (Fig. 3) from the experimental atomic distribution curve. Other assumptions about the relative weights of the statistical and ordered atomic distributions result in coordination numbers either in excess of 12 or below 10. Therefore we can safely assume that the fraction of atoms statistically distributed in the liquid alloy can only be slightly in excess of one half.

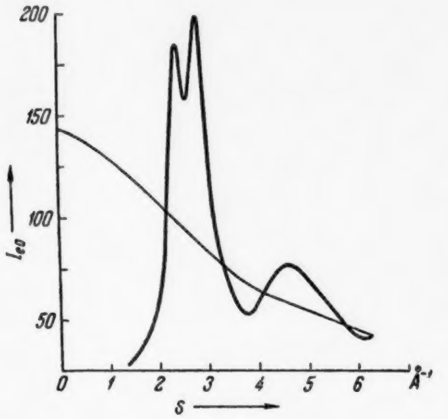

Fig. 3. Atomic distribution function of the AuSn alloy.

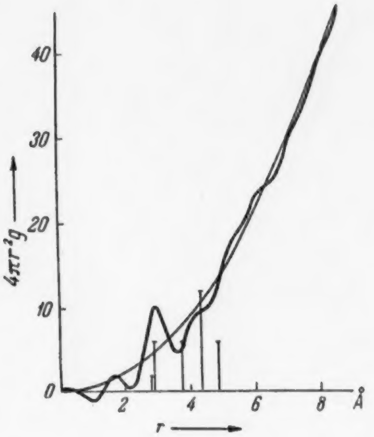

Fig. 2. Intensity distribution curve of liquid AuSn alloy.

From the above-presented data it follows that when AuSn alloy is melted the atoms are not completely randomnized. At any temperature near the melting point,about half the atoms preserve the closest packing of the same type as in the crystalline state. And namely, the first two coordination spheres of Au contain 2 Au atoms and 6 Sn atoms. Besides the ordered atoms about half the atoms in the liquid alloy have random statistical distribution and a coordination number of 10. As the temperature is raised the fraction of randomly distributed atoms increases at the expense of the ordered ones.

LITERATURE CITED

[1] V. I. Danilov and I. V. Radchenko, J. Exptl. Theor. Phys. 7, 1185 (1937).

[2] A. S. Lashko, Dopov AN URSR 1, 30 (1957).*

[3] A. S. Lashko, Problems in the Physics of Metals and Metal Science, Kiev, No. 8, 182 (1957).

[4] G. Voigtlaender-Tetzner, Zs. f. Phys. 150, 215 (1958).

[5] H. Hendus, Zs. Naturforsch. 2a, 505 (1947).

Received November 22, 1958

---

* Probably Proceedings of the Ukrainian Academy of Sciences.

THE THEORY OF THERMAL CHAIN FLAME PROPAGATION WITH TWO ACTIVE CENTERS HAVING DIFFERENT DIFFUSION COEFFICIENTS

L. A. Lovachev

The Institute of Chemical Physics of the Academy of Sciences of the USSR

(Presented by Academician V. N. Kondrat'ev, November 14, 1958)

For a reaction in which A and B are the primary reagents, C is the reaction product, and P_1 and P_2 are active centers, the reaction scheme is assumed to have the form:

$$M + A \rightarrow 2P_1 + M_1, \qquad \Phi = h_R R(T'); \tag{1}$$

$$P_1 + B \rightarrow C + P_2, \qquad Q_1 n_1 = h_1 F_1 n_1 = h_1 K_1 (T') n_B n_1; \tag{2}$$

$$P_2 + A \rightarrow C + P_1, \qquad Q_2 n_2 = h_2 F_2 n_2 = h_2 K_2 (T') n_A n_2; \tag{3}$$

$$P_2 + C \rightarrow B + P_1, \qquad Q_3 n_2 = h_3 F_3 n_2 = h_3 K_3 (T') n_C n_2; \tag{2'}$$

$$P_1 + C \rightarrow A + P_2, \qquad Q_4 n_1 = h_4 F_4 n_1 = h_4 K_4 (T') n_C n_1; \tag{3'}$$

$$2P_1 + M \rightarrow A + M, \qquad X n_1^2 = h_W W (T') n_1^2. \tag{4}$$

The symbolism, the dimensions, and the conditions for the validity of the expressions written on the right for the rates of evolution, or absorption, of heat, are the same as in the earlier article [1] where relations were obtained for determining the velocity of flame propagation in a system having two types of active centers whose diffusion coefficients were identical in value. That problem was solved by reducing it to the solution of a simplified chain reaction scheme with one type of active center [2]. The problem of the present article will be solved by a different method.

With the reaction scheme which has been assumed, and under the conditions which have been imposed, the system of equations for stationary laminar flame propagation will consist of the three members:

$$\lambda p p' - Bcp + Q_1 n_1 + Q_2 n_2 + Q_3 n_2 + Q_4 n_1 + X n_1^2 + \Phi = 0, \tag{5}$$

$$D_1 p^2 n_1'' - p n_1' (B - D_1 p') + F_2 n_2 + F_3 n_2 - F_1 n_1 - F_4 n_1 + R - W n_1^2 = 0, \tag{6}$$

$$D_2 p^2 n_2'' - p n_2' (B - D_2 p') + F_1 n_1 + F_4 n_1 - F_2 n_2 - F_3 n_2 = 0, \tag{7}$$

in which $B = u\rho$; $D_1 = \rho D_{P_1}$; $D_2 = \rho D_{P_2}$; $\underline{u}$ is the flow rate; D_{P_1} and D_{P_2} are the diffusion coefficients of P_1 and P_2; and the notation, dimensions, and conditions for the validity of the equations, and the remaining quantities and functions, are the same as those of [1].

Inclusion in the calculations of the rate of second-power rupture of the chains which proceed through triple collisions considerably complicates the final results without leading to an appreciable alteration in the theoretical value of the rate of flame propagation. For this reason, it will at first be assumed here that $W = 0$. It will then be shown that the earlier-obtained approximation relations can be used to evaluate the rate of flame propagation when allowance is made for the rate of the second-power chain rupture.

Supposing at first that $W = 0$, and working on the basis of (6) and (7), the concentrations of the active centers at $T = T_m$ ($p = p_m$) will, in conformity with [2], be written as:

$$n_{1m} = t_1 + (R_m + G_{2m}n_{2m} - G_{1m}n_{1m} - Bl_1p_m)\,N_1, \tag{8}$$

$$n_{2m} = t_2 + (G_{1m}n_{1m} - G_{2m}n_{2m} - Bl_2p_m)\,N_2, \tag{9}$$

where

$$l_1 = \frac{n_{1\mathrm{r}}^{*} - n_{10}}{T_\mathrm{r}}, \quad l_2 = \frac{n_{2\mathrm{r}} - n_{20}}{T_\mathrm{r}}, \quad N_1 = \frac{r}{2D_{1m}p_m^2}, \quad N_2 = \frac{r}{2D_{2m}p_m^2}, \quad t = n_{10} + l_1T_m,$$
$$t_2 = n_{20} + l_2T_m, \; r = T_m(T_\mathrm{r} - T_m), \; T_m = 0{,}5\,T_\mathrm{r}, \; G_1 = F_1 + F_4 \text{ and } G_2 = F_2 + F_3.$$

Solving (8) and (9), and rearranging, the result is

$$n_{1m} = \{t_1 + (R_m - Bl_1p_m)\,N_1 + [(t_1N_2 + t_2N_1) + (R_m - Blp_m)\;N_1N_2]\,G_{2m}\}\,M_1, \tag{10}$$

$$n_{2m} = \{t_2 - Bl_2p_mN_2 + [(t_1N_2 + t_2N_1) + (R_m - Blp_m)\,N_1N_2]\,G_{1m}\}\,M_1, \tag{11}$$

where $l = l_1 + l_2$ and $M_1 = 1/(1 + G_{1m}N_2)$.

Introducing (10) and (11) into (5) with $T = T_m$ (in which case $p = p_m$ and $p_m' = 0$), and taking into account the earlier-obtained [2] relation $B = \eta p_m = \eta p_*$ with $\eta = 4\lambda_0/cT_m$, an expression is obtained for the determination of p_*

$$A_1p_*^6 + A_2p_*^4 + A_3p_*^2 + A_4 = 0, \tag{12}$$

in which

$$A_1 = 4c\eta D_{1m}D_{2m}, \quad A_2 = 2c\eta r\,(G_{1m}D_{2m} + G_{2m}D_{1m}) + 2\eta r\;(S_{1m}l_1D_{2m} +$$
$$+ S_{2m}l_2D_{1m}) - 4\,D_{1m}D_{2m}(S_{1m}t_1 + S_{2m}t_2) - 4\,D_{1m}D_{2m}\Phi_m, \quad A_3 = \eta lr^2(S_{1m}G_{2m} +$$
$$+ S_{2m}G_{1m}) - 2r\,(t_1D_{1m} + t_2D_{2m})\,(S_{1m}G_{2m} + S_{2m}G_{2m}) - 2r\Phi_m\,(G_{1m}D_{2m} + G_{2m}D_{1m}) -$$
$$- 2r\,(S_{1m}R_mD_{2m}), \quad A_4 = -R_mr^2(S_{1m}G_{2m} + S_{2m}G_{1m}), \quad S_1 = Q_1 + Q_4 = h_1F_1 +$$
$$+ h_4F_4 \text{ и } S_2 = Q_2 + Q_3 = h_2F_2 + h_3F_3.$$

If it is supposed that $R = \Phi = 0$, (12) will lead to

$$A_1p_*^4 = A_2'p_*^2 + A_3' = 0, \tag{13}$$

where A_2' and A_3' are the values of A_2 and A_3 when $R = \Phi = 0$.

The rate of flame propagation is to be found from the relation

$$u_0 = \frac{1}{\rho_0}\,\eta p_*, \tag{14}$$

p_* being determined from (12), or from the approximation equation (13).

A third approximation is obtained from (13) by assuming that $A_1 \cong 0$, and, also, that $A_2' \cong 2c\eta\, r\,(G_{1m}D_{2m} + G_{2m}D_{1m})$:

$$p_*^2 = \frac{(t_1D_{1m} + t_2D_{2m})\,(S_{1m}G_{2m} + S_{2m}G_{1m})}{c\eta\,(G_{1m}D_{2m} + G_{2m}D_{1m})}\left(1 - \frac{2q}{\varkappa}\right), \tag{15}$$

where

$$\frac{2q}{\varkappa} = \frac{2q_1q_2(t_1 + t_2)}{t_1\varkappa_1q_1 + t_2\varkappa_2q_2}, \quad \varkappa_1 = \frac{cD_{10}}{\lambda_0}, \quad \varkappa_2 = \frac{cD_{20}}{\lambda_0}, \quad D_{10} = D_{1m}q_1, \; D_{20} = D_{2m}q_2,$$
$$q_1 = \frac{\mu_0}{\mu_m}\left(\frac{T_0'}{T_m'}\right)^{a_1-1} \text{when } D_{\mathrm{P}_1} \sim (T')^{a_1}, \qquad q_2 = \frac{\mu_0}{\mu_m}\left(\frac{T_0'}{T_m'}\right)^{a_2-1} \text{when } D_{\mathrm{P}_2} \sim (T')^{a_2},$$
$$\eta = 4D_mq\,\frac{1}{\varkappa T_m} \text{ and } D_m = \frac{t_1D_{1m} + t_2D_{2m}}{t_1 + t_2}.$$

---

* Γ designates combustion — Translator's note.

Substituting the expression for p_* from (15) into (14), and taking the symbolism of (8) and (9) into account, an approximation relation is obtained for the determination of the rate of flame propagation at $T_m = 0.5\, T_r$

$$u_0 = \varphi\xi\psi \frac{1}{\rho_0} \sqrt{\frac{n_r Q_m \rho_m D_{pm}}{2cT_r}}\,, \tag{16}$$

where

$$\varphi = 2\sqrt{\frac{2q}{\varkappa}\left(1 - \frac{2q}{\varkappa}\right)}\,, \tag{17}$$

$$n_r^* = (n_{1r} + n_{2r}) \frac{(n_{1r} D_{1m} + n_{2r} D_{2m})}{(n_{1r} + n_{2r})} \frac{(G_{1m} + G_{2m})}{(G_{1m} D_{2m} + G_{2m} D_{1m})}\,, \tag{18}$$

$$Q_m = \frac{S_{1m} G_{2m} + S_{2m} G_{1m}}{G_{1m} + G_{2m}}\,, \tag{19}$$

$$D_{pm} = \frac{n_{1r} D_{p_1 m} + n_{2r} D_{p_2 m}}{n_{1r} + n_{2r}}\,, \tag{20}$$

and the coefficients ξ and ψ (accounting for the effect of the rate of initiation, and for the second-power chain rupture, respectively) are to be evaluated according to [1] from the relations

$$\xi = \sqrt{\frac{1}{2}\left(1 + \sqrt{1 + \frac{16\, q\varkappa c T_r R_m}{(\varkappa - 2q)^2 n_r^2 Q_m}}\right)}\,, \tag{21}$$

$$\psi = \left[1 + \frac{qcT_r W_m}{\varkappa Q_m}\right]^{-1/2} \tag{22}$$

Supposing the concentration distributions of the active centers to be determined, as in [2], by the values of the quantities at $T = T_m$, the temperature dependence of the concentrations of these centers will be fixed through (10) and (11) by:

$$n_1(T) = \frac{(4\, D_{1m} D_{2m} p_m^4 l_1)\, T + [G_{2m} A_n + 2\, D_{2m} p_m^2 (R_m - \eta l_1 p_m^2)]\, T\, (T_r - T)}{4\, D_{1m} D_{2m} p_m^4 + 2 p_m^2 (G_{1m} D_{2m} + G_{2m} D_{1m})\, T\, (T_r - T)}\,, \tag{23}$$

$$n_2(T) = \frac{(4\, D_{1m} D_{2m} p_m^4 l_2)\, T + [G_{1m} A_n - 2\, D_{1m} \eta l_2 p_m^4]\, T\, (T_r - T)}{4\, D_{1m} D_{2m} p_m^4 + 2\, p_m^2 (G_{1m} D_{2m} + G_{2m} D_{1m})\, T\, (T_r - T)}\,, \tag{24}$$

where $A_n = 2\, p_m^2\, (l_1 D_{1m} + l_2 D_{2m})T + (R_m - \eta l\, p_m^2)\, T\, (T_r - T)$, and $p_m = p_*$ is to be found, either from (12), or the approximation equation (13).

For two instances of hydrogen-chlorine flames, (16) was used to calculate those theoretical values of the rate of flame propagation which, together with the corresponding experimental values from [3], are presented in Table 1. Rate constants for the chemical reactions as determined by kinetic methods independent of the flame were taken from [4]: $K_1 = 10^{13.9}\ \rho^2 \times \exp(-5500/RT')$, $K_2 = K_2'\ \rho^2 \exp(-2500/RT')$, $K_3 = 10^{13.4}\ \rho^2 \exp(-5200/RT^1)$. It was assumed that: $K_4 = 0$, $h_1 = -2 \cdot 10^3$, $h_2 = 4.6 \cdot 10^4$, $h_3 = 2 \cdot 10^3$. Diffusion coefficients and the thermal conductivity of each mixture were obtained from [5]: $(Dp_1)_0 = 0.19$ (atomic Cl), $(Dp_2)_0 = 1.04$ (atomic H), $\lambda_0 = 8.6 \cdot 10^{-5}$. Table 2 presents the results obtained from thermodynamic calculations (μ is the molecular weight of the mixture).

In estimating the highest possible values of the rate constants for processes (1) and (4) it was specified that $\xi = 1.00$ and $\psi = 1.00$. In view of the uncertainty in the value of the multiplying factor in the rate expression for process (3), calculations were carried out for two different values of this quantity (see Table 1).

TABLE 1

Experimental and Theoretical Values of the Rates of Flame Propagation (cm / sec) for Hydrogen-Chlorine Mixtures

Taken from	Composition of combustion mixture	
	$0.6H_2 + 0.4Cl_2$	$0.5H_2 + 0.5Cl_2$
Experimental of Bartolomé [3]	405	350
According to (16), with $K_2^0 = 10^{13.7}$	347	368
According to (16), with $K_2^0 = 10^{13.4}$	252	278

From a comparison of the theoretical values of the flame propagation rates as calculated from a relation analogous to (16) and the results obtained from a numerical integration of the initial system of equations, as presented in [2], and from the concordance between the experimental and theoretical values given in Table 1, the conclusion can be drawn that a theoretical study of a system having a reaction scheme similar to that which was presented in detail at the beginning of this paper will lead to a correct description of the actual propagation of such a flame.

The results which have been obtained (Table 1) confirm the possibility of the determination of the true constants and energies of activation of the elementary processes from experimentally determined relations between the rate of flame propagation and the combustion temperature; such a possibility was considered in [1] on the basis of a relation of the type of (16). For this purpose, use might also be made of the relation between the rate of flame propagation and the pressure. A more exact treatment of the experimental data can be had through (14) with the use of Equation (12), or (13).

TABLE 2

Data for the Thermodynamic Calculation

Composition of combustion mixture	T', °K	$n_B(H_2)$	$n_A(Cl_2)$	$n_C(HCl)$	$n_1(Cl)$	$n_2(H)$	μ, g/mole	c, cal/g·deg
		moles/g of mixture						
$0{,}5H_2 + 0{,}5Cl_2$	$T'_0 = 293$	$1{,}37 \cdot 10^{-2}$	$1{,}37 \cdot 10^{-2}$	0	0	0	36,5	0,208
	$T'_m = 1389$	$7{,}36 \cdot 10^{-3}$	$6{,}85 \cdot 10^{-3}$	$1{,}26 \cdot 10^{-2}$	—	—	35,8	0,225
	$T'_r = 2485$	$1{,}01 \cdot 10^{-3}$	$1{,}65 \cdot 10^{-5}$	$2{,}51 \cdot 10^{-2}$	$2{,}25 \cdot 10^{-3}$	$1{,}26 \cdot 10^{-4}$	35,1	0,241
$0{,}6H_2 + 0{,}4Cl_2$	$T'_0 = 293$	$2{,}03 \cdot 10^{-2}$	$1{,}35 \cdot 10^{-2}$	0	0	0	29,6	0,258
	$T'_m = 1337$	$1{,}36 \cdot 10^{-2}$	$6{,}75 \cdot 10^{-3}$	$1{,}32 \cdot 10^{-2}$	—	—	29,5	0,275
	$T'_r = 2380$	$6{,}97 \cdot 10^{-3}$	$1{,}67 \cdot 10^{-6}$	$2{,}64 \cdot 10^{-2}$	$6{,}08 \cdot 10^{-4}$	$2{,}23 \cdot 10^{-4}$	29,3	0,293

The relation between the rate of flame propagation, the temperature of combustion, and the pressure is principally determined by the alteration in the concentration of the leading type of active center [1] with temperature and pressure. Relation (16) makes possible a quantiative evaluation of the leading role of one of the two types of active center when the coefficients of diffusion are different.

Relation (16) permits the calculation of the variation of the rate of flame propagation under a simultaneous alteration in the coefficients of diffusion of the active centers and the thermal conductivity of mixture.

LITERATURE CITED

[1] L. A. Lovachev, Proc. Acad. Sci. USSR, 124, No. 6 (1959).*

[2] L. A. Lovachev, Proc. Acad. Sci. USSR, 120, No. 6, 1287 (1958).*

[3] E. Bartolomé, Zs. f. Elektrochem., 54, No. 3, 169 (1950).

[4] A. F. Trotman-Dickenson, Gas Kinetics, London, 1955, p. 182.

[5] K. Hellwig and R. C. Anderson, J. Am. Chem. Soc. 77, 232 (1955).

Received November 11, 1958

---

* Original Russian pagination. See C. B. Translation.

THE FORMATION OF HEXACHLOROETHANE BY γ-IRRADIATION OF CARBON TETRACHLORIDE

B. I. Losev, M. A. Troyanskaya and É. A. Bylyna

The Institute of Mineral Fuels of the Academy of Sciences of the USSR

(Presented by Academician A. V. Topchiev November 25, 1958)

Investigation has been made of the carbon chlorination product which is obtained from the γ-irradiation of fossil coals in carbon tetrachloride [1-3]. The experimental conditions were such that the coal was given a preliminary drying, pulverized, and screened through a 0.25 sieve. A weighed specimen of the coal of about 5 g was put into a glass ampule with a sixfold excess of CCl_4, and the ampule sealed in air. The source of the γ-radiation was Co^{60} at a source strength of 21000g-eq. of radium in the installation of the L. Ya. Karpov Physico-Chemical Institute [4]. Irradiation was carried out at dose rates of $3.5 \cdot 10^6$, and $1.15 \cdot 10^6$, r/hour. In every case, the integral dosage was 10^8 r.

After irradiation, the coal was separated from the CCl_4 and subjected to further investigation. The carbon tetrachloride, which had acquired a dark reddish-brown coloration after irradiation with the coal, was fractionally distilled. Fractions were taken at 76.5-78°, 78-80° and 80-90°, to leave a thick tarry residue from which a white crystalline substance with a sharp odor could be sublimed with further elevation of the temperature. This same white crystalline substance separated from the fractions after evaporation of the CCl_4. Solubility determinations showed this material to be completely insoluble in water and readily soluble in acetone, benzene, and carbon tetrachloride. After purification of the separated substance by a second sublimation, the melting point proved to be 183.5-184° and the molecular weight, 236.76 (M = 236.76).

Found %: C 10.21; Cl 89.60; H 0.0. C_2Cl_6. Calculated %: C 10.14; Cl 89.86; H 0.0.

From the elementary composition and melting point of this substance, and its ability to sublime, there was reason to believe that the compound was hexachloroethane.

For each 30 g of carbon tetrachloride which were taken in a single experiment at the fixed integral dose of 10^8 r, 0.46-0.6 g of hexachlorethane were obtained after irradiation, regardless of the dose rate ($3.5 \cdot 10^6$ or $1.15 \cdot 10^6$ r/hour). The variation in the amount of separated hexachloroethane was to be explained by loss due to sublimation of the compound during evaporation of the solvent.

As determined from the mean of the data of several experiments, the yield of the hexachlorethane was 1000 molecules per 100 ev.

In order to elucidate the role in the formation of the hexachloroethane which was played by the coal, or by the decomposition products of the latter which were present in the irradiated system, irradiation of a coal free of carbon tetrachloride was carried out under the same conditions and at the same integral dosage of 10^8 r. After irradiation, the CCl_4 was evaporated and a white crystalline substance which was identified as hexachloroethane was separated from the residue by sublimation. In this case, too, the yield of hexachloroethane was 1000 molecules per 100 ev.

Indication of the formation of hexachloroethane during radiolysis of CCl_4 has recently appeared in the literature [5, 6]. The formation of hexachloroethane from CCl_4 in ultraviolet light is also known to take place [7]. These papers do not contain data on the yield of hexachloroethane, either because the authors had not set themselves the task of separating this substance, or because other types of radiation were employed [8] and the dosage was less than that of the present work. The work of A. V. Zimin and Z. S. Egorova on carbon tetrachloride [5] has shown that the yield of radiolysis products is affected by the type of radiation and the dosage. Thus, the yield of free chlorine from CCl_4 under γ-irradiation is 2.5 times greater than that for radiation with α-particles at the same integral dosage.

These authors have represented the formation of radiolysis products from CCl_4 by the following scheme [5]:

$$CCl_4 \rightsquigarrow CCl_3^{\bullet} + Cl^{\bullet},$$

$$CCl_4 + Cl^{\bullet} \rightarrow CCl_3^{\bullet} + Cl_2,$$

$$2CCl_3^{\bullet} \rightarrow C_2Cl_6.$$

The authors of [5] considered that although hexachloroethane might be formed in the radiolysis of CCl_4, its amount was probably small and it was, for this reason, not separated. The high yield of hexachloroethane in the present case points to a chain reaction and can be interpreted, to a certain degree, by the addition of reaction (3) to the scheme proposed by A. V. Zimin and Z. E. Egorova.

$$CCl_4 \rightsquigarrow CCl_3^{\bullet} + Cl^{\bullet}, \quad (1)$$

$$CCl_4 + Cl^{\bullet} \rightarrow CCl_3^{\bullet} + Cl_2, \quad (2)$$

$$CCl_4 + CCl_3^{\bullet} \rightarrow C_2Cl_6 + Cl^{-}, \quad (3)$$

$$2CCl_3^{\bullet} \rightarrow C_2Cl_6. \quad (4)$$

In conclusion, we count it our duty to express our appreciation to A. Kh. Breger for his continual attention and for his aid in carrying out this work.

LITERATURE CITED

[1] B. I. Losev, F. Ya. Saprykin, et al., Herald Acad. Sci. USSR, No. 10 (1958).

[2] B. I. Losev, M. A. Troyanskaya and É. A. Bylyna, Proc. Acad Sci. USSR, 120, No. 2 (1958).*

[3] É. A. Bylyna, B. I. Losev and M. A. Troyanskaya, Bull. Acad. Sci. USSR, Div. Chem. Sci., No. 4 (1958).*

[4] Isotopes and Radiation in Chemistry (in Russian), Acad. Sci. USSR, Press, 1958.

[5] A. V. Zimin and Z. S. Egorova, Collected Papers on Radiation Chemistry (in Russian), Acad. Sci. USSR, Press, 1955.

[6] E. Bourne, Chem. and Ind., No. 46, 1372 (1956).

[7] K. Peordte, J. prakt. Chem. 5, No. 3/4, 196 (1957).

[8] W. Mund, et al., Bull. classe sci. Acad. Roy. Belg, 41, No. 9, 929 (1955).

Received November 25, 1958

---

* Original Russian pagination. See C. B. Translation.

DESIGN OF A NEW CELL FOR THE MEASUREMENT OF PRESSURES OF SATURATED METAL VAPORS

Yu. N. Lyubitov and V. M. Polyanskii

The A. A. Baikov Institute of Metallurgy

(Presented by Academician I. P. Bardin, October 1, 1958)

There is a continual demand from modern technology for the development of new alloys with the most diversified of properties. A knowledge of the thermodynamic characteristics of metals and alloys can be of great help in the solution of this problem. One basis for the determination of these characteristics is to be found in the measurement of the pressure of the vapors above metals and alloys.

Two methods are available for determining vapor pressures in the range from 10^{-2} to 10^{-8} mm: 1) that of Langmuir, in which measurement is made of the rate of sublimation (or vaporization from an open surface, and 2) that of Knudsen, which is based on the measurement of the rate of effusion of the vapors through an orifice in a special cell. With m designating the mass of metal condensing on unit surface area of an acceptor in unit time, M, the molecular weight of the particles constituting the vapor, R , the molar gas constant and T, the absolute temperature, the pressure, p, of the vapors can be calculated from the equations:

in the Knudsen method

$$p = m\sqrt{\frac{2\pi RT}{M}}; \tag{1}$$

in the Langmuir method

$$p = \frac{m}{\alpha}\sqrt{\frac{2\pi RT}{M}}. \tag{2}$$

The α of Equation (2) is the accommodation coefficient of the surface. For most metals, $\alpha = 1$ [1], but data indicating that α can reach a value of 0.2 is to be found in the literature [2].

In determining the vapor pressure, it is necessary to know either the area of the effusional orifice (Knudsen cell), or the area and the composition of the surface of evaporation (Langmuir "cell"). Due to the requirement that the experimental parameters, and especially the area of the effusional orifice, or the area of the surface of evaporation, be held constant in experiments of long duration (several hours), errors in the measured values of the vapor pressure reach ten percent or more. In the Langmuir method, it is necessary to have α, a quantity whose value is not known with exactness.

The Knudsen method permits a unique determination of the vapor pressure even when $\alpha = 1$. Thus, let h be the area of the effusional orifice, ν, the number of particles impinging per unit time on unit interior surface of a Knudsen cell with an effusional orifice, ν', the number of particles impinging in unit time on unit interior surface of this cell without the orifice, α, the accommodation coefficient of the cell surface and S, the area of this surface.

Then

$$\nu h = \nu'\alpha S - \nu\alpha S \tag{3}$$

or

$$\nu = \frac{\nu'\alpha}{h/S + \alpha}. \tag{4}$$

Multiplication of each number of Equation (4) by $m^* \sqrt{2\pi RT/M}$, (m^* is the mass of the vapor particle, in grams) leads to

$$p = p'\frac{\alpha}{h/S + \alpha}. \tag{5}$$

When $h/S \ll \alpha$, or $p \cong p'$.

The Knudsen method cannot, however, replace the Langmuir method when measurement is to be made of the vapor pressures of metals which evaporate with difficulty.

We have made the attempt to design a cell for the vaporization of metals which would be free of the defects of the Langmuir and the Knudsen cells, and would at the same time retain their desirable features. We have set up an analogy between the laws of vaporization and the thermal radiation, and have made use of the mathematical apparatus which was applied by O. N. Talenskii for the design of a cylindrical model of the ideal black body [3].

A number of assumptions are required for establishing this analogy. The most important among these are that the thermal radiation be characterized by the Lambert Law, and the vaporization, by the analogous Cosine Law of Knudsen. At pressures of 10^{-2}– 10^{-8} mm, the mean free paths are so long that there is scarcely any interaction between the vapor particles and they are, in this sense, similar to photons.

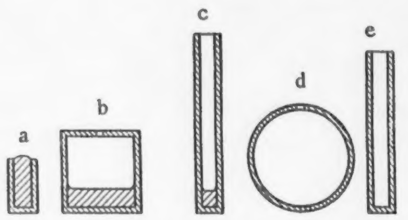

Fig. 1.

Let us turn to the diagram in which schematic representation is given of the Langmuir "cell" (Fig. 1,a), the Knudsen cell (Fig. 1,b), the cell which is to be discussed (Fig. 1,c), a "black body" model in the form of a spherical cavity (Fig. 1,d) and a "black body" model in the form of a cylindrical cavity (Fig. 1,e), which is a "black body" for a definite value of the ratio L/D [3].

The Langmuir Cell. Particles of the vapor phase which impinge on the metal surface can either remain there or be reflected and undergo condensation on an acceptor which is at a lower temperature than this surface. The vapor particle has possibility of a single-step approach to the surface. This cell is similar to a "gray body", in the sense of thermal radiation.

The Knudsen Cell. The surface of the vaporizing metal and the walls of the cell are at the same temperature. Every vapor particle impinging on the metal surface and undergoing reflection will be reflected (with a definite probability) from the walls, and will again impinge on the metal surface. The vapor particle has the possibility of repeated approach to the vaporizing surface. The Knudsen cell is similar to a "ideal black body". The escape of vapors through the effusional orifice does not essentially disturb the equilibrium.

A correspondence will now be established between the characteristics of radiation and those of vaporization. Under the conditions enunciated above, the pressure of the vapor is equal to one third of its energy per unit volume (only the kinetic energy of the particle, being taken into account) and the integral radiation density $\theta = \sigma T^4$ correspond to this vapor pressure.

Every radiating body is characterized by its coefficient of blackness, ϵ, which is equal to the ratio between the emissivity of the given body and the emissivity of a "black body"; when the latter is taken as unity,

$$1 - \varepsilon = \rho \tag{6}$$

is the reflection coefficient. Vaporization is characterized by the condensation coefficient, η, the number of particles condensing on unit surface in unit time; by the vaporization constant, μ, which is similarly defined; and by the accommodation coefficient,

$$\alpha = \eta/\nu, \tag{7}$$

ν being the same as in Equation (3).

At equilibrium:

with $\alpha = 1$

$$\nu = \eta = \mu; \tag{8}$$

with $\alpha \neq 1$

$$\eta = \mu \quad \nu = \mu + \gamma. \tag{9}$$

Setting $\nu = 1$, and taking (7) into account, gives

$$\alpha = \eta = \mu. \tag{10}$$

Thus α corresponds to ϵ, and

$$1 - \alpha = \gamma \tag{11}$$

corresponds to the reflection coefficient, ρ.

The accommodation coefficient was introduced by Knudsen [2] in order to account for processes of energy exchange between the solid walls and the impinging particles. The mechanism which he proposed for this interchange was similar to that for the interaction between thermal radiation and matter, while his "completely rough body" is the analog of the "ideal black body" of optics.

In the cell which is under consideration, the vapors interact with the specimen surface and with the cell walls. It will be supposed that this interaction between the vapor particles and the walls is limited to physical adsorption; this could be the situation in the case of walls of certain materials which have the complex structures of molecular crystals.

After a definite interval of time, equilibrium is established between the vapors and the film which is adsorbed on the walls. Within the cell, the vapors are characterized by the following equations:

$$\nu_M = \mu_M + \gamma_M, \tag{12}$$

$$\nu_W = \mu_W + \gamma_W \tag{13}$$

where the index M designates the metal and W, the walls, It is clear that $\nu_M = \nu_W$, $\mu_M \geq \mu_W$, $\gamma_M \leq \gamma_W$.

We will now determine the ratio of cell parameters under which vapors contained in the cell will be in equilibrium, i.e., for which our cell will correspond to the "ideal black body", just as does the Knudsen cell. Replacing the radiation characteristic in the formula for the design of a "black body" having the form of a cylindrical cavity [3] by the vaporization characteristic, an expression is obtained for the flux of particles leaving the cell (in relative units):

$$W(l) = 1 - \frac{\gamma_M e^{-(1+\alpha_W)l}}{1 + e^{-l} - e^{-\alpha_W l}} \tag{14}$$

and for the pressure of vapors at the open end of the cell:

$$p(l) = \left[1 - \frac{\gamma_M e^{-(1+\alpha_W)l}}{1 + e^{-l} - e^{-\alpha_W l}}\right] m \sqrt{\frac{2\pi RT}{M}}. \tag{15}$$

Here l is the ratio of the length of the cylinder to its diameter and m is the mass of material escaping through unit area of the outlet in unit time. When $l \to 0$ and (11) is taken into account, the result is

$$p(l) = \alpha_M m \sqrt{\frac{2\pi RT}{M}}. \qquad (16)$$

Equation (16) is formally different from (2), in which the left-hand member is $p = p(\infty)$. On the other hand, Equation (15) goes over into (1) for sufficiently large values of l (see Table 1).

Thus, (15) is a generalization of the equations of Langmuir and Knudsen. Table 1 contains the results of calculations of the cell parameters for various values of α_M and α_W; it is clear that the cell under consideration is similar to the Knudsen cell when $l \geq 6$.

TABLE 1

Values of $p(l)/p(\infty)$ for Various Values of α_M, α_W, and l · $p(l)$ is the Pressure Measured at the Cell Outlet, and $p(\infty)$, the Equilibrium Vapor Pressure

	l							
	0,5	1	2	3	4	5	6	7
$\alpha_M = 0{,}9$; $\alpha_W = 0{,}87$	0,961	0,985	0,998	0,999	0,9999	—	—	—
$\alpha_M = 0{,}8$; $\alpha_W = 0{,}1$	0,823	0,884	0,931	0,976	0,993	0,998	0,999	0,9998
$\alpha_M = 0{,}8$; $\alpha_W = 0{,}5$	—	0,941	0,992	0,997	0,999	0,9998	0,9999	—
$\alpha_M = 0{,}5$; $\alpha_W = 0{,}2$	0,61	0,725	0,902	0,974	0,998	0,999	0,9998	0,9999

Since the vaporous particles are only physically adsorbed on the cell walls (there is no chemical adsorption), and the wall temperature and the temperature of the metal are the same, there is no essential variation in the magnitude of the orifice with time, a condition which is not fulfilled in the Knudsen cell.

The cell which is under discussion can be looked upon as a container which is completely filled with the saturated vapors. Each section perpendicular to the cell axis is at equilibrium in regard to vaporization. Thus, the form of the meniscus of the metal in the cell is without significance, since any distorted surface at the bottom can be replaced by a plane section perpendicular to the cylindrical axis of the cell. In the Langmuir "cell", the form of the vaporization surface is of importance to the calculation of the vapor pressure. In the proposed cell, interest attaches only to the area of the outlet. Such a cell is very suitable for the measurement of the temperature with a pyrometer, since it is a "ideal black body" for $l > 5$ [3].

LITERATURE CITED

[1] J. Langmuir, Phys. Rev., 2, 239 (1923).

[2] M. Knudsen, Ann. d. Phys. 34, 593 (1911).

[3] O. N. Talenskii, A Photometric Method for Measuring the Emissivity of Molten Metals (in Russian), Dissertation, Moscow, 1953.

This article photostated 8/2/60 (W

THE EFFECT OF IONIZING RADIATION ON THE ELECTROCHEMICAL ACTIVITY OF METALS COVERED WITH SEMICONDUCTING OXIDE FILMS

I. L. Rozenfel'd and E. K. Oshe

(Presented by Academician A. N. Frumkin November 27, 1958)

The semiconducting character of the oxides has been known to the physicist for a considerable time. Nevertheless, up to the present, semiconduction in oxide films has not received its due attention in the electrochemistry and corrosion of metals where such films are known to play a very important role. Because of the specific nature of the semiconduction, the electrophysical parameters of these films can vary over the widest of limits as the result of various external effects (the introduction of alloying substances, the adsorption of different materials, irradiation, the alteration of temperature, etc.) which frequently seem to be quite insignificant. This can have a profound influence on the electrochemical and corrosional processes, as has been shown by ourselves, and by other investigators [1, 2].

In the present work, investigation was made of the effect of electronic irradiation (E = 0.1 Mev, I = 10 μ amp/cm^2) on the electrochemical behavior of a number of metals over a wide interval of polarization current densities. The attempt was also made to utilize electronic bombardment for developing differences in the electrochemical activity which is shown in cathodic and anodic reactions by metals carrying semiconducting surface oxide films which differ in conduction mechanisms (electronic or hole).

For investigation there were selected zirconium and titanium, which have oxide films showing electronic conduction mechanisms (n-type films), and nickel and chromium, which have oxide films showing hole conduction mechanisms (p-type films) [3, 4]. Investigation was carried out in distilled water, in 3% NaCl and in 0.1 N NaOH. The cathodic process was the reduction of oxygen, or ionic hydrogen; chemical analysis showed the anodic process to be the electrochemical oxidation of the metal.

It was found that electron bombardment lowered the overvoltages for the cathodic and the anodic processes, and increased their velocities. This is a reversible effect as we have shown earlier [2]; on breaking off irradiation, the overvoltage and the rates of both the anodic and the cathodic processes returned to almost exactly their initial values.* In its general form, these statements are applicable to all of the investigated metals, both those with n- and those with p- type films, and to all of the experimental electrolytes.

It was also found that there was a marked distinction in the behavior under irradiation of metal with n-type and metals with p-type films in regard to the anodic reaction. A similar distinction was not observed in regard to the cathodic reaction.

The results which were obtained are illustrated in Fig. 1, where polarization curves are given for zirconium, and nickel, in a 0.1 N NaOH solution, under irradiation (Curves 1, 2), and in the absence of irradiation (Curves 3, 4). It is to be seen from the figure that the irradiation of cathodically polarized zirconium (n-type film), and cathodically and anodically polarized nickel (p-type film) led to a considerable acceleration of the electrode reaction over the entire range of polarizations, the relative acceleration being greatest at the lower current densities. In irradiation of anodically polarized zirconium, the reaction acceleration was not pronounced and was not observed over the entire range of polarizations; at low current densities the relative acceleration was quite insignificant. With increasing current density, the acceleration passed through a maximum.

---

*No consideration will be given here to those irreversible effects which arise during irradiation and are related to the initiation and progress of the structural breakdown of the oxide film. Such effects were insignificant in this work.

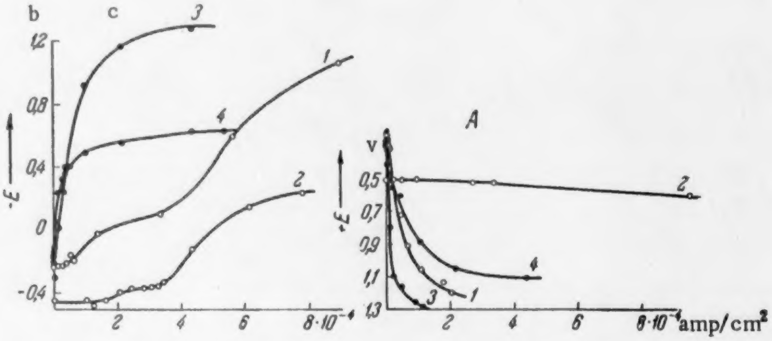

Fig. 1. Polarization curves for Zr (1 and 3) (n-type film), and for Ni (2 and 4) (p-type film), in a 0.1 N NaOH solution; 1, 2) under irradiation; 3, 4) without irradiation. C – cathodic polarization; A – anodic polarization.

The qualitative difference in the anodic behavior under irradiation of metals with p-type and metals with n-type films can be more clearly followed in curves showing the relation between the relative current effect under irradiation, i/i_0, and the density of the polarization current, i_0, as obtained with zirconium, titanium, nickel and chromium (Fig. 2).

The relative magnitude of this effect under irradiation is dependent on the type of electrolyte, being fixed by the nature and the extent of the interaction between the electrolyte and the oxide film on the metal. In Table 1 there are presented mean values of the relative current effect as obtained from several experiments on the irradiation of aluminum (n-type film) which was cathodically polarized in various electrolytes (i_0 interval, 1-3 μamp/cm²)

TABLE 1

Electrolyte	i/i_0
Distilled water	6.7
3% NaCl	5.9
0.1 N NaOH	1.0

In order to explain the experimental results it must be supposed that the principal factor limiting the rate of the electrode reaction is the low concentration of the current carriers (electrons and holes) in semiconducting films which the metal carries. Under the experimental conditions this assumption is justified for all the given metals and electrolytes with the exception of aluminum in 0.1 n NaOH solution.

Electronic irradiation with absorption resulted in a marked increase in the conductivity of the semiconducting oxide layer as a consequence of the ionization of the atoms (ions) in the lattice of the semiconductor. In other words, electronic irradiation increased the number of electrons and holes which were capable of participating in electrode reactions. On the basis of the above assumption that the rate of electrode reaction is limited by the concentration of the current carriers, the electrons or the holes, irradiation, by bringing about an increase in the carrier concentration, must lead to an increase in the rate of the electrode reaction with a corresponding alteration in the electrode potential, i.e., the result must be that which was, in general, observed experimentally. This conclusion finds partial confirmation in the fact that this same effect can be brought about by the illumination of the film with light which is photoelectrically active [1].

The cathodic reaction proceeds on the surface of the semiconductor with the consumption of the electrons. In the terminology of semiconduction, this reaction can be designated as an acceptor with respect to the semiconductor. The number of electrons is significant for the progress of the cathodic reaction and the mechanism by which these electrons reach the surface is a matter of indifference; they can be drawn from the conduction zone, or from the valence zone. This indifference of the cathodic reaction to the mechanism of semiconduction can be used to explain the observed absence of a qualitative difference in the cathodic behavior under irradiation of metal with n-type and metals with p-type films.*

According to our assumption, anodic reaction proceeds on the surface of a semiconductor with the consumption of holes.** It can be referred to as a donor reaction with respect to the semiconductor. The number of holes capable of participating in the reaction is significant for its progress. In other words, the rate of anodic reaction on a semiconductor is limited, at each instant, by the number of free energy levels (holes) in the surface into which the electrons of the oxidizing component can be transferred.

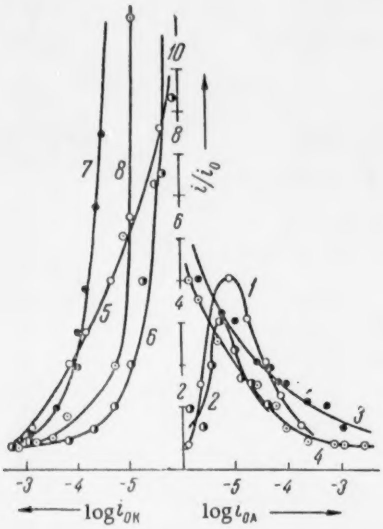

Fig. 2. Curves showing the relation between the relative current effect under irradiation and the direction and magnitude of the polarization current; 1,5) Zr; 2, 6) Ti (n-type film); 3,7) Ni; 4, 8) Cr (p-type film).

Starting from such concepts, the observed difference in the anodic behavior of metals with p-type, and metals with n-type, films can be explained in the following manner. In the majority of cases, the oxide semiconductors retain their inherent type of conduction under irradiation, even when carrier excitation occurs in the valence zone with the formation of electron-hole pairs. Experiment has shown that this is so because of attachment of the secondary carriers to subsidiary local levels which are formed by impurities, or defects, in the semiconductor [4, 5]. Thus, under irradiation of an anodically polarized metal with an n-type film, this localization of the secondary carriers, the holes, must oppose the acceleration of the anodic oxidation reaction, since exactly these holes are required for maintaining the reaction. This can be experimentally observed in the irradiation of anodically polarized zirconium, or titanium, at low polarization current densities (Fig. 1,A, Curve 1, and Fig. 2, Curves 1, 2). The observed increase in the relative effect with increasing current density is clearly the result of a stripping of the holes from the local levels by the increasing electrical field, the energy of activation for this process being less than that for natural conduction. Naturally, localization of the secondary carriers, the electrons, can not prevent an acceleration of the reaction in the irradiation of anodically polarized metals with p-type films. This is confirmed experimentally in the irradiation of anodically polarized nickel and chromium (Fig. 1, A, Curve 2 and Fig. 2, Curves 3, 4).

An experiment shows, the relative effect of irradiation in accelerating the electrode reaction diminishes with an increase in the density of the polarization current, since this latter serves as a background for the action of irradiation. Thus increase in the polarization current density in irradiation of an anodically polarized metal with an n-type film leads, on the one hand, to an increase in the relative effect due to the stripping of the secondary carriers from the local levels by the increasing electrical field, and results, on the other hand, in a decrease in this effect as a result of the rise in the background current. This accounts for the appearance of a maximum on Curves 1, 2 (Fig. 2) at that value of the polarization current density under which the relative effects of these two factors become equal. It is the second factor alone which acts from the very outset in the irradiation of an anodically polarized metal with a p-type film, or a cathodically polarized metal with n-, or p- type film. This is the explanation of the steady diminution of the relative effect which is observed in these cases as the density of the polarization current rises (Fig. 2, Curves 3, 4, 5, 6, 7, 8).

The results which are presented in Table 1 can be explained in a simple fashion by taking account of the fact that the oxide film on aluminum is maintained in distilled water, and in 3% NaCl solution, and that such film is lacking in a 0.1 N NaOH solution.

---

*From this, the conclusion should not, however, be drawn that there is no quantitative difference between the course of anodic reactions on metals with n-type, and on metals with p-type, films.

**This does not apply to anodic reactions of ionization of metal atoms, since, in this case, the process does not involve the passage of electrons through the semiconducting layer.

Finally, it can be concluded that in order for the existing concepts of the role and properties of protective films to be applicable to metals with dense protective films of the semiconducting type, it is clearly necessary to take into account the fundamental electrochemical properties of the semiconducting layer. These properties can be accounted for by a factor which characterizes the position of the Fermi level relative to the energy zones of the semiconductor and gives the most general reflection of the latter's electrophysical characteristics.

We consider it a pleasant duty to express our thanks to P. Ya. Glazunov, and to the group directed by him, for their aid in carrying out these experiments.

LITERATURE CITED

[1] V. I. Veselovskii, J. Phys. Chem. 22, vol. 12 (1948); K. Shwabe, Zs. f. Phys. Chem. 205,5 (1956).

[2] L. L. Rozenfel'd and E. K. Oshe, Proc. Acad. Sci. USSR, 114, No. 1 (1957).*

[3] M. Mallet, W. Albrecht and R. Bennett, J. Electrochem. Soc., 104, 6 (1957).

[4] G. Busch, Zs. Angew. Math. u. Phys. 1, 3 (1950).

[5] A. F. Ioffe, The Physics of Semiconductors (in Russian), Acad. Sci. USSR, Press, 1957; Semiconductors in Science and Technology (in Russian) 1, Chapter 1, Acad. Sci. USSR, Press, 1957.

Received November 27, 1958

---

* Original Russian pagination. See C. B. Translation.

This article photostated 5/2/60

QUANTUM MECHANICAL EFFECTS AND THE TEMPERATURE DEPENDENCE OF THE RATE OF THE ELECTROLYTIC EVOLUTION OF HYDROGEN AND DEUTERIUM

St. G. Khristov

The Department of Physical and Electrochemistry of the Chemicotechnological Institute
Sofia, Bulgaria

(Presented by Academician P. A. Rebinder December 4, 1958)

The author's preceding papers [1] have given a quantum-mechanical treatment of the theory of overvoltage, which was based on the supposition that the step of delayed discharge is realized, at least in part, by a tunnel transfer of ions through a potential barrier in the dense section of the double layer. The calculations presented by the author [1] have shown that this supposition is very probably justified in the case of the cathodic evolution of hydrogen and deuterium. It is also in agreement with the results of a theoretical evaluation of the factor multiplying the exponential in the classical expression for the rate of discharge of the hydrogen ion, for which the value obtained by Temkin [2] ($K_H^{cl} = 1 \cdot 10^5$ amp/cm^2) exceeds the experimentally determined values by factors of 5–50. The role of the tunnel effect in these processes has been experimentally confirmed by the measurements of Post and Hiskey [3], who give for the discharge of the deuterium ion on mercury a value of the multiplying factor ($K_D = 2 \cdot 10^4$ amp/cm^2) which is twice as great as that for the hydrogen ion ($K_H = 10^4$ amp/cm^2). It would seem to be impossible to explain this last on the basis of the classical ideas; actually, exactly the inverse relation would be expected in view of the fact that the vibrational frequency of hydrated deuterium is less than that of the hydrated proton by a factor of $1/\sqrt{2}$. But according to quantum mechanics, the tunnel effect must lead to a diminution, not only of the energy of activation, but of the multiplying factor as well [4]. It is clear that this diminution would be the greater, the smaller the mass of the particle (proton), and the results of the measurements of K_H and K_D by Post and Hiskey are thus to be explained [2].

Temkin considers that the slight discrepancy between the calculated, and the experimentally determined, values of K_H merely indicates that the tunnel effect plays a small role in the discharge of H_3O^+, if it is not entirely outside the limits of precision of the measurements and calculations. In order to clear up this matter, however, there is need for a more detailed quantum-mechanical investigation of the temperature dependence of the reaction rate, $v = f(T)$. Alterations in the form, and the dimensions, of the potential barrier have a great effect on this relation, as the author has shown for the cases of the retangular barrier and the Eckart barrier. In both cases, it proves to be so that the function $\log v = \varphi(1/T)$ is practically linear in the region of ordinary temperatures (0-100°).* As might be anticipated, the activation energy generally increases with increasing height and breadth of the barrier. But for the narrow Eckart barrier, alteration of the height over very wide limits leads to only an insignificant alteration in the activation energy. In this case, the multiplying factor diminishes with increasing height of the barrier; only for barriers which are sufficiently wide does this factor increase with the height.

These conclusions open the possibility of an indirect approach to the quantitative evaluation of the role of the tunnel effect in the discharge of H_3O^+ and D_3O^+, based on a study of the temperature dependence of the current density through an Eckart barrier, as compared to the direct approach, which presupposes a knowledge of the exact form and dimensions of the actual barrier. All that is known for certain is that the width of the actual barrier is no greater than that of the double layer, $d \simeq 1.5 \cdot 10^{-8}$ cm, and that its height is no less than would correspond to the experimentally determined energy of activation, E', as obtained from the relation

---

*This result is not in agreement with the calculations of Bell [4], which were carried out for an Eckart barrier $1 \cdot 10^{-12}$ erg high and 2 Å wide, and this is true, not only for this one particular case, but for other barrier dimensions, as well.

$$E'(\eta) \equiv -k\left(\frac{\partial \ln i}{\partial (1/T)}\right)_{\eta} = E_0' - \alpha\varepsilon\eta, \quad 0 < \alpha < 1, \tag{1}$$

in which i is the current density, ahd η is the overvoltage. According to the most precise experimental data [3], $E'_{0,H} = 1.50 \cdot 10^{-12}$ erg (21.7 kcal/mole) and $E'_{0,D} = 1.56 \cdot 10^{-12}$ ergs (22.5 kcal/mole) for the respective discharges of H_3O^+ and D_3O^+ on a mercury cathode in a 0.1 N HCl solution with an overvoltage $\eta = 0$.

For simplicity, use can be made of the symmetric Eckart barrier * which is described through the function

$$V(x) = 4E_0 \frac{e^{2\pi x/l}}{(1 + e^{2\pi x/l})^2}, \tag{2}$$

in which E_0 is the barrier height, and $\delta = 2(l)$ is the width of the base. The transmission coefficient of this barrier is given by the expression [5]

$$W(U) = \frac{\operatorname{ch} \frac{2\pi\delta}{h}\sqrt{2mU} - 1}{\operatorname{ch} \frac{2\pi\delta}{h}\sqrt{2mU} + \operatorname{ch} \pi\sqrt{8m\delta^2 E_0/h^2 - 1}}, \tag{3}$$

in which U is the energy of the particle, m is its mass and the condition is imposed that $8m\delta^2 E_0/h^2 > 1$.

Provisionally supposing that $K_H^{cl} = 1$, the current density can be calculated from the equation

$$i = \frac{K^{cl}}{kT}\int_0^\infty W(U)\,e^{-U/kT}\,dU \tag{4}$$

by numerical integration.

In order to decide to what extent the real barrier can be approximated by an Eckart barrier, calculation was first made of the activation energy of the proton, $E'_{0,H}$ for a number of values of and E_0.** The resulting values prove to be considerably less than those determined experimentally, and this is not only true for the mercury cathode, but for other metals as well. The highest value for $E'_{0,H}$ is $\sim 3.5 \cdot 10^{-13}$ erg (5 kcal/mole) which corresponds to $\delta = 1.5$ Å; and to barrier heights, E_0, ranging from $1 \cdot 10^{-12}$ to $8 \cdot 10^{-12}$ erg. In connection with this, there is a diminution of the multiplying factor, K_H*** with increasing barrier height, E_0, the value being considerably less than K_H^{cl}. From this it follows that the Eckart potential cannot be employed as an approximation expression for the barrier in the case of the discharge of H_3O^+ on the mercury cathode. It can, nonetheless, be used in indirectly fixing the role of the tunnel effect in this process. For this purpose it is necessary to select those values for E_0 and for $l = \delta/2$, which will yield the experimentally determined $E'_{0,H}$ and K_H; the actual barrier can then be replaced by such an Eckart barrier over the temperature interval which is under consideration (0-100°).

TABLE 1

$E_0 \cdot 10^{12}$, erg	$i = \delta/2$, Å	K_H^{cl}/K_H
1.80	1.75	80
1.70	1.90	10
1.60	2.20	6

---

*Similar results are obtained if use is made of an unsymmetrical Eckart barrier [5].

**On the basis of two values of the current density, i, at T equal to 273 and 373°.

***Calculated by graphic extrapolation of the linear relation $\log i = \varphi(1/T) = -E'_0/kT + \ln K$ to intersection with the axis of ordinates (log i).

The determination of the parameters of this equivalent barrier can be carried out by a graphical interpolation based on a study of the relation between E'_0 and K, to E_0 and = $2(l)$. By increasing δ at a fixed value of E_0 ($> 1.56 \cdot 10^{-12}$ erg !), the experimental value of $E'_{0,H}$ can be reached; by varying E_0 it is possible to attain the experimental value of K_H.

For the purposes of orientation, Table 1 gives for three values of E_0, those values of δ for which E'_0 is equal to $1.48 \cdot 10^{-12}$ erg (21.3 kcal/mole), the approximate value of $E'_{0,H}$. At such high values of δ, the data show K_H to diminish with diminishing E_0 to reach values which correspond to the result found by Temkin for the ratio K_H^{cl}/K_H.

For a more detailed investigation, selection was made of a barrier height of $1.6 \cdot 10^{-12}$ erg (23 kcal/mole), for which the tunnel effect should be comparatively small. The relation between the width of this barrier and the energy of activation is represented in Fig. 1 from which it follows that the experimental $E'_{0,H}$ is reached at values δ = 4.4 – 4.8.[*]. Results calculated for three values of δ taken out of this interval are shown in Table 2.[**] For these same parameter values, calculations were carried out for the discharge of D_3O^+ (Table 3), substitution of $K_D^{cl} = K_H^{cl}/\sqrt{2}$ being made in (4). The resulting values of $E'_{0,D}$ and K_D/K_H show good agreement with the experimental [3]. Table 4 indicates that the same is true of the values of the coefficient of separation of H and Ds = = $(i_H/i_D)\ \eta, T, \underline{c}$ which, according to the data of a number of authors [3, 6, 7], is approximately 3 for mercury (at T = 298°). These results show that an Eckart barrier, $1.6 \cdot 10^{-12}$ erg in height and 4.6-4.8 Å in width, can undoubtedly be considered as completely equivalent to the actual barrier for the discharge of H_3O^+ and D_3O^+ at $\eta = 0$, even though this width is approximately 3 times greater than the depth of the double layer.[***]

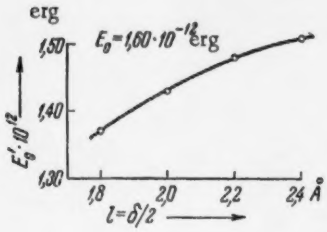

Fig. 1. The relation between the energy of activation and the barrier width at $E_0 = 1.6 \cdot 10^{-12}$ erg.

TABLE 2

The Discharge of $H_3O^+ \cdot E_0 = 1.6 \cdot 10^{-12}$ erg

$l = \delta/2$, Å	$T = 273°$, $i^{cl} = 3{,}71 \cdot 10^{-19}$			$T = 373°$, $i^{cl} = 3{,}21 \cdot 10^{-14}$			$E'_{0H} \cdot 10^{12}$, erg	K_H^{cl}/K_H[**]
	$i = i' + i''$[*]	i'/i	i''/i^{cl}	$i = i' + i''$	i'/i	i''/i^{cl}		
2,2	$1{,}43 \cdot 10^{-18}$	0,86	0,52	$5{,}20 \cdot 10^{-14}$	0,60	0,65	1,48	6,0
2,3	$1{,}18 \cdot 10^{-18}$	0,80	0,64	$4{,}88 \cdot 10^{-14}$	0,55	0,67	1,50	4,5
2,4	$9{,}86 \cdot 10^{-19}$	0,77	0,66	$4{,}57 \cdot 10^{-14}$	0,53	0,67	1,51	3,6

[*] "Tunnel current" $i' = \frac{1}{kT}\int_0^{E_0} W(U)e^{-U/kT}dU$, "quasi-classical current" $i'' = \frac{1}{kT}\int_{E_0}^{\infty} W(U)e^{-U/kT}dU$. [**] Accuracy of calculations, approximately 5%.

The data of Tables 2 and 3 show that the role of the quantum-mechanical effects of leakage through the barrier and reflection above the barrier are very considerable; all of the particles actually show nonclassical behavior, since they fall in the region of energies $1.2 - 1.8 \cdot 10^{-12}$ erg in which $W(U) < 1$.[****] In the case of H^+ the density of the "tunnel current", i', is approximately 55% of the total current density, i, at T = 373°, and 80%, at T = 273°; for D^+ the corresponding values are 30, and 50%.*

---

[*] According to the graph, the value $E'_0 = 1.5 \cdot 10^{-12}$ erg corresponds to δ = 4.6 Å.

[**] The accuracy of the calculation of the current density, $\underline{i}$, from Equation (4) is approximately 1%.

[***] With $E_0 > 1.6 \cdot 10^{-12}$ erg and the corresponding values of δ, the divergence between the calculated, and the experimental values of $E'_{0,D}$, K_D, K_H, and $\underline{s}$ for the mercury cathode become greater, due to the fact that K_H^{cl} K_H takes on larger values (> 5). For example, with $E_0 = 1.7 \cdot 10^{-12}$ erg and δ = 3.8 Å, the result is K_H^{cl} $K_H = 10$ (Table 1), so that $E'_{0,D} = 1.65 \cdot 10^{-12}$ erg (23.8 kcal, mole), K_D $K_H = 4.5$ and $s = 8$ (T = 273°). The value K_H^{cl} $K_H \simeq 4$ (Table 2) should be considered as the best; with $K_H = 1 \cdot 10^4$ amp/cm² [3], this gives $K_H^{cl} = 4 \cdot 10^4$, which is in good agreement with the calculations of Temkin [2].

[****] $W(U)$ reaches a value of ≃ 1 when $U \simeq 1.8 \cdot 10^{-12}$ erg (for H and D). The integrated function in Equation (4) has a maximum at $U = 1.55 - 1.60 \cdot 10^{-12}$ erg for H, and at $U = 1.60 - 1.63 \cdot 10^{-12}$ erg for D (this maximum is displaced by alteration of the temperature).

TABLE 3

The Discharge of $D_3O^+ \cdot E_0 = 1.6 \cdot 10^{-12}$ erg

$l = \delta/2$, Å	$T = 273°$, $i^{cl} = 2,62 \cdot 10^{-10}$			$T = 373°$, $i^{кл} = 2,27 \cdot 10^{-14}$			$E'_{0,D} \cdot 10^{12}$, erg	κ_D/κ_H *
	$i = i' + i''$	i'/i	i''/i^{cl}	$i = i' + i''$	i'/i	i''/i^{cl}		
2,2	$3,62 \cdot 10^{-10}$	0,55	0,62	$2,45 \cdot 10^{-14}$	0,35	0,64	1,56	3,0
2,3	$3,19 \cdot 10^{-10}$	0,49	0,63	$2,33 \cdot 10^{-14}$	0,31	0,70	1,57	2,4
2,4	$3,12 \cdot 10^{-10}$	0,46	0,63	$2,28 \cdot 10^{-14}$	0,30	0,70	1,57	1,9

*Accuracy of calculation, approximately 5%.

The difference in the null-point vibrational energies $U_H^0 - U_D^0$ is practically without influence on the value of i in Equation (4), a displacement of the lower limit of the integral from $U_D^0 = 0$ to $U_H^0 = 1.08 \cdot 10^{-13}$ erg scarcely altering its value.

TABLE 4

$E_0 = 1.6 \cdot 10^{-12}$ erg

$l = \delta/2$ Å	$s = i_H/i_D$		
	T = 273°	T = 298°	T = 373°
2.2	4.0	3.3	2.1
2.3	3.7	3.2	2.1
2.4	3.1	2.7	2.0

For the real barrier, it can be considered that the role of tunnel effect would be no less, and is possibly even greater, than that for the equivalent Eckart barrier;** the difference in the null-point energies of H^+ and D^+ is the undoubtedly small significance, regardless of the smaller base width.

LITERATURE CITED

[1] St. G. Khristov, Ann. Univ. Sofia, Fac. Phys.-Math., 42, 2, 69 (1945-1946); 42, 2, 63 (1946-1947); C. R. Acad. Bulg. Sci., 1, 43 (1948); Zs. Elektrochem., 62, 567 (1958).

[2] M. I. Temkin, Proc. Conference on Electrochemistry, Moscow, 1953 p. 181.***

[3] B. Post and C. F. Hiskey, J. Am. Chem. Soc., 72, 4203 (1950); 73, 161 (1951).

[4] R. P. Bell, Proc. Roy. Soc., A, 139, 466 (1933).

---

* It is interesting to note that $i_D \simeq i_D^{cl}$ at T = 373°, so that the effects of leakage and reflection (above the barrier) compensate one another almost completely; $i'/i + i''/i^{cl} = 1$.

** If, for all values of the energy, the "tunnel length is less for the real barrier then it is for the equivalent Eckart barrier, then the height must be greater than $1.6 \cdot 10^{-12}$ erg in order to obtain the same value of the current density; if the height of the two barriers are approximately the same, i.e., if $E_0 \simeq 1.6 \cdot 10^{-12}$ erg (the height must be greater than $1.56 \cdot 10^{-12}$ erg!), then, since the "tunnel length" in the lower portions of the real barrier is less than in the case of the Eckart barrier, it will be greater in the upper portions and the maximum in the integrated function of Equation (4) will correspond to lower values of the energy. And in both cases, the relative contribution of the tunnel effect, i.e., the value i'/i, will be less for the real barrier than for the equivalent Eckart barrier.

*** In Russian.

[5] C. Eckart, Phys. Rev. 35, 1303 (1903).

[6] J. Horiuti and G. Okamoto, Sci. Papers Inst. Phys. Chem. Res. Tokyo, 28, 231 (1936); cited from A. I. Brodskii, The Chemistry of Isotopes (in Russian), Moscow, 1957.

[7] A. Eucken and K. Bratzler, Zs. phys. Chem., (A), 174, 273 (1936).

Received September 10, 1958

THE EFFECT OF NEGATIVE GROUPS ON THE ELECTROCHEMICAL REDUCTION OF THE CARBON – HALOGEN BOND IN ORGANIC COMPOUNDS

THE POLAROGRAPHIC BEHAVIOR OF THE HALOGENATED NITROALKANES

S. G. Mairanovskii, A. A. Fainzil'berg, S. S. Novikov and
V. A. Klimova

The N. D. Zelinskii Institute of Organic Chemistry of the Academy of Sciences of the USSR

(Presented by Academician A. N. Frumkin, November 10, 1958)

The introduction of electronegative groups into the α-position with respect to a carbon atom which is bound with a halogen atom favors the electrochemical reduction of the C – Hal bond, a fact which finds expression in the displacement of the half-wave potential for the polarographic reduction of this bond in the direction of lower cathodic potentials. Thus, in passing from CH_3Br, to CH_2Br_2, $CHBr_3$ and, finally to CBr_4, the half-wave potentials corresponding to the reduction of the first C – Br bond are displaced from −1.6 to −1.44, −0.6 and, finally, to −0.26 v, respectively [1]. The magnitude of the displacement toward positive potentials resulting from the introduction of oxygen-containing groups into the α-position with respect to the C – Br bond increases in the sequence CHOH < CHO < COOH [2].

In the present work investigation has been made of the effect of nitro groups, in the α-position, on the ease of electrochemical reduction of the carbon – halogen bond. Although the nitro group is itself very readily reduced polarographically, experiment proves that its presence so far favors electrochemical rupture of the C – Hal bond that the wave corresponding to the reduction of the latter appears before that for the reduction of the nitro group.

This work was carried out on the recording polarograph of the TsLA Energochermet [3]. In order to obtain curves in which distortion due to the inertia of the recording system was at a minimum, polarograms were developed under a retarded rate of polarization without damping. To avoid those oscillations in the recording system which arise from the growth and fall of the mercury droplets, use was made of a capillary from which the drop was broken off by a hoe [4]. The characteristics of this capillary were: m = 3.93 mg/sec, t = 0.18 sec, and $m^{2/3} t^{1/6} = 1.906 \text{ mg}^{2/3} \text{ sec}^{-1/2}$. In order to have the possibility of obtaining polarograms at potentials more positive than that of the saturated calomel electrode, a buffer solution containing 0.1 N K_2SO_4 and 0.1 N H_2SO_4 was employed as the background. Ethyl alcohol (20% by volume) was added to increase the solubility of the test materials in this buffer solution. The anode was a saturated K_2SO_4 – mercury sulfate electrode. The potential of this electrode was more positive than the saturated calomel electrode by 0.4 v. The solutions were freed from dissolved oxygen by being aerated with nitrogen. The operational sequence was as follows: into the cell there was poured a definite volume of the background solution, and a curve developed for this, after removal of the oxygen. Then, using a calibrated pipette, a solution of the test substance in this same buffer mixture was introduced into the cell, aerated, and its polarogram developed on the same diagram as the earlier curve for the background. Then the capillary of the auxiliary saturated calomel electrode with its sulfate bridge was put into the cell, and after manually setting the slide wire on points corresponding to the vertical portion of the polarogram, values of the potential of the dropping electrode were determined potentiometrically for this portion of the wave. The resulting data were employed for the construction of a graph show-

---

* Central Laboratory of Automation – Publisher's note.

ing the relation between the scale setting of the slide wire (or the abscissa of the diagram) and the potential of the dropping electrode relative to the saturated calomel electrode. This relation was graphed for each wave separately, thus eliminating errors which might arise from slippage of the diagram tape, from lack of agreement of the potentials at the beginning of the readings, and from the ohmic potential drop in the cell. In the case of substances such as iodonitroform, which rapidly hydrolyze in aqueous solution, a definite quantity of the freshly prepared solution was rapidly introduced into the cell and the polarogram immediately developed. Because of the fall in the wave height with time, potentiometric control of the potentials of the separate points on the waves of such substances could not be carried out. For these substances, the value of $E_{1/2}$ relative to the sulfate electrode were directly recalculated to the saturated calomel electrode (a correction of + 0.40 v).

A comparison of the polarograms of the halogenated nitrocompounds with the waves for similar nitrc products which do not contain halogens shows the first wave of the former to correspond to the reduction of the C − Hal bond. Further proof of this statement is to be found in the fact that the $E_{1/2}$ value of the first wave is independent of the pH of the solution, which is characteristic of the wave for the rupture of the carbon − halogen bond. The second wave corresponds to the reduction of the nitro group and is displaced toward negative potentials with an increase in the pH of the solution. From the fact that the reduction of the nitrocompounds in acidic solution proceeds to the corresponding hydroxylamines and involves four electrons while the height of the second wave of the halogenated mononitroalkane is twice that of the first wave, it follows that the wave for the rupture of the C − Hal bond is associated with two electrons, just as is the case for the reduction of other halogenated derivatives.

The experimental data on the reduction of the C − Hal bonds in the investigated substances are presented in Table 1. Subsequent waves are those for the reduction of the nitro group, and their characteristics are not presented here.

TABLE 1

Characteristics of the Wave for the Reduction of the Carbon − Halogen Bond in the Halogenated Nitroalkanes

Formula of substance	$E_{1/2}$, v (with respect to sat. cal. elec.)	$\alpha' n_a$	Formula of substance	$E_{1/2}$, v (with respect to sat. cal. elec.)	$\alpha' n_a$
CH_2ClNO_2	−0,52	0,52	$C_2H_5CBr(NO_2)_2$	+0,25	0,78
CH_2BrNO_2	+0,06	0,61	$(NO_2)_3CCl$	+0,24	0,74
$CH_3CCl(NO_2)_2$	−0,03	1,20	$(NO_2)_3CBr$	+0,36	0,52
$CH_3CBr(NO_2)_2$	+0,28	0,65	$(NO_2)_3CI$	+0,42	0,54
$C_2H_5CCl(NO_2)_2$	−0,03	1,26			

It should be noted that the potential of the half-wave is only an approximation criterion for the ease of the reduction in the case of such irreversible processes as the reduction of the carbon − halogen bond. In actuality, the $E_{1/2}$ value of an irreversible wave is not only affected by the rate of rupture of the bond, but also by the electrode characteristics [5, 6], by the adsorbability of the initial, and the product, substances on the electrode surface and by the value of αn_a, the product of the transfer coefficient and the number of electrons participating in the potential-determining step [7]. With compounds of a single type, the difference between the energies of adsorption of the initial materials and of the products obtained from them can be considered as almost constant, so that, when the electrode characteristics and the experimental conditions are held fixed, and the effect of variation of αn_a on the value of $E_{1/2}$ is neglected, conclusions as to the ease of reduction of a bond in a substance representive of this same type of compound can be based on $E_{1/2}$, as has been indicated above.

From a comparison of the data of Table 1 with the values of the half-wave potentials of the alkyl halides (for example, for CH_3Br and C_2H_5Br, $E_{1/2} \approx 1.6$ v [1]) it is seen that the presence of the nitro group in the α-position considerably favors the reduction of the carbon − halogen bond and that this effect increases with the number of nitro groups. Thus, in passing in the series of bromides from bromnitromethane to bromtrinitromethane there is a displacement of the half-wave potential from + 0.06 to + 0.36, i.e., an alteration of 0.30 v. A similar situation is to be observed in the series of the chlorides, although here the difference between the first and the last member of the series reaches an even higher value (0.76 v).

As is to be anticipated, the bromides are more easily reduced than are the corresponding chlorides. This can be followed with special clarity in the mononitro compounds. Thus, the difference in the half-wave potentials is 0.58 v for chlor- and bromnitromethane, and 0.31 v for chlor- and bromnitroethane. The difference between the half-wave potentials for the chlorides and the bromides increases with the number of nitro groups, this being due to the continually increasing ease in the reduction of the chlorides under the action of the nitro group.

Among the iodides, only iodotrinitromethane was investigated. This compound possesses the most positive half-wave potential of all the substances which were studied in the present work.

In Table 1 there are also given values of $\alpha' n_a$ as obtained from the slopes of logarithmic plots of the waves of the investigated substances. These values differ (insignificantly, to be sure) from the true values of αn_a which are obtained with quiescent (not dropping) electrodes [8, 9].

It is very interesting that there is an alteration in these quantities over a series of substances in which there is an obvious change in the polarity of the C – Hal Bond. Thus the value of $\alpha' n_a$ increases twofold in passing from the chlorides of the mononitro compounds to the chlorides of the dinitro compounds and then again diminishes on passing to the derivatives of trinitromethane. This can be explained by the fact that the C – Cl bond becomes less polar in the chlorides of the nitroalkanes as a result of the high electronegativity of the NO_2 group, so that two electrons, and not one, participate in the potential-determining step, just as in the case with the halides of the alkanes [6, 10]. In the case of chlorotrinitroethane, the trinitromethyl group is clearly more electronegative than chlorine, so that here n_a is once more equal to unity.

In a series of the bromo derivatives, it is likely that the nitroalkyl group becomes more negative than the bromine even in the mono derivative, and thus $n_a = 1$ for all of the bromoderivatives which were investigated in this work.

The influence of the structure of a substance of the αn_a value for its wave will be the object of further investigation.

LITERATURE CITED

[1] M. Stackelberg and W. Strake, Zs. Elektrochem. 53, 347 (1949).

[2] P. Kirrman, E. Saito, and P. Federlin, J. Chim. Phys. 49, C 154 (1952).

[3] S. B. Tsfasman, Zav. Lab., 22, 131 (1956).

[4] E. M. Skobets and N. S. Kavetskii, Zav. Lab. 15, 1299 (1949).

[5] É. S. Levin and Z. Fondiman, J. Phys. Chem. 28, 601 (1954).

[6] N. Hush, Zs. Elektrochem. 71, 734 (1957).

[7] P. Delahay, New Apparatus and Methods in Electrochemistry (in Russian), Foreign Lit. Press, 1957, p. 103.

[8] V. S. Bagotskii, J. Phys. Chem. 22, 1466 (1948).

[9] S. G. Maironovskii, J. Phys. Chem. 32, No. 10 (1958).

[10] P. Elring, J. Markowitz, and J. Rosenthal, J. Electrochem. Soc., 101, 195 (1954).

Received November 10, 1958

THE SELECTIVE PENETRATION OF DISSOLVED ELEMENTS FROM A LIQUID PHASE INTO A CRACK

B. A. Movchan and I. Ya. Dzykovich

The E. O. Paton Institute of Electric Welding of the Academy of Sciences of the USSR

(Presented by Academician A. A. Bochvar, December 7, 1958)

The basic rules applying to the formation of "hot" cracks in alloys have been established in a number of investigations and the possibility of the "filling up" of these cracks with mother liquid enriched in the dissolved elements has been pointed out ([1, 2], etc.).

The results of visual observation of the filling up of cracks have been presented in other works [3], and instances of the movement of the enriched mother liquid along capillary canals in the hardened part of the pig to form, in the final analysis, a number of defects, have been cited [4-6].

It has been established by one of the present authors that the concentration of the dissolved elements in the capillaries can be in considerable excess of the centration in the body of the liquid phase, and that this is true when equilibrium exists between the liquid and the solid phases, as well as in the irreversible processes of solidification [7].

The present work has carried out with a view to determinating the concentration of the enriched lquid which penetrates into a crack that has been formed at the interface between the phases.

Experiments were carried out on aluminum – copper, and on aluminum – zinc alloys, which had been prepared from pure components (99.995%). The experimental scheme is sketched in Fig. 1. The test alloys were melted in the alundum crucible, 35 mm in diameter, which was held in a constant temperature bath. The temperature was set 5-10° higher than that corresponding to the solidus. A specimen of pure aluminum 4 × 6 mm in cross section, was so placed above the crucible that one of its sides was in contact with the molten alloy. The oxide film was removed from the contacting surface of this specimen, and complete wetting of the specimen by the molten alloy achieved, by a special curved lancet whch was immersed in the alloy. The specimen was bent with the aid of a punch, and a series of fissures appeared in it. In order to facilitate the appearance of these fissures, several transverse scratches had previously been made on the specimen surface. Following this, a stream of water was directed into the crucible and the alloy was solidified. The experiments were of no more than one-minute duration.

From the composite specimens, polished sections were prepared for metallographic investigation, and plates, for micro x-ray analysis.

Use was made of the method of qualitative and quantitative micro x-ray analysis in absorption [8]. In essence, quantitative micro x-ray analysis involves the simultaneous exposure of a finely grained film of the investigated specimen (the plate) and a comparison standard. Subsequent photometry of the micro x-ray diagram permits a determination of the chemical composition of the microsection in question. The accuracy of this method of quantitative micro x-ray analysis is ± 10-15% of the measured quantities.

The micro x-ray analysis of the test specimens showed that the content of zinc, or copper, in a crack was considerably in excess of the mean content of the element in the corresponding alloy.

A micro x-ray diagram of a specimen with a crack, obtained under irradiation from iron (x-ray tube with iron anode), is presented in Fig. 2.

Results from the quantitative micro x-ray analysis are presented in Table 1. (In the final column there are given the minimum and the maximum concentrations of copper, or zinc, as obtained from the analysis of 5 specimens.)

TABLE 1

Alloy	Mean content of Cu or Zn in alloy, wt. %	Content of Cu or Zn in crack wt. %
Al–Cu	2.9	27–30
	7.8	29–33
	26.0	26–27
Al–Zn	4.9	25–27
	15.0	42–44

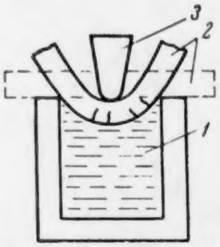

Fig. 1. 1) Molten alloy, 2) aluminum specimen, 3) punch.

It follows from Table 1 that the copper content of cracks which were in contact with molten aluminum – copper alloys containing 2.9 or 7.8% copper was approximately the same as that of the eutectic.

This is in good agreement with the results of metallographic analysis. The alloy which fills the crack has the eutectic structure (Fig. 3).

It should be noted that the tendency to surface cracking diminishes with an increase in the copper, or zinc, content of the respective alloy.

Thus, it is very difficult to induce surface cracking in a specimen which is in contact with an aluminum – copper alloy containing 26% copper. Such a specimen can be bent by almost 180°. Cracking can be obtained only by means of a deep, sharp scoring.

The selective penetration of the dissolved elements into a crack can be explained as the result of an attempt to establish equilibrium between the phases.

By comparing the concentration of the components in the filled cracks with the possible liquid-phase compositions as read from the phase diagrams for aluminum – copper, or aluminum – zinc, [9], the conclusion can be drawn that the content of copper or zinc in the cracks is, to within the limits of experimental error, that corresponding to the liquidus curves of these diagrams.

A departure of the concentrations from the equilibrium values was observed with one aluminum – copper alloy (2.9% copper), and with the aluminum -- zinc alloys, and was persistently repeated in successive runnings of the experiments; this can be explained as resulting from an imperfect knowledge of the true position of the liquidus curves for these alloys, or from peculiarities of concentrations in narrow capillary canals [7].

Fig. 2. Micro x-ray diagram of a specimen having a crack which had been brought into contact with a liquid aluminum-copper alloy (2.9% copper). 120 ×.

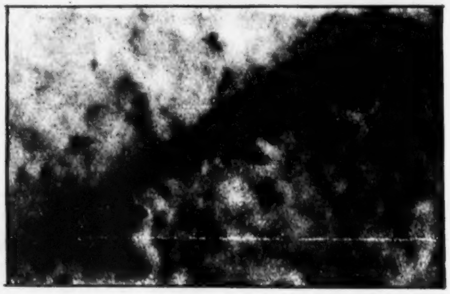

Fig. 3. Micro x-ray diagram of a specimen having a crack which had been brought into contact with a liquid aluminum-copper alloy (2.9% copper). 1400 ×.

LITERATURE CITED

[1] A. A. Bochvar and Z. A. Sviderskaya, Bull, Acad. Sci. USSR, Div. Chem. Sci., No. 3 (1947).

[2] A. A. Bochvar and I. I Novikov, Bull. Acad. Sci. USSR, Div. Chem. Sci., No. 2 (1952).*

[3] K. T. Matveeva and I. I. Novikov, Bull. Acad. Sci. USSR, Div. Chem. Sci., No. 5 (1957).*

[4] Yu. A. Nekhendzi, Steel Casting (in Russian), 1948.

[5] V. M. Tagaev, Monog. The Steel Ingot (in Russian), 1952.

[6] A. A. Ryzhikhov, The Theoretical Basis for Casting Practice (in Russian), 1954.

[7] B. A. Movchan, Bull. Acad. Sci. USSR, Div. Chem. Sci., No. 4 (1958).*

[8] B. A. Movchan, Zav. Lab., No. 7 (1956).

[9] Metals Handbook, Am. Soc. Met., 1948.

Received December 2, 1958

---

* Original Russian pagination. See C. B. Translation.

THE ASYMMETRY IN THE DISTRIBUTION OF THE COORDINATION NUMBERS OF THE MOLECULES OF WATER

V. K. Prokhorenko, O. Ya. Samoilov and I. Z. Fisher

The N. S. Kurnakov Institute of General and Inorganic Chemistry of the Academy of Sciences of the USSR. The V. I. Lenin Belorussian State University

(Presented by Academician I. I. Chernyaev, December 10, 1958).

A study of the coordination numbers of liquid particles leads to the problem of establishing a probability distribution function, w(z), for the coordination numbers, $z (z = 1, 2, \ldots)$, in a given liquid. If it is supposed that this distribution is Gaussian, or something sufficiently close to Gaussian, a knowledge of $\overline{z}$, and $\overline{(\Delta z)^2}$ is then sufficient for the construction of w(z). These two quantities can be evaluated for any liquid for which the pertinent x-ray data are available,as has been shown in [1, 2]. It proves to be so that $\overline{(\Delta z)^2}$ is always relatively large.

It is to be expected, however, that the actual distribution, w(z), would not be as symmetrical as the Gaussian. This fact could prove to be essential for an understanding of liquid microstructures. It can be supposed that fluctuations in the direction of diminishing coordination numbers will predominate in those liquids which are comparatively densely packed, whereas fluctuation in the direction of increasing coordination numbers will predominate in liquids in which the density of packing is low.

Especial interest attaches to the case of water, which has one of the most "open" of structures. At the present time, it is reasonably well established that the basic ice structure is maintained in water, at least in the sense of local ordering [3]. As a result, the tetrahedral lattice with its four coordination of the molecules acquires a particular stability in water; according to x-ray data, the mean coordination number only changes from 4.4 to 4.9 on raising the temperature from 1.5 to 83° [4]. The molecular distribution characteristic of ice is such that the structure contains many voids whose dimensions exceed those of the molecules. It is clear that the water molecules cannot fail to fall into the neighboring structural voids as a result of their thermal motion.* Energetically, the molecules which do fall into these voids are not equivalent to the molecules which are located at the lattice points, since they are to a higher degree free of the hydrogen bonding of the adjacent water molecules [3, 6]. On the other hand, account should be taken of that concept of the flexibility of the hydrogen bonds in water which has been introduced by Pople [7]. According to this author, contraction can occur without rupturing these hydrogen bonds. The idea of the partial filling of the voids of the tetrahedral structure by water molecules was introduced in [8] and has proven very useful in understanding the anomalous properties of this substance** [3, 5]. It is clear that this filling of voids is a mechanism accounting for the appearance of a second structure (dense packing) in the two-structure water model which has been proposed by Hall [5, 9]. But the translational movement of molecules among the voids in the tetrahedral lattice must lead to fluctuations in the direction of an increase in the coordination number.

---

*The hole which is left after movement of the molecule out of the lattice is "filled up" comparatively rapidly [5].

** As has been already noted in [3], filling of a void leads to an increase in the mean coordination number, even in the case where an "unfilled" hole is left by the passage of the molecule out of the lattice.

We will now pass to the quantitative determination of the asymmetry in the fluctuation of the coordination numbers. It will be supposed that the quantities $\overline{z}$ and $\overline{(\Delta z)^2}$ are already known [1, 2]. Then the sign, and the approximate magnitude of the asymmetry, of the distribution w(z) are fixed by the sign and magnitude of $\overline{(\Delta z)^3}$. The case $\overline{(\Delta z)^3} < 0$ corresponds to the predominance of fluctuations in the direction of decreasing coordination numbers; that of $\overline{(\Delta z)^3} > 0$, to fluctuations predominately in the direction of increasing coordination numbers. A knowledge of the fourth correlation function, $F_4(q, q', q'', q''')$, of the liquid particles is required for the exact evaluation of $\overline{(\Delta z)^3}$, [10], whereas only the binary function $F_2(q, q')$ can be developed from the x-ray data. For this reason, an exact calculation will not be attempted and instead of evaluating $\overline{(\Delta z)^3}$, determination will be made of $\overline{(\Delta N)^3}$, the mean cube of the deviation of the number of particles in a certain arbitrarily located unit volume of the liquid, equal in magnitude to the volume occupied by the selected liquid particle and its coordination sphere, from the mean value of this number. It can be supposed that such a substitution would not essentially distort the problem.

It is easy to see that the rule in this case should prove to be $\overline{(\Delta N)^3} < 0$. In determining the sign and magnitude of $\overline{(\Delta N)^3}$ it is possible to carry out an approximation calculation using the well-known semithermodynamic theory of fluctuation based on the Boltzmann Principle [11]. But in view of the fact that it is a matter here of very small volumes and numbers of particles, account must be taken, not only of the quadratic terms $(\Delta v)^2$, but also of the higher terms in a development of the thermodynamic potential as a power series in the deviation, Δv. The distribution of fluctuations in the volume and in the number of particles then proves to be non-Gaussian and the sign of the asymmetry of this distribution is fixed by the coefficient of $(\Delta v)^3$ in the series for the thermodynamic potential, i.e., by the sign of $(\partial^2 p/\partial v^3)_T$ (just as the fluctuation is determined by the value of $(\partial p/\partial v)_T$ when restriction is made to members of the order of $(\Delta v)^2$. But for all liquids $(\partial^2 p/\partial v^2)_T > 0$ and this leads, as is easily shown, to $\overline{(\Delta N)^3} < 0$.

This reasoning is exact for volumes over which $\overline{N}$ is relatively large. For dense-packed liquids $\overline{N} = \overline{z} + 1 \sim 10$ within the first coordination sphere, and for water, $\overline{N} \sim 5$. Thus further consideration of this problem is definitely needed, and it can be anticipated that the results in the case of water would be the opposite of the above.

We return to a strict statistical evaluation of $\overline{(\Delta N)^3}$. According to the methods which have been developed in [10], the quantity

$$\overline{(\Delta N)^3} = \overline{N^3} - 3\,\overline{N}\,\overline{N^2} + 2\,\overline{N^3} \tag{1}$$

can be evaluated with the aid of the expression

$$\overline{N} = \frac{1}{v}\int F_1(q)\,dq, \tag{2}$$

$$\overline{N^2} = \overline{N} + \frac{1}{v^2}\iint F_2(q,\ q')\,dq\,dq', \tag{3}$$

$$\overline{N^3} = -2\,\overline{N} + 3\overline{N^2} + \frac{1}{v^3}\iiint F_3(q,\ q',\ q'')\,dq\,dq'\,dq'', \tag{4}$$

in which v is the mean volume per liquid particle, $F_1(q)$, $F_2(q, q')$ and $F_3(q, q', q'')$ are, respectively, the monary binary, and ternary correlation functions for the particles in the liquid, and integration over each q is performed with the limits of the volume which is under consideration. All of these integrals can be evaluated by using the radial distribution function g(r), for the particles as obtained from x-ray data, provided the selected volume has the form of a sphere, and $F_1(q) = 1$, $F_2(q, q') = g(|q - q'|)$ and $F_3(q, q', q'') = g(|q - q'|)\,g(|q - q''|)\,g(|q' - q''|)$ are introduced into (2) – (4) (superpositional approximation). A certain additional simplication can be achieved if note is taken of the approximation relation

$$\begin{aligned}\iiint F_3(q,\ q',\ q'')\,dq\,dq'dq'' &\approx \iiint g(|q-q'|)\,g(|q-q''|)\;g(|q'-q''|)\,dq\,dq'dq'' \approx \\ &\approx \frac{4\pi}{3}\,r_1^3\iint g(|q|)\,g(|q'|)\,g(|q-q'|)\,dq\,dq',\end{aligned} \tag{5}$$

in which r_1 is the abscissa of the first minimum on the radial distribution curve.

For the two densely packed liquids, argon and mercury, at temperatures near the melting point, calculations carried out in this manner lead to negative values of $\overline{(\Delta N)^3}$ of the order of several tenths of a unit. This is in agreement with the results obtained from the semithermodynamic theory which was mentioned above.

TABLE 1

t, °C	r_1, A	$\overline{(\Delta N)^3}$
1.5	3.3	+25.1
13.0	3.3	+19.6
30.0	3.3	+15.5
62.0	3.45	+13.6
83.0	3.5	+15.7

In the case of water the results of calculation are quite different. For g(r), use was made of the experimental data out of [4]. Calculated results for several temperatures are shown in Table 1, where values of r_1 are also presented (values of $\bar{z}$ and of $\overline{(\Delta z)^2}$ for these same temperatures have been considered in [1]). The results of the last line are untrustworthy, since it is difficult to distinguish the first coordination sphere at the higher temperatures. It is significant, however, that $\overline{(\Delta N)^3} > 0$ in all cases, since this is a result which can clearly be carried over to $\overline{(\Delta z)^3}$. It is interesting that $\overline{(\Delta N)^3}$ shows a decrease with rising temperature.

A consideration of the asymmetry of the fluctuations in the coordination number in water is significant for explaining the nature of the translational movement of the molecules of this substance. The fact that fluctuations in the direction of an increase in the coordination number predominate in water (in distinction to the case of liquids which have a more dense packing) indicates the important role played by the movement of the molecules in the voids of the tetrahedral structure.

LITERATURE CITED

[1] I. Z. Fisher and V. K. Prokhorenko, Proc. Acad. Sci. USSR, 123, 131 (1958).*

[2] V. K. Prokhorenko and I. Z. Fisher, J. Phys. Chem. 31, 2145 (1957).

[3] O. Ya. Samoilov, The Structure of Aqueous Electrolytic Solutions and the Hydration of Ions (in Russian), Acad. Sci. USSR Press, 1957.

[4] J. Morgan and B. E. Warren, J. Chem. Phys. 6, 666 (1938).

[5] Yu. P. Syrnikov, The Compressibility of Electrolytic Solutions and Certain Problems in the Theory of These Solutions (in Russian), Dissertation, Leningrad State University, 1958.

[6] G. H. Haggis, J. B. Hasted and T. J. Buchanan, J. Chem. Phys. 20, 1452 (1952).

[7] J. A. Pople, Proc. Roy. Soc., A 205, 163 (1951).

[8] O. Ya. Samoilov, J. Phys. Chem. 20, 1411 (1946).

[9] L. Hall, Phys. Rev. 73, 775 (1948).

[10] N. N. Bogolyubov, Problems of Dynamics Theory in Statistical Physics (in Russian), Moscow, 1946.

[11] M. A. Leontovich, Statistical Physics (in Russian), Moscow, 1944.

Received December 2, 1958

---

* Original Russian pagination. See C. B. Translation.

THEORY OF SHOCK-INDUCED DETONATIONS

L. G. Bolkhovitinov

(Presented by Academician N. N. Semenov, December 13, 1958)

Many investigators had demonstrated that when a weighed sample of an explosive was subjected to any kind of mechanical stress, for example, shock, an explosive decomposition began in separate localized foci $10^{-3}-10^{-5}$ cm in size, from which it was then propagated throughout the bulk of the explosive. The only possible reason for the accelerated chemical reaction could be a temperature increase resulting from the change of the mechanical shock energy into thermal. Localized ignition of the material, when work is done on it, can thus only result from the friction between the particles of the explosive itself and the surrounding materials, or from a fluid deformation of the explosive. Bouden's hypothesis [1] that localized preheating arises in places of gaseous inclusions which are compressed by the shock is not correct, since the compression of a very small air bubble proceeds isothermally under ordinary experimental conditions. As evidence let us compare the thermal relaxation time τ of an air bubble of size $\underline{d}$ with the duration of shock. Since $\tau = d^2/\chi$ [χ is the thermal conductivity coefficient of air (0.2 cm^2/sec)], then for $d = 10^{-4}$ cm we get $\tau = 5 \cdot 10^{-8}$ sec, while the duration of shock and, consequently, compression is equal to approximately 500 μ sec, or 10,000 times longer than the thermal relaxation time of an air bubble. To ensure that the decomposition initiated in separate foci should not die out, the size and the temperature of a focus must have a definite value. Frank-Kamenetskii [2] discovered a simple relationship between the critical size d_* and temperature T_*,

$$\frac{d_*^2\, QEze^{-E/RT_*}}{KRT_*^2} = \delta,$$

where Q is the heat of reaction per unit volume, E the activation energy, $\underline{z}$ a preexponential coefficient, K the thermal conductivity coefficient, while $\delta = 3$ for a spherical focus. Knowing the values of these numbers we can calculate the critical temperature corresponding to any given focus size. In calculating the critical temperatures of various-size foci we used the activation energies obtained by A. I. Serbinov and based on numerous experiments on the thermal decomposition of explosives. These activation energies are presented in Table 1 alongside the results of our calculations. According to Serbinov the value of $\underline{z}$ is the same for all the compounds and equals $10^{13.6}$.

As one can see in Table 1, the critical temperatures T_* are above the melting points. Therefore the heating of an explosive, no matter in what way it is carried out, should proceed simultaneously with an over-all compression in order that $T_m \geq T_*$, since otherwise the energy supplied to the compound will be used to melt it. The relationship between the melting point and the applied pressure was studied by Bridgman. He found out [3, 4] that for aniline, bromoform, benzene, and nitrobenzene the melting-point elevations are the same and equal to about 0.02° per atmosphere. Assuming that the explosives have similar melting-point elevations we find out that the required pressure for an over-all compression $\sigma_* = (T_* - T_m)/0.02$.

The energy of formation of an ignited focus is negligibly small (due to the small dimensions) in comparison with the expansion energy of rollers, when a layer in the explosive attains the high pressure required for the formation of a hot focus with temperature T_*. The formation of a hot focus (a random phenomenon) obeys some statistical laws of which we know nothing so far. Therefore, we can only assume that if a layer in the

TABLE 1

Critical Temperatures for Various Size Foci

Compound	M.p., °C	E, kcal/mole	$d = 10^{-5}$ cm	10^{-4} cm	10^{-3} cm
			Temperature, °C		
TEN	141	32000	440	300	210
Hexogen	204	34000	490	340	240
Tetryl	129	35000	530	360	260
TNT	81	48000	860	720	470

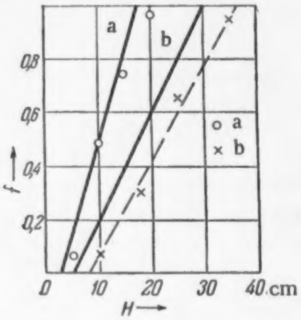

Fig. 1. Comparison between the calculated explosion probabilities of TEN*(a) and tetryl (b) and the experimental data (the experimental points are connected by a dotted line).

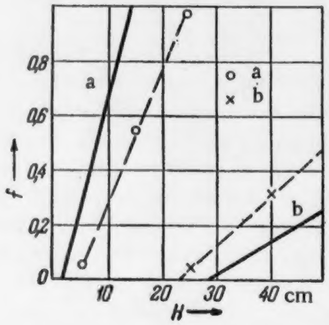

Fig. 2. Comparison between the calculated explosion probabilities of hexogen (a) and TNT (b) and the experimental data (the experimental points are connected by a dotted line).

explosive when subjected to shock attains a pressure at which the effective (i.e., inextinguishable) 10^{-5} cm large foci can form, then the explosion probability will be close to one. Experiments are usually carried out on powdered explosives, the particles of which are of the order of 10^{-3} cm in size. Considering that the maximum size of a hot focus is set by the particle dimensions, we can assume that when the shock raises the pressure to a point where the formation of an effective 10^{-3} cm large hot focus becomes possible, then the explosion probability becomes different from zero.

The maximum pressure developed by the shock under a drop hammer can be estimated in the following simple manner. Since the cross-section area of the rollers is about two orders of magnitude smaller than the area of the striking pin, we can presume that at the moment the load is stopped all the compression energy is concentrated in rollers. This energy is then transformed into the kinetic energy of the load and the height of recoil will be determined by this energy. Therefore we can take the maximum pressure in the rollers to be

$$\sigma_m = (2ePHE/V)^{1/2},$$

where P is the weight of the load, H the height from which the load is dropped, e the restoration coefficient of the drop hammer, E Young's modulus for the materials of which the rollers are made, and V their volume. From the condition that $\sigma_m = \sigma$ we can determine the range of explosion probability changes f as we increase the dropping height of the load. The calculated limiting dropping heights between which $0 \leq f \leq 1$ for a 10 kg weight and standard rollers with e = 0.5 are given in Table 2 and in Fig. 1 and 2, where the limiting points are linked by continuous lines. The same graphs also show the experimental probability curves obtained by V. N. Kozhlov. A comparison between our nominal "probability curves" and the experimental data shows that among

*Erythritol tetranitrate.

TABLE 2

Compound	f = 0		f = 1	
	σ_0, kg/cm^2	H_0, cm	σ_1, kg/cm^2	H_1, cm
TEN	3000	2.5	15000	17
Hexogen	1800	1.5	14300	15
Tetryl	6500	5.1	20000	30
TNT	19500	29.0	39000	110

the factors which determine the explosion probability during testing with a drop hammer the pressure attained under shock is of no less importance than the conditions of fluid flow in the substance.

LITERATURE CITED

[1] F. P. Bowden and A. D. Joffe, Excitation and Propagation of Shock in Solids and Liquids (IL, 1955) [Russian translation].

[2] D. A. Frank-Kamenetskii, Diffusion and Thermal Conductivity in Chemical Kinetics, Izd. AN SSSR, 1947 [in Russian].

[3] P. W. Bridgman, Phys. Rev. 3, 126, 153 (1914).

[4] P. W. Bridgman, Phys. Rev. 6, 1, 94 (1915).

Received December 13, 1958

AN INVESTIGATION OF THE THERMAL DEHYDRATION OF CRYSTALLINE AND AMORPHOUS SILICA BY THE METHOD OF MASS SPECTROGRAPHIC ANALYSIS

The M. V. Lomonosov State University, Moscow

(Presented by Academician M. M. Dubinin, December 24, 1958)

The heating of silica to temperatures in excess of 300°C, especially in vacuum, leads to the gradual removal of considerable amounts of the so-called "structural" water from the surface. A definite conclusion has not as yet been reached as to the nature of the elementary processes which then take place in the surface layer of the silica. Only hypothetical schemes [1-4] are available for describing the structural surface changes which occur in dehydrated silica. It is also unclear as to whether H_2O, which is usually detected macroscopically, is the initial, and the only, material leaving the silica surface on heating. Thus the theory of the silica surface which has been developed in [3] supposes that protons and the ions H_3O^+ can be removed along with H_2O in the course of the dehydration of silica gel.

By using mass spectrographic analysis, it is possible to determine the nature of the components in the gaseous phase which is liberated in the heating of adsorbents. In particular, the presence of positively charged particles can be detected readily with this method.

The thermal dehydration of silica has been studied on a MS-4 mass spectrometer. The search for positive ions which might be formed in natural dehydration was carried out by using a hot-anode ion source without forced ionization. A tungsten spiral served as the hot anode, a 40-50 mg cylinder of the compressed silica gel being placed within it.

The principal experiments in the mass spectrographic analysis of the neutral desorption components were carried out with a "gaseous" ion source into which the gaseous specimen was introduced and ionized by the electron beam. A considerable amount (2-10 g) of the silica was placed in a quartz tube which was outside the mass spectrometer and connected to a supplementary high-vacuum system; the silica was there heated by an electric furnace. The gases which were formed in this heating system could be introduced into the ion source through a series of connecting tubes and dosing valves. This permitted us to freeze out in passage the various components (H_2O, for example), and volatile foreign substances.

When the quartz tube was heated to the desired temperature, pumping was discontinued, and, after a definite time interval had elapsed, measurement was made of the ion currents due to the various components of the evolved gas. The chamber with the adsorbent was always pumped out in passing from one temperature to another. The temperature of the quartz tube was measured with a thermocouple.

We investigated two specimens of highly pulverized crystalline quartz which had been prepared at various times and possessed the specific surfaces 35.8 and 8 m^2/g and of three varieties of silica gel (K-2, KSK-2, KSK-3). The adsorption characteristics of these specimens have been presented in [5-6].

During this study, it proved necessary to purify the silica specimens with particular care. Experience showed that the generally applied methods of purification would not assure the complete absence of foreign substances, especially organic materials, or of CO_2 and the oxides of nitrogen.

Prior to each experiment, the charge of silica was subject to a preliminary heating at 300-400°C with simultaneous evacuation to 10^{-5} mm of Hg, the heating lasting from an hour and a half to eight hours. In order to exclude the "background," mass spectrographs of the atmosphere in the chamber of the apparatus during heating of the spiral anode (without the charge), and of the gases evolved by the heating of the empty quartz tube to 1000° were observed in each case.

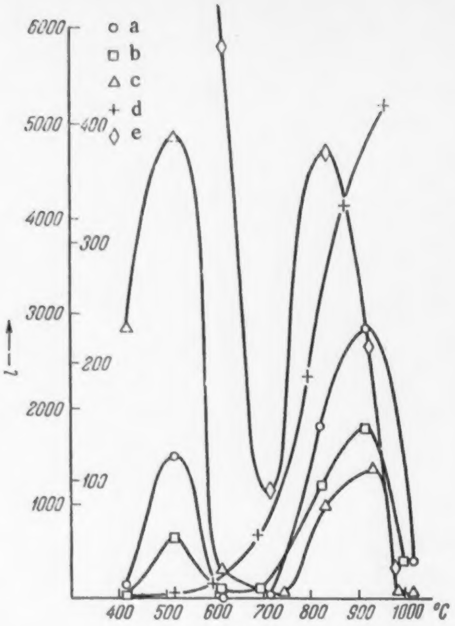

As the ordinate, there has been plotted the relative value of the O_2 ion current, as measured at a fixed time after reaching the temperature in question, this current being proportional to the amount of evolved oxygen. The scale to the right of the axis of ordinates refers to curves (a) and (b); the scale to the left, to the remaining curves. a) Quartz powder No. 1, b) quartz powder No. 2; c) silica gel KSK-2, which evolved a considerable amount of NO; d) silica gel KSK-3; e) silica gel KSK-3, which evolved a large amount of NO.

In all the experiments, the working range of temperatures was 400-1000°. Mass spectra in the interval from 1 to 50 m.e., were taken over 100-150°.

The intensities of the individual mass lines (the magnitudes of the ionic currents) varied markedly, even in experiments with different charges of a single adsorbent. It thus appeared to be most significant to compare the alteration in the intensity of a given line within a single series of measurements.

Negative results were obtained from a study of the dehydration of the silica gel K-2 in the hot-anode ion source, which was carried out with a view to disclosing the presence of charged particles. Up to temperatures of 900-1000°, there was complete absence of any kind of positive ions above the heated silica gel surface. At 1000°, weak currents of ions of mass numbers 23, 39 and 41 were observed; these lines also appeared on heating the spiral without the charge and were due to the thermal ionization of the sodium and potassium which were present as contaminants in the metal of the spiral.

Thus, when mass spectrographic analysis is performed in this manner, the data point to the conclusion that there is no spontaneous emission of ions by a silica gel surface during thermal dehydration, at least to within the sensitivity of the MS-4 spectrometer. It can be claimed that it would have been possible to detect the formation of ions if their ratio to the number of desorbed neutral H_2O molecules was at least $1:10^5$. It is clear that this fact supports neither the mechanism of the thermal dehydration, nor the scheme of the structure of the surface of the dehydrated silica gel proposed in [3]. With each type of silica, the mass spectrum of the neutral components of the desorbed gaseous phase proved to be relatively complex. In addition to H_2O and the "splinter" lines (OH, for example), lines of CO_2, N_2, CO, and O_2 were observed in the most cases, sometimes H_2 and NO, and other oxides of nitrogen, as well as the lines of various organic compounds. The lines belonging to the particles SiO_2, SiO, O_2, and O which arise from sublimation of the solid phase of silica, are known from [7] to appear in the mass spectrum only at temperatures of around 1500°

Both the absolute and the relative amounts of the materials represented in the mass spectra of the dehydrated material varied from specimen to specimen, and depended on the temperature, and the time of heating as well. From data gathered in a great number of experiments it was established that all of the components of the mass spectra, with the exception of H_2O and O_2, arose from extraneous factors which were not characteristic of the processes involved in the alteration in the structure of the silica surface. In particular, the presence of the lines of organic molecules, and of CO and CO_2, clearly indicated that the adsorbent readily picked up vapors of organic materials during its drying, storage, etc., and these substances were desorbed and partially oxidized during the dehydration. As a rule, these components showed their highest intensity at the beginning of the range of working temperatures, i.e., at 400-600°, and almost completely disappeared at temperatures above 700°.*

---

* The total amount of foreign materials in the adsorbents was comparatively small. For purified specimens, these materials could be estimated as making up several tenths of a percent of the amount of "structural" water.

The evolution of H_2O was almost completely analogous: a maximum was recorded in the region 450-650°, with a sharp fall-off to an infinitesimal amount at a temperature of 750-800°, facts which are in full agreement with data such as that presented in [4].

In our experiments, we could find no confirmation that the evolution of considerable quantities of molecular hydrogen occurred in the dehydration of silica, as was reported in [4, 8]. The H_2 which appeared in the mass spectrum was clearly of secondary origin, and arose from the breakdown of H_2O molecules in the electron beam. On freezing the H_2O out of the desorbed gases, the H_2 almost entirely disappeared as well.

The evolution of molecular oxygen in considerable quantities during the dehydration of crystalline quartz and two varieties of silica gel (KSK-2 and KSK-3) proved to be something essentially new. The temperature dependence of this process was quite different from that observed for the other components of the mass spectra. In the figure the typical curves which illustrate this dependence for four specimens of silica are sketched. These curves have two maxima; one in the region 500-550° and the other (in most cases) in the region 900-950°, with a sharp diminution, sometimes to total disappearance of the O_2, in the region 600-700°. This evolution of O_2 was quite reproducible, although its relative intensity varied markedly from specimen to specimen and there was, at times, a marked diminution in the region of one, or the other, of the maxima. A certain divergence in results was noted in the case of the silica gel KSK-3 where the second maximum was either displaced into the temperature range 800-850°, or was not detectable even at 950°.

A comparison of the specific amount of structural water in the investigated silicas with the amount of oxygen evolved in the interval of temperature 700-1000° made it possible to draw certain conclusions concerning the absence of a direct relation between these quantities.

In regard to the evolution of O_2, the behavior of the silica gel K-2 proved to be anomalous. Despite repeated experiments, it was impossible to state with certainty that O_2 was present in the mass spectra. Only in separate cases were traces of O_2 to be observed in the region 400-700°; these then disappeared, and possibly, reappeared only at a temperature of $\approx 1000°C$. In every case it could be stated that if O_2 was evolved by the silica gel K-2, the amount was 2-3 orders less than in the case of the other types of silica.

The peculiar temperature dependence of the evolution of O_2 can be interpreted in the following manner. The oxygen which appears at moderate temperatures (first maximum) should be looked upon as extraneous oxygen which is relatively weakly bound to the adsorbent. It was definitely noted in a number of experiments that the evolution of considerable quantities of NO at 450-650° was paralleled by a marked increase in the first maximum for O_2. In certain cases, this maximum was lacking and the curve rose steadily over the interval 450-900°. From these facts the conclusion follows that the oxygen which is liberated at moderate temperatures arises, at least in part, from the breakdown of oxides of nitrogen which are retained by the adsorbent after the latter's purification. This conclusion is supported by the presence of molecular nitrogen among the desorption components, since this could also arise from the oxides. It is obvious that only on heating would there be a full vaporization from the surface of the CO and CO_2 which are formed in the oxidation of organic compounds during the treatment of the adsorbent with nitric acid vapors.

It is clear that evolution of O_2 which begins at 700° and continues up to 1000° cannot be connected with foreign substances. Not only are N_2 and NO not observed in this temperature region, but even H_2O appears in only an insignificant amount, whereas the evolution of O_2 continually increases and reaches very considerable proportions. Obviously, here it could be oxygen which was more firmly bound with the silica surface, so that this evolution in the region of high temperatures could be considered a reflection of some type of surface alteration.

Thus, the evolution of "structural" oxygen with a maximum intensity at 900-950° can be looked upon as the basic result from the mass spectrometric analysis of the thermal dehydration of silica. The lower temperature limit for this process could not be established with satisfactory precision because of the complicating action of contaminants. It is possible that it is about 600°.

The observation of the evolution of O_2 during the thermal dehydration of silica is accompanied by difficulties in the case of specimens which are insufficiently pure. A considerable portion of the oxygen liberated on heating can be expended in the oxidation of organic contaminants, with the result that there will be an increase in the observed evolution of CO and CO_2, and an accompanying diminution, or even disappearance, of O_2. It is possible that this would explain the almost total absence of oxygen at medium temperatures, and the diminished amount of this material at higher temperatures, which was observed in certain of our experiments. As a rule, large amounts of organic substances were to be noted in the mass spectra of the specimens in question.

The present work has been carried out in collaboration with the Laboratory of Surface Phenomena of the Physics Department of the Moscow State University as a part of a group investigation of the properties of adsorbents.

I would like to express by thanks to A. S. Predvoditelev, Corresponding Member of the Academy of Sciences of the USSR, for his attention to, and his interest in, this work.

LITERATURE CITED

[1] A. V. Kiselev, Collected Papers, The Surface Chemical Compounds and Their Role in Adsorption Phenomena (in Russian), Moscow, 1957, p. 90.

[2] R. K. Iler, The Colloid Chemistry of Silica and Silicates, N. Y., 1955.

[3] W. A. Weyl, Research, 3, No. 5, 230 (1950).

[4] W. Stöber, Koll. Zs. 145, No. 1, 17 (1956).

[5] M. M. Egorov, V. F. Kiselev and K. G. Krasil'nikov, J. Phys. Chem. 32, No. 10, 2448 (1958).

[6] M. M. Egorov, T. S. Egorov, V. F. Kiselev and K. G. Krasil'nikov, J. Phys. Chem. 32, No. 11 (1958).

[7] R. F. Porter, W. A. Chupka, and M. G. Inghram, J. Chem. Phys. 23, No. 1, 216 (1955).

[8] L. Miller, Koll. Zs. 142, No. 2/3, 117 (1955).

Received December 17, 1958

THE ROLE OF OXYGEN IN RADIOLYTIC DISCOLORATION OF AQUEOUS SOLUTIONS OF INDIGO CARMINE

A. A. Zansokhova, V. D. Orekhov and M. A. Proskurnin

(Presented by Academician V. A. Kargin, December 20, 1958)

According to the data of Mongini and Zimmer [1],the radiolytic discoloration of aqueous indigo carmine solutions saturated with air is a very high-yield reaction (14.7 moles/100 e.v.). The fact that in solutions saturated with nitrogen radiation had no visible effects led these workers to the conclusion that HO_2 radicals (3 oxidation equivalents) are of paramount importance in the oxidation of this compound whereas H and OH radicals have no effect. These conclusions of Mongini and Zimmer contradict the current ideas on the reactivity of H, OH and HO_2 radicals.

The authors of the present communication endeavored to explain the role of oxygen in the oxidation of indigo carmine by using the method in which conjugated acceptors are introduced [2-5] while the dosage and other factors are varied (oxygen pressure, pH, etc.). As regards the method, the work is similar to the previously published ones, but one should note the great importance of insuring a high purity of the reagents used in the investigation systems. The indigo carmine was recrystallized twice from water and from sulfuric acid, then fractionally distilled. All solutions were prepared from twice-distilled samples.

Irradiation of oxygen-free acidic solutions of indigo carmine ($2 \cdot 10^{-4}$ M) by γ-rays resulted in both a reversible and irreversible discoloration, which corresponded to the reduction and oxidation of the dye,respectively. The absolute values and the ratio between the yields of these two reactions are highly dependent on the radiation dosage (curve 1 and 2, Fig. 1). The sharp increase in the reaction yield over a narrow range of low dosages (< 1r/sec) is evidently connected with the more favorable conditions for the rearrangement of the intermediate dye products to 5-isatinsulfonic acid [1] after oxidation, or to a leuco base after reduction. With increasing dosage the recombination of intermediate products becomes the predominant reaction and the over-all effect of radiolysis declines. The evolution of gases is also somewhat decreased (G_{gas} = 0.5 mole/100 ev).

The reduction as well as oxidation of indigo carmine can be either sensitized or inhibited by means of various additives. Compounds able to bind the oxidation and reduction products will shield the dye against radiation.

We have experimentally established the fact that in solutions saturated with air,acetanilide, thiourea, and ferrous ions will exhibit such shielding action if present in sufficiently high concentrations (of the order of 0.01 M).

When we introduced into solution certain acceptors of the oxidized components of radiolyzed water, such as benzene, formic and oxalic acids, et al., the yield of reduced dye increased from 0.1 mole/100 ev to 0.5, 1, and 1.7,respectively. We could recover the dye after irradiation by bubbling oxygen through the solution. Irreversible reactions are very insignificant in such systems.

Oxidation of indigo carmine was sensitized by introducing scavengers of atomic hydrogen. A 1 M concentration of NO_3^- ions (at pH $\geq$ 4) at a γ-ray dosage of 22 r/sec increased the oxidation yield of the dye from 0.01 moles (in unsensitized solutions) to 2 moles per 100 ev (and the same amount of NO_2^- ions). One should note that the presence of oxygen in solution had no effect on the oxidation of this system. This can be explained by the fact that oxygen can not compete with the excess of NO_3^- ions as an acceptor of H atoms, while

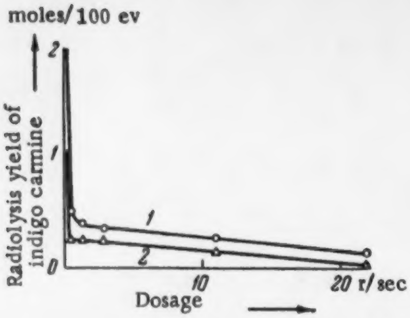

Fig. 1. Irradiation of $2 \cdot 10^{-4}$ M indigo carmine (pH 1.1) solutions in the absence of oxygen; reaction yield as a function of γ-ray dosage. 1) Change in reduction yield, 2) change in oxidation yield.

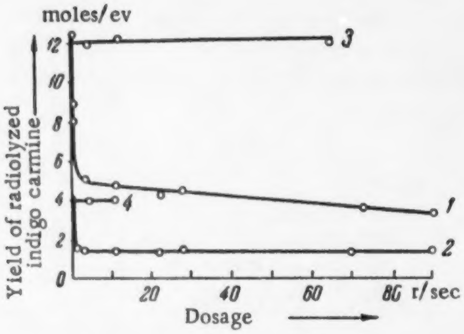

Fig. 2. The yield of oxidation products from indigo carmine ($2 \cdot 10^{-4}$ M) as a function of dosage. 1) Solution containing 1 equiv. of H_2SO_4 saturated with oxygen at atmospheric pressure; 2) solution of pH = 6, saturated with oxygen at atmospheric pressure; 3) solution containing 1 equiv. of H_2SO_4, saturated with oxygen at 80 atm; 4) solution of pH = 6, saturated with oxygen at 80 atm.

it does not seem to participate directly in the oxidation of the dye. Thus we can assume that O_2 has sensitizing action similar to that of NO_3^-, and the investigation of oxidation of indigo carmine in the presence of O_2 assumes a new interest.

An analysis of curves which represent the yield of oxidation products (neglecting secondary effects) as a function of radiation dosage in saturated solutions of different acidities (Fig. 2) leads to the conclusion that the oxidation of indigo carmine involves, besides the OH radicals, also hydrogen peroxide, which is formed in the following manner:

$$H + O_2 \rightarrow HO_2, \quad HO_2 + HO_2 \rightarrow H_2O_2 + O_2.$$

Some of our experiments on the oxidation of indigo carmine by H_2O_2 showed that this reaction was very slow. The rate declined with increasing pH attaining 0 at pH ≥ 6. This would indeed explain the secondary reactions detected in solutions containing $1 > H_2SO_4 > 10^{-6}$ N (pH ~6) at a dosage > 0.5 r/sec, i.e., under conditions where H_2O_2 had no time to react with the dye during the reaction and accumulated in solution. It can be identified by the colored compound it forms with titanium. Besides this, the hydrogen peroxide was detected and measured by the oxidation of an additional amount of dye when the irradiated solutions were later acidified (amongst them also solutions whose initial pH was ≥6). The oxidation yield, with secondary oxidation taken into account, never exceeded 12 moles/100 ev.

Increased oxygen pressure in solution made the reaction yield independent of dosage, while for each pH there was a certain maximum yield. Thus at pH ≥ 6, where the forming H_2O_2 is unable to oxidize the dye, the limiting oxidation value G = 4 moles/100 ev (oxidation by OH radicals) (curve 4, Fig. 3).

When we introduced an OH-radical scavenger (for example NO_2^- ions) into a solution of pH ≥ 6, then despite the presence of oxygen, the dye was completely shielded.

In a 1 N dye solution the oxidation yield attained a maximum value of 12 moles/100 ev (Fig. 2, curve 3) which agreed with the assumption that 12 water molecules were involved in the radiolysis (4 ionized and 8 excited) in the following fashion:

$$H_2O \rightarrow H + OH; \quad H + O_2 \rightarrow HO_2; \quad 2HO_2 \rightarrow H_2O_2;$$

$$\text{Indigo carmine} + OH + H_2O_2 \rightarrow \text{oxidation products.}$$

The increased concentration of dissolved oxygen (80 atm pressure) left the yield unchanged and equal to ~12 moles/100 ev.

In bearing with the above-discussed data, a chain mechanism is considered very unlikely in this radiolytic oxidation.

In concluding let us note that the high oxidation yield obtained by Mongini and Zimmer in solutions saturated with air we were able to reproduce only by introducing into the irradiated solution some finely ground methyl methyacrylate; this was the material of which the cells used by those workers in their irradiation were made of.

LITERATURE CITED

[1] L. Mongini and E. L. Zimmer, J. Chim. Phys. 50, 491 (1953).

[2] V. D. Orekhov, A. I. Chernova and M. A. Proskurnin, Coll. Works on Radiation Chemistry, Izd. AN SSSR, 1955, pp. 85-91.

[3] A. I. Chernova, V. D. Orekhov and M. A. Proskurnin, J. Phys. Chem. 30, 1343 (1956).

[4] V. D. Orekhov, M. A. Proskurnin, A. Sharpatyi and A. A. Zansokhova, Trans. 1st All-Union Conference on Radiation Chemistry, March 1957, Izd. AN SSSR, 1958, p. 100.

[5] V. A. Sharpatyi, A. A. Zansokhova and V. D. Orekhov, J. Phys. Chem. 32, 1686 (1958).

Received December 15, 1958

SEPARATION COEFFICIENTS FOR THE CHLORINE ISOTOPES IN THE REVERSIBLE VAPORIZATION OF HCl

K. I. Matveev, O. V. Uvarov and N. M. Zhavoronkov,
Corresponding Member, Acad. Sci. USSR
The L. Ya. Karpov Physicochemical Scientific Research Institute

Among the several extant methods for the determination of separation coefficients [1-3], Rayleigh distillation is the most frequently employed.

In 1902, Rayleigh derived an equation [4, 5] giving the relation between the alteration in the concentration of a liquid phase resulting from evaporation, and the amount of vaporized liquid. This equation has the following form:

$$\frac{N}{N_0}\left(\frac{1-N_0}{1-N}\right)^{1/\alpha}=\left(\frac{G_0}{G}\right)^{(\alpha-1)/\alpha}, \qquad (1)$$

in which N_0 and N are the initial, and the final, concentrations of the less volatile component; $1-N_0$ and $1-N$ are the initial, and the final, concentrations of the more volatile component; G_0/G is the ratio between the initial and the final amounts of the liquid, and α is the separation coefficient. The enrichment coefficient, F, is given by the expression $\frac{N(1-N_0)}{N_0(1-N)}$.

Since 1932, Rayleigh distillation has been used for the determination of the separation coefficients in such various isotopic systems as H_2-D_2 [6]; $C^{12}O-C^{13}O$ [7]; and $N^{14}H_3-N^{15}H_3$ [8]. In carrying out Rayleigh distillation, up to the present time, effort has been made to employ only very pure isotopic mixtures which were free of low-volatile impurities, since these tend to concentrate in the final volume in a higher degree than does the low-volatile component of the system. Using the Rayleigh equation, we have carried through some rough calculations to determine the effect of the amount of impurities on the value of the separation coefficient. The results of these calculations are shown in Fig. 1.

It is to be seen that the accuracy of determination of α depends only slightly on that of the determination of G_0/G at low enrichment, and that this is particularly true for high values of G_0/G when the coefficient of enrichment does not exceed 1.04. Thus, if $F \leq 1.04$ and $G_0/G \geq 4000$, an error of ± 1000 in the determination of G_0/G is practically without influence on α, so that with corresponding values of G_0/G, and F, up to 15% of impurities is permissible in the final volume, if the impurity peaks do not coincide with the peaks for the isotopic substance in mass spectrographic analysis. In practice, it is impossible to obtain a degree of reduction (G_0/G) in excess of 500-1000 by evaporation from a single vessel, because the volume of the gaseous phase must be taken into account in the determination of G_0/G. Thus, in order to increase the ratio G_0/G, the effect of the gaseous phase is minimized by carrying out the vaporization of two steps.

EXPERIMENTAL

HCl was vaporized from a cylindrical vessel having a conical bottom. The vessel was surrounded by a vacuum jacket to stabilize the vaporization process. The construction of the vessel is shown in Fig. 2. The

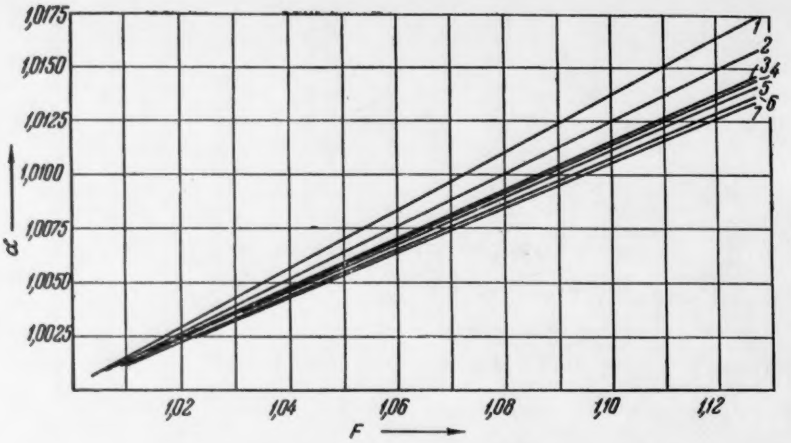

Fig. 1. The separation coefficient as a function of the coefficient of enrichment, and the coefficient of reduction. 1) G_0/G = 1000; 2) 2000; 3) 3000; 4) 4000; 5) 5000; 6) 7000; 7) 8000.

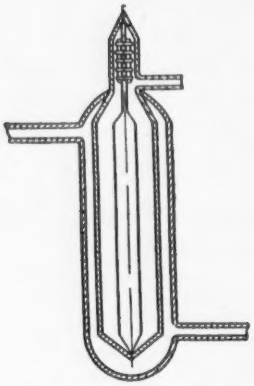

Fig. 2. Vaporization vessel.

liquid was agitated by a worm stirrer, to the upper end of which the ring winding from the rotor of a Warren motor was attached. The stirrer was powered by the magnetic field of the stator of this same motor, which was set on the upper part of the vessel. Splashing was avoided by this stirrer construction.

A sketch of the entire vaporization apparatus is given in Fig. 3.

The vaporization vessel was inserted into a special seat in the thermostat 34. This thermostat was in the form of a copper block which was set on the steel plate 33. This copper block was covered with the steel cover 4 which was well seated in the plate. To diminish thermal losses, air was pumped out of this cover to a pressure of 10^{-2} mm of Hg. The thermostat was cooled by the introduction of liquid nitrogen, or oxygen, into the cavity 32 in the copper block. In order to follow the vaporization of the liquid, the cover was equipped with a viewing mirror and a slot was made in the copper block. Special orifices were arranged in the plate for the delivery of the electric current and the cooling agent, for the removal of the HCl, etc. The apparatus was considered ready for operation when the pressure in the cover had fallen to 10^{-2} mm. The thermostat was then cooled to −110° to −120°C. At the same time, the cooling agent was introduced into the jacket of the vessel through the inlet tubes a and b. The vaporization vessel was then filled with HCl by condensation of gaseous HCl from the trap 11. The amount of the condensed HCl was determined from the liquid level in the vaporization vessel. After the necessary temperature had been reached by the thermostat and the working pressure established in the vessel, a specimen of gas was taken to serve as a standard (ampule 35). The rate of evaporation was regulated by the cocks 22 and 23, and was checked by the manometers 8 and 9, and by the liquid level in the vessel. The last portions of the liquid phase and the vapors remaining in the large vessel were carried into the small vessel 6, which had the same construction as the larger vessel, and a volume of 9 cm^3. An ordinary Dewar flask served as the thermostat. The remaining portions of the liquid and the vapors from the smaller flask were completely transferred into the space between the stopcocks 22 and 23. The final values of G was determined from the pressure and the known volume. The ampule 10 was then sealed off, its contents serving as a specimen in what followed. For the evacuation of the entire apparatus there was employed a vacuum system consisting of the fore pump 16, the diffusion pump 15, and the fore vacuum balloon 14. The hydrogen chloride for the experiments was obtained from the action of concentrated H_2SO_4 (98%) on hydrochloric acid (35%). The liquid HCl was distilled three times, the first and the last fractions being discarded. The temperature dependence of α was determined at a vaporization rate of 0.25-0.33 cm^3/hour per 1 cm^2 of evaporating surface, with the stirrer rotating at 240-300 rev/min.

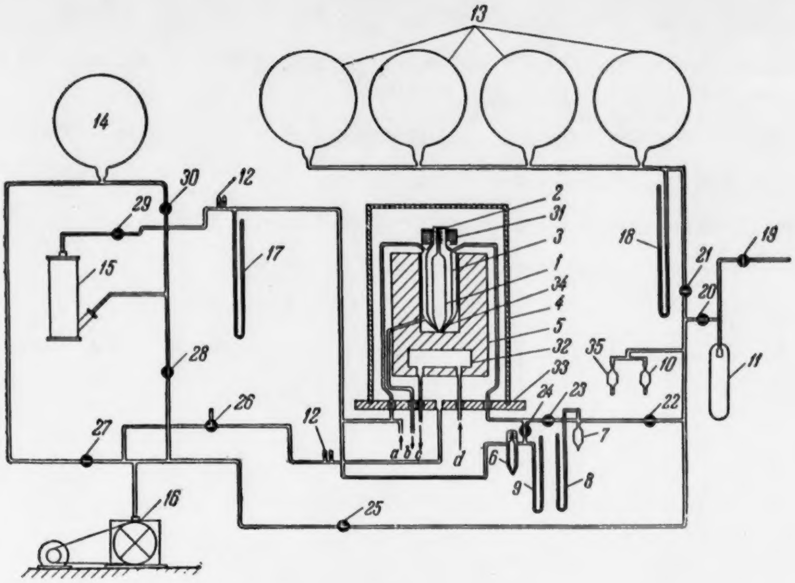

Fig. 3. Sketch of the apparatus for reversible vaporization.

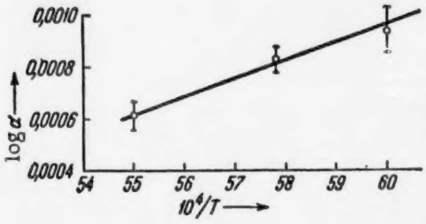

Fig. 4. The relation between log α and $10^4/T$.

The experimental results are summed up in the Table where there are given values of α, calculated from equation (2), and determined experimentally. Since the temperature interval between boiling (−84°C) and freezing (−114°C) is a narrow one, separation coefficients were determined for only three temperatures. The temperature dependence of log α on $10^4/T$ which is shown in Fig. 4, can be expressed by the equation:

$$\ln \alpha = \frac{1.2846}{T} - 0.0055, \qquad (2)$$

in which T represents the absolute temperature.

By distilling HCl in a column at a temperature of 185°K, I. G. Gverdtseteli, T. A. Gagua and Yu. V. Nikolaev [9] found the value α = 1.0008 – 1.001.

TABLE 1

T	P	F	α_{exp}	α_{col}
167	190	1,0221	1,0022 ±0,00025	1,0022
173	285	1,017	1,00193±0,000125	1,00194
181	534	1,012	1,0014 ±0,0001	1,0016
185	—	—	—	1,0014
189	760	—	—	1,0013

The low value obtained for α (1.0013, at the normal boiling point) indicates that the rectification of HCl, even in highly efficient columns, is not a suitable method for the separation of the isotopes of chlorine.

LITERATURE CITED

[1] I. Kirschenbaum, Heavy water (in Russian), Foreign Lit. Press, 1953, p. 28; D. Othmer, Ind. and Eng. Chem. 39, 2, 779 (1947).

[2] H. G. Thode, J. Am. Chem. Soc. 62, 581 (1940).

[3] Distillation, Foreign Lit. Press, 1954, p. 36; K. Kohen, J. Chem. Phys. 8, 588 (1940); S. I. Babkov and N. M. Zhavoronkov, Proc. Acad. Sci. USSR, 106, 877 (1956).*

[4] A. I. Brodskii, The Chemistry of Isotopes (in Russian), Acad. Sci. USSR, Press, 1952, pp. 66-68.

[5] Rayleigh, Phil. Mag., 4, 521 (1902).

[6] G. Urey, F. G. Brickwedde and C. M. Murphy, Phys. Rev. 4, 1 (1932).

[7] A. D. Zorin, Master's Dissertation, Moscow, 1955 (in Russian).

[8] M. H. Whal, I. F. Hoffman and I. A. Hipple, J. Chem. Phys. 3, 435 (1935).

[9] I. G. Gverdtseteli, T. A. Gagua and Yu. V. Nikolaev, Atomic Energy, 4, 294 (1958).*

Received December 10, 1958

---

* Original Russian pagination. See C. B. Translation.

A CONTRIBUTION TO THE THEORY OF RADIATION CHEMISTRY

L. S. Polak and A. Ya. Temkin

The Institute of the Syntheses of Petroleum Chemistry of the Academy of Sciences of the USSR

(Presented by Academician A. V. Topchiev, December 11, 1958)

Two problems will be treated in the present work: the evaluation of the interaction of tracks and the development of an approximation method for calculating the number of free radicals and final products resulting from (γ- or β-) radiolysis.

It is one of the characteristics of radiation chemistry that fundamental significance can be attached to the tracks of the particles of the ionizing radiation in which almost all of the principal primary steps of the radiochemical reactions develop [1]. A consideration of the effect of the structure of these tracks, their spatial distribution and interaction, is of importance for the study of low-yield radiochemical reactions (~ 10 molecules per 100 ev) where the chemical process is exhausted by the reaction of molecules excited in the initial step, with one another and with neighboring molecules; in chain reactions, the role of these tracks is much less significant. One must resort to ionizing radiation of high density in order to obtain high yields per unit of time of the final products from radiochemical reactions which are not of the chain type (or from reactions in which the chains are very short), including such important processes as the radiational cracking of hydrocarbons, certain types of radiational polymerization, nitration, etc., etc. But, at higher densities of radiation, track interaction naturally arises. The formation of this or the other type of ionizing centers for the chemical reaction, and the diffusion and recombination of these centers, are directly bound up with the existence of such track interaction. Thus, at high densities of ionizing radiation, it is necessary to take account of the mutual effects of the tracks of the various ionizing particles.

In this case the problem of the theory of radiation chemistry can be formulated in the following terms: given the initial distribution of the ions and radicals, to find the change in the distribution of the ions and free radicals in the irradiated medium at the time $\underline{t}$ which results from the formation of a track at the instant $t_0 = t - t'$.

Let $n_i([\tau], N_1, \ldots, N_i, \ldots, N_m, t, t', \mathbf{r})$ represent the change in the number of free radicals, or ions, of the i-th type at the point of radius vector $\mathbf{r}$ resulting at the instant $\underline{t}$ from the formation at $t_0 = t - t'$ of a track which at that moment contained N_i ($i = 1, 2, \ldots m$) particles of each type, the initial distribution of these particles in space being completely characterized by that certain set of numbers, or functions, which is designated by τ. In general, the symbol $f[\tau]$ will indicate that the quantity $\underline{f}$ is a functional of τ. In conformity with this, we will write $\delta\tau$ instead of $d\tau$, and consider that $\delta\tau$ can represent either a product of differentials of several variables, or the variations of several functions.

Through

$$w[\tau],\ N_1,\ \ldots,\ N_i,\ \ldots,\ N_m,\ t)\,dt\,\delta\tau\prod_{i=1}^{m} dN_i$$

we will now designate the number of tracks formed in the time interval $(t, t + dt)$, the initial numbers of particles of each type in these tracks to be included in the intervals $(N_i, N_i + dN_i)$ ($i = 1, 2, \ldots m$), with τ falling in the interval $(\tau, \tau + d\tau)$.

The total change in the density of the particles of type i at the point r, resulting from all of the tracks, $\nu_i(t, \mathbf{r})$, can be found by summing n_i over all of the tracks which have been formed in the irradiated volume V from the beginning of irradiation (t = 0) up to the instant t. It is clear that $\nu_i(t, \mathbf{r})$ represents the total density of the particles of the i-th type at the point r at the instant t.

If it is supposed that the number of tracks formed in each element of volume, dV, in each element of time, dt, is very great, it will then be possible to replace summation by integration, writing

$$\begin{gathered}\nu_i(t,\ \mathbf{r}) = \int_0^t dt' \int \delta\tau \int_0^{N_{1\max}} dN_1 \int_0^{N_{2\max}} dN_2 \ldots \int_0^{N_{m\max}} dN_m \times \\ \times w([\tau], N_1, \ldots, N_k, \ldots, N_m, t-t') n_i([\tau], N_1, \ldots, N_k, \ldots, N_m, t, t', \mathbf{r}),\ (1)\end{gathered} \tag{1}$$

where the τ range will cover all τ values corresponding to tracks formed in the volume V, and $N_{i\ \max}$ designates the largest of all of the values of N_i which are met in the entire course of the irradiation.

It is now possible to derive an equation which must be satisfied by the functions n_i. Let us consider the elementary volume dV with the radius vector r, and the time interval (t, t + dt). At the instant $t_0 = t - t'$, let one track be formed which at this moment contains N_i ($i = 1, 2, \ldots, m$) particles of each type, the initial distribution being determined by τ. Over the time dt, the formation of this track brings about an alteration in the number of particles of the i-th type in the volume element dV which is equal to $\frac{\partial(n_i + \nu_i)}{\partial t}$ dV dt. It is clear that this alteration is also equal to $\Gamma_i([n_i])$ dV dt, the number of particles of the i-th type which diffuse into the volume element dV in the time dt, minus the sum over j of $R_{ij}([(n_i + \nu_i)(n_j + \nu_j)])$ dV dt, the number of particles of the type i recombining in this same time in this same element of volume with particles of the type j, plus $S_i([\tau], N_i, t, t', \mathbf{r})$ dV dt, the change in the number of particles of the type i in the time dt in the volume element dV resulting from the passage of the given ionizing particle.

We are thus led to the equation:

$$\frac{\partial n_i}{\partial t} = \Gamma_i([n_i]) - \sum_j R_{ij}([(n_i + \nu_i)(n_j + \nu_j)]) - \frac{\partial \nu_i(t,r)}{\partial t} + S_i([\tau],\ N_i,\ t, t',\ \mathbf{r}), \tag{2}$$

in which Γ_i is a linear differential expression in n_i, and R_{ij} is a bilinear functional, or a bilinear function. (2) is an integrodifferential equation, since ν_i is fixed by equation (1).

It should be noted that S_i will depend only on t', and not on t, for irradiation under steady conditions of a medium of constant properties. At high irradiation densities, however, the properties of the irradiated medium can alter so rapidly that a dependence of S_i on t must be taken into account.

It follows from the derivation itself that equation (2) essentially describes only bimolecular reactions; no account is taken in it of the possibility of secondary reactions.

We will now consider certain special cases.

In the instance of the interaction between high-density radiation and a polymer, there is almost no diffusion of the polymer radicals, and the first member of the right-hand side of equation (2) can be neglected; here the solution of (2) is greatly simplified.

At high irradiation density in reactions which yield atomic hydrogen (and this is especially important for the radiation chemistry of the hydrocarbons), the system (2) must include an equation describing the diffusion, and various types of reactions, of the hydrogen atoms; when the radiation density is low, this member can be, and usually is, neglected.

At low irradiation densities, ν_i can be neglected in (2), and this system of equations describing the processes in a single track can then be written as:

$$\hat{L}_i n_i = -\sum_j R_{ij} + S_i, \tag{3}$$

where $\hat{L}_i$ is the linear operator determined from the equation

$$\hat{L}_i n_i \equiv \frac{\partial n_i}{\partial t} - \Gamma_i([n_i]). \tag{4}$$

We will now outline an approximation method for the solution of the system of equations (3), which is suitable for cases in which recombination is much slower than diffusion. Since recombination is bilinear in n_i and n_j and diffusion depends only linearly on n_i, this condition will be fulfilled for those tracks which are formed by particles yielding low-density ionization(electrons or photons). Before giving the method of its solution, we will first transform (3) into an integral equation. Let $g_i(\mathbf{r}, \mathbf{r}_1, t, t_1)$ be the Green function corresponding to the operator $\hat{L}_i$. Equation (3) can then be written in the form

$$n_i = -\sum_j \widetilde{R}_{ij}([n_i n_j]) + \widetilde{S}_i, \tag{5}$$

where for any function $F(\mathbf{r}, t)$,

$$\widetilde{F}(\mathbf{r}, t) = \int_V d\mathbf{r}_1 \int_0^\infty dt_1 F(\mathbf{r}_1, t_1) g(\mathbf{r}, \mathbf{r}_1, t, t_1). \tag{6}$$

The method which we propose involves solution of (5) with the aid of integration. Having supposed that recombination is much slower than diffusion, it is possible to assume in the 0-th approximation that

$$n_i^{(0)} = \widetilde{S}_i. \tag{7}$$

Setting (7) into (5), we find that

$$n_i^{(1)} = -\sum_j \widetilde{R}_{ij}([\widetilde{S}_i \widetilde{S}_j]) + \widetilde{S}_i. \tag{8}$$

Continuing this process, we find that in the l-th approximation the function n_i can be written as:

$$n_i^{(l)} = -\sum_j \widetilde{R}_{ij}([n_i^{(l-1)} n_j^{(l-1)}]) + \widetilde{S}_i. \tag{9}$$

Setting approximate expressions for n_i [which can be calculated to any desired degree of accuracy from equation (9)] into (1), we find that

$$\begin{gathered} \nu_i^{(l)} = \int_0^t dt' \int \delta\tau \int_0^{N_{1\,\max}} dN_1 \ldots \int_0^{N_{k\,\max}} dN_k \ldots \int_0^{N_{m\,\max}} dN_m \cdot w([\tau], N_1, \ldots \\ \ldots, N_k, \ldots N_m, t - t') \Big\{ -\sum_j \widetilde{R}_{ij}([n_i^{(l-1)} n_j^{(l-1)}]) + \widetilde{S}_i \Big\}. \end{gathered} \tag{10}$$

The number of recombinations of particles of the types $\underline{i}$ and $\underline{j}$ per unit volume per unit time, being summed, as it is, over all of the tracks, is equal to

$$\rho_{ij} = \int_0^t dt' \int \delta\tau \int_0^{N_{1\max}} dN_1 \ldots \int_0^{N_{k\max}} dN_k \ldots \int_0^{N_{m\max}} dN_m w([\tau], N_1, \ldots, N_k, \ldots \qquad (11)$$
$$\ldots, N_m, t - t') R_{ij}([n_i n_j]).$$

Setting $n_i^{(l-1)} n_j^{(l-1)}$ into (11) in the place of $n_i n_j$, we obtain an approximation for ρ_{ij}:

$$\rho_{ij}^{(l)} = \int_0^t dt' \int \delta\tau \int_0^{N_{1\max}} dN_1 \ldots \int_0^{N_{k\max}} dN_k \ldots \int_0^{N_{m\max}} dN_m w([\tau], N_1, \ldots, N_k, \ldots \qquad (12)$$
$$\ldots, N_m, t - t') R_{ij}([n_i^{(l-1)} n_j^{(l-1)}]).$$

Through the equations which have been derived here, it is possible to determine the number of free radicals and final products from the radiolysis, the calculation being reduced to the solution of the diffusional equation satisfied by g and evaluation of quadratures.

The proposed method is suitable for calculations on a discreetly acting electrical calculating machine since the successive approximations can be evaluated on such machines without the necessity of setting up separate programs for each integration.

It is to be noted that equation (3) can be looked upon as the equation of the 0-th approximation when the interaction of the tracks is weak. Introducing its solution into (1) in place of n_i, we obtain an approximation for ν_i which can be set into (2). Under these conditions, the solution of equation (2) will approximately allow for the effect of the remaining tracks; at that level, this is equivalent to the introduction of a background [2]. In principle, any desired degree of accuracy can be attained by repeating the above-described process several times.

Note added during the correction of proofs. A paper [3] presenting experimental curves covering the relation between ν and t for solid oxalic acid, during irradiation with rapid electrons at low dose strengths, and immediately after breaking off irradiation, appeared after the present work was ready for the press. If the member $\Gamma([n])$ in (3) is neglected, calculations which we have carried out show that the $\nu(t)$ function obtained through (1) will well describe the experimental curves of [3] for all t. Despite the affirmations of [3], it proves to be so that: a) saturation is not reached in irradiation, b) the coefficient k of [3] is not the coefficient of recombination, since it is inversely proportional to the dose received by the substance during the period of its irradiation.

LITERATURE CITED

[1] A. Shapiro, Radiation Res., 6, 11 (1957).

[2] J. L. Magee, J. Am. Chem. Soc. 73, 3270 (1951).

[3] Yu. N. Molin, A. T. Koritskii, N. Ya. Buben and V. V. Voevodskii, Proc. Acad. Sci. USSR, 124, 121 (1959).*

Received December 10, 1958

---

*Original Russian pagination. See C. B. Translation.

THE INFRARED SPECTRA OF NITRIC OXIDE ADSORBED ON FERRIC AND CHROMIC OXIDES

L. M. Roev and Academician A. N. Terenin

The A. A. Zhdanov State University, Leningrad

The molecule of NO with its unpaired electron can readily enter into covalent binding, either giving up an electron to form the cation NO^+ or combining with an electron to form the anion NO^-. In earlier papers from this laboratory [1], it has been shown that the alteration in the frequency of the infrared absorption band of the NO molecule can serve as a criterion for judging the behavior of the latter as an electron acceptor, or electron donor, in intermolecular compounds and complexes. Whereas the frequency of the neutral molecule in the gaseous state lies at 1876 cm^{-1}, this band falls within the range 2000-2400 cm^{-1} when an electron is lost to form a positive ion, and within the range 1000-1100 cm^{-1} when a negative ion is formed.

The oxides of the transition metals with their incomplete d-orbits are catalysts for many reactions. It has been assumed [2] that adsorption on these metals involves participation of the d-orbits of the metallic atoms with the formation of covalent bonds. In the present work, investigation has been made of the infrared absorption spectra of NO on ferric and chromic oxides, the aim being to use the above-mentioned spectral criterion for detecting the presence of electron-acceptor centers on these surfaces.

The adsorbents in powdered form were deposited on films of CaF_2. In mass units, the specimen thickness was about 5 mg/cm^2. The specimens were held in vacuum at 150° for several hours. Measurements over the frequency range 1000-2300 cm^{-1} were carried out on an IKS-11 spectrometer with a NaCl prism. The spectra presented below give the ratio I/I_0, I_0 being the transmission of the specimen prior to, and I the transmission after, adsorption. The spectral width of the slit varied from 10 to 20 cm^{-1}. Each of the spectra which are presented were recorded 2-3 times, with good reproducibility. The nitric oxide was obtained through the reaction of potassium nitrite and potassium iodide in sulfuric acid, and was purified by passage through a trap cooled with dry ice; P_2O_5 was used for dehydrating the gas.

NO on Fe_2O_3. A ferrigel with a specific surface of the order of 100 m^2/g* was employed as the adsorbent. Gas adsorption was carried out at 20° and at 150° with no detectable difference in the spectra.

The infrared spectrum of molecular NO adsorbed on ferrigel is reproduced in Fig. 1. The spectrum of gaseous NO did not appear at the pressure (30 mm), and cell depth which were employed. A comparison of curves 1 and 2 of Fig. 1 shows that the number of bands is not influenced by an increase in the time of contact of the gas, but there is an increase in the intensities of the bands at 1865, 1806, and 1770 cm^{-1}. On freezing out the gas with liquid air and evacuating the adsorbent, the relative intensities of the bands at 1806 and 1738 cm^{-1} diminish, and the bands at 1865 and 1770 cm^{-1} disappear (Fig. 1, 3). The spectral curve 4 was observed after desorption of the gas at 150°.

A comparison of the observed spectra with the spectrum of liquid nitric oxide presented schematically at the bottom of Fig. 1, makes it possible to identify the bands at 1865 and 1770 cm^{-1} with bands of liquid NO containing the dimer N_2O_2 [3]. Clearly, dimerization occurs during the condensation of the gaseous molecules in the narrow pores of the adsorbent. Two groups of bands are present in the NO absorption spectrum; one at

---

*We wish to express our indebtedness to T. G. Plachenov and G. M. Belotserkovskii for their immeasurable help in furnishing these gel specimens.

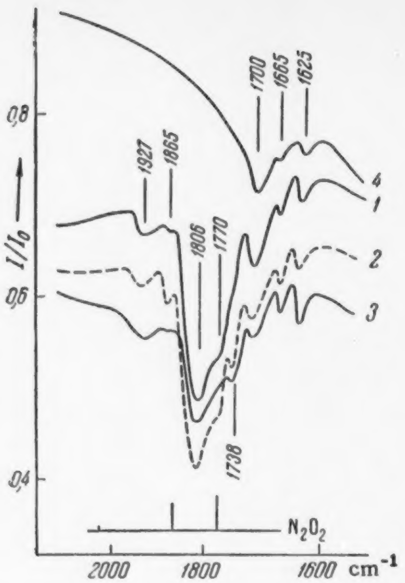

Fig. 1. Infrared absorption spectra of NO adsorbed on a Fe_2O_3 gel: 1) after 20 minutes of adsorption of the gas (20 mm of Hg) at 20°; 2) after 12 hours of adsorption at 20°; 3) after evacuation for 1 hour at 150°; 4) after desorption of the gas at 150°.

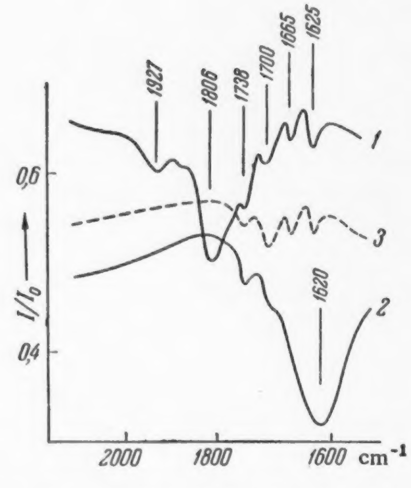

Fig. 2. The effect of the admission of O_2 to NO adsorbed on a Fe_2O_3 gel: 1) adsorbed NO after 1 hour of evacuation at 20°; 2) after 1 hour in the presence of O_2 (200 mm of Hg); 3) after 30 minutes of evacuation at 20°.

1625, 1665, and 1700 cm^{-1}, and the other at 1738, 1806, and 1927 cm^{-1}; the second of these groups disappears on evacuation at 150°, as is seen from Fig. 1, leaving the first group which disappears only on evacuation at 350°.

The alterations which arise in the spectrum of the adsorbed NO molecules from the introduction of oxygen are sketched in Fig. 2. The result in the one group is the disappearance of the bands at 1927 and 1806 cm^{-1} and the appearance of a high-intensity band at 1620 cm^{-1}, whereas in the other group (1625-1700 cm^{-1}), the bands do not disappear (curve 3). These latter bands clearly belong to molecules of NO which are firmly chemosorbed and are incapable of reacting with O_2, while the group of bands at 1738, 1806, and 1927 cm^{-1} belongs to the less firmly adsorbed molecules which react with the oxygen, forming NO_2; obviously, it is to this latter compound that the intense band at 1620 cm^{-1} is to be ascribed.

The bands of the strongly chemosorbed NO molecules at 1700, 1665 and 1625 cm^{-1} can be ascribed to the formation of covalent bonds with the oxygen atoms of the adsorbent. In fact, according to the data of Tarte [4], the absorption band of the group $-O-N=O$ is to be found in the frequency range 1690-1610 cm^{-1}. Moreover, absorption bands, together with the known dimer bands which have been referred to above have been detected by us in this same region in the adsorption of NO on silica gel, aluminogel and aluminosilicate catalysts.

In comparison with the gas, the bands at 1806 and 1738 cm^{-1} are displaced toward the long wavelengths; they should be ascribed to molecules of NO which have entered into coordination, or covalent, binding with the iron atoms of the surface. This interpretation is based on the values of the frequencies 1800 and 1844 cm^{-1}, these same frequencies being observed in the nitrosylhalides where the NO forms covalent bonds with the halogen [5, 6]. It is natural to ascribe the band at 1927 cm^{-1}, with a frequency greater than that of the gaseous NO molecule, to donor interaction with the adsorbent and accompanying formation of a cation.

NO on Cr_2O_3. Specimens of chromic oxide obtained by ignition of ammonium dichromate* were investigated and, also, specimens of a chrome gel with a high specific pore surface (200 m^2/g). For each of these adsorbents, gas adsorption at 20°, and at 150°, gave the same spectrum. The spectra sketched in Fig. 3 show that a number of bands can be identified with bands which were observed in the case of the ferrigel. The bands at 1625, 1663, and 1698 cm^{-1} are to be ascribed to molecular NO, which is presumably adsorbed on the oxygen atoms. The bands at 1734, 1810, and 1842 cm^{-1} are at frequencies lower than those for the molecular gas, and these we also ascribe to covalent, or coordination, binding with the metal atoms. From the criterion mentioned earlier, the bands of higher frequencies at 2028 and 2093 cm^{-1} are

---

[*] At our request, this compound was kindly prepared by V. A. Komarov of the Chemical Faculty of the Leningrad State University, to whom we express our deep gratitude.

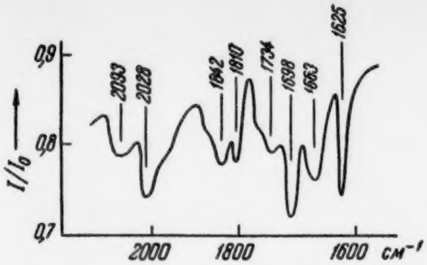

Fig. 3. Infrared absorption spectra of NO adsorbed on Cr_2O_3. Gas adsorption (20 mm of Hg) for 30 min at 20° with subsequent evacuation for 1 hour at 20°.

known to belong to the form NO^+, i.e., to the donor bonding of the molecules with the chromium atoms of the surface. The presence here of two frequencies, instead of one, probably arises from state differences in the adsorption centers, or may even be due to a simultaneous addition of two molecules, such as is observed in the case of CO chemosorbed on Pd [7]. The bands at 1842, 1810, and 1734 cm^{-1} are at frequencies lower than those of the gaseous molecules and can, as in the case of the ferrigel, be ascribed to covalent, or coordination, bonding with chromium atoms on the surface. It should be noted that the number of bands is greater for the adsorption of NO on chromium than for the adsorption on iron. The appearance of many vibrational frequencies as the result of the adsorption of NO on the same centers indicates the existence of differences, not only in the centers themselves, but also in their mode of interaction with the molecules.

It was not possible to detect a band of molecular adsorption in the region 1000-1200 cm^{-1}, where the band for the NO^- ions might be expected to appear.

SUMMARY

Proof has been given for the existence of three types of centers for the adsorption of NO on the oxides of iron and chromium, these being manifest through differences in the magnitude, and the direction of displacement, of the infrared absorption bands relative to the gas. Covalent bonding, obviously with the metallic atoms, occurs on these types of centers. On the centers of the second type there is donor binding, the state of the NO molecule approximating the electron configuration of NO^+. These centers clearly belong to the metal ions, since we have observed a similar displacement in the case of NO chemosorbed on dispersed iron. The centers of the third type arise from the formation of strong covalent bonds between the NO and the oxygen atoms of the oxide.

LITERATURE CITED

[1] V. I. Filimonov, D. S. Bystrov and A. N. Terenin, Optics and Spectroscopy, 3, 480 (1957).

[2] B. Treinel, Chemical Adsorption (Russian translation), Foreign Lit. Press, 1958.

[3] A. L. Smith, W. E. Keller and H. L. Johnston, J. Chem. Phys. 19, 189 (1951).

[4] P. Tarte, J. Chem. Phys. 10, 1570 (1952).

[5] W. G. Burns and H. J. Berstein, J. Chem. Phys. 18, 1669 (1950).

[6] D. W. Magnuson, J. Chem. Phys. 20, 380 (1952).

[7] A. S. Yang and S. W. Garland, J. Phys. Chem. 61, 1509 (1957).

Received January 28, 1959

ADSORPTION OF PENICILLIN ON POLYMERIC ADSORBENTS

G. V. Samsonov, V. V. Vedeneeva and A. A. Selezneva

Institute of High-Molecular Compounds of the Academy of Sciences USSR,
Leningrad Chemico-Pharmaceutical Institute

(Presented by Academician M. M. Shemyakin, December 12, 1958)

Penicillin is quite a strong acid. Thus the pK_a of benzylpenicillin is approximately 2.7 [1]. As a result of this, penicillin can be adsorbed on weak anion exchange resins, for example, resins prepared by the condensation of metaphenylenediamine [2, 3], as well as on strong ones synthesized by the chloromethylation of styrene and the condensation of the resulting product with tertiary amines [4, 5]. The amount of penicillin adsorbed depends on the compactness of the resin. On a strongly basic anion exchange resin (amberlite IRA-400), when the coefficient of swelling is decreased by a factor of 4-4.5, the adsorbing capacity of the resin (with respect to penicillin) is decreased by a factor of 32 [5].

Despite the large adsorption of penicillin on various anion exchange resins, its purification encountered several substantial difficulties. Thus, for example, a great number of anion exchange resins would adsorb penicillin reversibly from aqueous solutions in the absence of extraneous products, but irreversibly from culture solutions.

The data listed in Table 1 show that the principal cause of the irreversible adsorption of penicillin from culture solutions rests in the presence of sulfates, phosphates, and anions of other acids. After these anions were precipitated with barium the penicillin adsorption became almost completely reversible, although the adsorbability did not increase. Thus, for example, the amount of penicillin adsorbed from solutions containing sodium phosphate was greater than from the culture solution after precipitation of $SO_4^{=}$ and $PO_4^{\equiv}$; nevertheless, in the first case we were able to desorb less than one fourth of the penicillin, while in the second almost all the penicillin could be desorbed. All this points to a possible additional interaction between penicillin and the phosphate and sulfate anions adsorbed alongside it. As we shall demonstrate later on, a hydrogen bond is formed between these compounds.

The complex nature of the interaction between penicillin and the anion exchange resin makes it essential to investigate the possibility of applying the fundamental anion exchange laws to this phenomenon. As one may see in Fig. 1 we are dealing here with an equivalent ionic exchange, where the number of chloride ions desorbed from the ÉDÉ-10 exchange resin is equal to the number of adsorbed penicillin molecules.

As we have already noted, penicillin can be almost entirely desorbed from anion exchange resins by use of sodium phosphate and sulfate solutions, provided these anions had not been previously adsorbed on the resin. It seems that this can be explained by the fact that the additional bond formation between penicillin and the adsorbed anions takes some time. When aqueous solutions are used as eluents, despite the full yield, desorption of penicillin proceeds very slowly with the formation of a chromatographic tail (Fig. 2). Yet the addition of only 10% acetone increases the maximum concentration of penicillin in the eluate by a factor of three, and the average concentration by more than five. Disregarding the factors which were important in the desorption of the tetracyclin group of antibiotics as a result of transition to nonaqueous solvents [6], and which were connected with the formation of a sharp boundary in the dynamic ionic exchange process, it seems that in our case the acetone was able to form hydrogen bonds, and consequently also disturb those already existing. The probability that such a process is real becomes even greater due to the fact that addition of 0.1% urea (a compound capable of forming hydrogen bonds) improves the desorption of penicillin to the same extent as acetone.

The utilization of an anion exchange method for the separation and purification of penicillin by starting

TABLE 1

Reversible Adsorption of Penicillin on an ÉDÉ-10 Anion Exchange Resin. Desorption by an Aqueous Solution Containing 10% Acetone, 0.25 N Na_2HPO_4, and 0.25 N Na_2SO_4

Initial solution	Adsorbability, mequiv./g	Desorption, %
Penicillin G, 3000 units/ml	3.71	99.5
Penicillin V, 3000 units/ml	3.3	97
Mother liquor of penicillin G	0.041	18
Mother liquor of penicillin V	0.048	13.8
Penicillin G, 3000 units/ml in 0.02 N Na_2SO_4	0.248	22.5
Penicillin G, 3000 units/ml in 0.2 N Na_2HPO_4	0.403	22.7
Penicillin G, 3000 units/ml in 0.02 N $Na_2C_2O_4$	0.308	18.0
Penicillin G, 3000 units/ml in 0.02 N NaCl	0.96	97.7
Penicillin G, 3000 units/ml in 0.02 N CH_3COONa	1.4 0.149	97.7 95.5
Mother liquor of penicillin G after precipitation of phosphates and sulfates		
Mother liquor of penicillin V after precipitation of sulfates and phosphates	0.284	93

TABLE 2

Adsorbability of Penicillin on Cation Exchange Resins

Cation exchange resin	Functional group	Adsorbability units/g · 10^3
SbS-3	$-SO_3Na$	175
SKhV	$-SO_3Na$	95
PF	$-PO_3H_2$	200
KFU	$-COONa$	100
KFUKh	$-COONa$	100
KFUKh	$-COOH$	275

TABLE 3

Desorption of Penicillin by 0.1% Urea

Resin	Functional group	Desorption yield, %
SKhV	$-SO_3Na$	93
KFUKh	$-COOH$	96
KFUF	$-COONa$	93
KB-4P-2	$-COOH$	90
KB-4P-2	$-COONa$	92

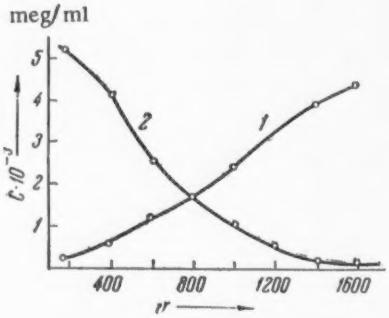

Fig. 1. Equivalent exchange between penicillin and chloride ions on an ÉDÉ-10 anion exchange resin, 1) penicillin; 2) chloride.

with a culture solution is based on the principles (put forth in this paper) of a reversible selective adsorption and desorption of penicillin on anion exchange resins. The choice of exchange resins plays a very important part in this process. A transition from a moderately basic resin ÉDÉ-10 to strongly basic ones, such as AV-16 and SMA, greatly increases the selectivity of penicillin adsorption. Specific extraction of penicillin by anion exchange resins from culture solutions, followed by desorption and precipitation, yields pure penicillins V and G.

The effect of sulfate and phosphate anions on the reversibility of penicillin adsorption on anion exchange resins was explained by the formation of additional bonds between the adsorbed anions. In connection with this there arose a hypothesis that it should be possible to adsorb penicillin on cation exchange resins which contain sulfate and phosphate radicals. The study of this phenomenon enabled us to work out a basically new application of selective penicillin adsorption. The results presented in Table 2 show that penicillin is strongly adsorbed on sulfate, phosphate, and carboxyl cation exchange resins.

One could assume that such a great adsorbability was connected with the formation of hydrogen bonds between the peptide groups in penicillin and the oxygens of the corresponding acidic groups. To prove this assumption we determined the infrared spectra of penicillin adsorbed on a thin film of a sulfate cation exchange

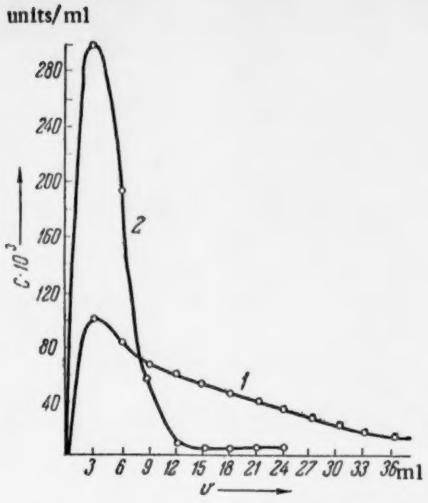

Fig. 2. Outgoing penicillin desorption curves on ÉDÉ-10 anion exchange resin. 1) 0.25 N Na_2HPO_4 and 0.25 N Na_2SO_4; 2) 0.25 N Na_2HPO_4, 0.25 N Na_2SO_4, 10% acetone.

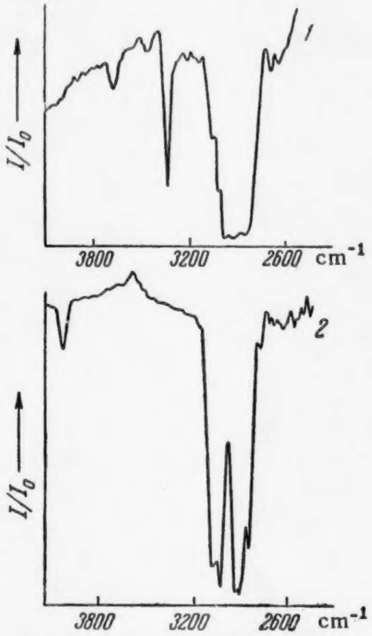

Fig. 3. Infrared spectra of penicillin. 1) Penicillin; 2) penicillin adsorbed on film (sulfate cation exchange resin).

resin prepared from sulfostyrene and divinylbenzene. We found that the characteristic absorption band (~ 3300 cm^{-1}) disappeared after penicillin was adsorbed (Fig. 3). In view of the fact that it is impossible to form an ionic bond with the peptide group, this effect can only be ascribed to the formation of a hydrogen bond between penicillin and the adsorbent. The same can be deduced from the fact that penicillin can be almost completely desorbed from cation exchange resins by a 0.1% urea solution (Table 3); as is well known, urea can form hydrogen bonds and is frequently used to break the hydrogen bonds in albumen. All these results indicate that the formation of hydrogen bonds between the adsorbent and the adsorbate is a new form of adsorption, the existence of which was previously experimentally demonstrated by Terenin and co-workers [7] in the adsorption of amines on silica gel.

The fact that penicillin can be adsorbed on cation exchange resins due to an interaction between its peptide group and the adsorbent can obviously be utilized for the separation of penicillinfrom other acids, the great majority of which do not possess similar properties. In fact, through a simple direct process one can fully separate penicillin G from, for example, phenylacetic acid, which is not adsorbed on cation exchange resins at all. The specific adsorption of penicillin on cation exchange resins constitutes one of the most effective processes for its fine purification. The possibility of a full desorption makes this method especially successful in the separation and purification of pencillins V and G.

We want to thank V. N. Nikitin and E. I. Pokrovskii for running the infrared spectra of penicillin.

LITERATURE CITED

[1] M. M. Shemyakin and A. S. Khokhlov, Chemistry of Antibotics, 1949, p. 284.*

[2] R. Kubo and D. Sasano, Jap. Pat. 2496 (51); Chem. Abstr. 47, 834 (1953).

[3] D. Sasano, Jap. Pat. 4499 (53); Chem. Abstr. 48, 9632 (1954).

[4] Ch. H. McBurney, Patent USA, 2689227; Chem. Abstr. 49, 1285 (1955).

[5] R. Kunin and R. J. Myers, Disc. Farad. Soc. No. 7, 114 (1949).

[6] G. V. Samsonov, S. E. Bresler and N. A. Rozentsveig, Colloid J. 18, No. 4 (1956).**

[7] A. N. Terenin, Coll. Chemical Surface Compounds and Their Role in Adsorption Phenomena, Moscow, 1957, p. 206.*

Received December 9, 1958

---

* In Russian.

** Original Russian pagination. See C. B. Translation.

KINETIC POLAROGRAPHIC CURRENTS FROM THE DELAYED DISCHARGE OF THIOCYANATE COMPLEXES OF NICKEL

Ya. I. Tur'yan and G. F. Serova

The Kishinev State University

(Presented by Academician A. A. Grinberg, December 10, 1958)

With a view to elucidating the nature of the three waves of nickel thiocyanate complexes (Fig. 1) which had been discovered earlier [1], we investigated the relationship between the wave heights, the concentration of KCNS ($\mu = 1$: KCNS + KNO_3) at $C^0_{Ni^{2+}}$ = const (0.140 mmole/1), and the concentration of nickel at C_{CNS^-} = = const (12.6 mmole) (Fig. 2, and Table 1). The capillary characteristic was:

$$m^{2/3}t^{1/6} = 1{,}81 \text{ mg}^{2/3} \text{ sec}^{-1/2} (t = 2{,}4 \text{sec}).$$

A study of the effect of the elevation of the mercury reservoir on the values of the limiting currents showed that i_k and Σi_k (Fig. 1) were kinetic currents, and i_d (Fig. 1) was a diffusional current.

Using [2], in which determination was made of the dissociation constants of the nickel thiocyanate complexes, it can be shown that, in principle, only the Ni^{2+} and the $NiCNS^+$ ions diffuse to the electrode in the investigated interval of KCNS concentrations.

The following scheme will be accepted as determining the limiting currents for the electrode processes: first wave

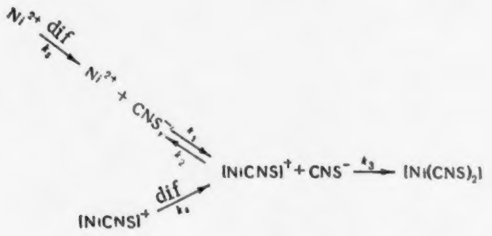

(1)

first wave + second wave

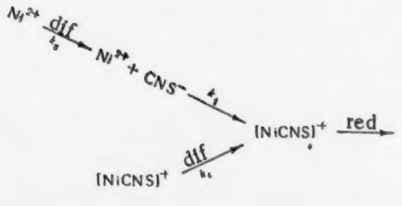

(2)

first wave + second wave + third wave

$$\mathrm{Ni}^{2+} \xrightarrow[k_s]{\text{dif}} \mathrm{Ni}^{2+} \xrightarrow{\text{red}}$$

$$[\mathrm{NiCNS}]^{+} \xrightarrow[k_c]{\text{dif}} [\mathrm{NiCNS}]^{+} \xrightarrow{\text{red}} \tag{3}$$

For the time being, the question will be left open as to which ion it is that undergoes reduction at the potentials of the first wave. This could be a particle of $\mathrm{Ni(CNS)_2}$, or, according to [3], of a complex of anodic type resulting from a very rapid reaction between $\mathrm{Ni(CNS)_2}$ and $\mathrm{CNS^-}$.

The total height of the i_d wave should be fixed by the diffusion rate, according to the scheme of [3], and this is actually observed in practice.

In order to obtain equations describing the relationship between $C_{\mathrm{CNS^-}}$, and the kinetic currents i_k and Σi_k, recourse will first be had to the approximation theory of Brdicka and Weisner [4, 5]. Taking (1) into account

$$i_k = \frac{\frac{k_s}{a}(i_d - k_s C_M) + \mu_1 k_1 C_X i_d}{\frac{k_s}{a} + \frac{k_c}{a}\frac{\mu_1 k_1}{\mu_3 k_3} + \frac{k_s}{a}\frac{1}{\mu_3 k_3 C_X}\left(\frac{k_c}{a} + \mu_1 k_1 K_1\right) + \mu_1 k_1 C_X}; \tag{4}$$

can be obtained from this theory; here k_s and k_c are the constants of the diffusional currents of Ni^{2+} and of NiCNS^+, respectively, C_M is the concentration of the simple Ni^{2+} ions at a thiocyanate concentration C_X, $a = nFq \cdot 10^{-3}$ (q is the mean surface area of the mercury drop), i_1 and k_3 are reaction velocity constants [see scheme (Σ)], μ_1 and μ_3 are the depths of the corresponding reaction layers, and K_1 is the dissociation constant for NiCNS^+.

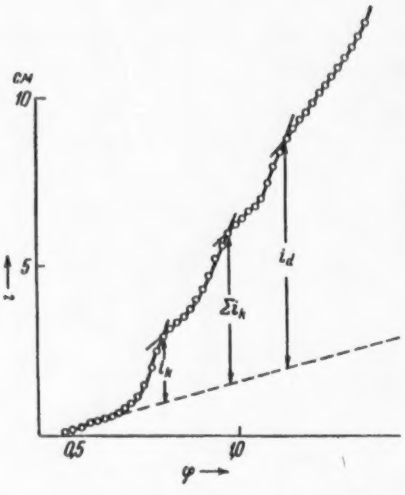

Fig. 1. Polargram of Ni^{2+} on a $7.84 \cdot 10^{-3}$ M KCNS + 1 M $\mathrm{KNO_3}$ background.

An expression for the kinetic current Σi_k can be found from (4) by assuming that $k_3 \gg k_s \gg k_3 \gg k_c$, and $k_3 \gg k_1$:

$$\Sigma i_k = \frac{\frac{k_s}{a}(i_d - k_s C_M) + \mu_1 k_1 C_X i_d}{\frac{k_s}{a} + \mu_1 k_1 C_X}, \tag{5}$$

here k_3 is to be calculated from the value of i_d in 1 M $\mathrm{KNO_3}$, and k_c determined by a graphic method based on the equation

$$i_d = k_c C_M^0 - -(k_c - k_s) C_M^0 K_1 \frac{1}{K_1 + C_X}, \tag{6}$$

which follows from the relations

$$i_d = k_s C_M + k_c C_{MX}; \tag{7}$$

$$C_M^0 = C_M + C_{MX}; \tag{8}$$

$$K_1 = \frac{C_M C_X}{C_{MX}}. \tag{9}$$

From Fig. 3, it is to be seen that i_d depends linearly on $\frac{1}{K_1 + C_X}$, just as is to be expected from equation (6). This is indirect confirmation of the correctness of the dissociation constants which were obtained in [2]. Extrapolation of the straight line to $\frac{1}{K_1 + C_X}$ gives $k_c C_M^0$. The result, $k_c > k_s$ ($D_{[\mathrm{NiCNS}]^+} > D_{[\mathrm{Ni}]^{2+}}$), explains the increase of i_d with increasing C_X (Fig. 2).

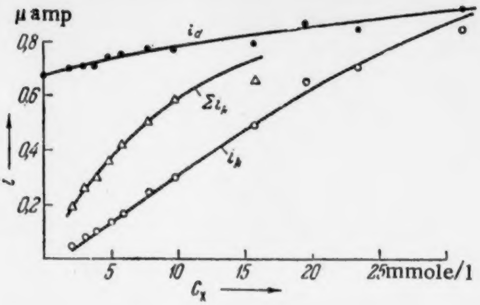

Fig. 2. The dependence of the kinetic, and the diffusional, currents on the thiocyanate concentration.

On setting $\mu_1 k_1 = 0.23$ cm · sec^{-1} (mole /l)$^{-1}$ and $\mu_3 k_3 = 1.3$ cm · sec^{-1} (mole /l)$^{-1}$, good agreement is found between $i_{k,\mathrm{cal.}}$ and $\Sigma i_{k,\mathrm{cal.}}$ [equations (4) and (5)], and the corresponding experimental values (see Fig. 2; the curves correspond to experimental, and the points, to calculated, values).

Using Weisner's equation, and assuming $D_{[\mathrm{NiCNS}]^+} = D_{\mathrm{Ni(CNS)_2}}$, the reaction velocity constants, $k_1 = 3.5 \cdot 10^2$ sec^{-1} (mole /l)$^{-1}$ and $k_3 = 3.8 \cdot 10^3$ sec^{-1} (mole/l)$^{-1}$, were obtained. As is to be seen, the velocity constant for the addition of $\mathrm{CNS^-}$ to $[\mathrm{NiCNS}]^+$ considerably exceeds the constant for the addition of a $\mathrm{CNS^-}$ ion to the $\mathrm{Ni^{2+}}$ ion.

A relation between i_k and C_M^0 can be obtained from (4), (7), (8), and (9); namely

$$i_k = \frac{\mu_1 k_1 C_X k_s \dfrac{K_1}{C_X + K_1} + \left(\dfrac{k_s}{a} + \mu_1 k_1 C_X\right) k_c \dfrac{C_X}{C_X + K_1}}{\dfrac{k_s}{a} + \dfrac{k_c}{a}\,\dfrac{\mu_1 k_1}{\mu_3 k_3} + \dfrac{k_s}{a}\,\dfrac{1}{\mu_3 k_3 C_X}\left(\dfrac{k_c}{a} + \mu_1 k_1 K_1\right) + \mu_1 k_1 C_X}\, C_M^0, \tag{10}$$

and, changing to Σi_k ($k_3 \gg k_s$, $k_3 \gg k_c$ and $k_3 \gg k_1$):

$$\Sigma i_k = \frac{\mu_1 k_1 C_X k_s \dfrac{K_1}{C_X + K_1} + \left(\dfrac{k_s}{a} + \mu_1 k_1 C_X\right) k_c \dfrac{C_X}{C_X + K_1}}{\dfrac{k_s}{a} + \mu_1 k_1 C_X}\, C_M^0 . \tag{11}$$

TABLE 1

The Relation Between the Concentration of Metal and the Limiting Currents for the First Wave (i_k), the First Wave + Second Wave (Σi_k), and the Total Wave (i_d), of Nickel. KCNS concentration, 12.7 mmole/l; h = 59 cm

$C_{\mathrm{Ni^{2+}}}$, mole/liter	i_k, μa	$\dfrac{i_k}{C_{\mathrm{Ni^{2+}}}}$ (mmole/ /liter)$^{-1}$	Σi_k, μa	$\dfrac{\Sigma i_k}{\mu\text{amp}}$ (mmole/l)	i_d, μa	$\dfrac{i_d}{C_{\mathrm{Ni^{2+}}}}$ μamp (mmole/l)
0,140	0,36	2,57	0,55	3,93	0,67	4,79
0,264	0,72	2,73	1,09	4,13	1,22	4,62
1,18	2,99	2,54	4,60	3,90	5,24	4,44
2,00	4,95	2,47	7,94	3,97	9,10	4,55
Average		2,58		3,98		4,60

From equations (10) and (11) with C_X = const, there follows that proportionality between C_M^0 and the kinetic current which is observed experimentally. The calculated values, $(i_k/C_M^0)_{\mathrm{theo}} = 2.54$ μ amp (mmole/l)$^{-1}$ and $(\Sigma i_k/C_M^0)_{\mathrm{theo}} = 3.88$ μ amp (mmole /l)$^{-1}$, are in good agreement with the experimental data (see table). This once more points to the validity of the theoretical assumptions, and to the correctness of the resulting values of the constants k_1 and k_3.

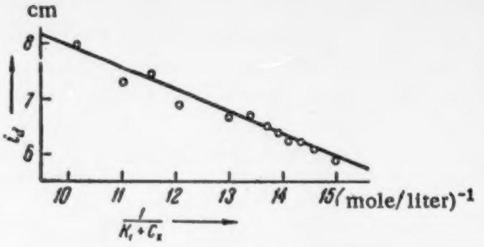

Fig. 3. Determination of the constant for the [NiCNS]$^+$ diffusion current.

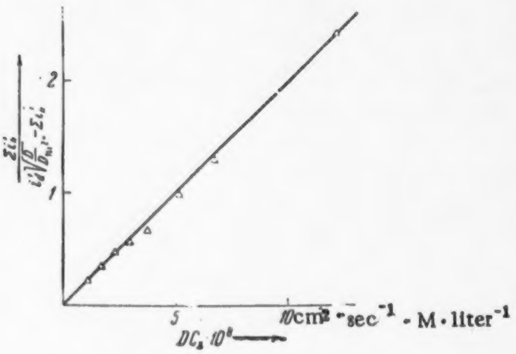

Fig. 4. Establishment of the nature of the kinetic current through the Koutecky equation.

In addition to the approximate theory, application to scheme (2) of the more exact Koutecky equation [6] was also made to the case in which the diffusional coefficients are different. Taking a simultaneous diffusion of [NiCNS]$^+$ into account, corrected expressions for Σi_k and i_d:

$$\Sigma i'_k = \Sigma i_k - k_c C_{MX}; \quad (12)$$

$$i'_d = i_d - k_c C_{MX}. \quad (13)$$

were introduced into the Koutecky equation.

After simple rearrangements, the Koutecky equation took the form [6]:

$$\frac{\Sigma i'_k}{i'_d \sqrt{D/D_{Ni^{2+}}} - \Sigma i'_k} = -0{,}87 \sqrt{\frac{D_{[NiCNS]^+} k_1 t_1}{D^3_{Ni^{2+}} K_1}} DC_X; \quad (14)$$

in which D is the mean diffusion coefficient.

It follows from Fig. 4 that equation (14) is in good agreement with the experimental results, i.e., that the proposed mechanism for the origin of the second kinetic wave is also confirmed by the more exact theory. (Fourteen) gives $k_1 = 0.9 \cdot 10^2$ sec^{-1} (mole/l^{-1}), i.e., a value which is less than the approximate by a factor of 1/4; this is in agreement with the results of [7] which, it is true, were obtained for identical values of the diffusion coefficients. The Budevskii correction to the Weisner equation brings the results closer to the exact value.

Because of the impossibility of taking into account a simultaneous diffusion of one of the intermediates of the reaction, we were, unfortunately, not able to apply the Koutecky equation of [9] to scheme (1), or to use the Koutecky equation of [10] for establishing the nature of the particles which undergo reduction.

LITERATURE CITED

[1] Ya. I. Tur'yan, J. Phys. Chem. 31, 2423 (1957).

[2] S. Fronaeus, Acta Chem. Scand. 7, 21 (1953).

[3] A. N. Frumkin and G. M. Florianovich, Proc. Acad. Sci. USSR 80, 907 (1951).

[4] R. Brdička and K. Wiesner, Coll. Czechoslov. Chem. Commun. 12, 138 (1947).

[5] K. Wiesner, Chem. Listy, 41, 6 (1947).

[6] J. Koutecky, Collected Czech. Chemical Commun. 19, 857 (1954).

[7] J. Koutecky, Collected Czech. Chemical Commun. 18, 597 (1953).

[8] P. Delehaye, New Equipment and Methods in Electrochemistry (Russian translation), Foreign Lit. Press, 1957.

[9] J. Koutecky, Collected Czech. Chemical Commun. 19, 1093 (1954).

[10] J. Koutecky, Collected Czech. Chemical Commun. 21, 1056 (1956).

Received December 6, 1958

THE DIMINUTION OF THE MELTING POINT OF WATER IN THE CAPILLARIES OF A POROUS BODY

V. A. Bakaev, V. F. Kiselev and K. G. Krasil'nikov
The Institute of Physical Chemistry of the Academy of Sciences of the USSR

(Presented by Academician M. M. Dubinin, December 24, 1958)

The relation between the diminution of the melting point of a substance, ΔT, and the radius of the capillary, r, in which this substance is adsorbed, has been studied in [1-5]. In these investigations, we determined the temperatures at which phase changes occurred in a substance adsorbed in pores, and proof was given [4, 5] that the ΔT, r relation is independent of the chemical composition of the adsorbent. Thus it is possible to obtain a quantitative characterization of the structure of a porous body from data on the temperature variation of the phase composition of an adsorbed substance, determination being made not only of the radii, but also of the volumes of the capillaries in which the phase transitions are occurring. This type of problem has not been treated in [1-5].

The amount of adsorbate, per 1 g of adsorbent, which is in the molten condition at the temperature T can be determined from the heat capacity of the adsorbent–adsorbate system. Obtaining direct and reasonably exact measurements over a wide temperature interval of the heat capacity of a heterogeneous system in which phase transformations are taking place is, however, an experimentally difficult problem. A simpler but still sensitive method involves the indirect evaluation of the heat capacity through measurement of the thermal diffusivity, λ. This latter quantity is related to the heat capacity, c, through the equation

$$\frac{k}{\rho}\,\frac{1}{\lambda}=c,$$

in which ρ is the density, and k, the coefficient of thermal conductivity, of the system. The amount of thermal energy which must be supplied to the system in order to heat it from the temperature T_1, where all of the adsorbate in the capillaries is in the solid form, to the temperature T, where a part of this adsorbate has passed over into the liquid state, is given by the expression

$$Q=\int_{T_1}^{T} c_0(T)\,dT+qF(T),$$

in which c_0 (T) is the heat capacity of the entire system, q is the specific heat of fusion of the adsorbate, and F(T) is the amount of liquid which has been formed at the temperature T. The heat of the phase transition over the working interval of temperature [7] is implicitly contained in the experimentally measured heat capacity, i.e.,

$$c=\frac{dQ}{dT}=c_0(T)+q\,\frac{dF(T)}{dT}$$

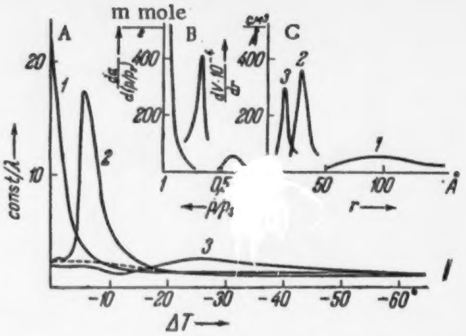

Fig. 1. A) The relation between the reciprocal thermal diffusivity* and the diminution of the melting point of water sorbed at $p/p_s = 1$ on specimens of BS-1 (1), KSK-2 (2)**, and KSM-1 (3), B) derivatives from the desorption branches of the 20° isotherms for the adsorption of water vapor, C) differential curves giving distributions of pore volumes over radii, as calculated from B by using equation (3).

In order to determine c from the thermal diffusivity data, the density, ρ, of the system, and its thermal conductivity, k, must also be known. These quantities alter with changing phase composition. k/ρ can be determined only for the limiting cases of T_1, where the adsorbate is in the solid state, and T_2, where the adsorbate has melted, i.e., only when the phase composition of the adsorbate in the capillaries is known. For water adsorbed on silica gel, evaluations of k/ρ which we have made for values of λ experimentally determined for these extreme cases prove to differ by no more than 10%. With a view to simplifying the calculations, it will be supposed that $k/\rho = \text{const.}$* Then

$$c = \frac{\text{const}^*}{\lambda} = c_0(T) + q\frac{dF(T)}{dT}.$$

Within the limits of this approach to the evaluation k/ρ, it is natural to assume the specific heats of water and ice, and the latent heat of transition, q, to be independent of the temperature. In this case, c_0 (T) will alter with change in the phase composition of the system, just as does F(T). dF(T)/dT can be found from the calorimetric measurements by a method of successive approximations. It should be noted that since the specific heat of fusion is large, the melting of even a relatively small amount of the substance, dF(T), can lead to a considerable alteration in c, and, accordingly, in λ also. Thus, despite the various assumptions which are involved in these calculations, this method can be used in practice for the determination of the volume of liquid which has been formed at a given temperature in the pores of an adsorbent.

Measurements of the thermal diffusivity of these systems were carried out by a modification of the method of "linear increase in temperature" [6]. The silica gels KSK-2 and KSM-1, and a specimen of the nonporous silica BS-1 were used as adsorbents; the adsorption isotherms for water vapor had been measured for these gels. These specimens were held in saturated water vapor until their weight remained constant, after which they were placed in the calorimeter for the determination of λ. Measurements of the thermal diffusivity were carried out from the temperature of liquid nitrogen (where it was assumed all of the water was in the frozen condition) up to 275°K. Figure 1A shows the const/λ temperature relations for the investigated specimens. In order to establish the dF/dT temperature relation, equation (1) shows that it is necessary to subtract from each of these curves the const/λ curve corresponding to c_0 (T). With the values of const λ obtained from various experiments at the extreme temperatures T_1 and T_2, it is possible to develop this curve by the method of successive approximations. Such a curve, calculated in a first approximation for the KSK-2 specimen, is presented in Fig. 1A. The dF(T)/dT curve must be integrated in order to obtain F(T), the volume of water formed expressed as a function of temperature. The results of graphic integration of such a curve for the KSK-2 specimen are shown in Fig. 2B. Since the function dF(T)/dT [and F(T), as well] contains a constant quantity which is not experimentally evaluated, the results of Fig. 2B are given in the relative units F(T)/F(273°), F(273°) being the total amount of water in the pores at 273°K.

The theory of capillary condensation establishes a relation between the lowering of the temperature of a phase transformation and the radius of the capillaries in which the sorbed material is held. Starting from the fact that a liquid in a capillary will solidify when the temperature is such that the vapor pressure of the liquid is the same as that of the substance in the solid state [8] has given the following equation to relate the freezing point of the liquid and the relative vapor pressure:

---

* Into the value of the "const" there enter the constants of the apparatus, and also such experimental constants as the density of coverage, etc.

** In view of the assumption involved in this calculation, there is no need of a second approximation for c_0 (T).

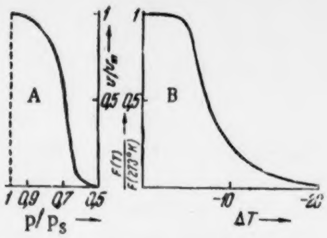

Fig. 2. A) Desorption branch of the isotherm giving the relative filling of the pore volume with water for the specimen of KSK-2, B) the relative amount of water formed at $\Delta T = 273° - T$ during heating of a specimen of KSK-2 which had been first saturated with water and then frozen.

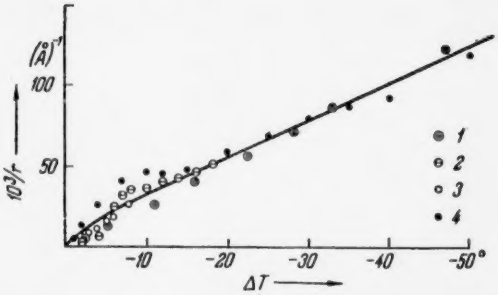

Fig. 3. The relation between the reciprocal pore radius and the diminution of the melting point of water. The points have been obtained from calculations on the data of [5] (1), and from measurements on the specimens KSK-2, BS-1 (3); and KSM-1 (4).

$$\ln\left(\frac{p}{p_s}\right)_{T_0} = \frac{\Delta H \Delta T}{RT_0T}, \qquad (2)$$

here T_0 is the normal melting point of the material which is under investigation, T is the melting point of this same substance in the capillary, ΔH is the heat of fusion, and $\Delta T = T - T_0$. On the other hand, when combined with the Kelvin equation, the theory of capillary condensation establishes a relation between the vapor pressure of a liquid in a capillary and the capillary radius, namely:

$$\ln \frac{p}{p_s}\left(\frac{\varphi(r)}{T}\right)_{T_0}, \qquad (3)$$

here $\varphi(r)$ is a function of the radius of the capillary. By setting this result into (2), a relation can be developed between the lowering of the melting point and the capillary radius:

$$\Delta T = \frac{RT}{\Delta H}\varphi(r) \qquad (4)$$

It should be noted that the ΔT, p/p_s relation is usually established from experimental data obtained at temperatures other than T_0. Carrying out an investigation of the freezing of a liquid in the pores of an adsorbent, the authors of [3] consider that the agreement between their experimental data and equation (4) confirms the validity of the theory of capillary condensation. This conclusion is, however, not well founded. In actuality, the experiment of [3] gives a relation between the lowering of the freezing point, ΔT, in the capillary and the relative pressure of the vapors above the liquid. For comparison with the theoretical equation (4), equation (3) is used to carry this over into a relation between ΔT and the capillary radius which is then compared with equation (4). Thus the function $\varphi(r)$ enters into (4), and is also used in working up the experimental data. It follows that this function can be chosen at will without disturbing the agreement between theory and experiment.

In conformity with the concepts of the theory of capillary condensation, the melting of a substance in a capillary of radius r can be said to be independent of the melting in capillaries of other radii. Then the volume of all of the pores of radii up to r is numerically equal to the amount of material in these pores which has melted at the temperature T. Experiment gives the derivative of this quantity, $dF(T)/dT$, which can be compared with the values of $da/d(p/p_s)$, or dv/dr, as obtained from equation (3). In such a comparison, however, it is necessary to postulate at once the type of relation existing between the lowering of the melting point, ΔT, and the quantities p/p_s and r. It is for this reason that the integral quantities $F(T)$ and $v(r)$ are compared in Fig. 2. In the case of the KSK-2 specimen, this figure shows the form of the curve for the melting of water to be near to that of a structural curve independently obtained from adsorption data; similar agreement is observed for the other specimens, as well. By equating corresponding abscissa of the curves of Fig. 2, it is possible to establish a relation between the freezing point of water and the pore radius. It can be seen from Fig. 3 that points obtained from various types of measurements, on various specimens [4], satisfactorily satisfy a linear equation.

Within the limits of the accuracy of measurement, the results of [4, 5] indicate that the lowering of the melting point of a substance in pores is independent of the nature of the adsorbent. This detail, together with the fact that evolution of phase-transition heat is not observed when the relative pressure of vapor above the adsorbent is less than that corresponding to the beginning of reversible hysteresis on the adsorption isotherm, have been considered in [3-5] as confirming the validity of the theory of capillary condensation. According to this theory, the temperature of solidification of a liquid sorbed in a capillary is fixed by diminution of its vapor pressure and, as has been shown above, by the curvature of the meniscus. From this point of view it is, however, difficult to explain a lowering in the melting point of a solid substance located in a capillary, since the concept of a meniscus applies only to the liquid and no data is available on the form of the free surface of a solid substance in a capillary. These phenomena can be interpreted independently of the form of the meniscus by starting from the properties of materials in the dispersed state, where the translatory motion of the molecules and the resulting conditions for melting and crystallization are different from those prevailing in the bulk of a normal liquid or solid body.

A determination of the nature of the porosity of an adsorbent is usually made by working up the results of time consuming adsorption measurements which must be carried out with relatively complicated apparatus. With the proposed technique for determining const/λ, it is possible to obtain a melting curve for a substance adsorbed on a porous body in a much shorter time; using this curve and the relation given in Fig. 3, the curve showing the distribution of pores in terms of effective radii can be developed. When automatic temperature recording is introduced into the measurement of const/λ, a $dF(T)/dT$ curve can be obtained on the tape of a recording potentiometer in the course of several hours.

The authors wish to express their thanks to L. V. Radushkevich for his interest in this work.

LITERATURE CITED

[1] W. A. Patrick and W. A. Kemper, J. Phys. Chem. 42, 369 (1938).

[2] R. W. Batchelor and A. G. Foster, Trans. Farad. Soc. 40, 300 (1944).

[3] J. Higuti and I. Iwagami, J. Phys. Chem. 56, 50 (1952).

[4] B. R. Puri, L. R. Sharma and M. Lakhanpal, J. Phys. Chem. 19, 3 (1954).

[5] B. R. Puri, D. D. Singh and I. R. Myer, Trans. Farad. Soc. 53, 4 (1957).

[6] A. V. Lykov, The Theory of Thermal Conductivity (in Russian) 1952.

[7] A. V. Chudnovskii, Heat Exchange in Dispersed Media (in Russian), 1954, p. 285.

[8] P. Kubelka, Zs. Elektrochem. 38, 611 (1932).

Received December 17, 1958

A METHOD FOR THE DETERMINATION OF THE PHASE STATE IN BINARY SYSTEMS

I. B. Borovskii and I. D. Marchukova

The A. A. Baikova Institute of Metallurgy of the Academy of Sciences of the USSR

(Presented by Academician A. A. Bochvar, December 27, 1958)

Up to the present time, the great majority of the field boundaries in binary, ternary, and higher-order phase diagrams have been located by classical methods. Even with the simplest of binary systems, it is necessary to carry out chemical, x-ray, and dilatometric studies as well other investigations on several score of alloys. For these reasons, the search for more rapid methods of constructing phase diagrams was begun long ago [1, 2].

In recent years, an x-ray method for investigating the chemical composition of microvolumes has been successfully developed [3]. Since it is highly localized and possesses a high degree of local sensitivity to elements of atomic numbers ranging from 12 (magnesium) to 92 (uranium), this method has been fruitfully applied to the study of diffusional processes, to the investigation of the compositions of microscopic grains and the distribution of the elements within these grains and on their boundaries, and for other purposes as well [4].

The essential feature of this method is the replacement of the anode of a special x-ray tube by a polished section of the alloy which is under investigation. By a system of electromagnetic lenses, an electron beam, accelerated to 30 – 40 kv, is focused onto a narrow zone, 0.1 – 2 μ, on the surface of the section. Over this region, the probe electrons excite the characteristic x-ray radiation, which is then spectrally decomposed by a bent crystal and recorded by quantum counter. By determining the wavelength of the x-ray radiation which is excited here, it is possible to fix qualitatively the alloy composition in this region. A comparison of the intensity of a line from an element in the specimen with the intensity of this same line in a "standard" permits a quantitative evaluation of the amount of the element in question.

By using this method to investigate diffusion layers in various binary systems (Cu – Zn, Cu – Au, Mo – Be, Mo – Si, Al – Si, etc.), it was shown that the diffusion layer obtained from suitably selected specimens will contain all of those phases which are predicted by the phase diagram of the system in question. In certain systems (U – Mo, U – Zr), this same fact has been established by other investigations [5]. It has also been noted thar regions of phase mixing cannot be obtained in the diffusion layer.

As our investigations have shown, the composition of the phases in the diffusion layer and the phase composition boundaries are not consistent with the concentration boundaries in the phase diagram. This is due to the specific conditions of phase stability in the diffusion layer. From this fact, it follows that data obtained in the study of diffusion layers can serve only for the construction of a skeleton form for a phase diagram. Such data cannot give exact limits for the existence of the various phases. If, however, investigations on diffusion layers obtained between pure metals are supplemented with data on phase compositions in alloys corresponding to two-phase regions, the phase diagram can be built up in its entirety.

The following method is proposed for constructing the phase diagram for a binary system. Using the contact method, a diffusion layer is formed for the binary system, and from this, quantitative determination is made of the phases present in the system at the annealing temperature, and of the concentration ranges of these phases.

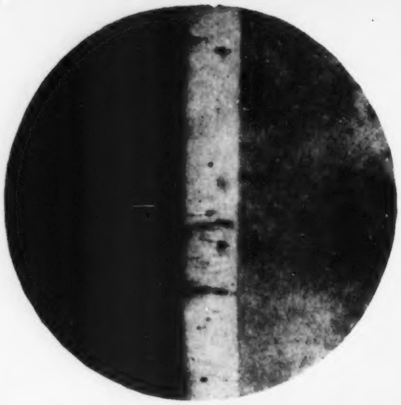

Fig. 1. Microrelief of the diffusion layer between metallic Cu and Zn.

Specimens of concentrations corresponding to the region of phase mixing are then prepared. These specimens are annealed at various temperatures and the temperature dependence of the concentration boundaries of the resulting phases determined by investigating the phase compositions. The regions corresponding to phase mixing are fixed directly from the concentration curves (Fig. 2) obtained for the diffusion layers.

Because of the high degree of localization of this method, a layer width of 5 – 10 μ is sufficient for a trustworthy determination of the chemical composition of a phase. There are times, however, when it is necessary to prepare special specimens in order to obtain the requisite phase width, resort being made to diffusion between phases which are neighboring in the phase diagram.

This method has been tested on the classic systems, copper – zinc and copper – gold. In studying the copper – zinc system, diffusion layers between the pure metals were prepared over the temperature interval 300 – 400°. According to the phase diagram, the diffusion layer in this temperature interval should contain the α and the η solid solution and three intermetallic compounds, the β-, the γ- and the ϵ- phases. The presence of the γ- and the ϵ- phases was established by microanalysis of the point composition in the resulting diffusion layers, these phases being adjoined from the side of the pure metals by the α- and the η- solid solutions. The width of the region of solid solutions was approximately 2-4 % of the total width of the layer. Very careful measurements were required in order to detect these regions. As was to be anticipated, regions of phase mixing were not observed on the concentration curves, the composition changing abruptly on passing from one phase to another.

TABLE 1

Batch composition	Annealing temperature, in °C	Phase composition, in wt. %	Batch composition	Annealing temperature, in °C	Phase composition, in wt. %
40 wt. % zinc $\alpha + \beta$	400	α 38±1 (of Zn) β 45±1,5 (of Zn)	75 wt. % zinc $\gamma + \varepsilon$	400	γ 31,5±0,8 (of Cu) ε 22±0,8 (of Cu)
	550	α 38±1 (of Zn) β 43,5±1,5 (of Zn)		500	γ 30,0±0,7 (of Cu) ε 22±1 (of Cu)
55 wt. % zinc $\beta + \gamma$	550	β 49,5±0,5 (of Cu) γ 42±1,5 (of Cu)	90 wt. % zinc $\varepsilon + \eta$	550	γ 29,6±0,8 (of Cu) ε 22±1 (of Cu)
	400	β 50±1 (of Cu) γ 42±1 (of Cu)		400	ε 12±0,5 (of Cu) η 2±0,2 (of Cu)

It was established that the existence of a phase in the diffusion layer was limited to a concentration range which was considerably narrower than would be expected from the phase diagram. Thus, at 370°, the region of existence of the γ-phase in the diffusion layer ranges from 66 to 68 weight % instead of from 58.5 to 68.5 weight % (of zinc). For the ϵ-phase, the range is from 82 to 85 weight % instead of from 78.5 to 86.5 weight % (of zinc). This indicates that the conditions for phase stability in the diffusion layer are different from those in the equilibrated alloy.

The β-phase, the third intermetallic compound of the system, can be detected in the diffusion layer between the pure metals only with difficulty, just as is the case with the α- and the η- solid solutions. For this reason, the determination of the composition of the β-phase (up to 20 μ) could be obtained on these specimens by annealing for a comparatively brief time (40 hours) at a reasonably low temperature (300°).

For studying the exact concentration limits of the phases, four alloys of compositions corresponding to two-phase regions were prepared. Specimens of these alloys were annealed at various temperatures (see Table 1).

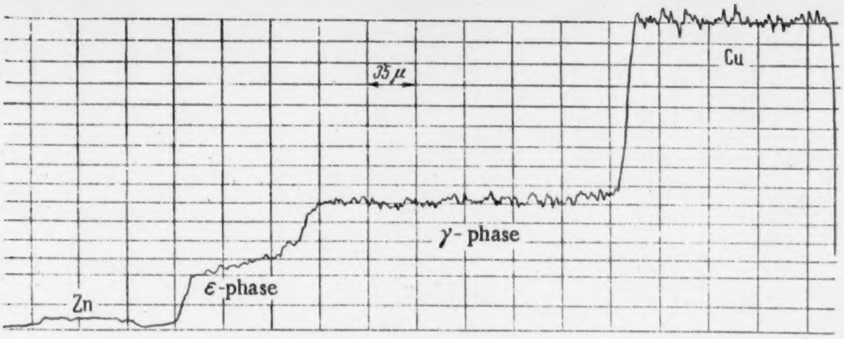

Fig. 2. Concentration curve for the layer between Cu and Zn, as recorded with the K_α line of copper (see Fig. 1).

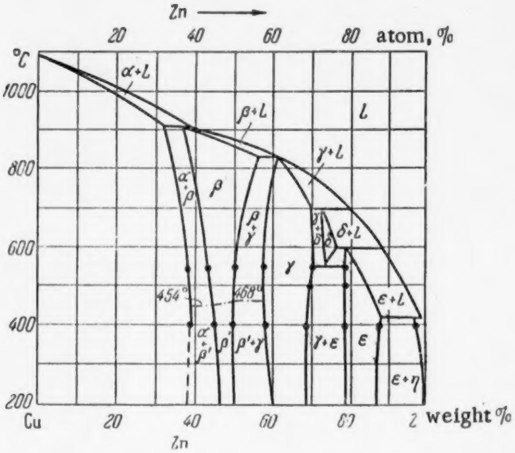

Fig. 3. Phase diagram for the Cu – Zn system (from collected papers in conjunction with the calculations of S. T. Konobeevskii). The points designate experimentally determined values.

By investigating the chemical compositions of the individual phases in the two-phase regions, it was possible to determine the exact boundaries for the existence of these phases and their temperature dependence. The data obtained are presented in Table 1 and plotted in the phase diagram of Fig. 3. These results agree with the literature data, which have been repeatedly verified.

The phase diagram of the Cu – Au system is especially interesting because it consists of a series of solid solutions and ordered phases of the composition CuAu and Cu_3Au [6]. Both of these phases are clearly recorded in a diffusion layer obtained by annealing at a temperature lower than that of ordering [7]. Thus this method is applicable even to the case in which the system contains ordered phases.

LITERATURE CITED

[1] S. A. Vekshinskii, New Methods of the Metallographic Investigation of Alloys (in Russian), Moscow – Leningrad, 1944.

[2] A. S. Palatnik and V. V. Levitin, Proc. Acad. Sci. USSR, 96, 975 (1954).

[3] I. B. Borovskii, Problems of Metallurgy, Collected Papers in Honor of the 70-th Birthday of Academician I. P. Bardin, Acad. Sci. USSR, Press, 1953 [in Russian].

[4] I. B. Borovskii and N. P. Il'in, Plant Lab. No. 10 (1957); I. B. Borovskii, et al., Bull. Acad. Sci. USSR phys. ser. 21, No. 10 (1957).

[5] G. Philibert and J. Adda, Compt. rend. 245, 2507 (1957); J. Adda, G. Philibert and H. Faraggi, Rev. de Métallurgie, 54, No. 8, 597 (1957).

[6] F. N. Rhines, N. E. Band and R. A. Rummel, Trans. Am. Soc. met. 47 (1955).

[7] I. B. Borovskii, N. P. Il'in, L. E. Loseva and I. D. Marchukova, Scientific Investigations of the Institute of Metallurgy of the Academy of Sciences of the USSR, 1957, p. 92 [in Russian].

Received December 3, 1958

SENSITIZED RADIOLYTIC OXIDATION OF LEUCO METHYLENE BLUE IN AQUEOUS SOLUTIONS

A. N. Zansokhova and V. D. Orekhov

L. Ya. Karpov Physicochemical Institute

(Presented by Academician A. N. Frumkin, December 15, 1958)

An investigation of the effects of ionizing radiation on leuco bases of dyes in aqueous solutions will provide a quantitative means of determining the amount of radiolytically oxidized water by a direct colorimetric method. By choosing a dye with a high molar extinction coefficient we can follow the reaction kinetics in the range of low radiation dosage – from several tens to hundreds of roentgens.

The first reports on the radiolysis of leuco bases of dyes in organic solvents appeared in a review article by Miller [1]. Later, Vereshchinskii and co-workers [2] investigated the radiolytic oxidation of leuco bases of triarylmethane and other type dyes in ethyl alcohol; they determined the oxidation yields of a large number of compounds and noted the sensitizing action of oxygen.

The investigation of similar reactions in aqueous solutions was initiated by us; we used samples of leuco indigo esters [3]. We established the fact that the oxidation, which by itself proceeds very slowly, becomes highly enhanced when scavengers of atomic hydrogen are introduced into solution; molecular oxygen and nitrate ions were used by us for this purpose. The presence of both oxygen and nitrate ion created conditions favorable to the initiation of a chain oxidation of the leuco base to the corresponding dye, while the yield attained values which would make this reaction suitable for practical uses.

In a recently published paper, Armstrong and Grant [4, 5] described some experiments on the radiolytic oxidations of sensitized leucodyes of thiophenediarylmethane type. When radiolyzed in aqueous solution saturated with air these dyes were oxidized into the colored form with a yield of 1.1 moles/100 ev. The above-mentioned workers have also tried to sensitize the reaction by introducing sodium chloride, salts of copper, iron, nickel, cesium, and manganese.

In the present paper we have studied the necessary conditions for sensitized oxidation of leucodyes by carrying out conjugated radiolytic oxidation–reduction reactions. By means of this method (previously described in [3, 6]) the fraction of the compound oxidized or reduced by the radiolysis products of water can be established with an accuracy of almost 12 equiv/100 ev. The oxidation was followed by means of leuco methylene blue. In highly acidic solutions under the effect of radiation this dye undergoes a transition into an intermediate form (semiquinone) (which was established by Swallow [7]), while in moderately acidic aqueous solutions there is usually a reduction to the leuco base [8]. The advantages of using this dye rest in a high molar extinction coefficient of its colored form and high solubility of the leuco base, making it possible to prepare high enough concentrations to achieve appreciable sensitization.

The choice of nitrate ion as the conjugated acceptor was guided by the fact that it does not react with the leuco base within the investigated pH range (in the absence of light).

Since a solution of leuco methylene blue and nitrate ion is highly sensitive to light and to traces of oxygen, the samples to be irradiated were prepared under red light and in a special oxygen-free chamber filled with nitrogen. The leuco base was prepared by reducing the dye with zinc powder in an acid medium. The optical densities of solutions were measured on FÉK-M model photoelectric colorimetric. A laboratory-type

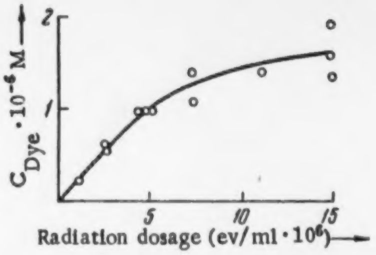

Fig. 1. Dye formation as a function of the radiation dosage in $2 \cdot 10^{-2}$ M leuco methylene blue saturated with nitrogen (pH = 1, dosage = 0.05 r/sec).

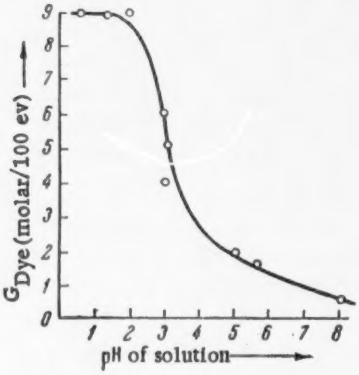

Fig. 2. Yield of the colored dye as a function of pH during irradiation of solutions 10^{-2} M in leuco methylene blue and 2 M in sodium nitrate (solution saturated with nitrogen γ-ray dosage 0.05 r/sec).

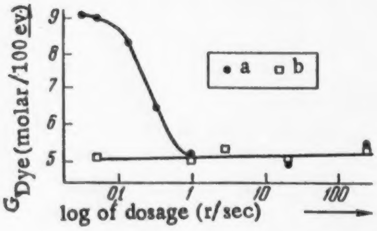

Fig. 3. Yield of the dye as a function of γ-ray dosage in solutions 10^{-2} M in leuco methylene blue and 2 M in $NaNO_3$. a) Solutions with pH ≤ 2; b) solutions with pH ≥ 3.

Co^{60} set-up with an activity of 0.1 to 30 radium equiv., was used as the γ-ray source. The dosage was varied from 0.05 to 20 r/sec. All the experiments were done in glass ampules.

In the absence of any promoting compounds the yield of the colored form of methylene blue was very low. The initial yield (Fig. 1) did not exceed 1 mole/100 ev, and with increasing dosage it rapidly decreased to zero.

The solutions became strongly sensitized when high concentrations of sodium nitrate (2 moles/liter) were introduced. In such cases the yield was strongly dependent on the pH of solutions. In the range of high acidities (pH < 2.5) it attained a maximum of about 9 moles/100 ev (Fig. 2). With increasing pH the yield of the colored form declined quite sharply down to 0.5 mole/100 ev at pH = 8. The curve shown in Fig. 3 was recorded at a dosage of 0.5 r/sec.

Increased radiation dosage in solutions of pH ≤ 2.0 decreased the yield to 5.0 moles/100 ev (Fig. 3, a). Under these conditions we also observed secondary reactions. The dosage had no effect on solutions of pH > 3, nor were there any secondary effects (Fig. 3, b).

The results obtained can be interpreted in the following manner. The low yield of the colored dye in irradiated leuco base solutions free of sensitizers can be explained by reversible reactions and radical recombinations, which are favored by the divalent mechanism proposed for the transition from the leuco base to the colored dye and the comparatively long life of the intermediate (semiquinone).

The sensitizing action of the nitrate ion may be attributed mainly to its ability to bind hydrogen atoms and form less reactive products, which in turn enhances the conjugated oxidation of the leuco base by hydroxyl free radicals. If we assume that the number of chemically active pairs (H and OH) capable of participating in the reactions of dissolved compounds attains 12 [3], then the maximum yield of the colored dye should be 6 moles/ev; this is born out experimentally in solutions of pH = = 3.0 and in more acidic solutions at higher dosages. The increased yield (9 moles/100 ev) and the secondary effects observed at high dosages in solutions of pH = 2.5 are due to the participation of nitrite ions in the oxidation of the leuco base; the nitrite is produced by the conjugated reduction of nitrate. This may account for up to 3 moles of dye per 100 ev (corresponding to 6 nitrite ions). In the above-mentioned pH range we achieved the maximum utilization of water radiolysis products in the oxidation of the leuco dye, while the gas evolution did not exceed G = 0.1 moles/100 ev. The oxidation of the leuco base by nitrite proceeds rather slowly and the rate declines rapidly with increased pH. This should explain the decline in the yield between pH 2 and 3, as well as the effects of dosage strength and secondary reactions mentioned before. The continuing decline in yield with increasing pH (above 3) is probably connected with the decreased oxidizing power of hydroxyl free radicals. It should be noted that as the end reaction products (dye, nitrite or its reduction products) accumulate in solution they begin to compete in various reactions with the products of water hydrolysis.

Consequently, just as in the case of a pure leuco base solution (Fig. 1) the optical density function of the dye in irradiated solutions loses its linear character at dosages > 1000 r.

In concluding the authors wish to thank M. A. Proskurnin for his valuable advice and remarks made in the course of this work and during discussion of results.

LITERATURE CITED

[1] N. Miller, Actions chimiques et biologiques des radiations, Paris, 1956, p. 168.

[2] I. V. Vereshchinskii, L. P. Karpushkin and V. N. Shcheglov, Trans. 1st All-Union Confer. On Radiation Chem. Izd. AN SSSR, 1958, p. 249.*

[3] V. D. Orekhov, M. A. Proskurnin, V. A. Sharpatyi and A. A. Zansokhova, Trans. 1st All-Union Confer. On Radiation Chem. Izd. AN SSSR, 1958, p. 100.*

[4] W. A. Armstrong and G. A. Grant, Rad. Research 8, No. 5, 375 (1958).

[5] W. A Armstrong and G. A. Grant, Canad. J. Chem. 36, No. 10, 1398 (1958).

[6] A. I. Chernova, V. D. Orekhov and M. A. Proskurnin, J. Phys. Chem. 30, 1343 (1956).

[7] A. J. Swallow, J. Chem. Soc. 1957, 1553.

[8] V. D. Orekhov, A. I. Chernova and M. A. Proskurnin, Coll. Works on Radiation Chem. Izd. AN SSSR, 1955, p. 85.*

Received December 15, 1958

---

* In Russian.

THE THEORY OF SINGLE ELECTRON QUANTUM MECHANICAL SYSTEMS WHICH INCLUDE A LARGE SUBSYSTEM

Jaroslav Koutecký and Antonin Fingerland

The Institute of Physical Chemistry of the Czechoslovakian Academy of Sciences,
Prague CzSR

(Presented by Academician A. N. Frumkin, January 7, 1959)

I. Introduction. A method for the theoretical treatment of crystalline distortions has been developed by Lifshits [1], Koster and Slater [2], and Baldock [3]. This method has been generalized by one of us (J. Koutecký) and applied to the general theory of the surface states of crystals, and to the theory of chemical adsorption [6]; in the first of these applications use was made of the approximations of the methods of simple molecular orbitals [4] and the self-consistent field [5]. We believe that this method should be useful for the treatment of problems in the theory of chemical bonding; in essence, it gives a theoretical basis for the Dewar variant of the method of molecular orbitals [7].

The principle of the method is as follows. The state of a single electron is studied (in the simple method of molecular orbitals), or that of several electrons (in the method of the self-consistent field), in the field of a certain configuration of atomic residues, S (the term atomic residue is to be understood as designating the atomic nucleus together with those electrons which do not participate in bond formation). It will be supposed that the system S can be built up from the various subsystems, D_I, D_{II},..., D_R, of atomic residues. One, at least, of these subsystems is presumed to be much larger than its region of contact with the remaining subsystems. It is then supposed that the potential acting on the electron in one of these large subsystems is approximately the same as in the corresponding portion of the system S. This assumption is justified when the interaction between this large subsystem and the remaining subsystems is sufficiently weak.

It is then necessary to find an electronic state function for the system S, this function to have the form of a linear combination of the molecular orbitals of the subsystems. In order to use the properties of symmetry, it will in certain cases prove expedient to employ the Vannier* function, not only for infinite crystals, but for finite crystals as well (see, for example, [6]). It then proves possible to construct a linear combination of molecular orbitals of the various large subsystems, the amplitude of each of these orbitals being large over only a small region of the corresponding subsystem. Such linear combinations exist for crystals (the Vannier function), and for certain molecules (equivalent orbitals).

As will be shown, the equations for the unknown coefficients in this development of the electronic eigenfunction in terms of the orbitals of the subsystems can be written so as to involve a small number of the coefficients for the development of the Vannier functions, or the equivalent orbitals.

As possible examples in which it is clearly possible to apply this method of treatment, there can be mentioned:

1. A molecule which arises from two subsystems of atomic residues. The original molecules would be considered as the subsystems.

2. A finite crystal. The infinite crystal could be considered as the initial system.

3. Molecular chemisorption. As the subsystems there could be selected either the molecule and a finite crystal, or the molecule and an infinite crystal.

---

* Transliteration of Russian — Publisher's note.

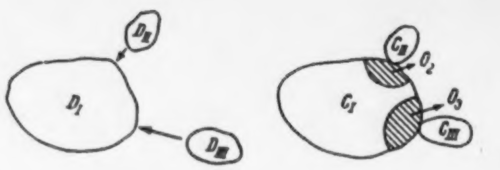

Fig. 1. Schematic representation of the system S. D_I, D_{II}, and D_{III} are subsystems; C_I, C_{II}, and C_{III} are portions of the system S which are joined to the subsystems D_I, D_{II}, and D_{III}; O_2 and O_3 are regions which contain no matrix elements, $V_{ik}^{\alpha,\beta}$, which can be neglected.

4. A polyene. Here, an infinite chain of atoms, joined by double bonds, could serve as the initial system.

The realization of this program in the approximation methods of molecular orbitals and the self-consistent field, will be shown below.

II. The simple method of molecular orbitals. It will be supposed that the eigenfunction ψ_i^α and the eigenenergies, E_i^α, of the single-electron Hamiltonians, H^α,

$$H^\alpha \psi_i^\alpha = E_i^\alpha \psi_i^\alpha$$
$$(\alpha = I, \ldots . R), \tag{1}$$

are known; here $H^\alpha = -\frac{h^2}{2m}\Delta + V^\alpha$ is the effective potential of the selected electron in the individual subsystem, D^α. The state of the electron in the system S is given by the solution of the Schrodinger equation

$$H\Phi = W\Phi, \text{ where } H = -\frac{h^2}{2m}\Delta + V \tag{2}$$

The solution, Φ, of equation (2) can be represented in the form of a linear combination of a finite number, N, of characteristic functions, each of which satisfies equation (1); here

$$N = \sum_{\alpha=1}^{R} N^\alpha \tag{3}$$

With the aid of unitary transformations, it is possible to pass from the molecular orbitals to functions which, to a satisfactory degree of precision, can be considered as localized in a certain part of a subsystem [9]. When the N^α are correctly chosen, these transformations can be written in the form

$$\varphi_r^\alpha = \sum_{i=0}^{N^\alpha-1} C_{ir}^{*\alpha} \psi_i^\alpha, \quad \psi_i^\alpha = \sum_{r=0}^{N^\alpha-1} C_{ir}^\alpha \varphi_r^\alpha \tag{4}$$

(the identity transformation is not excluded here). The solution of equation (2) will be taken in the form of the linear combination

$$\Phi = \sum_{\alpha=1}^{R} \sum_{j=0}^{N^\alpha-1} d_j^\alpha \varphi_j^\alpha. \tag{5}$$

Equation (5) can be represented as

$$\Phi = \sum_{\alpha=1}^{R} \sum_{j=0}^{P^\alpha-1} d_j^\alpha \varphi_j^\alpha, \quad \text{where} \quad P^\alpha \leqslant N^\alpha. \tag{6}$$

For an infinite system, the integral square number of elementary cells in the cyclic crystal will be selected as the value of N^α. By the usual variational procedures, the condition

$$\sum_{\beta=1}^{R}\sum_{k=0}^{P^{\alpha}-1} d_k^{\beta} P_{jk}^{\alpha\beta} = 0 \quad (\alpha = 1, \ldots, R;\ j = 0, \ldots, N^{\alpha}-1), \tag{7}$$

where

$$P_{jk}^{\alpha\beta} = \int \varphi_j^{*\alpha} \,|\, H^{\beta} + (V - V^{\beta}) - W \,|\, \varphi_k^{\beta}\, d\tau. \tag{8}$$

is obtained for the coefficients of equation (5).

By making use of the relation

$$H^{\alpha}\varphi_j^{\alpha} = \sum_{s=0}^{N^{\alpha}-1} \varepsilon_{js}^{\alpha}\varphi_s^{\alpha}, \text{where} \quad \varepsilon_{js}^{\alpha} = \sum_{r=0}^{N^{\alpha}-1} C_{rj}^{*\alpha} E_r^{\alpha} C_{rs}^{\alpha}, \tag{9}$$

equation (7) can be put into the form

$$\sum_{\beta=1}^{R}\sum_{k=0}^{P^{\beta}-1} d_k^{\beta}\,[(\varepsilon_{ki}^{\alpha} - W\delta_{ik})\,\delta_{\alpha\beta} + V_{jk}^{\alpha\beta}] = 0, \tag{10}$$

where the matrix of the perturbation integrals can be determined from:

$$V_{jk}^{\alpha\beta} = \sum_{s=0}^{N^{\alpha}-1} \varepsilon_{ks}^{\beta} S_{js}^{\alpha\beta} - W S_{jk}^{\alpha\beta} + V_{jk}^{\prime\alpha\beta}, \quad \alpha \neq \beta; \qquad V_{jk}^{\alpha\alpha} = V_{jk}^{\prime\alpha\alpha}; \tag{11}$$

$$S_{js}^{\alpha\beta} = \int \varphi_j^{*\alpha}\varphi_s^{\beta}\, d\tau; \quad V_{jk}^{\prime\alpha\beta} = \int \varphi_j^{*\alpha}(V - V^{\beta})\,\varphi_k^{\beta} d\tau. \tag{12}$$

Though this form of the equations for the development coefficients is characteristic for large systems, it is quite unsuitable here, since the system of homogeneous linear equations (12) has very many members. This difficulty can be circumvented in the following manner. Equation (10) is multiplied by $C_{pi}^{*\alpha}$ and summation carried out over $\underline{i}$. When use is made of the definition of ϵ_{js}^{α} from (9), and of the fact that the transformation is unitary, the result is

$$\sum_{i=0}^{P^{\alpha}-1} C_{pi}^{*\alpha} C_{ri}^{\alpha} + \sum_{i=P^{\alpha}}^{N^{\alpha}-1} C_{pi}^{*\alpha} C_{ri}^{\alpha} = \delta_{pr},$$

$$\sum_{k=0}^{P^{\alpha}-1} d_p^{\alpha} C_{pk}^{*\alpha}(E_p^{\alpha} - W) = \sum_{k=0}^{P^{\alpha}-1}\sum_{i=P^{\alpha}}^{N^{\alpha}-1} \varepsilon_{ki}^{\alpha} d_k^{\alpha} C_{pi}^{*\alpha} - \sum_{\beta=1}^{R}\sum_{k=0}^{P^{\beta}-1}\sum_{i=0}^{P^{\alpha}-1} d_k^{\beta} C_{pi}^{*\alpha} V_{ik}^{\alpha\beta} \tag{13}$$

$$(\alpha = 1, \ldots, R;\ p = 0, \ldots, N^{\alpha} - 1).$$

Assuming that

$$(E_p^{\alpha} - W) \neq 0, \tag{14}$$

dividing by the expression $E_p^{\alpha} - W$, multiplying by C_{ps}^{α}, and summing over $P^{\alpha} - 1$, the result is

$$\sum_{k=0}^{P^\alpha-1} d_h^\alpha \delta_{ks} = \sum_{\beta=1}^{R}\sum_{i=0}^{P^\alpha-1}\sum_{k=0}^{P^\beta-1} L_{si}^\alpha V_{ik}^{\alpha\beta} d_k^\beta - \sum_{i=P^\alpha}^{N^\alpha-1}\sum_{k=0}^{P^\alpha-1} L_{si}^\alpha \varepsilon_{ki}^\alpha d_k^\alpha \tag{15}$$

$$(\alpha = 1, \ldots, R;\ s = 0, \ldots, N^\alpha - 1),$$

where

$$L_{si}^\alpha = \sum_{p=0}^{N^\alpha-1} \frac{C_{pi}^{*\alpha} C_{ps}^\alpha}{W - E_p^\alpha}. \tag{16}$$

Since $k < P^\alpha$, $\delta_{ks} = 0$ for $s \geq P^\alpha$, so that the system (15) splits into two subsystems:

$$d_s^\alpha = \sum_{\beta=1}^{R}\sum_{i=0}^{P^\alpha-1}\sum_{k=0}^{P^\beta-1} L_{si}^\alpha V_{ik}^{\alpha\beta} d_h^\beta - \sum_{i=P^\alpha}^{N^\alpha-1}\sum_{k=0}^{P^\alpha-1} L_{si}^\alpha \varepsilon_{hi}^\alpha d_k^\alpha \tag{15a}$$

$$(\alpha = 1, \ldots, R;\ s = 0, \ldots, P^\alpha - 1);$$

$$0 = \sum_{\beta=1}^{R}\sum_{i=0}^{P^\alpha-1}\sum_{k=0}^{P^\beta-1} L_{si}^\alpha V_{ik}^{\alpha\beta} d_h^\beta - \sum_{i=P^\alpha}^{N^\alpha-1}\sum_{h=0}^{P^\alpha-1} L_{si}^\alpha \varepsilon_{hi}^\alpha d_k^\alpha$$

$$(\alpha = 1, \ldots, R;\ s = P^\alpha, \ldots, N^\alpha - 1). \tag{15b}$$

Equations (15) can be successfully applied when the matrix elements for the perturbation potential, $V_{ik}^{\alpha,\beta}$ are essentially different from zero only for a small number of values of the index k. If the second summation on the right-hand side of equation (15) also contains only a small number of members, this form will be suitable for the case of $P^\alpha < N^\alpha$, as well.

The system of (15a) is essentially homogeneous, so that the condition for solubility is:

$$\det|D| = \det\left|\sum_{i=0}^{P^\alpha-1} L_{si}^\alpha V_{ik}^{\alpha\beta} - \sum_{i=P^\alpha}^{N^\alpha-1} L_{si}^\alpha \varepsilon_{ki}^\alpha \delta_{\alpha\beta} - \delta_{\alpha\beta}\delta_{sk}\right| = 0. \tag{17}$$

From the roots which are obtained here, it is of course necessary to select those which will at the same time satisfy the system of (15b). Due to the fact that certain coefficients of high indices will disappear, this matrix can be brought to the form

$$D = \left(\begin{array}{c:c} D_1 & 0 \\ \hdashline & \begin{matrix} 1 & 0 & 0 \\ 0 & 1 & 0 \\ 0 & 0 & 1 \end{matrix} \end{array}\right)$$

so that

$$\det|D_1| = 0. \tag{18}$$

can serve as the condition for the solution of (17).

III. The self-consistent field method. Relations analogous to (15)-(18) can be obtained by the use of the method of the self-consistent field. It is necessary, however, to assume that the Hartree-Fok* equations for the system S, and for the subsystems $D_I, \ldots, D_R$ will here reduce to the type

---

* Transliteration of Russian — Publisher's note.

$$F^{\alpha}\psi_i^{\alpha} = E_i^{\alpha}\psi_i^{\alpha}, \quad F\Phi_j = W_j\Phi, \tag{19}$$

where F^{α}, F are the Hartree-Fok operators for the respective systems; ψ_i^{α}, Φ_j, are the molecular orbitals; and E_i^{α}, W_j, are the orbital energies. It is known that the self-consistent field method does not always lead to equations of the type of (19), although such equations are always approximately valid [10]. For infinite crystals, it has been shown that there are linear combinations of the characteristic functions of the Hartree-Fok operator which possess properties similar to those of the Vannier function (in the sense of localization, for example). For molecules, it is also possible to construct functions which will be analogous to equivalent orbitals [11]. Thus, there is a complete analogy between the formulations of our problem in terms of molecular orbitals and in terms of the self-consistent field.

LITERATURE CITED

[1] I. M. Lifshits, J. Exp. Theo. Phys. 17, 1017 (1947); 17, 1076 (1947).

[2] G. F. Koster and J. C. Slater, Phys. Rev. 95, 1167 (1954); 96, 1208 (1954).

[3] G. R. Baldock, Proc. Cambr. Phil. Soc. 48, 457 (1952).

[4] J. Koutecký, Phys. Rev. 108, 13 (1957).

[5] J. Koutecký, Čs. časopis pro fysiku, 8, 153 (1958).

[6] J. Koutecký, Zs. Elektrochem. 60, 835 (1956).

[7] J. Koutecký and R. Zahradník (unpublished).

[8] M. J. S. Dewar, Proc. Cambr. Phil. Soc. 36, 193 (1940).

[9] G. Pavzen, Phys. Rev. 89, 237 (1953).

[10] H. C. Longuet-Higgins and J. A. Pople, Proc. Phys. Soc. A 68, 591 (1955).

[11] J. Lennard-Jones, Proc. Roy. Soc. A 198, 1 (1949).

Received December 22, 1958

THE GENERAL PRINCIPLES OF THE COPRECIPITATION OF MICROADDITIVES DURING CRYSTAL GROWTH

I. V. Melikhov, M. S. Merkulova and G. Éval'd

The M. V. Lomonosov State University, Moscow

(Presented by Academician V. I. Spitsyn, December 29, 1958)

Crystals containing small amounts of isomorphous additives have recently found wide application in industry and in research. In most cases, these additives form solid solutions with a limited range of miscibility with the basic material of the crystals. We have made an attempt to develop the principles applying to the distribution of an additive between a supersaturated solution (supercooled melt) and the crystals of that macrocomponent which is involved in the formation of the solid solution of limited miscibility.

Let us consider the mechanism of the coprecipitation of an additive with crystals which are growing from a vigorously agitated supersaturated solution. The first step in the coprecipitation of this additive will be its interaction with the phase interface. It is only when the supersaturation on the crystallization front, S, is equal to, or in excess of, a certain minimum value, S_0, that crystal growth from the solution becomes possible [1]. Dynamic adsorptional exchange occurs between the surface and the solution when $S < S_0$. A kinetic equilibrium will exist between the crystal surfaces and the solution on the crystallization front at each instant τ, if the rate of exchange is considerably greater than the rate of diffusion of the solution components through the surface of the diffusion layer. The condition required for the establishment of such an equilibrium is that the rate of adsorption of the additive, V_a, should be equal to the rate of desorption of this substance from the crystal surfaces, V_d:

$$V_a = \alpha (A - \theta) C_\tau, \tag{1}$$

$$V_d = \beta\theta, \tag{2}$$

here, A is the total number of positions per 1 cm² which are available for the adsorption of the additive, θ is the number of adsorbed ions per 1 cm² of surface at the instant τ, C_τ is the concentration of the additive at this same instant, and α and β are constants.

From this equilibrium condition, it follows [2] that the weight of the microcomponent, q, per 1 cm² of surface will be:

$$q = \frac{\frac{\alpha}{\beta} n A C_\tau}{1 + \frac{\alpha}{\beta} C_\tau}, \tag{3}$$

n being the weight of the individual adsorbed ion.

When the supersaturation at the crystallization front reaches the value S_0, growth of a monolayer, dy, of the macrocomponent takes place on the crystal surfaces. At the same time, a partial desorption of the additive is observed. The concentration of this substance in the surface monolayer, dx/dy, is determined by the equation

$$C_s = \frac{dx}{dy} = \frac{\alpha}{\beta R} An \frac{C_t}{1 + \frac{\alpha}{\beta} C_t}, \tag{4}$$

where R is the coefficient of secondary desorption, and C_t is the concentration of the additive on the crystallization front at the instant when $S = S_0$. If the interaction of this substance with the crystal surfaces is such that $\frac{\alpha}{\beta} C_t << 1$, it follows that

$$C_s = \frac{dx}{dy} = \frac{\alpha}{\beta R} AnC_t = \lambda C_t. \tag{4a}$$

The results of integrating equations (4) and (4a) will be different, depending on the conditions of formation, and growth, of the crystals of the solid phase. When there is a rapid growth of crystals from a small number of nuclei in a supersaturated solution, the additive will be homogeneously distributed over the entire crystal volume [3]. In this case, C_s will be independent of the amount of the macrocomponent which has passed into the precipitate, which, in turn, is equal to:

$$x = \int_0^y C_s \; dy = \left| \frac{\alpha}{\beta R} An \frac{C_t y}{1 + \frac{\alpha}{\beta} C_t} \right| \tag{5}$$

where $\underline{y}$ is mass of the precipitate which has been formed up to the time $\underline{t}$. Since the concentration of the additive in the precipitate is independent of time, it follows that $C_t = a/b = a_0/b_0$, $\underline{a}$ and $\underline{b}$ being the amounts of the micro- and the macro- components present on the crystallization front of the solution at the instant $\underline{t}$, and a_0 and b_0, the total amounts of these same materials in the system.

From equation (4a) there then follows

$$\frac{x}{y} = \lambda \frac{a}{b}. \tag{5a}$$

A similar expression has been theoretically and experimentally obtained by Riehl [3].

When the crystal growth is slow (the method of isothermal evaporation, or homogeneous precipitation), diffusion through the diffusion layer to the crystal surfaces could be expected to ensure that at each instant the concentrations of the micro- and the macro- components in the crystallization front equals the concentration of those components in the entire volume of the solution. In this case, integration of equation (4a) will lead to the Doerner – Hoskins formula [4].

$$\ln \frac{a_0 - x}{a_0} = \lambda \ln \frac{b_0 - y}{b_0} \tag{6}$$

Integration of equation (4) gives the approximation

$$\frac{x}{y} = \frac{\lambda a_0}{b_0 + \frac{\alpha}{\beta} a_0 + \left[b_0 (\lambda - 1) - \frac{\alpha}{\beta} a_0 \right] \left(1 - \frac{a_0 - x}{a_0} \right) \frac{1}{2\lambda}} \tag{6a}$$

In order to confirm these equations experimentally, investigation was made of the coprecipitation of small amounts of $PbCl_2$ and of $CdCl_2$ with crystals of NaCl formed in the isothermal breakdown of solution supersaturation. Previously, the kinetics of nucleation and crystal growth of sodium chloride were studied under experimental conditions. At a temperature of 25°, a supersaturation of 3-4%, and a rate of solution agitation of 200 rev/min, nucleation of a small number of crystals was found to take place over a long period of time, after

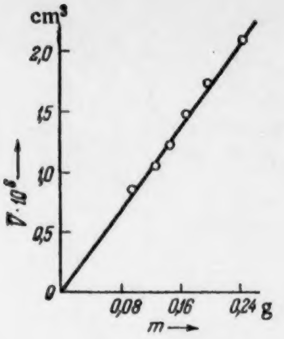

Fig. 1

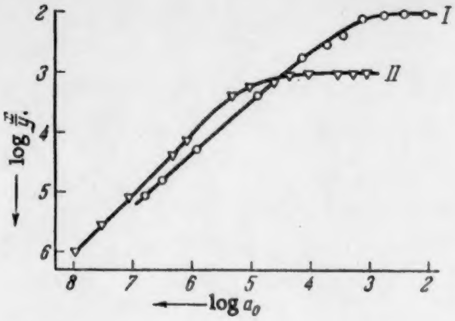

Fig. 2

Fig. 1. The relation between the mean volume of the crystals in the precipitate and the amount of NaCl which has passed into the solid phase.

Fig. 2. The relation between the concentration of the additive in the precipitate and the total amount of this substance in the system. I) System $NaCl-CdCl_2-H_2O$; II) system $NaCl-PbCl_2-H_2O$.

which crystal growth was observed to proceed rapidly. Microscopic observations showed that the mean volume of the crystals of the precipitate increased linearly with an increase in the amount of the NaCl present in the solid phase (Fig. 1), i.e., there is no nucleation of new crystallization centers during the period of growth. The breakdown of supersaturation results in the growth of a comparatively small number of crystals in the supersaturated solution. Thus,the conditions applying to the formation and growth of crystals of the macrocomponent are those for which the relations (5) and (5a) were derived.

We have carried out an investigation of the distribution of isotopes of Pb and Cd between crystals of NaCl and a saturated solution, and the dependence of this distribution on the concentration of the microcomponent in the liquid phase. The amount of the microcomponent in the solid and in the liquid phases could be determined to an accuracy of ±3% by the use of radioactive indicators. The experimental results are given in Fig. 2.

The applicability of equation (5) could be anticipated in this case, since in preceding papers [5] it has been surmised that $PbCl_2$, $SrCl_2$, and $CdCl_2$ would form solid solutions of limited miscibility with crystals of sodium chloride. The experimental data satisfactorily follow equation (5) when the values used for the coefficients are: for the system $NaCl-PbCl_2-H_2O$, $\alpha/\beta = 1.2\cdot10^5$, $An/R = 8.8\cdot10^{-4}$; for the sytem $NaCl-CdCl_2-H_2O$, $\alpha/\beta = 4.4\cdot10^3$, $An/R = 1.0\cdot10^{-2}$.

Thus, the results obtained in this experimental investigation of the mechanism of the coprecipitation of an additive with crystals growing from a supersaturated solution, are in accordance with the derived equations; thus, the following conclusions might be drawn:

1. The rate of exchange between the surface and the solution on the crystallization front is considerably greater than the rate of diffusion of the components through the surface of the diffusion layer.

2. The amount of additive which passes into the solid phase during the crystal growth, and the distribution of this additive in the body of the crystals, can be determined from the equations (5), (5a), (6), and (6a).

LITERATURE CITED

[1] R. Kaischew and J. Stransky, Phys. Zs. 36, 393 (1935); M. Volmer and W. Schultze, Zs. phys. Chem. A, 156, 1 (1931).

[2] J. Langmuir, J. Am. Chem. Soc. 40 (2), 1361 (1918).

[3] N. Riehl, Zs. phys. Chem. 14, H. 5/6, 361 (1958).

[4] H. A. Doerner and W. M. Hoskins, J. Am. Chem. Soc. 47, 662 (1925).

[5] M. S. Merkulova, J. Inorg. Chem. 3, No. 1 (1958); M. S. Merkulova and I. V. Melikhov, Isotopes and Radiation in Chemistry (in Russian), Acad. Sci. USSR, Press, 1958, p. 21.

Received December 24, 1958

THE EFFECT OF CONJUGATION BETWEEN AN ANTHRACENE RING AND A DOUBLE BOND IN AN ALKENE SUBSTITUENT ON THE FLUORESCENCE AND ABSORPTION SPECTRA

A. S. Cherkasov

(Presented by Academician A. N. Terenin, December 19, 1958)

Earlier [1-3] we came out with a hypothesis that the strong smearing observed in the vibrational structure of fluorescence spectra (with only insignificant changes in the absorption spectra) when aryl substituents were introduced into the meso position of an anthracene ring was caused by an increased conjugation between the benzene and anthracene rings in the excited state; this conjugation results in a rearrangement where the molecule assumes a more planar configuration* after absorbing a quantum of light, and such a modified molecule has electronic levels different from those in the unexcited state [4].

In order to obtain a more definite proof that the observed facts were really caused by conjugation we examined the adsorption and fluorescence spectra of certain mesoalkenyl derivatives of anthracene: 9,10-diallylanthracene (I), 9-n-prop-1-enyl-10-n-propylanthracene (II), 9,10-di-n-prop-1-enylanthracene (III), and 9-vinylanthracene (IV).

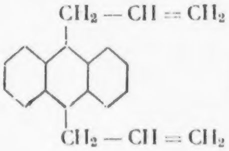

I

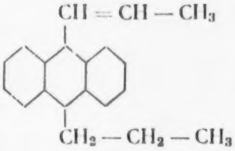

II

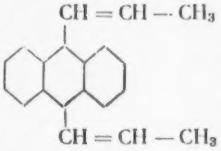

III

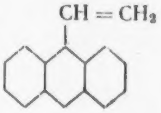

IV

Dialkylanthracene (m. p. 135-136°) was prepared by using phenylhydrazine to reduce [4] 9,10-dialkyl-9,10-dihydroxy-9,10-dihydroanthracene, which was in turn prepared by reacting $CH_2 = CH - CH_2MgCl$ with anthraquinone. Propenylpropylanthracene (m. p. 124-125°) was prepared [5] by treating 9,10-di-n-propyl-9,10-dihydroxy-9,10-dihydroanthracene (synthesized from anthraquinone and n-CH_3H_7MgBr) with dilute hydrochloric acid, while dipropenylanthracene (m. p. 164-165°) was prepared by isomerization of diallylanthracene with alcoholic potassium hydroxide [4]. 9-Vinylanthracene (m. p. 66-67°) was prepared by dehydration [6] of 9-α-hydroxyethylanthracene, which was in turn synthesized by reducing 9-acetylanthracene with aluminum isopropoxide. All the compounds used for spectral work were thoroughly purified by repeated recrystallization and chromatography on aluminum oxide.

The absorption spectra were determined on a SF-4 spectrophotometer, while fluorescence,on a UM-2 monochromator with a photomultiplier as an energy recorder. The spectroscopic sensitivity of the latter set-up was determined by means of a source with known energy distribution. Ethyl alcohol was used as solvent in our spectroscopic work.

---

* The planes of benzene rings in mesoaryl derivatives of anthracene should normally be at a large angle to the plane of the anthracene ring, due to the steric interaction between hydrogens (or groups in its place) in the o-position of the benzene ring and α-hydrogens in anthracene.

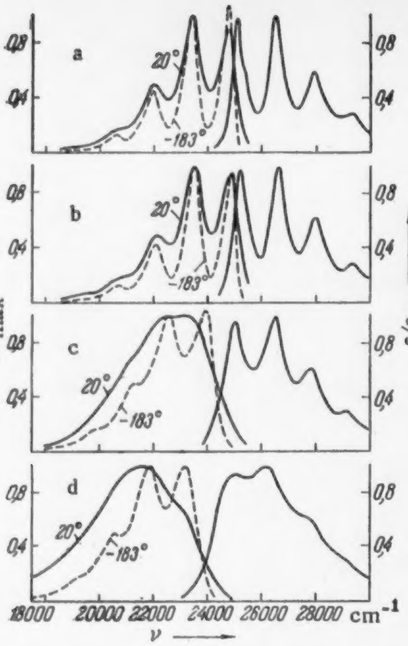

Fig. 1. Fluorescence (left) and absorption (right) spectra. a) 9,10-Di-n-propylanthracene; b) 9,10-diallylanthracene; c) 9-n-prop-1'-enylanthracene; d) 9,10-di-n-prop-1'-enylanthracene. Ethyl alcohol was used as solvent. The left ordinate gives relative quantum intensities of fluorescence, the right, relative molar absorption coefficients.

The dialkenylanthracenes studied in this paper were very similar structurally but differed in the fact that in diallylanthracene the double bonds were isolated from the anthracene ring while propenylpropyl and dipropenylanthracene had, respectively, one and two double bonds conjugated with the ring. It should be noted that an examination of scale models indicated that free rotation of either an alkyl or aryl group in the meso position was sterically hindered due to the overlap between the hydrogen spheres in the alkenyl group and in the α-position of anthracene.

The fluorescence spectra and the long-wave absorption spectra of the investigated dialkenylanthracene and of the corresponding dialkylanthracene (9,10-di-n-propylanthracene) are shown in Fig. 1. In Fig. 2 we have plotted the spectra of 9-vinylanthracene and its corresponding alkyl derivative, 9-ethylanthracene.[*]

One may see in Fig. 1 that the effect of alkenyl substituents with the double bonds isolated from the anthracene ring is similar to the effect of alkyl substituents, and the absorption and fluorescence spectra of 9,10-diallylanthracene are almost identical with those of 9,10-di-n-propylanthracene, not only in the general shape, but also in the location of maxima. The vibrational structure of the spectra is well resolved, and the amount of shift from the anthracene spectrum is not very different from the shift observed in dipropylanthracene.

The existence of double bonds conjugated with the anthracene ring in both propenylpropyl and dipropenylanthracene has a very pronounced effect on the fluorescence spectra, which become much more displaced towards shorter frequencies than those of dialkylanthracene, and are also very strongly smeared. The displacement caused by one propenyl group[**] (1700 cm^{-1}) is more than double the shift resulting from an alkyl group (750 cm^{-1}). The effect of a mesovinyl group on the shape of fluorescence spectra (Fig. 2) is compatible with the effect of a mesopropenyl group; while the shift (1575 cm^{-1}) is similar to that caused by a propenyl group, it is sharply different from the displacement caused by a corresponding alkyl (ethyl) group (725 cm^{-1}).

As had already been noted with other anthracene derivatives [1, 7, 9] the smeared fluorescence spectra observed in derivatives where the substituents contain double bonds conjugated with the anthracene ring are accompanied by an increased separation between the maximum in the fluorescence spectra and in the long-wave absorption band. In 9,10-diallylanthracene this separation is 3100 cm^{-1} (in anthracene and derivatives with structured spectra it is 3000-3100 cm^{-1}), while in propenylpropylanthracene 3950 cm^{-1}, dipropenylanthracene 4600 cm^{-1}, and vinylanthracene 3800 cm^{-1}.

---

[*] Individual vibrational maxima in the absorption and fluorescence spectra of compounds, I, II, III, and IV, are located at the following respective frequencies (in cm^{-1}): I) 25,200, 26,600, 28,000, 29,400, 30,800 and 24;900, (24,900), 23,500 (23,500), 22,100 (22,075), ~20,750 (20,700), (~19,400); II) 25,050, 26,500, 27,900, 29,300, ~30,800 and 23,300 (23,950) 22,550 (22,550), (21,250), (~19,900); III) 25,000, 26,200, ~27,600, ~29,200 and ~23,000 (23,250), 21,600 (21,900), (20,600), (~19,200); IV) 25,900, 27,250, 28,650, ~30,000, ~31,500 and ~24,500 (24,850), 23,450 (23,450), ~22,400 (22,050), (~20,700), (~19,200). The parentheses give corresponding

[**] The magnitudes of this shift were similar (1700 and 1675 cm^{-1}, respectively) when calculated by either starting with the maximum shift in the fluorescence spectrum of 9,10-dipropenylanthracene, or by starting with the shift in the maximum of 9-propenyl-10-n-propylanthracene, pointing to the additive effect of these substituents on the spectral shift [2, 7, 8].

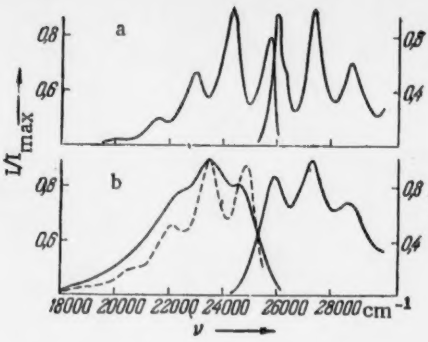

Fig. 2. Fluorescence (left) and absorption (right) spectra. a) 9-Ethylanthracene; b) 9-vinylanthracene.

When the temperatures of solutions containing the investigated compounds were lowered from 20° to the boiling point of liquid air the fluorescence spectra of substituents with unconjugated and conjugated double bonds were affected in entirely different ways. While the first ones exhibited only an improved resolution of the vibrational structure, the others underwent a change in the general nature of their spectra (Fig. 1 and 2), which became very similar to the usual anthracene spectrum with the characteristic difference between the vibrational maxima of 1400 cm^{-1}*. Besides all this they were slightly shifted towards higher frequencies, whereas among derivatives with unconjugated substituents their position remained either unchanged or was slightly shifted towards lower frequencies. Thus, the decrease in temperature sort of diminished (to a certain extent) the specific influence of conjugated substituents – it decreases the effect of conjugation with the anthracene ring.

By adhering to the scheme which proposed that in the excited state molecules of the examined compounds have a different equilibrium ring configuration than in the ground state, we can obviously explain the above-described singular effects of temperature on the fluorescence spectra by the fact that such a molecular rearrangement requires a certain activation energy. Then at lower temperatures the rate at which equilibrium is established will be greatly decreased, and at certain temperatures it may even be never attained during the lifetime of the excited molecule.

The absorption spectra were much less affected by the presence of substituents with double bonds conjugated with the anthracene ring. Their location practically coincided with that of corresponding alkyl derivatives, while the vibrational structure, although somewhat smeared, still remained well pronounced. The effect of the investigated substituents was much more apparent in the increased optical density in the region of the long-wave absorption band. Thus the force constant** increased from 0.133 in diallylanthracene (the value of 0.13-0.14 is characteristic for dimesoalkyl derivatives of anthracene) to 0.147 in propenylpropylanthracene and 0.176 in dipropenylanthracene. The force constant in 9-vinylanthracene (0.133) was also appreciably larger than in monomesoalkylanthracenes (0.11-0.12).

Thus, on the basis of our research on the fluorescence and absorption spectra of alkenyl-substituted anthracenes we can conclude that when the substituent contains double bonds conjugated with the anthracene ring there is an interaction between the π-electrons in the substituent and in the ring (even if the conjugated system is not coplanar), and the interaction in the excited state is stronger than in the unexcited. The similar effects of the examined alkenyl and aryl substituents on the fluorescence and absorption spectra makes it possible to assume that certain previously observed pecularities in the fluorescence spectra of mesoarylanthracenes were also caused by the existence of conjugation between the benzene and anthracene rings in the excited state, with only insignificant amounts (or complete absence) of it in the ground state.

In concluding it should be emphasized that due to their high sensitivity to molecular conjugation the fluorescence spectra can be used in several cases to establish the structure of unknown compounds more successfully than can absorption spectra. One should only keep in mind the fact that if the conjugated system can not acquire a configuration close to a coplanar one due to strong steric hindrance, the effect of conjugation may be absent even in the excited state.

LITERATURE CITED

[1] A. S. Cherkasov, Bull. Acad. Sci. Phys. Ser. 20, 478 (1956).

[2] A. S. Cherkasov, Data from the 10th All-Union Conference on Spectroscopy, 1, L'vov, 1957.

---

*The fluorescence spectra of mesoarylanthracenes undergo similar changes when temperature is lowered.

**Force constants were calculated from the formula [10], $f = 4.32 \cdot 10^{-9} \int \epsilon_{\nu}\, d\nu$.

[3] B. S. Neporent, J. Phys. Chem. 30, 1048 (1956); Transactions of GOI,* 25, No. 150, 1957.

[4] K. J. Clark, J. Chem. Soc. 1956, 1511.

[5] G. M. Badger, J. Chem. Soc. 1952, 1175.

[6] E. G. E. Hawkins, J. Chem. Soc. 1957, 3858.

[7] A. S. Cherkasov and T. M. Vember, Optics and Spectr. 1, 663 (1956).

[8] A. S. Cherkasov, Optics and Spectr. 6, No. 4 (1959).

[9] A. S. Cherkasov, J. Phys. Chem. 29, 2209 (1955).

[10] J. R. Platt and H. B. Klevens, Rev. Mod. Phys. 16, 182 (1944).

Received December 10, 1958

---

* State Optical Institute.

THE ALTERATION OF THE PHOTOELECTRIC WORK FUNCTION OF ZnO, NiO, AND Cr_2O_3, BY THE ADSORPTION OF GASES AND VAPORS

F. I. Vilesov and Academician A. N. Terenin

The A. A. Zhdanov State University, Leningrad

The photoelectric emission from ZnO, NiO, and Cr_2O_3, prior to, and after, their adsorption of a number of gases and vapors has been studied, the aim being to obtain new data on the electron donor-acceptor interaction between molecules and the surfaces of typical semiconducting adsorbents.

The method used here in the study of these surface phenomena is one which was used in earlier investigations of the adsorption of the alkali metal atoms, and certain diatomic molecules (hydrogen, oxygen), on tungsten, and other high-melting metals [1]. Mention should be made of work which has recently been carried out by Suhrman [2], where the surface photoelectric effect has been useful in elucidating the electron-donor mechanism of chemisorption on metals.

Since a study of the photoemission from oxide semiconductors encounters a number of difficulties, in particular, difficulties arising from the considerable magnitude of the work function (of the order of 6 ev), it was necessary to alter fundamentally the apparatus which had earlier been applied in such work [3].

For obtaining monochromatic radiation in the far ultraviolet region of the spectrum, we used the vacuum monochromator described in [4]; in conjunction with a high-voltage hydrogen lamp, it was possible to obtain monochromatic radiation of the order of 10^9-10^{10} photons/sec in the region from 2500 to 1200 A. With radiation of such low intensity, there could be no perceptible photochemical alteration of the layer of adsorbed molecules during the brief period of illumination in the course of the measurements (of the order of 20 minutes). In view of the low quantum yield of the photoemission from semiconductors, the Geiger counter was used as the most sensitive device for the registration of the photoelectrons; in its simplest form, a similar application had been made earlier by Bäsken [5].

In the first series of experiments, the adsorbent was placed directly into a counter filled with argon (15 mm of Hg) to which the adsorbing gas had been added. The cathode of this counter had the form of a plate (Cu, Al), 8×20 mm^2 in dimensions. The oxide was deposited in a thin layer over the entire cathode surface. The anode was a tungsten wire, 0.1 mm in diameter, situated 5 mm from the cathode and running parallel to it. In the second series of experiments, the counter was separated by a vacuum-tight collodion film, 0.1-0.2 μ in thickness, from a vacuum cell containing the specimen. The photoelectrons were accelerated to 4-5 kv by a system of annular electrodes, 3, (see Fig. 1), and passed through this collodion film into the sensitive volume of the end-window counter, where they were recorded. The adsorbent, deposited onto a finger, in the form of a layer (0.5 -1 mm) could be heated to a temperature of 350-400° by a furnace set over the finger. In order to make electrical contact with the adsorbent, this finger was coated with a tin oxide film obtained by thermal decomposition of vapors of tin chloride. With this arrangement, it was possible to carry out high temperature vacuum aging of the adsorbent independently of the counter; the adsorption of gases onto this adsorbent could be made independent of the counter's working mixture, and the photoelectric emission studied in high vacuum. The accuracy in the determination of the photoelectric threshold was of the order of 0.1 ev. The value of the work function was fixed from the beginning of the sharp rise in the photoemission curve.

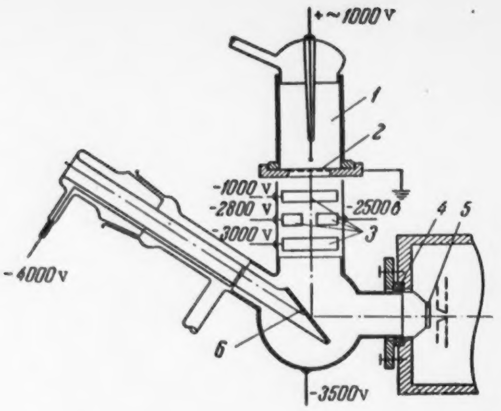

Fig. 1. Design of the vacuum cell for the study of the photoemission from semiconducting surfaces; 1) electron counter; 2) vacuum-tight collodion film; 3) system of accelerating electrodes; 4) packing; 5) lithium fluoride window; 6) finger with specimen.

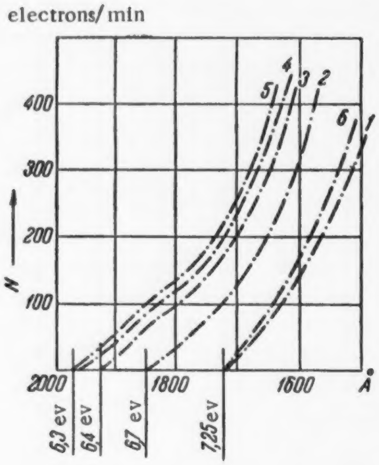

Fig. 2. Yield from photoemission of a zinc oxide surface with adsorption of oxygen: 1) specimen surface saturated with oxygen; 2) specimen heated to 300-350° for 20 minutes with evacuation; 3, 4, 5) similar thermal treatment with evacuation; 6) surface treated with oxygen (3-5 mm of Hg, 10 minutes).

Measurements of the photoelectric work function for a zinc oxide surface onto which oxygen had been adsorbed gave the following principal results.[*] Specimens of oxygen-saturated zinc oxide had a photoelectric-emission threshold at 7.25 ev (Fig. 2, 1). After heating such specimens at 300-350° for 20 minutes, with evacuation and subsequent cooling to room temperature, this threshold was displaced to 6.7 ev (Fig. 2, 2). With repetition of this thermal treatment, the threshold continued to be displaced toward the long-wave side of the spectrum, approaching 1970 A (6.3 ± 0.1 ev) as a limit. This is the value of the photoelectric work function associated with a clean zinc oxide surface, its magnitude being fixed by the position of the upper level of the filled zone. With the introduction of dry air or oxygen, there was a gradual reversal in the displacement of the threshold to a value of 7.2-7.3 ev. These processes were completely reversible and could be repeated many times with a single specimen.

The rather considerable increase of approximately 1 ev in the photoelectric work function of a zinc oxide surface resulting from the adsorption of oxygen is an indication of the existence of a negative charge in the surface layer. It is clear that the oxygen, acting as an electron acceptor, will be negatively charged, whereas the zinc oxide surface, functioning as an electron donor, will be positively charged. The resulting dipolar layer hinders the emission of electrons and increases the work function by an amount $\Delta\varphi$

$$\Delta\varphi = 4\pi ne\mu$$

n being the number of elementary dipoles per 1 cm^2 of surface, e, the electronic charge, and μ, the moment of the elementary dipole. These results are in agreement with the work of many authors [6] where it has been shown that there is a diminution of the dark conductivity of zinc oxide as a result of oxygen adsorption.

Considering oxygen to be chemisorbed as O_2^-, using the values which we have found for the work function of pure zinc oxide and of zinc oxide saturated with oxygen, namely, 6.3 and 7.3 ev, respectively, and the values 0.87 ev for the electron affinity of the oxygen molecule [7] and 3.1 ev for the width of the forbidden zone [8], a review of the energy cycle for the transfer of a conduction electron from the zinc oxide into the oxygen has shown the level of the adsorbed negative O_2^- ion to be 0.2-1.2 ev below the bottom of the conduction zone, a conclusion which is in agreement with the results of other publications from our laboratory [9] in which this was conjectured to be the case. The adsorption of CH_4, CO, or H_2O vapors, on a zinc oxide surface which had been cleaned by thermal treatment, was

---

[*] Use was made of a finely dispersed, catalytically active, zinc oxide which was obtained by thermal decomposition of zinc oxalate at 350-400°. The zinc oxide layer was deposited from an ethanol suspension.

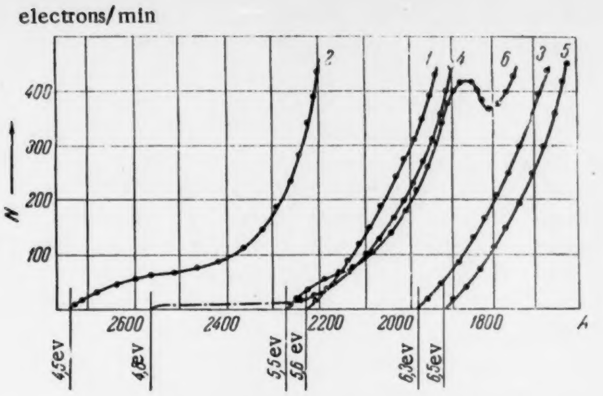

Fig. 3. Yield of photoemission from NiO, ZnO, and Cr_2O_3 surfaces with adsorption of ethanol: 1) NiO after thermal treatment with evacuation; 2) NiO in ethanol vapors (3-5 mm of Hg); 3) ZnO after thermal treatment with evacuation; 4) ZnO in ethanol vapors (3-5 mm of Hg); 5) Cr_2O_3 after thermal treatment with evacuation; 6) Cr_2O_3 in ethanol vapors (3-5 mm of Hg).

observed to give a slight displacement of the photoelectric threshold in the direction of longer wave lengths by 0.1-0.3 ev. Since a considerable portion of the CO is weakly adsorbed in the zinc oxide surface [10], these measurements of the threshold for photoemission were carried out in an atmosphere of CO. For this purpose, the specimen was placed in a counter which was filled with CO (5 mm of Hg) and A (15 mm of Hg). Prior to filling the counter with this mixture, the zinc oxide specimen was cleaned by a glow discharge in an atmosphere of argon. The threshold value of 6.0 ev obtained thereby was in agreement with the 6.1 ev measured in the vacuum cell. The good agreement between these values of the threshold for photoemission indicates that weakly adsorbed carbon monoxide is without influence on the work function of a zinc oxide surface. The insignificant alteration of the photoelectric work function of a zinc oxide surface resulting from an adsorption of CO, or even H_2O vapors, shows the surface bonding of these molecules to be covalent at 20°. The slight decrease in the work function can be explained by this fact, or by the permanent dipole moments of these molecules, the latter so orienting themselves in adsorption that the positive charges will be outward.

In a number of papers (see, for example [11]), indication has been given that there is a certain displacement of the valence electrons toward the adsorption centers when aliphatic and aromatic hydrocarbons are adsorbed on oxide catalysts. In order to test this point, the alteration in the work function of ZnO, NiO, and Cr_2O_3 surfaces from the adsorption of benzene or ethanol was studied. Chromic oxide* is catalytically active, promoting the decomposition of alcohols [12]. The nickel oxide was in the form of a finely dispersed, catalytically active preparation. In view of the fact that the vapors of both benzene and ethanol dissolve in collodion, these measurements were carried out directly in a counter which was filled with the adsorbing vapors (3-5 mm of Hg) and A (15 mm of Hg).

With each of the oxides, there was a diminution of 0.8-1 ev in the photoelectric work function (Fig. 3) as a result of the adsorption of ethanol, although the emission curves were markedly different for these adsorbents; this latter fact could be due to differences in the degree of uniformity of the surfaces, or to differences in the decomposition of the ethanol molecules during chemical adsorption. Thus, by the adsorption of ethanol on nickel oxide, the threshold was displaced from 5.5 to 4.5 ev, the yield of photoemission being comparatively low in the region 4.5-5.2 ev and increasing only slightly with a diminution of the wavelength of the acting radiation. By the adsorption of ethanol on chromic oxide, the work function diminished from 6.5 to 5.5 ev, and, in addition a selective maximum of photoemission was observed in the region of 1900 A (6.5 ev). A similar maximum in the photoemission is to be observed in the adsorption of the dye eosin on a tin oxide surface at low degree of coverage.

---

* This chromic oxide was prepared from ammonium dichromate by V. A. Komarov, Lecturer of the Leningrad State University; for this we wish to express our deep thanks to him.

In the first case, the selective maximum in the photoemission could be due to the photoionization of the surface compounds which are formed by the decomposition of the ethanol on the chromic oxide surface [13]; in the second case, the maximum could result from the photoionization of the eosin molecules. There is little likelihood of the photoionization of the adsorbed molecules of ethanol themselves, since the ionization potential of this compound in the gaseous state is approximately 10 ev. With benzene vapors in the counting tube, there was also a displacement of the thresholds of these adsorbents, the movement being in the direction of the long-wave portion of the spectrum. The largest displacement was observed with zinc oxide. The displacement was least (0.2 ev) in the case of nickel oxide. With benzene vapors, the displacement of the threshold had an intermediate value of the order of 0.5 ev for Cr_2O_3, but the exact position of the threshold could not be determined because of the strong absorption of benzene vapors in this region. The emission curves in the case of the adsorption of benzene were similar to those for clean oxide surfaces. In view of this fact, and the high mobility of the π-electrons of the benzene ring, the diminution of the work function can be explained as arising from a polarization of the adsorbed molecules, with an accompanying extension of the electron cloud toward the adsorbent. In comparison with the emission from the pure oxide surfaces, no marked displacement of the threshold resulted from the adsorption of methane on the oxides of nickel and zinc, this being due to the high symmetry and low polarizability of the adsorbed molecules.

The results of these experiments indicate that benzene and ethanol adsorb on the oxides of zinc and chromium (electron semiconductors), and on nickel oxide (hole semiconductor), with a certain accompanying displacement of the negative charge toward the adsorption centers. The magnitude of the decrease in the work function is independent of the type of semiconduction of the oxide, and is fixed by the nature of the adsorbed molecules and the adsorption centers.

LITERATURE CITED

[1] Z. G. De-Bur, Electron Emission and Adsorption Phenomena (in Russian), Moscow-Leningrad, 1936.

[2] R. Suhrman, Zs. Electrochem. 56, 351 (1952); R. Suhrman and K. Shulz, Naturwiss, 40, 139 (1953).

[3] A. N. Arsen'eva-Geil', The Surface Photoeffect in Semiconductors and Dielectrics (in Russian), Moscow, 1957.

[4] F. I. Vilesov, Instruments and Experimental Techniques, 4, 89 (1958).

[5] J. Bäsken, Rec. Trav. Chim. 47, 1037 (1928).

[6] E. Mollwo and F. Stockman, Ann. d. Phys. 3, 340 (1928); F. I. Vergunas and G. A. Konovalov, J. Exp. Tech. Phys. 23, 712 (1952); I. A. Myasnikov and S. Ya. Pshezhetskii, Problems of Kinetics and Catalysis, 8, 34 (1955).

[7] H. O. Pritschard, Chem. Rev. 52, 529 (1953).

[8] P. Miller, Semiconducting Materials, Foreign Lit. Press, 1954, p. 227.*

[9] K. V. Tagantsev and A. N. Terenin, Proc. Acad. Sci. USSR, 112, 241 (1957).**

[10] N. P. Keier and G. I. Chizhikova, Proc. Acad. Sci. USSR, 120, 830 (1958).**

[11] B. Trepnel, Chemical Adsorption, Foreign Lit. Press, 1958.*

[12] V. A. Komarov, J. Phys. Chem. 27, 1754 (1954).

[13] L. M. Roev and A. N. Terenin, Proc. Acad. Sci. USSR, 125, No. 3 (1959).*

Received January 28, 1959

---

* Russian translation.

** Original Russian translation. See C. B. Translation.

SUPPRESSED CATALYTIC ACTIVITY OF POLYVALENT METALS IN RUBBER

A. S. Kuz'minskii, V. D. Zaitseva and N. N. Lezhnev
Scientific Research Institute of Rubber and Latex Products

(Presented by Academician P. A. Rebinder, January 3, 1959)

It is known that the salts of metals with variable valences exhibit catalytic activity with respect to the conjugated chain oxidations and structural changes in rubber.

According to current ideas [1, 2], metallic ions play a double role in the oxidation of hydrocarbons – they catalyze the initial reaction of chain formation and accelerate the decomposition of peroxides into free radicals [3].

The decomposition of peroxides can be represented by the following reaction scheme:

$$\mathrm{ROOH} + \mathrm{Me}^{+} \rightarrow \mathrm{RO}^{\cdot} + \mathrm{OH}^{-} + \mathrm{Me}^{++}$$
$$\mathrm{ROOH} + \mathrm{Me}^{++} \rightarrow \mathrm{ROO}^{\cdot} + \mathrm{H}^{-} + \mathrm{Me}^{+}.$$

According to our data, the activation energy (E) for the thermal decomposition of stable peroxides in purified NR*(polyisoprene) is 31 kcal/mole; however, in the presence of 0.1% Fe^{+++} (in the form of its naphthoxide) this number is reduced to 23.5 kcal/mole). Although it is obvious that the large decrease in E during oxidation of rubber is partially compensated by a decreased entropy factor, the polyvalent ion still has a very substantial effect on this reaction.

The suppression of the catalytic activity of polyvalent metal ions present in rubbers is a very important but little-studied problem. The present paper partially fills up this gap. The behavior of metallic salts was investigated in two types of rubbers: divinylstyrene and natural.

We measured the rate of oxygen absorption at various temperatures and determined the structural changes in rubber from the viscosity and its solutions in benzene. The results are presented in Fig. 1, 2, and 3.

It is of utmost importance to study the binding of metal ions into stable, catalytically inactive complexes [4, 5].

These complexes are evidently formed by one d electron in Cu^{++} or five unpaired electrons in Fe^{+++} and Mn^{++}; the central ion is completely blocked by the adduct molecules, with the result that electronic transitions from the ion to the substrate (rubber peroxides), and vice versa, become impossible.

The catalytic activities of metal ions with a variable valence, both free and bound in complexes of various stabilities, have been examined in connection with several problems in biocatalysis [6], where it was established that the activity of metal ions decreased as the stability of the complex increased; less stable complexes may be very active in promoting the oxidation of the material or the decomposition of its peroxides.

The catalytic properties of complexes have been studied mainly in homogeneous aqueous systems. There is only scant information on the possibility of using complexes to catalyze reactions in hydrocarbon media and on the suppressed activity of complexed metal ions.

---

* Natural rubber.

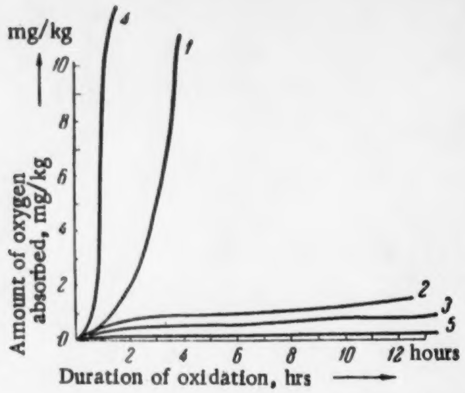

Fig. 1. Oxidation kinetics of technical solid NR (polyisoprene). Temperature 100°. 1) Rubber + + 0.003 moles of copper per 100 g of rubber; 2) rubber + 0.003 moles of copper + 0.05 moles of sodium diethylthiocarbamate (mixed on a roller) per 100 g of rubber; 3) rubber + copper complex of diethylthiocarbamic acid (synthesized), estimated at 0.003 moles of copper per 100 g of rubber; 4) rubber + 0.003 moles of copper per 100 g of rubber; 5) rubber.

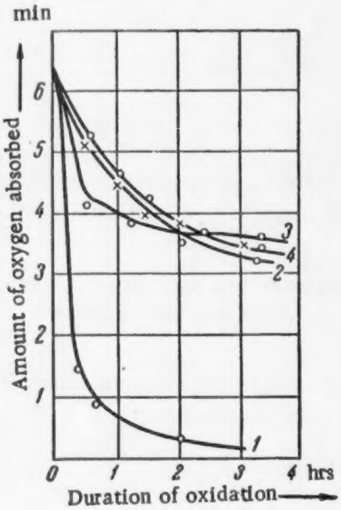

Fig. 3. Viscosity changes in oxidized films of NR (purified). Temperature 100°. 1) Rubber + 0.03 moles of iron per 100 g of rubber; 2) rubber; 3) rubber + 0.03 moles of iron + 0.15 moles of parahydroxyphenyl-β-naphthylamine per 100 g of rubber; 4) rubber + ferric salt of parahydroxyphenyl-β-naphthylamine (synthesized) estimated at 0.03 moles of iron per 100 g of rubber.

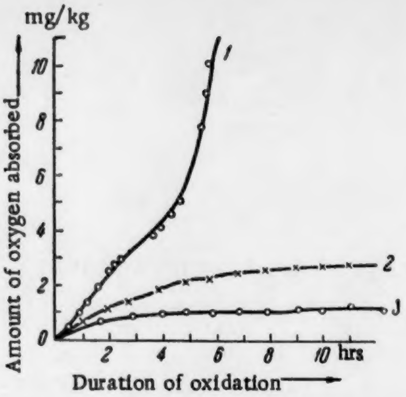

Fig. 2. Oxidation kinetics of technical NR in the solid phase. Temperature 100°. 1) Rubber + 0.003 moles of iron per 100 g of rubber; 2) rubber + 0.003 moles of iron + + 0.25 moles of parahydroxyphenyl-β-naphthylamine (mixed on a roller) per 100 g of rubber; 3) rubber + ferric salt of parahydroxyphenyl-β-naphthylamine (synthesized) estimated at 0.03 moles of iron per 100 g of rubber.

The formation of such complexes in viscous molecular media has not been studied at all.

In the first part of this work we investigated the ability of metal salts to complex with various ingredients of resinous mixtures: in solutions of low molecular weight compounds and in rubber.

The complexing of cupric ions by the antioxidant in a benzene solution was followed by the suppressed fluorescence in benzene and in alcoholic solutions of these compounds.

The conditions ensuring full suppression of fluorescence are given in Table 1.

Since the suppression of fluorescence can be related to the blocking of the ion, it demonstrates the decreased probability of electronic transitions and consequently a decreased catalytic activity of the metal ion.

Further work was directed towards finding out if it was possible to form such complexes in rubber.

The compounds between iron and copper and certain ingredients in the latex form stable complexes which can be obtained by precipitation from aqueous acidic or alkaline solutions and a subsequent thorough washing to remove all components which did not participate in the reaction.

The composition of these compounds is listed in Table 2.

TABLE 1

Chelating agent	Starting formula	Number of copper atoms complexed with one molecule of the chelating agent
Phenyl-β-naphthylamine (neozone-D)	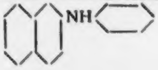	1.5
Parahydroxyphenyl-β-naphthylamine (hydroxyneozone)	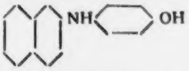	3
Dinaphthylparaphenylenediamine	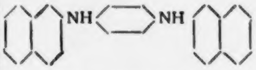	4
Aldol-α-naphthylamine	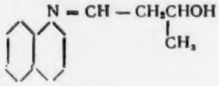	3
1,4-Diphenylphenylenediamine	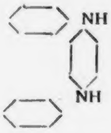	7.5
Diaminodiphenylsulfide	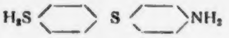	5
Parahydroxydiphenylamine	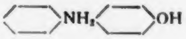	0.1
Phenothiazine	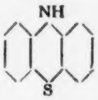	5

TABLE 2

Name of the complex	Number of metal atoms complexed with one molecule of chelating agent
Salt of iron and tetramethylthiuramdisulfide	1
Salt of iron and parahydroxyphenyl-β-napthylamine	2
Salt of iron and diethyldithiocarbamic acid	0.5
Salt of copper and tetramethylthiuramdisulfide	1
Salt of copper and parahydroxyphenyl-β-naphthylamine	3
Salt of copper and diethyldithiocarbamic acid	0.5

The ratios given in Table 1 and 2 between the organic molecules and metallic atoms cannot in the majority of cases be easily represented by any definite structure, so the problem still requires further research.

Let us note that in a rubber medium the reaction between the chelating agent and the metal also proceeds to completion, but very slowly. However, mechanical stirring (rolling) accelerates the process considerably, so that in this case it may be completed in 3-5 minutes.

In Fig. 1, 2, and 3 we have presented kinetic data on the oxidation of rubber in the presence of complexes formed directly in the hydrocarbon medium of the rubber and also complexes introduced into the rubber; the composition of the latter ones is given in Table 2.

In those same figures we have shown, for the sake of comparison, the effects of free Cu^{++} and Fe^{+++} ions. The complexed metal ions had no effect on the oxidation rate and on structural changes in rubber; i.e., they lost their catalytic activity.

Accordingly, rubber containing compounds capable of complexing with Cu^{++}, Fe^{+++}, and other ions is more stable in the presence of salts of polyvalent metals than is the crude latex from which it was prepared.

LITERATURE CITED

[1] A. R. Dabald, Rub., Age, 71, No. 5 (1952).

[2] C. E. Frank, Chem. Rev. 46, No. 1 (1950).

[3] C. H. Bown, J. Oil and Coulor Chem. Assoc. 36, 443 (1953).

[4] P. Chovin, Compt. rend. 219, No. 19, 297 (1941).

[5] G. Salomon, Rev. gén. Cautch. 27, No. 11, 276 (1950).

[6] L. A. Nikolaev, J. Phys. Chem. 31, No. 6 (1957).

Received December 22, 1958

JOULE EFFECT ASSOCIATED WITH THE FLOW AND STOPPING OF ABNORMALLY VISCOUS SUBSTANCES

V. P. Pavlov and G. V. Vinogradov

Institute of Petrochemical Synthesis of the Academy of Sciences USSR

(Presented by Academician V. A. Kargin, January 5, 1959)

When deformation conditions of slightly viscous liquids or generally of systems with short relaxation times, are changed,the state of equilibrium is attained in very short periods of time. This also applies to processes connected with the evolution of heat from internal friction. In systems with sufficiently long relaxation times the transition rates from one equilibrium state to another may have finite values. In such cases it becomes easier to determine the energy required for a transition from one state of the system to another. From the heat evolved after flow is stopped or after the rate of deformation (D) is slowed, it is possible to estimate the energy of structure formation in abnormally viscous systems. So far, nobody has looked into this. However, quite some time ago we had already shown in our work on capillary viscosimetry of homogeneous greases [1, 2] that the evolution of heat in a stream of highly structured systems is considerably below the theoretically expected value in the flow of Newtonian liquids with equivalent viscosities. After the grease flows out of the capillary, for a certain distance away from the orifice the temperature in the stream is slightly elevated. We were already then able to postulate that after an abnormally viscous system comes out of the capillary heat is evolved due to the setting in of structure formation—thixotropic reduction.

The study of heat evolution during flow is also important in that it will help determine the necessary conditions for conducting isothermal viscosimetric experiments and make the corresponding corrections. This is particularly essential in cases where highly viscous and structured systems are investigated in rotation viscosimeters, where D varies over a wide range of values.

The simplest way to study heat evolution during flow is in cases where the field of shearing stress is homogeneous. Therefore, in the present work the evolution of heat was investigated in a previously described [3] rotation viscosimeter, in which the radius of internal cylinder was 6.3 mm, and the width of the gap was 0.25 mm. The cylinders had smooth (polished) working surfaces. To permit instantaneous halting and at the same time to free the apparatus from external moments the setup was outfitted with a powerful braking mechanism and a special coupling. The temperature increase (ΔT) in the stream was determined with an accuracy of ± 0.005° by a differential thermocouple. The hot end of the thermocouple, which was located in the annular gap at a distance of approximately 0.1 mm from the surface of the internal cylinder, was continuously washed by the investigated compound. The cold end and the viscosimeter itself were placed in a circulation thermostat. The water in the thermostat was vigorously stirred and the temperature was maintained within ± 0.005°. The changes in ΔT with time were registered on a mirror galvanometer and recorded photographically with a special camera.

A typical photogram showing the kinetics of changes in ΔT in experiments with Newtonian liquids is represented by the curve OABCL in Fig. 1. The abcissa here represents time. Point O corresponds to the beginning of experiment where D is taken to be a constant. The segment OA of curve AOB shows a rise in temperature at D = const, until steady thermal conditions are established (line AB). Under conditions of steady flow all the thermal energy is transferred to the thermostat and $\Delta T = \Delta T_s = \text{const}$. At point B (at time t_0) the flow was stopped ($D = 0$). The curve BCD gives the kinetics of the cooling process in the investigated material.

Let us analyze the problem of temperature changes in the stream. It is known that the specific force

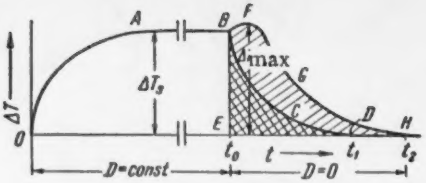

Fig. 1. A photogram of thermal effects in Newtonian liquids and highly structured systems during beginning of flow, under steady flow conditions, and when flow is stopped.

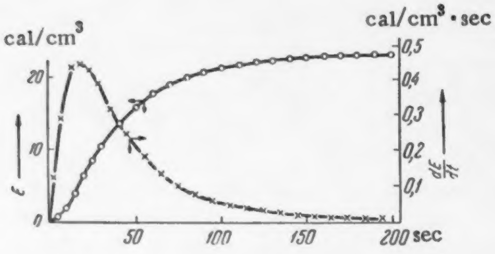

Fig. 2. Time variations of the integral and differential heats of structure formation when a stream of hydrated Ca-grease is halted.

(N_{sp}, expressed per unit volume) necessary to maintain a constant deformation rate in laminary flow and a homogeneous field of shearing stress is $D\tau$. Let all the supplied N_{sp} be converted to heat. One part of it will be used to warm up the material under study, the other will be absorbed in the thermostat. Then the balanced equation for the heat changes will be

$$D\tau = c\frac{d(\Delta T)}{dt} + k\Delta T. \qquad (1)$$

Where c is the specific heat (at constant volume) of the material under study, k the coefficient of thermal conductivity from this material to the liquid in the thermostat.

Equation (1) when used with Newtonian liquids becomes the analytical expression for curve OABCD. Its linear segment AB can be represented by equation

$$D\tau = k\Delta T_s, \qquad (2)$$

For the case where flow is halted, equation (1) gives us

$$c\frac{d(\Delta T)}{dt} + k_1\Delta T = 0. \qquad (3)$$

Under stationary conditions the thermal conductivity coefficient may have a value different from that in equations (1) and (2). Therefore in Eq. (3) it is denoted by k_1. However, due to the fact that it is very difficult to experimentally determine k_1 we assumed that $k_1 = k$.

Assuming that c and k are independent of t and ΔT, and also that c is constant both under conditions of rest and flow, we integrate Eq. (3) and get

$$c\Delta T_s = -k\int_{t_0}^{t_1}\Delta T dt = kmS_1 = E_1. \qquad (4)$$

Here n is a proportionality constant connecting the numerical value of the integral with the area BCDE in Fig. 1, denoted by S_1. From equation (4) it follows that the amount of heat E_1 transferred to the thermostat (proportional to the area S_1) equals the decrease in heat content of the liquid ($c\Delta T_s$).

In order to determine coefficient k we investigated the dependence of ΔT_s on $D\tau$ values from 10^6 to 10^8 ergs/cm³·sec. The investigation was conducted on Newtonian liquids (hydrocarbon oils), fluid disperse systems of the same type as homogeneous greases, highly structured concentrated solutions of ethyl cellulose and aluminum naphthoate in several solvents, as well as some other compounds. The applicability of equation (2) was confirmed, and it was shown that k is constant for a given viscosimeter and independent of $D\tau$ and of rheological properties of the investigated compounds. In our case $k = (5\cdot 10^7 \pm 3\%)$ ergs/cm³·sec·deg.

Knowing the value of k and utilizing equation (2) we can ensure isothermal conditions in our determinations of viscosity at various $D\tau$. According to equation (2) we have to calculate ΔT_s from known values of τ and D. If ΔT_s turned out to be larger than the allowed deviations from the controlled temperature, then the liquid in the thermostat had to be cooled by ΔT_s degrees. Our experiments fully proved the effectiveness of this procedure.

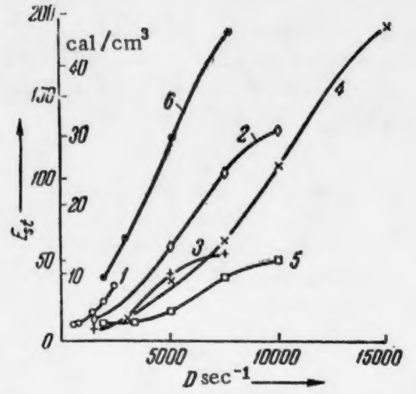

Fig. 3. Heat of structure formation as a function of the deformation rate at which the flow was stopped. 1) 15% Lithium stearate in bright stock of chosen purity; 2) aliphatic "solidol"; 3) synthetic "solidol"; 4) 10% lithium stearate in a low-viscosity oil; 5) 5% aluminum naphthoate in a low-viscosity (machine) natural oil; 6) 10% aluminum naphthoate in the same oil.

Let us now find out what happens when the flow of highly structured systems with the same heat capacities as Newtonian liquids is stopped. The curve BFGH in Fig. 1 corresponds to such a case. After the instrument was suddenly turned off the temperature of the system inclosed in the gap of the viscosimeter increased, attaining in several seconds a maximum value at point F. Later, for about two or three minutes it decreased along curve FGH and at time t_2 became equal to the water temperature in the thermostat. The value of $\delta = \Delta T_{max} - \Delta T_s$ may attain several tens of degrees.

The temperature increase, after the flow of highly structured systems was stopped in rotational viscosimeters, agreed beautifully with the previously mentioned experiments where we determined the temperature of a grease stream coming out of a capillary.

Let E_2 denote all the heat evolved when the stream of a structured system is stopped. To this corresponds the area BFGHE in Fig. 1, equal to S_2. If the initial heat contents of a Newtonian and a structured system are equal (point B in Fig. 1), the excess (over a Newtonian liquid) heat evolved when a flowing structured system is stopped will be $E_{st} = E_2 - E_1 = km(S_2 - S_1)$. Besides the over-all excess of heat evolved (E_{st}) we can also make use of the instantaneous (at any given time) excess of heat evolved (E).

The increased evolution of heat when flowing structured systems are stopped does not result from the work done by the elastic (potential) energy stored in the system. The maximum elastic energy (E_e) can be easily calculated if we assume that (within the available limits of accuracy) Hooke's law is applicable. One obtained in such a case variable values of E_e. Nevertheless, in highly structured grease-like systems these are at least 4-tenths of an order of magnitude smaller than E_{st}.

TABLE 1

D, sec^{-1}	1500	5000	7500	10000
E_{st}, joule/cm^3	14	58	104	130
τ_s, g/cm^2	15	25	33	40
$E_{st}(D\tau_s)^{-1}$, sec	6.2	4.6	4.2	3.3

The increased evolution of heat and the rise in temperature after the flow of abnormally viscous systems is stopped occurs due to a structure-formation process which proceeds with time – during a thixotropic reduction of structure. The amount of heat evolved determines the energy of structure formation (E_{st}). With reversible thixotropic transformations E_{st} should be equal to the energy of structural breakdown.

The rapid damping of the heat evolution is connected with the high values of k and the fact that the rate of thixotropic reduction in structured systems declines rapidly with time.

In Fig. 2 we have drawn some typical curves for the changes in integral (E) and differential (dE/dt) heats with time after the flow was suddenly stopped. The material used in this study was "solidol", a grease composed of spindle oil thickened with 18.5% of the calcium soap of cottonseed oil. Experiment was carried out at D = 7200 sec^{-1} and room temperature. The thing most obvious in Fig. 2 is that E_{st} is very large (more than 20 kcal/cm^3), comparable in value to the heats of fusion of many compounds. In Table 1 we have made a comparison between the energy of structural breakdown and the specific powers of steady flow in a stream of "solidol" at room temperature; it is obvious that E_{st} and $D\tau_s$ are comparable in magnitude and that with increasing deformation rate $D\tau_s$ increases faster than E_{st}.

The value of E depends on D and on the nature of the structured systems. This is well illustrated by the data in Fig. 3, where we illustrated experiments done on several systems at room temperature. Figure 3 shows that with increasing depth of structural breakdown,if D exceeds a certain critical value the rate of increase of E_{st} decreases. We can assume that with less-structured systems at sufficiently high D we should be able to attain the maximum values of E_{st}.

In this paper we have described for the first time a direct method of determining the structure formation and breakdown energies in systems with very long relaxation times; the method is based on the determination of heat evolved when the flow of an abnormally viscous system is halted. Since it was demonstrated that the breakdown and spontaneous restoration of structure are accompanied by appreciable amounts of heat, the classical definition of thixotropy proposed by Freundlich does not strictly hold.

The authors wish to thank Academician V. A. Kargin for discussing this work and some valuable advice.

LITERATURE CITED

[1] G. V. Vinogradov and V. P. Pavlov, Proc. Acad. Sci. 58, 1391 (1947).

[2] G. V. Vinogradov and V. P. Pavlov, Coll. Properties of Petroleum Products at Low Temperatures, 1949, p. 61.*

[3] V. P. Pavlov, Coll. Annotations to the Papers on the Chemistry and Technology of Petroleum and Natural Gases Published in 1956, Petroleum Institute of the Acad. Sci. USSR, 1957, p. 69.*

Received December 17, 1958

---

* In Russian.

THE COMBINED ACTION OF ORGANIC CATIONS AND HALIDE ANIONS ON THE EVOLUTION OF HYDROGEN ON A MERCURY ELECTRODE

Tza Chyuan-hsin and Z. A. Iofa

M. V. Lomonosov Moscow State University

(Presented by Academician A. N. Frumkin, December 8, 1958)

The hydrogen overvoltage on mercury cathode depends on the nature and concentration of the surface-active agents present in solution, for the adsorption of these products at the boundary between the electrode and solution changes the structure of the electrical double layer in which the elementary processes of hydrogen ion discharge occur.

By taking into consideration the effect of double-layer structure on the surface concentration of discharging ions and the activation energy for the discharge, A. N. Frumkin derived [1] the following equation for the hydrogen overvoltage in acid solutions

$$\eta = \frac{RT}{\alpha F} \ln i - \frac{1-\alpha}{\alpha} \frac{RT}{F} \ln[H_3O^+] + \frac{1-\alpha}{\alpha} \psi_1 + \text{const}, \qquad (1)$$

where ψ_1, is the average potential one ionic radius away from the electrode surface.

The action of various surface-active ions differs in that, first of all, their adsorption may vary differently with changes in electrode potential, and second, that when adsorbed they may produce different (in magnitude and sign) changes in the potential ψ_1. Halide ions become predominantly adsorbed on a neutral or positively charged electrode surface, displace the ψ_1 potential in the negative direction, and (in accordance with equation 1) decrease the hydrogen overvoltage. Tetraalkylammonium cations displace the ψ_1 potential towards more positive values and increase the hydrogen overvoltage [2].

The present work was undertaken to explain the mechanism of a joint action by organic cations and halide anions. We often encounter such combined systems in practice, so it was interesting to find out if the effects of individual ions on the kinetics of electrochemical reduction of hydrogen ions are preserved when above-mentioned ions are present in solution together.

In Fig. 1 we have plotted curves of η vs. log $\underline{i}$ obtained on a dropping-mercury electrode by a method described in paper [3]. The electrode was polarized at a constant potential (φ = const.) during the lifetime of a drop; the true current density* in this case was,

$$i = {}^5/_3 \frac{\bar{I}}{S_2}, \qquad (2)$$

---

* The condition φ = const. was attained at minimum resistance in the polarization circuit. In such a case (according to Tafel's equation) i = const., while current I changes with increase in drop area. Since $I_2 = iS_2$ (where I_2 and S_2 are the current and drop area at τ_d – the moment the drop is detached) then $S = S_2 t^{2/3} \tau_d^{-2/3}$, $I = iS_2^{2/3} \tau_d^{-2/3}$, and the average current $\bar{I} = \frac{1}{\tau_d} \int_0^{\tau_2} I_2 t^{2/3} \tau_d^{-2/3} dt = {}^3/_5 I_2 = {}^3/_5 iS_2$.

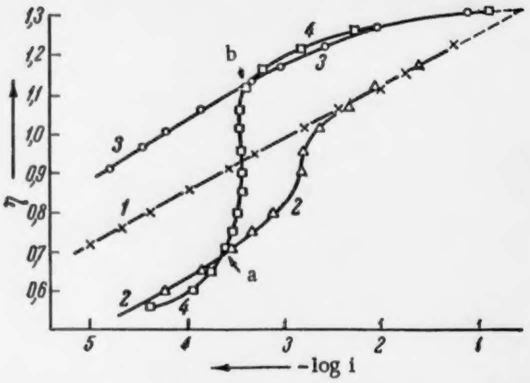

Fig. 1. Overvoltage curves in solutions of: 1) 2 N HCl + + 2 N KCl; 2) 2 N HCl + 2 N KI; 3) 2 N HCl + 2 N KCl + + $4.5 \cdot 10^{-4}$ moles/liter of $N(C_4H_9)_4Br$; 4) 2 N HCl + 2 N KI + $4.5 \cdot 10^{-4}$ moles/liter of $N(C_4H_9)_4Br$.

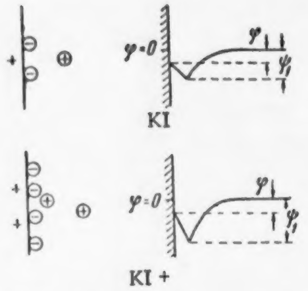

Fig. 2. Schematic representation of an electrical double layer at $\varphi_r = -0.6$ v.

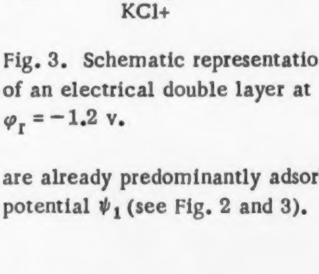

Fig. 3. Schematic representation of an electrical double layer at $\varphi_r = -1.2$ v.

where $\bar{I}$ is the average current measured with a well-damped mirror galvanometer; S_2 is the maximum area of a drop, calculated from the formula $S_2 = 0.850\ (\tau_d m)^{2/3}$ cm^2 (τ_d = dropping period, m = rate of mercury flow). Experiments were conducted at 20 ± 1°. An equilibrium hydrogen electrode in 2 N HCl + 2 N KCl was used as reference.

One can see from curve 1 in Fig. 1 that in the range of potentials where it was possible to measure hydrogen overvoltage on a dropping-mercury electrode the adsorption of Cl^- ions was small, and one could not detect any effects on the overvoltage. Addition of some $N(C_4H_9)_4^+$ cations increased the overvoltage considerably (curve 3). Iodide ions, which were strongly adsorbed over a wide range of potentials at low current densities, decreased the overvoltage (curve 2). The introduction of $N(C_4H_9)_4^+$ cations in this case produced an additional decrease in the overvoltage in the region of low overvoltages (compare curves 2 and 4). With increasing current density the overvoltage increased sharply and attained a value greater than that in a solution of 2 N HCl + + 2 N KCl + $N(C_4H_9)_4^+$. When the current density was increased some more the excessive overvoltage decreased and the η vs. log $\underline{i}$ curve coincided with the same curve for solutions free of organic cations (curve 4). The reduced action of organic cations in regions of high negative potentials has already been described [4].

It is obvious that the section of decreased η in the region of low polarizations is associated with a predominant adsorption of iodide anions; the section of increased η corresponds to predominant adsorption of organic cations, and finally the decreased effect of cations adsorption at higher polarizations corresponds to desorption of these cations.

The observed mutual reinforcement in the action of the adsorbed ions can be explained by some "secondary adsorption" of oppositely charged surface-active ions on the neutral surface of the electrode. Secondary adsorption enhances the adsorption of those same ions, which are already predominantly adsorbed in the given range of potentials, and thus produces a greater change in potential ψ_1 (see Fig. 2 and 3).

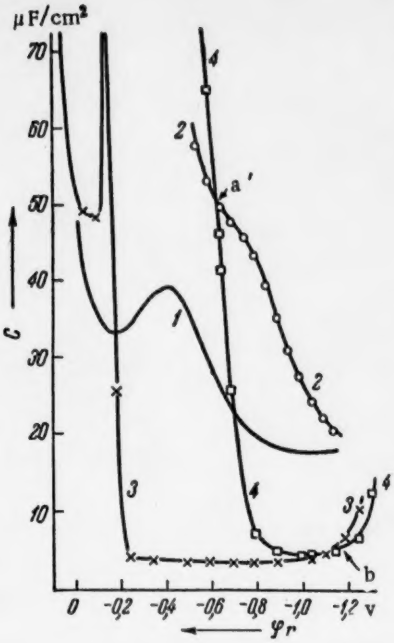

Fig. 4. Differential capacitance curves as a function of potential. The solutions are labeled just as in Fig. 1. Curves 1 and 2 were recorded at a frequency of 400 hertz, curves 3 and 4 at 5000 hertz.

This description of the combined ionic action is confirmed by the differential capacitance of an electrical double layer determined on a dropping-mercury electrode in those same solutions. The impedance bridge used in this work did not differ in its basic design from those described in papers [5-7]. The time interval between the detachment of a drop and the subsequent achievement of bridge balance was determined accurately with an electronic relay and an electric timer.

As one can see from Fig. 4 (where differential capacitance was plotted as a function of electrode potential φ_r), at potentials more negative than -0.63 v, curve 4, obtained with a solution containing quaternary salt cations, fell above the one with just HCl + KI in solution (curve 2). This means that with increasing potential at $\varphi_r > -0.63$ v, the electrode surface becomes charged more rapidly under the influence of quaternary cations. It is quite obvious that if only anions had any effect on the structure of the double layer at low polarizations then the left portions of curve 2 and 4 would have to coincide.

Iodide anions act similarly at high polarizations. Comparing curve 3 and 4 one can see that at potentials more negative than -1.13 v, the adsorption of quaternary cations in the presence of iodide anions decreases the capacitance more abruptly (with increasing potential), whereas the desorption of the organic cation begins at more negative potentials.

It is interesting to note that the potentials at the intersections of curves 2 and 4 and curves 3 and 4 (points a' and b' in Fig. 4) practically coincide with the potentials at the intersections of the corresponding polarization curves (points a and b in Fig. 1). It seems that to the first approximation this coincidence can be used to support the proposed hypothesis on the mutual reinforcement of adsorbed ions, although it would be more appropriate to compare the locations of a and b at the intersections of $(\eta, \log i)$ curves with the intersections of curves representing not the differential capacitance, but the electrode charge as a function of potential.

We wish to thank Academician A. N. Frumkin for his interest in this work and valuable advice.

LITERATURE CITED

[1] A. Frumkin, Zs. Phys. Chem. A 164, 121 (1933).

[2] Z. Iofa, B. Kabanov, E. Kuchinskii and F. Chistyakov, J. Phys. Chem. 13, 1105 (1939).

[3] Z. A. Iofa and A. I. Kolychev, J. Phys. Chem. 14, 58 (1940); Acta physicochim. URSS, 12, 231 (1940).

[4] E. P. Andreeva, J. Phys. Chem. 29, 699 (1955); Z. A. Iofa, E. P. Andreeva and N. V. Nikolaeva, Trans. Conf. on Electrochem. Izd. AN SSSR, 1953, p. 294.*

[5] D. C. Grahame, J. Am. Chem. Soc. 68, 30 (1946); 71, 2976 (1949).

[6] V. I. Melik-Gaikozyan, J. Phys. Chem. 26, 560 (1952).

[7] B. B. Damaskin, J. Phys. Chem. 32, 2199 (1958).

Received December 1, 1958

---

* In Russian.

THE MECHANISM OF THE ANODIC FORMATION OF THE PERSULFATE ION

Ts'u Yung-ts'ao and Mi Tien-ying

The Institute of Applied Chemistry of the Academy of Sciences of the
Chinese People's Republic, Changchun

(Presented by Academician A. N. Frumkin, January 7, 1959)

Since the discovery of persulfuric acid by Berthelot (1878), two theories concerning its anodic formation, the "active oxygen" theory (OH, O, H_2, O_2), and the theory of direct discharge [1, 2], have been in vogue, although neither of these theories has been confirmed by adequate experimental data. Using O^{18} as an indicator, A. N. Frumkin and his co-workers [3] have shown that the oxygen of the water does not enter into the make-up of the $S_2O_8^{2-}$ which results from electrolysis. This makes it seem all the more likely that $S_2O_8^{2-}$ arises from the discharge of the SO_4^{2-} ion. At the same time, these authors have indicated that there are other hypotheses, which, though they are less likely to be valid, are still consistent with the data obtained through the method of tagged atoms. Thus, it might be supposed that the OH radical is the initial product of electrolysis, and that this radical subsequently oxidizes the SO_4^{2-} through an electron transfer without an accompanying displacement of oxygen. On the basis of the relation between the concentration of the HSO_4^- ions and the current efficiency of the formation of persulfuric acid, E. A. Efimov and I. A. Izgaryshev [4] have postulated that persulfuric acid is formed by direct discharge of HSO_4^-.

In order to explain the mechanism of the anodic formation of the persulfate ion, it is necessary to obtain direct experimental data on the kinetics of this process and the relation to the kinetics of the evolution of oxygen.* This calls for a separation of the total current density, i_T, into those current densities i_I and i_{II}, which are associated with the formation of O_2 and $S_2O_8^{2-}$, respectively, i.e., partial-polarization curves must be constructed for these latter processes. The evolution of O_2 on a Pt electrode is an unstable process which is strongly affected by the adsorption of oxygen and anions on the electrode. Thus, it is necessary to determine the most stable polarization curve for this reaction [5].

Electrolysis was carried out in a cell which was divided by a glass diaphragm equipped with ground joints. The anode was a smooth platinum wire, 1 mm in diameter and about 1 cm^2 in area. In order to assure energetic agitation, a magnetic stirrer was placed beneath the anode. The anode section of the cell was equipped with a horizontal glass tube, with a scale, into which a soap film was introduced. From the movement of this film, it was possible to determine the rate of evolution** of the O_2; this permitted a calculation of the current efficiency of the formation of $S_2O_8^{2-}$. Comparison was made with a mercurous sulfate electrode, the potentials being recalculated to the normal hydrogen electrode. Experiments were carried out at a temperature 7°.

Prior to measurement, the electrode was subjected to a strong anodic polarization, after which measurements were begun at low current densities (10^{-4} or 10^{-5} amp/cm^2). After each alteration in the current density, the stable value of the electrode potential was measured, these measurements being performed when the change in potential had proven to be no more than 3 mv in 30 minutes.

---

*When the present paper was ready for the press, we became acquainted with another paper [8], also in press, in which the concurrent formation of $S_2O_8^{2-}$ and O_2 was also considered. In a future communication, it is hoped to compare the results of this work with our own conclusions.

**Under the experimental conditions, ozone is formed in only insignificant amounts, and, in a first approximation, can be neglected.

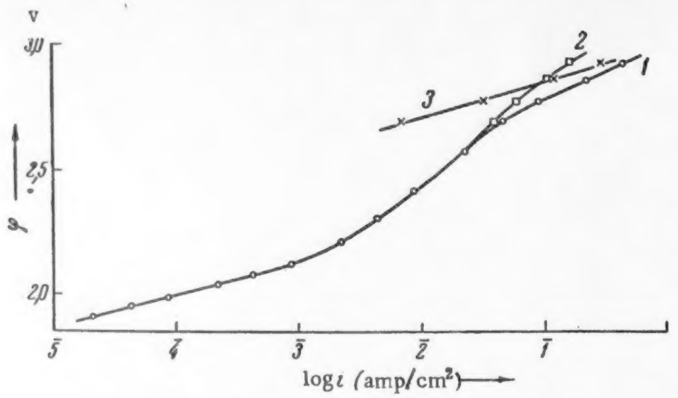

Fig. 1. Anodic polarization curves in 3.5 N $(NH_4)_2SO_4$ + 3.5 N H_2SO_4 solution: 1) total-polarization curve; 2) partial-polarization curve for the evolution of O_2; 3) partial-polarization curve for the formation of $S_2O_8^{2-}$.

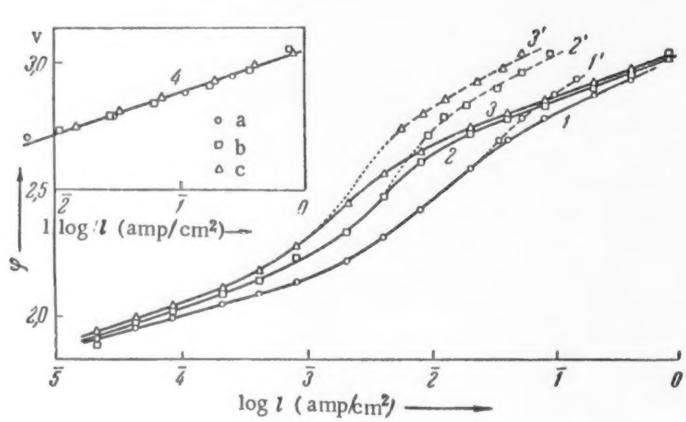

Fig. 2. Anodic polarization curves for 3.5 N $(NH_4)_2SO_4$ + 3.5 N H_2SO_4 + + NH_4F solutions. The full curves 1, 2, 3 are total-polarization curves; the dotted curves 1', 2', 3' are partial-polarization curves for the evolution of O_2. NH_4F concentrations: 1 and 1') 0; 2 and 2') $3 \cdot 10^{-4}$ N; 3 and 3') 10^{-3} N. 4 is partial-polarization curve for the formation of $S_2O_8^{2-}$; NH_4F concentrations; a) 0; b) $3 \cdot 10^{-4}$ N; c) 10^{-3} N.

Figure 1* represents polarization curves which were obtained in a 3.5 N $(NH_4)_2SO_4$ + 3.5 N H_2SO_4 solution. The total-curve 1, (the potential rise on this curve is especially marked at the higher current densities) is similar in form to the curves which have been obtained by other authors [6]. Over a wide interval of current densities, curve 2 is a straight line. It is to be seen from Fig. 1 that the rate of the formation of the $S_2O_8^{2-}$ ion is much less than the rate of evolution of O_2 in the region of low current densities. On elevating the current density, a stable oxide film, incorporating the acid anions in its make-up, is formed on the platinum surface [5, 6]. It is clear that the formation of this film results in a diminution in the energy of adsorption of the OH radicals (or of the O atoms) and thus leads to a marked retardation in the evolution of O_2. As a result, the potential for the separation of O_2 is raised to such a value that the formation of $S_2O_8^{2-}$ becomes possible. At the point of intersection of the curves 2 and 3, the rate of formation of the $S_2O_8^{2-}$ becomes equal to the rate of evolution of O_2. Under more positive potentials, the rate of formation of $S_2O_8^{2-}$ becomes higher than that of the formation of O_2 and the current efficiency for the formation of $S_2O_8^{2-}$ is in excess of 50%.

---

* These data form a part of the material which was published in the Reports of the Academy of Sciences of the Chinese People's Republic for 1958-1959.

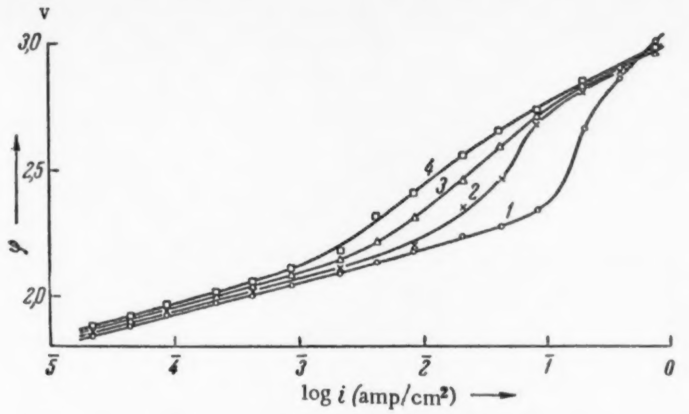

Fig. 3. Anodic-polarization curves for $H_2SO_4 + (NH_4)_2SO_4$ solutions. Total electrolyte concentration, 7 N. $(NH_4)_2SO_4$ concentrations: 1) 0; 2) 0.5 N; 3) 3.5 N; 4) 5 N.

The effect of added NH_4F is shown in Fig. 2. From this figure, it follows that the adsorption of the F^- ions leads to a marked increase in the overvoltage for the evolution of O_2, this effect being especially marked in the region of the sharp potential increase. Curve 4 shows that, within the limits of experimental error, points obtained from solutions free of F^- ions lie on the same straight line as those obtained with solutions containing various concentrations of F^- ions. Thus, the adsorption of F^-, although markedly retarding the evolution of O_2, is without influence on the kinetics of the anodic formation of the $S_2O_8^{2-}$. This fact makes understandable the effect of the F^- ions on the current efficiency of the formation of $S_2O_8^{2-}$.

The action of SCN^- and Cl^- ions is similar to that of F^-; i.e., these ions increase the overvoltage of O_2, but are practically without effect on the kinetics of the formation of $S_2O_8^{2-}$. As the result of the oxidation of SCN^- and Cl^-, there is, however, a limiting diffusion current of each of these ions in the region of low current densities.

These facts confirm convincingly the theory of the direct formation of $S_2O_8^{2-}$, since a retardation of the discharge of the water molecules would be accompanied by a retardation in the formation of the $S_2O_8^{2-}$ if the first of these processes were an intermediate stage in the second (theory of "active oxygen").

Kinetic calculations on this process confirm the correctness of this conclusion and show the direct discharge of the ion of sulfuric acid to be the decisive stage in the anodic formation of $S_2O_8^{2-}$:

$$HSO_4^- \, (SO_4^{2-}) \rightarrow HSO_4 \, (SO_4^-) + e^-. \tag{I}$$

A review of the kinetic equations also shows that the evolution of O_2 at high current densities can proceed, in part, through such an intermediate discharge of HSO_4^- (SO_4^{2-}) as:

$$HSO_4 \, (SO_4^-) + H_2O \rightarrow H_2SO_4 \, (HSO_4^-) + OH_{ad}; \tag{II}$$

$$2\,OH_{ad} \rightarrow O_{ad} + H_2O, \tag{III}$$

$$2\,O_{ad} \rightarrow O_2. \tag{IV}$$

rather than through discharge of the water molecules.

The effect of the addition of ammonium ions on the total polarization curve for the process is shown in Fig. 3.* It is to be seen that addition of these ions markedly increases the potential, especially in the region where there is a sharp rise in the curve. The mechanism of cation action requires further investigation. According to Frumkin, the effect of cations can be due to their action on the oxide film on the platinum surface [7].

The authors express their heartfelt thanks to Academician A. N. Frumkin for his valuable advice, and to Professor B. N. Kabanov for his review of the manuscript.

LITERATURE CITED

[1] S. Glasstone and A. Hickling, Electrolytic Oxidation and Reduction, 1936.

[2] W. Machu, Das Wasserstoffperoxyd u. die Perverbindungen, 1951.

[3] A. N. Frumkin, R. I. Kaganovich, M. A. Gerovich and V. N. Vasil'ev, Proc. Acad. Sci. USSR, 102, 981 (1955).

[4] E. A. Efimov and I. A. Izgaryshev, Proc. Acad. Sci. USSR, 106, 1039 (1956).**

[5] Ts'u Yung-ts'ao, Lo Hsiu-ching, Chou Shuo-wu, et al., Bulletin Acad. Sci. Chinese People's Republic (Sciences Record) (1958).

[6] R. I. Kaganovich, M. A. Gerovich and É. Kh. Enikeev, Proc. Acad. Sci. USSR, 108, 107 (1956);** M. A. Gerovich, R. I. Kaganovich, V. M. Vergelesov and A. N. Gorokhov, Proc. Acad. Sci. USSR, 114, 1049 (1957);** R. I. Kaganovich and M. A. Gerovich, J. Phys. Chem. 32, 957 (1958).

[7] A. N. Frumkin, V. S. Bagotskii, Z. A. Iofa and B. N. Kabanov, The Kinetics of Electrode Processes (in Russian) 1952.

[8] A. A. Rakov, V. I. Veselovskii, K. I. Nosova, É. V. Kasatkin and T. I. Borisova, J. Phys. Chem. 32, No. 12 (1958).

Received December 1, 1958

---

*This diagram has been taken from the work of Lo Hsiu-ch'ing and Chou Shuo-wu (unpublished).

**Original Russian pagination. See C. B. Translation.

THE EFFECT OF SURFACE HYDRATION ON THE ADSORPTION OF ALIPHATIC ALCOHOLS (FROM SOLUTION) ON SILICA

L. G. Ganichenko, V. F. Kiselev and K. G. Krasil'nikov
M. V. Lomonosov Moscow State University

(Presented by Academician M. M. Dubinin, December 30, 1958)

Differences in the degree of hydration of a silica surface have great effect on the adsorption of water vapor [1], but relatively little effect on the adsorption of saturated aliphatic hydrocarbons [2] whose adsorption is primarily determined by the dispersion forces between the molecules and the surface atoms of the adsorbent. It was interesting to investigate the adsorption of the homologous series of alcohols, since those molecules contain a hydroxyl group and hydrocarbon chains of various lengths. In this work we measured the adsorption of several normal alcohols (from CCl_4 solutions) on silica samples with various degrees of surface hydration. The literature contains very little information on the effects of hydrated silica surfaces on the adsorption of various compounds from solution. We only know that the adsorption of dissolved compounds silica gel decreases after thermal treatment; thus, in paper [3] it was shown that the maximum adsorption of acetic and stearic acids from CCl_4 solutions decreased as the firing temperature of silica gel was raised; however, the authors of [3] did not determine the specific surface of the investigated samples and therefore could not separate the effects caused by a changed degree of surface hydration from those caused by decreased surface area. Recently it was observed [4] that the dehydration of a silica gel surface was accompanied by a decreased maximum adsorption of lauric acid from pentane solutions. While investigating the maximum adsorption from CCl_4 solutions in a homologous series of n-alcohols, certain workers [5] have shown that as the length of the hydrocarbon chain was incteased the porosity of the silica gel began to have a greater influence on the maximum adsorption. Therefore, in order to find out just what effect does the nature of the surface have on the adsorption in a homologous series of molecules, it is necessary not only to determine the degree of surface hydration but also conduct all the measurements on nonporous silica samples.

We used two samples of nonporous silica (powdered silica gel [6]) in our work, PSG-1 and PSG-2. Both samples were fired at 300° before the experiment; a separate sample was also fired at 700°C. The method used in determining the specific surface and structural-water content was described in paper [7]; our results are presented in Table 1. An interferometer was used to measure the equilibrium concentrations of solutions.

As one can see in Figs. 1 and 2 the maximum adsorptions of the investigated alcohols, when expressed per 1 m^2 of the surface of each sample, decrease with increasing hydrocarbon chain length. The degree of surface hydration had a noticeable effect on the maximum adsorption, and the effect (most pronounced in the case of methanol) decreased with increasing chain length of the alcohol. The area ω, occupied by one adsorbed methanol molecule (Fig. 2, b) on the most hydrated sample (PSG-2-300°) is 11.7 A^2, which is close to 12.5 A^2 [8], the area occupied by a hydroxyl group. Thus, each adsorbed methanol molecule is associated with one surface hydroxyl (Fig. 2, d). With increasing surface dehydration the number of methanol molecules per one surface hydroxyl increases, the settling area ω increases, and the thickness of the adsorbed layer decreases (Fig. 2b and 2c). However, such calculations based solely on adsorption data still do not allow any definite conclusions about the true nature and number of bonds formed between the adsorbed molecules and the adsorbent surface, nor about bonds between the adsorbed molecules, and in particular about the formation of intermolecular aggregates [9]. Any assumptions made in this connection can only become confirmed and well established if one introduces into the solution of this problem some other independent data, especially heats of adsorption. As one proceeds

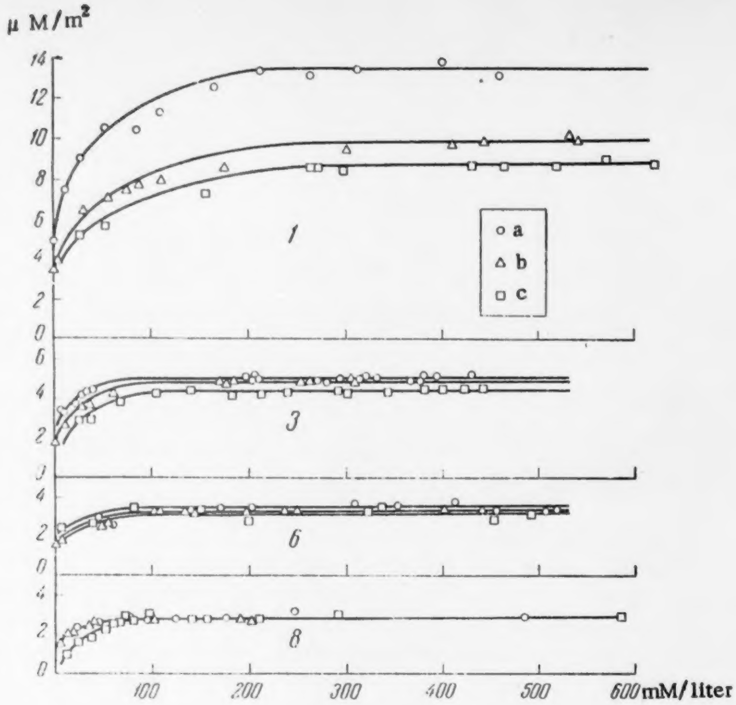

Fig. 1. Adsorption isotherms of n-alcohols (from CCl_4) on powdered silica gel. a) PSG-2-300°; b) PSG-1-300°; c) PSG-2-700°. The numbers next to the curves denote the number of carbon atoms in a molecule of alcohol.

TABLE 1

Adsorption Characteristics of the Powdered Silica Gel Used in this Experiment

Sample	Processing temp., °C	Specific surface, in m^2/g	Structural water content, in $\mu M/m^2$
PSG-2	300	169	7.9
PSG-1	300	244	4.2
PSG-2	700	129	2.8

towards higher alcohols the ratio between the number of adsorbed molecules, and the number of surface hydroxyls decreases. The molecules become attached to the surface at an angle [5] and seem to shield some of the hydroxyl groups; consequently the adsorption of hexanol already begins to be almost independent of the hydroxyl concentrations (as far as we had investigated). And as follows from Figs. 1 and 2a, the absorption of octanol is practically independent of the surface hydration. In connection with this, we should note that as we go from methanol to propanol the heat of wetting becomes less dependent on the degree of surface hydration; the heat of wetting (of silica gel) by n-heptane remains practically constant when the samples are thermally dehydrated [10]. With increasing length of the hydrocarbon chain its role in the adsorption process increases, and the adsorption properties of higher alcohols begin to resemble those of the corresponding hydrocarbons. On the other hand, it should not be assumed that the alcohols are adsorbed only on the silanol portion of the area. If we assume that the limiting adsorption of alcohols (shown in Fig. 2a) remains a linear function of the degree of surface hydration all the way to complete dehydration, then we can readily see that there would still be considerable adsorption on the siloxane surface.

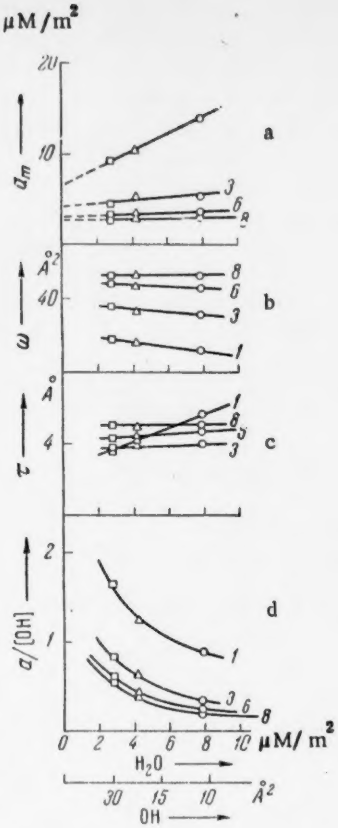

Fig. 2. Maximum adsorption a_m (a), settling area of molecule ω (b), thickness of the adsorbed layer τ (c), ratio between the number of adsorbed molecules and the number of hydrogen groups a/[OH] (d), all as a function of the degree of surface hydration. The numbers denote the number of carbon atoms in an alcohol molecule.

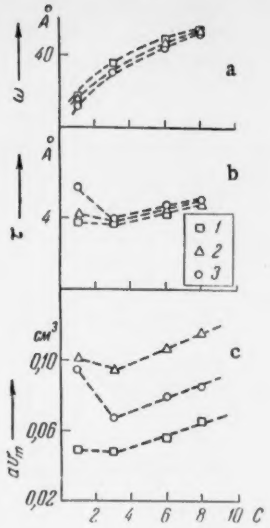

Fig. 3. Settling area ω (a), thickness of the adsorbed layer τ (b), and maximum volume av_m (c) of normal alcohols on samples of powdered silica gel. 1) PSG-1-300°; 2) PSG-2-300°; 3) PSG-2-700°.

According to [11] the maximum adsorption in a homologous series of alcohols should remain constant on nonporous lyophilic adsorbents, which would correspond to a representation where the molecules on the surface layer are oriented in such a way that the adsorption occurs through the hydroxyl group in the alcohol while the hydrocarbon chains are arranged normal to the surface. However, some direct experiments carried out on nonporous silica and reported in paper [5] contradicted this assumption. With increasing hydrocarbon chain length the limiting adsorption of alcohols decreased, the settling area of molecules increased correspondingly, but in the homologous series the increase per CH_2 group became smaller. From this it was deduced that most of the adsorbed alcohol molecules "lie" on the surface, while with higher alcohols they become inclined to the surface. The data obtained in our present work (presented in Fig. 3) permit an extension of the conclusions made in [5] to surfaces with various degrees of hydration. On inspecting these data we can't fail to notice the small size of the settling area and the greatly increased layer thickness when methanol is adsorbed on PSG-2-300°; since this sample had the most hydrated surface, it seems that the above-mentioned facts must be connected with changed orientation of the methanol molecules.

The surface of silica is not homogeneous [12]; it consists of qualitatively different segments, or places with varying energy and adsorption properties. This nonhomogeneity is characterized by varying distribution of the silicon – oxygen tetrahedra, and consequently different degrees of surface hydration, i.e., by varying ratios between the silanol and siloxane portions of the surface. Variations in the distribution of SiO_4 tetrahedra on the surface may arise during the preparation and subsequent processing of the samples. Thermal treatment, in particular, renders the structural elements of the silica lattice (SiO_4 tetrahedra) somewhat labile; this fact is evidenced by polymorphic transitions in the SiO_2 systems [15] [$\beta-\gamma$-tritonite, $\alpha-\beta$-crystobalite (117-270°), as well as $\alpha-\beta$-quartz (575°)]. It seems that the rearrangement of SiO_4 tetrahedra will begin and proceed most readily on the surface of the samples, where their one-sided bonds to the outside phase would provide favorable conditions for such transformations. The thermal dehydration of the surface is accompanied by such a rearrangement. At the same time, as we have shown in this work, the orientation of the adsorbed alcohol molecules varies,depending on the degree of surface hydration. Since the orientation of molecules depends on their interaction with each other, with the outside phase, and with the adsorbent surface, then as the latter becomes covered up a situation may arise such that a change from the original molecular orientation to a closer packing would be energetically more favorable. The increased adsorption would in this case show up as a jump on the adsorption isotherm [13, 14]. It is obvious that any changes in the nature of the adsorbent surface may influence this effect. It was shown in paper [13] that by using the same silica gel sample one can obtain either a stepwise or a smooth adsorption isotherm, depending on the preliminary thermal treatment.

The authors wish to thank B. V. Il'in for supporting this work and discussing the results,

LITERATURE CITED

[1] B. V. Il'in, V. F. Kiselev and K. G. Krasil'nikov, Bulletin of the Moscow University, No. 6, 35 (1957).

[2] L. D. Belyakov and A. V. Kiselev, Proc. Acad. Sci. USSR 119, 298 (1958).*

[3] A. V. Kiselev, I. A. Vorme, et al., J. Phys. Chem. 19, 83 (1956).

[4] I. H. de Boez, M. E. Hermans and I. M. Vleeskens, Proc. Konikl. nederl. akad. wet. 60, 45 (1957).

[5] A. K. Bonetskaya and K. G. Krasilnikov, Proc. Acad. Sci. USSR 114, 1257 (1957).*

[6] A. K. Bonetskaya, E. A. Leont'ev and E. A. Kharlamov, J. Appl. Chem. 30, 1237 (1957).

[7] M. M. Egorov, K. G. Krasil'nikov and V. F. Kiselev, J. Phys. Chem. 32, 2448 (1958).

[8] R. K. Ilez, The Colloid Chemistry of Silica and Silicates, N. Y., 1955.

[9] N. N. Gryazev, Proc. Acad. Sci. USSR 118, 121 (1958).*

[10] G. I. Aleksandrova, V. F. Kiselev, et al., Proc. Acad. Sci. USSR 108, 283 (1956).*

[11] A. V. Kiselev, J. Phys. Chem. 23, 452 (1949).

[12] M. M. Egorov, K. G. Krasil'nikov and E. A. Sysoev, Proc. Acad. Sci. USSR 108, 103 (1956).*

[13] V. F. Kiselev and K. G. Krasil'nikov, J. Phys. Chem. 32, 1435 (1958).

[14] K. V. Topchiev and I. V. Smirnova, Proc. Acad. Sci. USSR 123, 316 (1958).*

[15] V. Éitel', Physical Chemistry of Silicates, 1936.[in Russian].

Received December 24, 1958

---

* Original Russian pagination. See C. B. Translation.

CERTAIN REGULARITIES IN THE PROPERTIES OF SOLUTIONS OF STRONG ELECTROLYTES

A. I. Gorbanev, Yu. M. Kessler, Yu. M. Povarov and
É. S. Sevost'yanov
The Institute of Electrochemistry of the Academy of Sciences of the USSR

(Presented by Academician A. N. Frumkin, January 14, 1959)

The deviations which exist between the limiting form of the Debye-Hückel Law and experimental data in the region of low concentrations, $c \sim 0.01$ mole/l, can be formally explained either: a) by assuming incomplete ionization [1], or b) by taking account of a variation in the amount of "free solvent" resulting from solvation of the ions [2], or, c) by considering the specific interaction of the ions [3, 4]. Assumption a) is clearly not applicable to the case of positive deviations, since it is impossible to explain a rise in the activity coefficient in terms of an increase in the intensity of interionic action. If b) is to be used as a point of departure, it is necessary to postulate an increase in hydration in the direction $Cl^- \rightarrow I^-$, although this is in contradiction with both theory and experiment [4]. Only by starting from c) is it possible to avoid these and certain other contridictions and obtain a general theory which is qualitatively consistent with experimental results [4].

On the basis of ideas which have been developed earlier [4], f_c, the contribution to the activity coefficient arising from the interaction of nearest ions, can be represented (for 1-1 electrolytes) in the form

$$\ln f_c = {}^4/_3 \pi a^3 Bc - B\beta_1 c, \tag{1}$$

$$\beta_1 = 4\pi \int\limits_a^{a_i + a_j} \left[\exp\left(-\frac{U_c(r_{ij})}{kT}\right) - 1\right] r^2 \, dr, \tag{2}$$

$$U_c(r_{ij}) = -\left|u_e(r_{ij})\right| - \left|u_c^m(r_{ij})\right| + \left|\sum u_c^i\right| - \left|u_k(r_{ij})\right|, \tag{3}$$

where $B = 6.024 \cdot 10^{20}$; $a = r_+ + r_-$; r_+ and r_- are the crystallographic radii of the cation and the anion, respectively; a_i and a_j are the respective radii of the solvation spheres of these ions; $U_c\,(r_{ij})$ is the potential energy of the ionic pair; $u_e\,(r_{ij})$ is the energy of the electrostatic interaction of the ions; $u_c^m\,(r_{ij})$ is the energy of solvation of the ionic pair; u_c^i is the energy of solvation of the free ion, and $u_k\,(r_{ij})$ is the quantum-mechanical energy. Supposing, in agreement with experiment, that the contribution to $\underline{f}$ arising from other factors is much less than that given by (1), we obtain the approximate expression

$$\lg f_{\exp} = \lg f_D + \lg f_c, \tag{4}$$

in which $\log f_D$ is to be obtained from the limiting Debye-Hückel equation. By applying the relations (1)-(4), it is possible to elucidate the experimental data and establish certain generalizations.

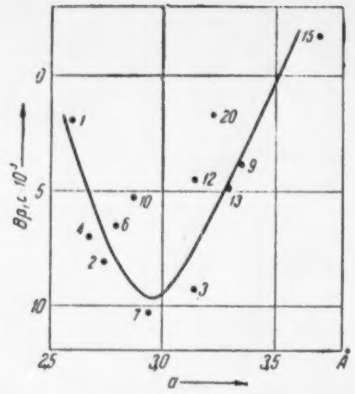

Fig. 1. Departure from the limiting law as a function of a: H_2O, 0°. 1) LiCl, 2) LiBr, 3) $LiClO_4$, 4) $LiNO_3$, 5) NaF, 6) NaCl, 7) NaBr, 8) NaI, 9) $NaClO_4$, 10) $NaNO_3$, 11) KF, 12) KCl, 13) KBr, 14) KI, 15) $KClO_4$, 16) RbCl, 17) CsF, 18) CsCl, 19) CsBr, 20) KNO_3.

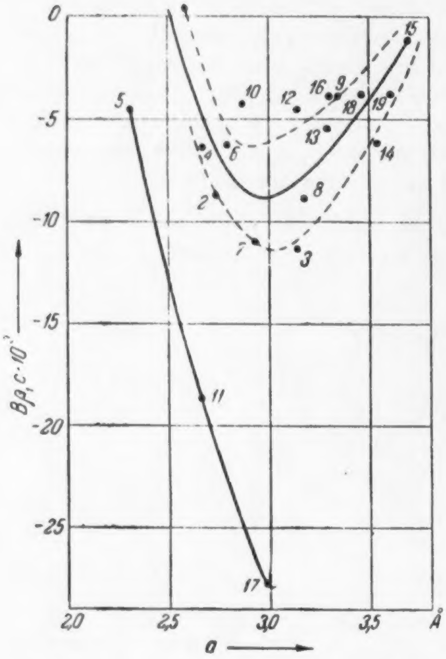

Fig. 2. Departure from the limiting law as a function of a: H_2O, 25°. 1) For notation, see Fig. 1.

For 25° aqueous solutions at c = 0.01, the difference $\log f_{exp} - \log f_D$ increases in the sequence $LiCl < KClO_4 < NaF$, $NaNO_3$, $NaClO_4$, RbCl, CsCl, $CsBr < KCl < KBr < LiNO_3$, $NaCl < KI < LiBr < NaI < NaBr < LiClO_4 < KF < CsF$. From this, it can be seen that there is no parallelism between the value of this difference and the ability of the ions to undergo solvation. Preliminary calculations have shown that the variation of $u_e(r_{ij})$ and $u_k(r_{ij})$ with increasing ionic radius is such that these quantities approximately compensate one another. Thus, the lack of a parallelism must arise from those individual differences in the ionic pairs which appear in $u_c^m(r_{ij})$. If such is the case, $u_c^m(r_{ij})$, and $B\beta_1c$, must be nonmonotonic functions of some parameter which characterizes the solvating tendency of the ionic pair. On the basis of the most general ideas concerning the factors which determine the energy of solvation, the quantity a might be selected as such a parameter.

Making use of equations (1) and (4), and the experimental data for 0° or 25°, on aqueous salt solutions at c = 0.01, the quantity $B\beta_1c$ has been evaluated and graphs of $B\beta_1c = f(a)$ constructed (Figs. 1 and 2). Although the scattering of points is considerable, these graphs show that a relation between $B\beta_1c$ and a actually exists. This is not unexpected, however, since in the evaluation of $B\beta_1c$, only the covolume effect has been considered as contributing to the departure from the limiting law, all other factors being neglected. The positions of the fluorides on these various curves can be clarified by considering that the energy of hydration of F^- is 30% greater (in terms of the modulus) than that of Cl^-, the most strongly hydrated of the ions involved in the salts which are under study. Thus, for the fluorides, the upper limit of the integral of (2) must be larger, because of a_j, than is the case for the other salts. In view of the strong dependence of β_1 on $a_i + a_j$, this fact is sufficient for a clarification of the behavior of the fluorides. In addition, it is clear that account should also be taken here of the possibility of hydrolysis.

It is interesting to note that the resulting curves have an extreme at $a \approx Zr_{H_2O}$. Although the ratio of the dimensions of a solvated object and a molecule of the solvent is an important quantity [6], it is likely that the ratio between a and the length of the dipole of the solvent molecule plays an even greater role in the case of solvated ionic pairs. In the water molecule, the distance between the opposite charges (for the quadrapole model) differs but little from the diameter of the molecule as a whole, and this fact leads to the observed relation.

Since the energy of solvation of the ions is a function of $b = 1/r_+^2 + 1/r_-^2$ (ion – dipole interaction), or of $g = 1/r_+ + 1/r_-$ (polarization of the continuum, and charge – charge interaction), it is necessary to determine the type of relation existing between $B\beta_1c$, and b and g. The points in the plots of $B\beta_1c = f(b)$ and $B\beta_1c = f(g)$ prove to be distributed completely at random over the entire area of each graph, i.e., there is an absence of any sort of interrelationship. This indicates that the hydration of the ionic pair is the factor determining the deviation from the limiting law.

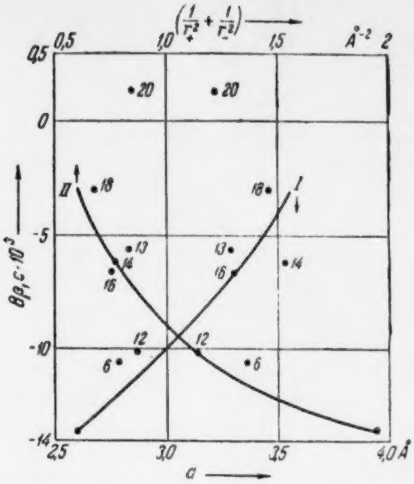

Fig. 3. Deviation from the limiting law as a function of a (I), and b (II); formamide, ~2°. For notation, see Fig. 1.

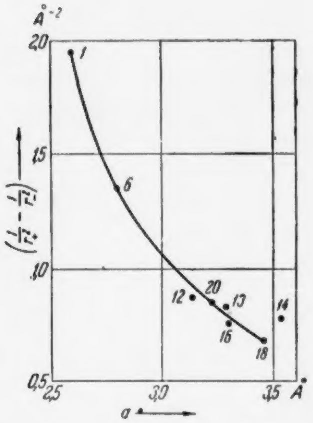

Fig. 4. Relation between a and b. For notation, see Fig. 1.

Among other solvents with high dielectric constants, data on activity coefficients is available only for formamide solutions [7]. Values of $B\beta_1c$ calculated from this data at ~2° and c = 0.02, are represented as a function of a in Fig. 3. The tendency for an extremum to appear on the curve as the value of a approaches the length of the dipole (~ 2A, for formamide) is maintained, although not clearly, in this case. The salts for which data are available accidently prove to be such that a continuous relation exists between a and b, g; this is shown in Fig. 4 for the case in which a = f(b). Therefore $B\beta_1c$ also depends continuously on b. If an arbitrary pair of values, a and b, is selected and the corresponding values of $B\beta_1c$ then found from curves I and II of Fig. 3, the resulting values of $B\beta_1c$ will be practically identical. For example, a = 3.0 corresponds to b = 1.06; the values found for $B\beta_1c$ are $1.0\cdot10^{-2}$, respectively. The same thing is observed in the case of the relation $B\beta_1c$ = f(g). This indicates that only one of the variables, a, b, or g is the true argument of the function $B\beta_1c$. In order to decide which one of the variables this is, data are needed for salts which do not fall on the curve of Fig. 4 (for example LiBr, NaF, NaI, $LiClO_4$).

This is no definite relationship between a, b,or g, and deviations from the limiting law for the heats of dilution of aqueous solutions at c = 0.01 and 25°. This might have been anticipated in view of the earlier noted [4] fact, that the various effects, contributing differently to the activity coefficient, make approximately the same contribution to the heat of dilution. In other words, it is not permissible to neglect the entropy term. Thus, in order to establish regularities in the case of the heat dilution it is necessary to separate out the contribution arising from a given effect.

LITERATURE CITED

[1] W. Nernst, Zs. Elektrochem. 33, 428 (1927); Zs. phys. Chem. 135, 237 (1928).

[2] R. H. Stokes and R. A. Robinson, J. Am. Chem. Soc. 70, 1870 (1948); E. Glueckauf, Trans. Farad. Soc. 51, 1235 (1955).

[3] E. A. Guggenheim, Phil. Mag. 19, 588 (1935).

[4] Yu. M. Kessler and A. I. Gorbanev, Proc. Acad. Sci. USSR, No. 6, 50 (1957).*

[5] G. Harned and B. Owen, The Physical Chemistry of Solutions of Electrolytes (Russian translation), Foreign Lit. Press, 1952; S. Glasstone, Introduction to Electrochemistry (Russian translation), Foreign Lit. Press, 1951.

[6] O. Ya. Samoilov, The Structure of Aqueous Solutions of Electrolytes and the Hydration of Ions, Acad. Sci. USSR Press, 1957 [in Russian].

[7] E. N. Vasenko, J. Phys. Chem. 21, 361 (1947); 22, 999 (1948); 23, 959 (1949).

Received December 26, 1958

CONCERNING THE MECHANISM OF THE INTERCRYSTALLINE CORROSION OF STAINLESS STEELS IN NITRIC ACID

A. I. Krasil'shchikov, L. M. Volchkova, I. K. Burtseva
and V. D. Plyasunov

(Presented by Academician A. N. Frumkin, January 22, 1959)

It is well known that an unequal access of oxygen to two iron or two zinc electrodes which are immersed in a solution of neutral electrolyte gives rise to a differential aeration current, the electrode which is supplied with oxygen becoming the cathode and the other electrode, to which the supply of oxygen is impeded, undergoing anodic dissolution.

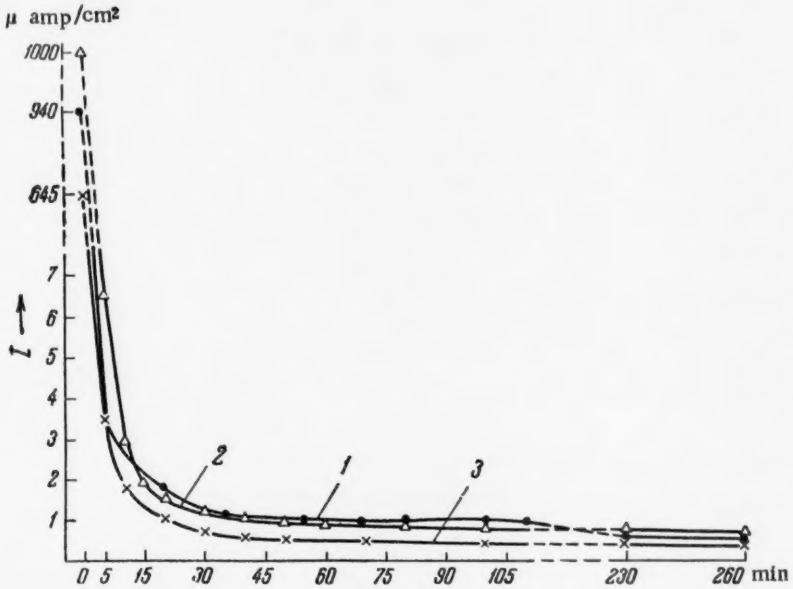

Fig. 1. The effect of concentration differences in HNO_3 on the behavior of Ya1-T steel at 60°. In the left side of the cell, 56% HNO_3; in the right side: 1) 2%, 2) 0.6%; 3) 0.06% HNO_3.

This effect cannot be due to any of the specific properties of the oxygen, and, in principle, a similar effect could arise from an excessive delivery to one of the electrodes of some oxidizing agent other than oxygen.

In the present work it is shown that a current arises between two stainless steel electrodes immersed in nitric acid solutions of different concentrations, the electrode in the more concentrated acid serving as the cathode and the electrode in the more dilute acid undergoing anodic dissolution.

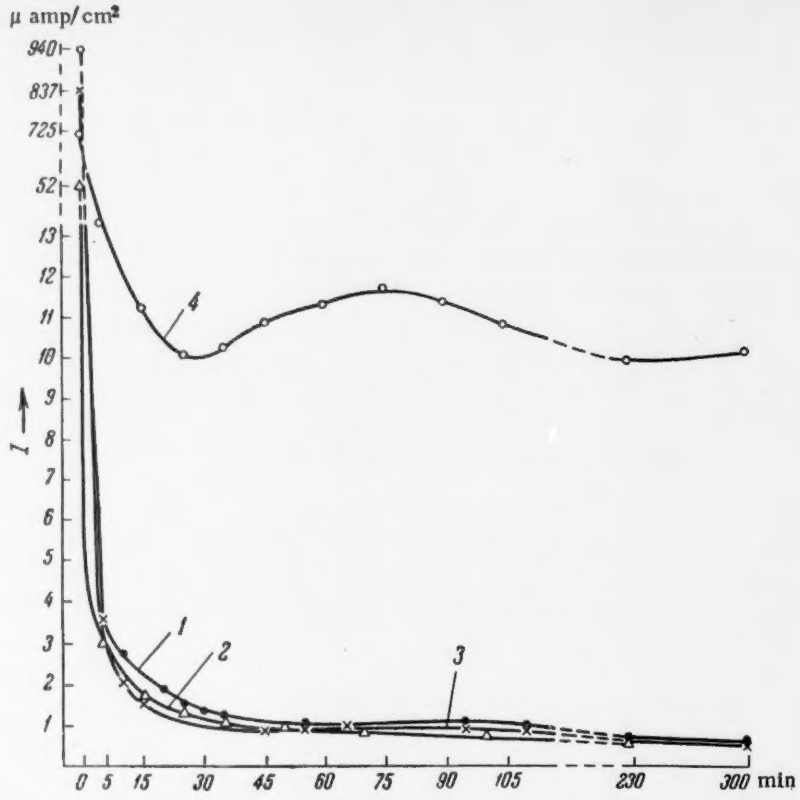

Fig. 2. The effect of concentration differences in the HNO_3, and of various additions of Cr^{3+}, Cr^{6+}, and Fe^{3+}, on the behavoir of Yal-T steel at 60°. In the right side of the cell, 2% HNO_3; in the left side: 1) 56% HNO_3; 2) 56% HNO_3 + Fe^{3+}, 3 g/l; 3) 56% HNO_3 + Cr^{3+}, 3 g/l; 4) 56% HNO_3 + Cr^{6+}, 3 g/l.

In Fig. 1 the 60°-differential depolarization currents which arise between two stainless steel electrodes in a cell containing solutions of nitric acid separated by a porous divider are shown (the cathode is in the 56% acid and the anode in the more dilute acid). The existence of these currents is clearly related to a certain difference in the degree of passivity of the two electrodes, the cathode being passive to a somewhat greater extent than the anode.

Let us now imagine a specimen of stainless steel in nitric acid.

The supply of acid into the microfissures on the metallic surface will be hindered, and the concentration of the acid within these fissures will fall as the result of corrosion, the concentration gradually becoming much less than on the surface of the metal. Because of the differential depolarization currents, it is clear that the total metallic surface will serve as the cathode and that the processes of anodic dissolution will begin to develop within the microfissures, which usually run along the grain boundaries. Such intercrystalline corrosion will, under favorable conditions, develop progressively, penetrating into the depth of the metal.

It is to be seen from Fig. 1 that though the differential depolarization current is at first quite large, it rapidly falls to a value of 0.5-1.0 μamp/cm², and then remains constant over a long period of time.

A current strength of 1 μ amp/cm² corresponds to a rate of dissolution of about one micron per month. In view of the fact that the grain dimensions are of the order of a fraction of a micron, dissolution at this rate can quickly lead to a breakdown of the bonds between the grains.

Figure 2 shows that addition of trivalent iron, or chromium, to the nitric acid is without effect on the differential depolarization current. On the other hand, the addition of an oxidizing agent in anodic form (hexavalent chromium) markedly increases this current.

In hot, concentrated nitric acid, it is possible that there is a direct chemical oxidation of trivalent chromium, which passes from the stainless steel into solution in the hexavalent form [1]. In actuality, it is known that it is exactly under these conditions that there is an especial intensification of the intercrystalline corrosion of stainless steel [2]. The intercrystalline corrosion of stainless steel in a standard acid solution of copper sulfate proceeds in a similar fashion, the role of the oxidizing agent being filled by the mixture of the ions of divalent and monovalent copper.

The application of tensile stresses to a specimen of stainless steel should aid in the development of microfissures on the metal surface, especially in those positions where there is a localization of strains which should therefore favor the process of microcrystalline corrosion. This effect is well known from the literature [3, 4].

The observed character of the corrosion depends on the ratio between the differential depolarization current, i_1, and the total corrosional dissolution current of the metallic surface, i_2. The corrosion is predominantly intercrystalline when $i_1 > i_2$. In the event that $i_2 > i_1$, a uniform corrosion of the metal is to be observed.

LITERATURE CITED

[1] J. E. Truman, J. Appl. Chem. 4, 273 (1954).

[2] H. T. Shirley, J. Iron and Steel Inst. 171, 111 (1952).

[3] A. V. Ryabchenkov, The Corrosional-Fatigue Resistance of Steel (in Russian) 1953.

[4] G. L. Shvarts and M. M. Kristal', The Corrosion of Chemical Apparatus (in Russian) 1958.

Received January 22, 1959

CERTAIN DETAILS OF THE CATHODIC PROCESS ON STAINLESS STEELS IN NITRIC ACID SOLUTIONS

E. N. Mirolyubov, M. M. Kurtepov and N. D. Tomashov

The Institute of Physical Chemistry of the Academy of Sciences of the USSR

(Presented by Academician A. N. Frumkin, January 24, 1959)

It is generally admitted that the corrosion of metals and alloys, including the stainless steels, in electrolytic solutions is an electrochemical process. In this connection, a consideration of the electrode processes occurring on various constructional materials in aggressive media is undoubtedly interesting. In publications dealing with the kinetics of the electrode processes on stainless steels in nitric acid solutions, there has generally been no account taken of the specific properties of the acid, or of the possibility of a breakdown of the passive condition through cathodic polarization [1]. These problems are treated in the present work.

The method of cathodic-polarization curves was adopted for the study of the cathodic processes on stainless steels in nitric acid solutions. At each assigned value of the density of the external cathodic current, the potential was measured and the weight loss of the electrodes in the course of the experiment (30 minutes) was determined. Each point on the cathodic polarization curves was obtained with a fresh specimen. Stainless chrome steels containing 17% and 28% chromium, annealed at 760°, and an 18-8 chrome-nickel steel containing niobium tempered at 1050° were studied. Throughout the diagrams,the potential values given are with respect to the normal hydrogen electrode.

In Fig. 1 polarization curves have been plotted for a number of stainless steels and for a smooth platinum electrode in 3% nitric acid, which is fully dissociated [2, 3], and in 30% HNO_3, which contains undissociated homopolar molecules of nitric acid. From this figure, it is seen that the polarization curves for the steels in the 3% nitric acid show inflection points and have limiting currents, the magnitude of which depends on the composition of the electrode. In the case of the platinum electrode, a limiting current is to be observed only in the 30% nitric acid solution (curve 7). The presence of inflection points and limiting currents on the cathodic polarization curves points to [4] a change-over from a cathodic process whose rate is controlled by an electrode reaction to a process controlled by the rate of supply of the reducing particles of a depolarizer to the electrode surface, this change-over beginning at a definite potential for each material. It is clear that this depolarizer can be supplied, either through its diffusion from the mass of the solution, or by its formation on the surface of the electrode by a chemical reaction.

It is also to be seen from Fig. 1 that the overvoltage for the cathodic process on stainless steel electrodes (for example, on the steels 1Kh17 and 1Kh18N11B), in both 3% and 30% nitric acid solutions, can be lower than on platinum under the same conditions.

The literature data [5] show that an evolution of hydrogen occurs on a platinum cathode in fully dissociated nitric acid solutions (less than 18-20%), but that the evolution of hydrogen in more concentrated solutions containing homopolar nitric acid molecules is preceded by the reduction of nitric acid to nitrous acid, this process taking place at the more positive potentials and being autocatalyzed by the nitrous acid. The reduction of nitric acid on the platinum electrode can also proceed in fully dissociated solutions to which nitrous acid has been added.

It is known that the hydrogen overvoltage is at a minimum on the platinum cathode [6]. The presence

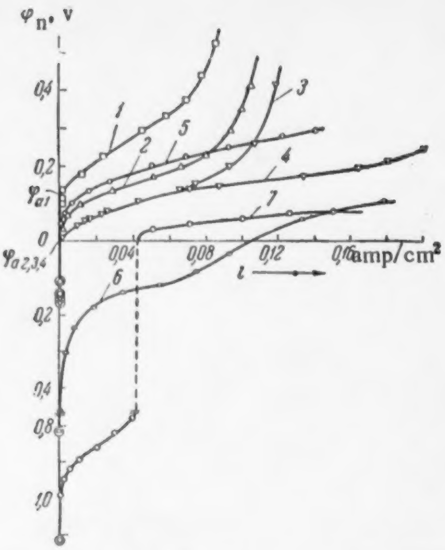

Fig. 1. Cathodic polarization curves for stainless steels, and platinum, in nitric acid solutions at 20°; without agitation: 3% HNO_3: 1) 1Kh28; 2) 1Kh17; 3) 1Kh18N11B, with agitation of the solution at 2500 rev/min; 5) Pt; 30% HNO_3; 6) 1Kh18N11B; 7) Pt.

on the stainless steels of cathodic overvoltages which are less than the overvoltage for hydrogen on platinum justifies the assumption that it is not the evolution of hydrogen, but some other cathodic process which takes place on these steels in nitric acid solutions over the region of investigated potentials.

It will be shown later that the cathodic process on stainless steels in nitric acid solutions can be interpreted in terms of a breakdown of passivity. In distinction to the inert platinum electrode, stainless steel electrodes are subject to corrosion during cathodic polarization in nitric acid solutions [7]. The relation between the rate of corrosion of these stainless steels and the potential is represented in Fig. 2. It is seen that the stainless steels are subject to a measurable corrosion once the activation potential (φ_a) has been reached, the rate of this corrosion increasing as the potential is displaced in the direction of negative values, reaching a maximum at the potential of the active state (φ_{ac}); with potentials more negative than φ_{ac}, the rate of corrosion diminishes and electrochemical cathodic protection of the active steel sets in.

By comparing the cathodic-polarization curve (Fig. 1) with the curves expressing the relation between the potential and the rate of spontaneous dissolution of the stainless steels (Fig. 2), it can be seen that it is only after the activation potential has been reached that the cathodic process on stainless steels in fully dissociated nitric acid solution proceeds with measurable velocity. The potential of the inflection point on the polarization curve is approximately that corresponding to the active state of the steel, i.e., the potential at which the rate of the spontaneous dissolution begins to diminish. These facts indicate that the products from the spontaneous dissolution of the steels in nitric acid solutions affect the rate of the cathodic process, increasing it. This conclusion is supported by the fact that accelerating the spontaneous dissolution of the stainless steels by agitation of the acid leads to an increase in the limiting current on the steel cathode (Figs. 1 and 2, curves 3 and 4).

To a first approximation, a mechanism can be developed for the effect of the products of spontaneous dissolution on the rate of the cathodic process of activated stainless steels by taking account of the fact that in the active state elements such as iron and chromium which are present in these steels pass into solution as divalent ions [8]. Because of their oxidation in solution, these ions are analytically determined in nitric acid in trivalent form. The oxidation of these ions can proceed according to the reaction.

$$NO_3' + 2\,Me^{2+} + 3H^+ \rightarrow HNO_2 + 2\,Me^{3+} + H_2O \qquad (A)$$

with a reduction of the nitrate ions to nitrous acid. There is experimental proof of the possibility of the reduction of nitric acid by divalent iron ions [9].

If the products of the spontaneous dissolution can reduce the nitrate ion to nitrous acid, an autocatalyst for the reduction of nitric acid, then, in principle, the cathodic reduction of nitric acid on the active steels must be analogous to the cathodic process on a platinum cathode in a fully dissociated solution of nitric acid to which nitrous acid has been added.

The mechanism of the cathodic reduction of nitric acid on an inert electrode has been considered by Vetter [10, 11]. The over-all reduction reaction

$$NO_3 + 3H^+ + 20 \rightarrow HNO_2 + H_2O \qquad (B)$$

proceeds through the steps

$$NO_3' + H^+ \rightleftarrows HNO_3 \qquad (1)$$

$$HNO_3 + HNO_2 \rightarrow N_2O_4 + H_2O \qquad (2)$$

$$N_2O_4 \rightleftarrows 2NO_2 \qquad (3)$$

$$NO_2 + \theta \rightarrow NO_2' \qquad (4)$$

$$NO_2' + H^+ \rightleftarrows HNO_2 \qquad (5)$$

It is step (4) which limits the rate of the cathodic reduction of the nitric acid. The value of the limiting current for the reduction of the nitric acid is fixed by the rate of the chemical reaction (2) which produces the reducing molecules of nitrogen tetroxide. The observed diminution of the limiting cathodic current on platinum [6, 10] which results from agitating the nitric acid is explained by the removal of this nitrogen tetroxide from the electrode surface. As Vetter has shown, reaction (2) is heterogeneous.

For the case of the reduction of nitric acid on a spontaneously dissolving electrode, the step represented by equation (A) must be added. The total reaction for the reduction of nitric acid on a spontaneously dissolving electrode is then represented by:

$$NO_3' + Me^{2+} + 3H^+ + \theta \rightarrow HNO_2 + Me^{3+} + H_2O \qquad (C)$$

The absence of an agitation effect on the overvoltage of this process (Fig. 1; 3, 4) justifies the assumption that the rate of the cathodic reduction of nitric acid on the active steels is limited, just as on platinum by the electrode reaction (4). According to equation (2), the value of the limiting cathodic current at given nitric acid concentration is fixed by the concentration of the nitrous acid in the pre-electrode layer; in the case of a stainless steel electrode, this value must also depend on the rate of reaction (A), which produces the nitrous acid. Since the rate of this reaction depends on the nature of the electrode, and the rate of its spontaneous dissolution, the value of the limiting current should be fixed by the electrode composition, just as is actually observed to be the case.

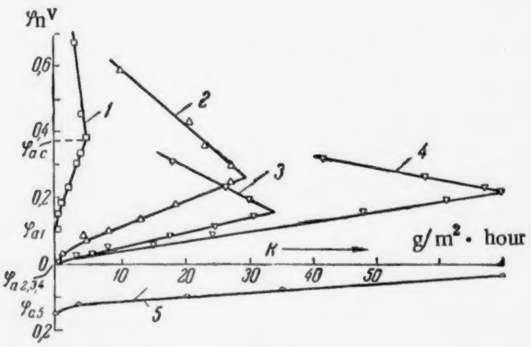

Fig. 2. The relation between the potential and the rate of corrosion of stainless steels in nitric acid solutions at 20°, without agitation: 3% HNO_3: 1) 1Kh28; 2) 1Kh17; 3) 1Kh18N11B; 4) 1Kh18N11B, with agitation of the solution at 2500 rev/min; 30% HNO_3: 5) 1Kh18N11B.

As established in the present work, the details of the cathodic processes on stainless steel electrodes in nitric acid solutions (namely the existence of a relation between the value of the limiting current and the electrode composition, and of lower overvoltage for the cathodic process than that for the platinum electrode) can be explained by the breakdown of the passive state of the steel during cathodic polarization with a subsequent formation of nitrous acid (the autocatalyst of the process) through the reduction of the products from the spontaneous dissolution of the steel in the nitric acid solution.

LITERATURE CITED

[1] S. Mints, Bull. Polish Acad. Sci. Section 3, I, 333 (1953).

[2] T. G. O. Berg, Zs. allg. anorg. Chem. 265, 33 (1951).

[3] I. V. Oknin, J. App. Chem. 24, 167 (1951).

[4] N. D. Tomashov, The Corrosion of Metals with Oxygen Depolarization (in Russian) Acad. Sci. USSR, Press, Moscow-Leningrad, 1947, p. 82.

[5] A. N. Frumkin, V. S. Bagotskii, Z. A. Iofa and B. N. Kabanov, The Kinetics of Electrode Processes (in Russian) Moscow, 1952.

[6] J. T. Ellingham, J. Chem. Sco. 1, 1565 (1932).

[7] N. D. Tomashov, M. M. Kurtepov and E. N. Mirolyubov, J. Phys. Chem. 32, 904 (1958).

[8] T. Heumann, Passivierende Filme und Deckschichten, Berlin, 1956, p. 256.

[9] K. J. Vetter and H. J. Booss, Zs. Elektrochem. 56, 16 (1952).

[10] K. J. Vetter, Zs. Phys. Chem. 194, 199 (1950).

[11] K. J. Vetter, Zs. Elektrochem. 55, 121 (1951).

Received January 24,1959

AN X-RAY METHOD OF STUDYING THE DENSITY ON THE DETONATION FRONT OF GASEOUS MIXTURES

M. A. Rivin,* Academician Ya. B. Zel'dovich, V. A. Tsukerman, V. V. Sof'ina and A. S. Beregovskii

Institute of Chemical Physics of the Academy of Sciences USSR

It has been suggested that the gas in a detonation wave is first compressed by shock and only then undergoes combustion. At any time the detonation wave should contain a layer of compressed gas between the unexcited gaseous mixture at the initial state and the combustion products in a thermodynamically defined state. The thickness of this layer is proportional to the time needed for the dissipation of the heat evolved in the chemical reaction taking place in the compressed gas. Despite the fact that more than 15 years have passed since these relationships have been clearly formulated [1-3], the experimental data on the compressed layer at the detonation wave front are still very scant [4-6]. Attempts by Kistiakowsky and co-workers [7, 8] to detect this layer with an x-ray densitometer by using a scintillation counter and an oscillographic technique failed to given any unequivocal results due to the low resolving power of their technique. Later developments of this technique were done mainly towards increasing the accuracy of gas density measurements [9].

In 1945 M. A. Rivin, Ya. B. Zel'dovich and V. A. Tsukerman began to study the densities on the detonation front of oxyhydrogen gas mixed with hydrogen iodide by using an x-ray pulse technique; however, due to the serious illness and subsequent death of M. A. Rivin the research was discontinued.

Experiments were resumed in 1957. The special features of the method used in the present work were the use of a point source x-ray pulse tube [10] with a zirconium anode and the addition of krypton (as quencher) to the oxyhydrogen gas. The characteristic zirconium radiation ($\lambda_{k\alpha} = 0.788$ A) falls within the krypton absorption band. The above-mentioned combination of emitter and quencher made it possible to record density variations in relatively thin layers of gaseous mixtures. In the main set of experiments we used plexiglass tubes 1.5 mm thick and 20 mm in internal diameter to study the detonation of oxyhydrogen gas mixed with krypton. The initial gas pressure was 0.5 kg/cm^2. To test the x-ray photographic technique we carried out experiments on shock waves in pure krypton in 5 mm (diameter) tubes and at an initial pressure of 1 kg/cm^2.

Detonations in gaseous mixtures and shock waves in pure krypton were initiated by an electric spark; a low induction (20 μF) condenser was charged to 5-6 kv, then discharged through a 0.1 mm nichrome wire in the gas. While recording the x-ray picture of the wave we simultaneously measured the detonation rate by means of an electron-beam oscillograph.

When the x-ray bursts lasted for about 0.2 μ sec, the smearing of the image in the direction of detonation did not exceed 0.3 mm. The deflections of the x-rays from the plane of the front were controlled and in most cases did not exceed 1°. Additional smearing connected with the final dimensions of the focal length (1.5 mm) did not exceed 0.1 mm in the instrument's designed geometry. The over-all image smearing in the described method can be estimated at 0.4-0.5 mm.

The principal results of this work are the observations which demonstrated beyond any doubt the presence at the detonation wave front of a narrow gaseous layer whose density was 3-4 times the initial value (so-called chemical peak region). Its width in most experiments (allowing for the smearing) was 0.1-0.3 mm and was just at the limit of the resolution available to our method.

---

[*] Deceased.

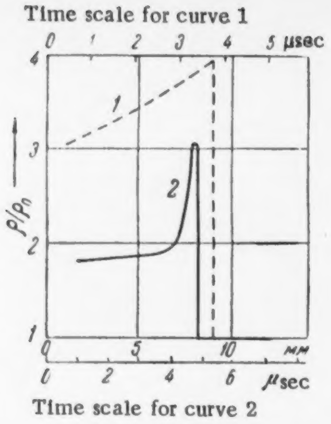

Fig. 1. Relative density distribution of the gas, ρ/ρ_0. 1) Shock wave in pure krypton with the front 42 mm away from the initiation point and traveling at a rate of 2.4 km/sec; 2) detonation wave in a mixture of 20% H_2 + 10% O_2 + 70% Kr with the front 400 mm away from the initiation point and traveling at a rate of 1.3 km/sec.

Figure 1 shows curves for the distribution of densities in a shock wave of pure krypton and the detonation wave of oxyhydrogen gas mixed with krypton; the curves were obtained by a microphotometric processing of the pulse x-ray pictures. The region in which the density on the detonation wave front is much higher than that calculated for the reaction products is very clearly exhibited. Our experimental value of $\rho/\rho_0 \approx 3$ is evidently too low, due to the fact that the width of the chemical peak region is close to the maximum spatial resolution possible with our method.

Despite the large number of experiments it was not possible at the present time to establish any definite correlation between the peak-width and the composition and pressures of mixtures. Any further work requires that the method be improved with respect to resolution in space and time. It is also possible that by choosing a different explosive mixture one may be able to extend the high-density region on the detonation wave front and thus obtain more accurate quantitative data with the available measuring techniques.

We take this opportunity to express our deep gratitude to N. N. Orlova, who participated in the above-described work, to E. I. Leont'eva, who conducted experiments in 1945, and to R. M. Zaidel' for his help in calculations and valuable discussions.

LITERATURE CITED

[1] Ya. B. Zel'dovich, J. Exptl.-Theoret. Phys. 10, 542 (1940).

[2] W. Doering, Ann. Phys. 43, 421 (1943).

[3] Ya. B. Zel'dovich, Combustion and Detonation Theory, Izd. AN SSSR, 1944.*

[4] S. M. Kogarko and Ya. B. Zel'dovich, Proc. Acad. Sci. 63, 553 (1948).

[5] W. R. Gilkerson and N. Davidson, J. Chem. Phys. 23, 687 (1955).

[6] R. E. Duff and E. Houston, J. Chem. Phys. 23, 1268 (1955).

[7] G. B. Kistiakowsky, J. Chem. Phys. 19, 1611 (1951).

[8] G. B. Kistiakowsky and P. H. Kydd, J. Chem. Phys. 25, 824 (1956).

[9] H. T. Knight and D. Venable, Rev. Sci. Instr. 29, 92 (1958).

[10] V. A. Tsukerman and M. A. Manakova, J. Tech. Phys. 27, 390 (1957).

Received February 16, 1959

---

* In Russian.

THE COLLOIDAL STATE OF DYES AND METACHROMATISM

M. V. Savost'yanova and L. G. Matsinova

(Presented by Academician A. N. Terenin, January 24, 1959)

Problems connected with the color changes observed in solutions of basic (cation) dyes (metachromatism)* in the presence of certain high polymeric compounds (chromotropes) are currently receiving a great deal of attention due to the application of this phenomena to biology, particularly histochemistry, as a means of differentiating tissues.

At present all the workers agree [1, 2] that the new absorption maximum M, which appears in the presence of chromotropes and is distinct from the known monomeric (α) and dimeric (β) maxima, can be attributed to active centers made of dye aggregates. However, neither the nature of these aggregates nor the conditions of their formation are as yet understood.

On the other hand, it is known that certain highly aggregated colloidally dispersed ** dyes will likewise exhibit characteristic extinction maxima [3]. In order to correlate these two sets of phenomena we compared the spectroscopic properties of certain colloidally dispersed dyes with the properties of those same dyes in aqueous solutions in the presence of a typical metachromatizing compound, agar-agar.

Below we are presenting some data on the following dyes: methylene blue (MB), fuchsin (F), crystal violet (CV), and a cyanine (3,3-diethyl-9-methylthiocarbocyanine iodide) dye (C).

The colloidal solutions of MB in benzene were prepared by a method described by one of the workers [3] in connection with F (several drops of an acetone solution of the dye were introduced into thoroughly purified benzene; the dye separated out in the form of colloidal particles). Neither F nor MB gave a constant location for their extinction maxima (it depended on conditions of preparation, growth of the sol, and temperature); according to the optical theory*** of turbid media containing absorbing particles,this phenomenon is caused by variations in the diameters (2ρ) of colloidal particles. The locations of MB extinction maxima are listed in Table 1; in the investigated solutions they were located between 540 and 580 mμ. In Fig. 1 we have plotted the curves for the extremally located maxima. As regards experimental conditions, the colloidal solutions of MG possess a greater stability than those of F, while the absorption maximum of its molecular form is much weaker and farther displaced from the colloidal λ_{max} than in the case of F.

The absorption curve for the smallest particles ($2\rho/\lambda \to 0$)**** of CV in water, calculated by the Rayleigh-Mie formula from the data given in [7], was plotted in Fig. 2.

---

* This phenomenon was discovered as early as 1875 during staining of biological specimens. An exhaustive review of work done up to 1955 is given in [1].

** We have in mind particles with a "phase separation surface" for example, cubosols, see [4] and not "colloidal electrolytes" (benzopurpurin et al.).

*** This theory was developed by Mie on the basis of equations derived by Rayleigh in his "The Theory of Sound." See for example [5], Chap. II and III.

**** In this case there is no scattering and we can only talk of absorption. The applicability of Rayleigh-Mie Theory to colloidal solutions of metals has been known for a long time [5, 6]; in paper [3] the agreement between experimental and calculated data was also demonstrated for dyes. In our case the location of the extinction maximum was determined with an accuracy of 15-20 mμ. We couldn't do any calculations for MB and C due to the lack of reliable data on the optical constants of their solid films.

TABLE 1

Methylene Blue Colloidal Solutions in Benzene. Dye Concentration in Acetone $\sim 10^{-3}$ g/ml. Measurements Done at 17-20°

Test Nos.	Expt. Nos.	% Acetone in benzene	Standing time in days	λ_{max} in mμ
1	1	1.7	0	555
2			1	560
3			3	565
4			6	570
5	*		7	540
6	2	1.7	0	565
7			1	575
8			3	580
9	3	4.1	0	545
10			2	555
11			3	555
12			4	560
13			5	555
14			10	565

---

* After 3 hr heating at 40°.

TABLE 2

Methylene Blue. Metachromatic Coloration

Test Nos.	Expt. Nos.	Conc., in g/ml		Measured at °C	Time after film formation, in hrs	Location of the maximum M, in mμ
		agar	dye			
1	1*	$2 \cdot 10^{-3}$	$0.8 \cdot 10^{-7}$	17	0.5	560
2				41	1.0	570
3				56	1.5	570
4				38	2.0	560
5				17	2.2	570
6	2**	$1 \cdot 10^{-2}$	$1 \cdot 10^{-3}$	20	0.5	570
7	3***	$1 \cdot 10^{-2}$	$1 \cdot 10^{-4}$	20	>24	545
8				20	>24	570
9				20	>24	575
10				20	>24	595

---

* Solution in the cell; concentrations given for the agar + dye mixture.

** Film on the gel; dye concentration in the initial solution.

*** Isolated film (dry) fragments, measured on a cytospectrophotometer (Nos. 7 and 10, see Fig. 1). The dye concentration in the initial solution.

In our experiments the metachromatic coloration appeared whenever aqueous solutions of agar-agar and the dye (at a concentration > 10^{-7} g/ml) were mixed.

When the dye concentration was > 10^{-6} g/ml an insoluble colored precipitate was formed [1, 2, 14]. The colored flakes which formed in agar solutions looked like film scraps several square millimeters in size; a continuous film could be prepared by depositing the dye solution on the surface of jellied agar. During the first hours after its formation the film could be destroyed by being treated up to 60-70°; after a more extended period of time it became completely stable even at ~100° and would not dissolve in organic solvents (except in a

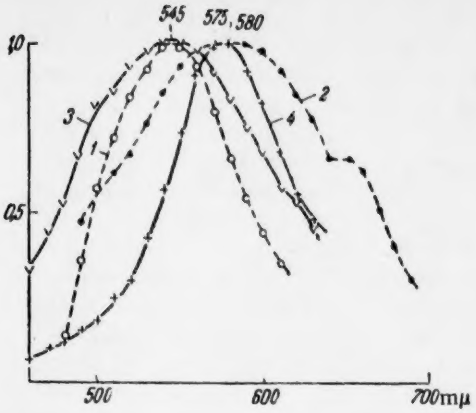

Fig. 1. Extinction curves in relative units. Methylene blue. 1 and 2) Colloidal solutions in benzene (Table 1, Nos. 9 and 8); 3 and 4) dry films of agar + MB (Table 2, Nos. 7 and 9).

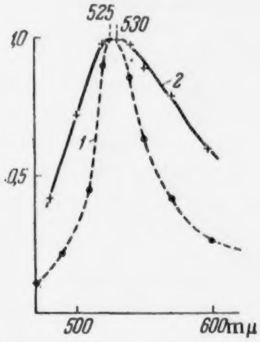

Fig. 2. Extinction curves in relative units. Crystal violet. 1) Colloidal solutions in water (data calculated for the smallest particles); 2) dry film of agar + CV.

pyridine + water mixture). After removing the film from solution and washing excess dye and agar away, we followed the spectroscopic changes in its absorption on a cytospectrophotometer* [8]. The spectra of dried films were displaced towards longer wavelengths (by 15-20 mμ) with respect to those of the moist films.

At dye concentrations $< 10^{-6}$ g/ml the agar solution became transparent;** in this case the spectroscopic absorption changes were followed on an SF-4 spectrophotometer by using an agar solution of the same concentration as a blank. The absorption curves always exhibited a more or less intense α and β maxima (absorption curves of the film gave pure metachromatic spectra). When the solution was heated these maxima increased at the expense of maximum M; the reverse process was observed on cooling.

In order to get some ideas as to whether the maximum M had a fixed location for a given set of conditions used in preparing the coloring centers we made up several solutions with various relative concentrations of agar and dye, and we also followed the changes in the absorption spectrum of dye solutions by varying the temperature (this was done with the help of a constant temperature attachment to the SF-4).

Some of the results obtained on both films and solutions of MB are listed in Table 2 and Fig. 1; a close examination of the data reveals the fact that the location of maximum M is not as constant as that of α and β;*** it is particularly sensitive to temperature variations (it is not reproducible during cooling of solution) and to the conditions of preparing the centers (different films or even fragments of a film may have varying λ_{max}). A comparison between the data obtained on the colloidal and on metachromatic dyes showed that the extinction maxima were located in the same spectral region and that the curves had the same general shape.

Other dyes also behave in a similar fashion. According to [3] the extinction maxima of colloidal solutions of F are located in the range of 500-560 mμ; with solutions and films (dried) we obtained curves similar to those of MB in that the location of their maximum M (485-505 mμ) was determined by the same factors. The clearing curve of a CV film was similar to that of the colloidal solution (Fig. 2). In Fig. 3 we have plotted the band M of dye C; its shape and location coincides with the so-called H-band previously detected [9, 10] in aqueous gelatin solutions of some cyanine dyes. The type of change [9] exhibited by this band when the relative concentrations of dye and gelatin or the temperature were varied were metachromatic. This indicates that both phenomena must be identical. On the other hand the H-band was also detected in an aqueous solution [11, 12] of a similar dye (bromide) at a concentration of $1 \cdot 10^{-2}$ M. One was obviously dealing with colloidal dye particles formed at high concentration.

The data so far presented indicate that the maximum M depends on centers which are of a colloidal nature. (This opinion was first expressed by Lison [13], yet it was immediately rejected by him).

---

* We wish to thank L. S. Agroskin for assisting us with the measurements.

** Sometimes if the solution is allowed to stand for a long time some flakes may be formed.

*** This is supported by the literature data on several dyes and chromotropes.

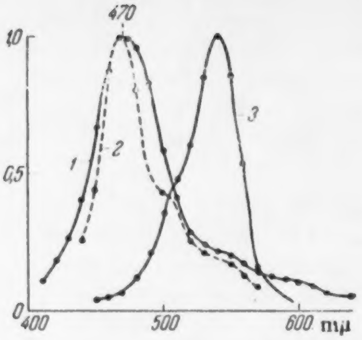

Fig. 3. Extinction curves in relative units. 1) Iodide used as sensitizer, a layer of jellied agar-agar ($5 \cdot 10^{-4}$ g/ml) was imbued with $3 \cdot 10^{-5}$ g/ml dye; 2) bromide used as sensitizer, aqueous dye solution at a concentration of 10^{-2} mole/liter (colloidal?) [11]; 3) alcoholic solution of the dye (iodide), conc. = 10^{-4} g/ml.

Starting out with the description proposed by Sylven [2] for the formation of metachromatic centers* (the dye is absorbed on the negatively charged groups in the chromotrope, then the interaction between adjoining dye ions results in the formation of aggregates with new intermolecular bonds) we can define the concepts associated with these aggregates more accurately. These aggregates are several tens of millimicrons in diameter and have optical constants typical of the dye in the solid state (consequently their extinction spectrum is identical with the spectrum of colloidal particles possessing those same constants). The size of 2ρ (which we estimated from the location of λ_{max} on the M-band) varied with the experimental conditions. Thus with F the experimental distribution in λ_{max} was 20 mμ, which (according to calculations done in [3]) corresponded to a change in 2ρ from 0 (smallest particles) to 40 mμ.

According to [14] one heparin molecule can bind 40-50 dye molecules (acridine orange); by taking 0.4-0.5 mμ as the average distance [12] between adsorbed molecules, we get in this case a colloidal particle with a diameter of the order of 20 mμ (the values may be different for other combinations of dyes and chromotropes). In water the chromotrope molecules, with the colloidal dye particles bound to it, give a colored colloidal solution characterized by the largest value of M; with particles of the above-mentioned size light scattering in such solutions is still insignificant. Precipitation of the above-described stable colored films may be ascribed to the aggregation of the dyed chromotrope molecules; meanwhile the colloidal dye particles may either remain isolated (retain the same diameter) and consequently have the same location of maximum M, or may combine into larger size particles all the way to a solid layer, which is confirmed by the "metallic" luster observed at higher dye concentrations. The previously discussed reversible shift in the maximum M observed when the film is dried and which according to theory indicates increasing particle size seems to be connected with some sort of structural changes in the polymeric portion of the film.

LITERATURE CITED

[1] M. Schubert and D. Hamerman, J. Histochem. and Cytochem. 4, 159 (1956).

[2] B. Sylven, Quart. J. Microsc. Sci. 25, 327 (1954).

[3] M. V. Savost'yanova, Bull. Acad. Sci. USSR, Phys. Ser. 17, 747 (1953).

[4] L. I. Belenskii et al., J. Phys. Chem. 31, 1564 (1957).

[5] K. S. Shifrin, Light Scattering in Turbid Media, Moscow-Leningrad, 1951.**

[6] M. V. Savost'yanova, Progr. Phys. Sci. 22, 1 (1939).

[7] N. N. Pribytkova and L. S. Agroskin, Optics and Spectroscopy, 2, 628 (1957).

[8] N. V. Korolev and L. S. Agroskin, Biophysics, 2, 513 (1957).

[9] A. V. Borin and I. A. Pobedonostseva, J. Sci. and Appl. Photography and Cinematography 3, 256 (1958).

[10] H. Dickinson, Coll. Physical Chemistry of Photographic Processes (IL, 1954, p. 208).***

[11] B. Carroll and W. West, Physical Chemistry of Photographic Processes (IL, 1954, p. 242).***

[12] W. West, B. Carroll and D. Whitcomb, Physical Chemistry of Photographic Processes (IL, p. 280).***

---

* Similar scheme is used also for centers causing the H-band [9, 10].

** In Russian.

*** Russian translation.

[13] L. Lison, Arch. Biol. 46, 599 (1935).

[14] W. Appel and V. Zanker, Zs. Naturforsch. 13b, 126 (1958).

Received October 15, 1958

THE OXIDIZING PROPERTIES OF ATOMIC HYDROGEN IN THE RADIATIONAL OXIDATION OF DIVALENT IRON IONS

V. N. Shubin and P. I. Dolin

(Presented by Academician A. N. Frumkin, January 21, 1959)

In order to explain the high efficiency obtained in the radiational oxidation of divalent iron in acid solution in the absence of oxygen, Weiss has proposed the reaction: $Fe^{2+} + H_2^+ = Fe^{3+} + H_2$, in which atomic hydrogen enters as the oxidizing agent, forming a molecular ion, H_2^+, by uniting with a H^+ ion. This explanation of the high efficiency in the oxidation of Fe^{2+} has called forth objections from a number of investigators. Attempts have been made to interpret the high efficiency in the oxidation of Fe^{2+} in terms of the reaction of OH radicals formed by the breakdown of excited water molecules.

If the oxidation of the Fe^{2+} depended entirely on the OH radicals, it is clear that the reaction: $OH + H_2 \rightarrow H + H_2O$, in which the OH radicals are transformed into H atoms, would cause the efficiency of oxidation to diminish with an increase in the concentration of molecular hydrogen in solution. Up to the present, there has been no investigation of the effect of the concentration of molecular hydrogen on the reaction efficiency.

In the present work, the efficiency of oxidation of divalent iron in acid solution under the action of the γ-radiation from Co^{60} has been measured, investigation being made over the interval of concentrations of molecular hydrogen corresponding to hydrogen pressure above the solution ranging from one to 180 atmospheres.

PROCEDURE

The investigated solution of Mohr's salt in 0.8 N H_2SO_4, in a glass cell, was saturated with hydrogen at atmospheric pressure. The cell (Fig. 1) was sealed and put into a steel bomb which was connected with a vacuum line and with a pressure system. After evacuation and threefold flushing with hydrogen, the vacuum line was cut off and hydrogen run into the bomb to the desired pressure. The thin-walled bulb on the cell was thereby broken and the hydrogen bubbled through the solution.

The reactants were of "chemically pure" grade. The working solutions were built up from doubly distilled water. The concentration of the $Fe(NH_4)_2(SO_4)_2$ was $\sim 1.3 \cdot 10^{-3}$ M. The dose strength was $\sim 3 \cdot 10^{15}$ ev/cm^2 · sec. The hydrogen was purified, either by diffusion through a palladium capillary, or on a copper catalyst [1] at $t = 200°$.

DISCUSSION OF RESULTS

The initial section of the oxidation curve was developed at each H_2 concentration. The initial yield of oxidation, as calculated from this data, has been plotted as a function of the pressure of hydrogen above the solution in Fig. 2. From this figure, it is to be seen that the reaction yield proved to be independent of the concentration of hydrogen in the solution. The yield of oxidation was somewhat lower than in a solution saturated with hydrogen at atmospheric pressure ($G = 8.1$), and was equal to 7.7 ± 0.25 mole/100 ev.

We have assumed the initial efficiency of oxidation to be determined under our conditions by the course of the following reactions:

$$H_2O \xrightarrow{\gamma} OH, H, H_2O_2, H_2. \qquad (0)$$

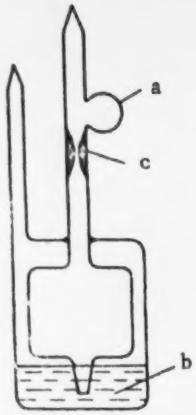

Fig. 1. Irradiation cell: a) thin walled bulb; b) solution c) constriction.

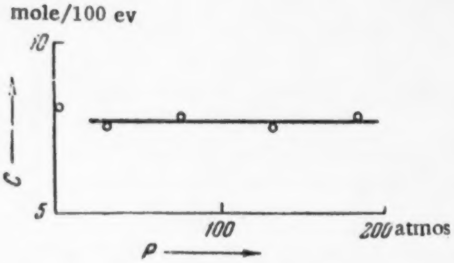

Fig. 2. The relation between the yield of oxidation of Fe^{2+} and the hydrogen pressure above the solution.

$$Fe^{2+} + OH \xrightarrow{k_1} Fe^{3+} + OH^-,$$

$$Fe^{2+} + H_2O_2 \xrightarrow{k_2} Fe^{3+} + OH + OH^-, \qquad (2)$$

$$H_2 + OH \xrightarrow{k_3} H_2O + H, \qquad (3)$$

$$H + H^+ \xrightarrow{k_4} H_2^+, \qquad (4)$$

$$Fe^{2+} + H_2^+ \xrightarrow{k_5} Fe^{3+} + H_2. \qquad (5)$$

According to this system, atomic hydrogen is produced through reactions (0) and (3), and then participates in the oxidation of the Fe^{2+} in reactions (4) and (5), so that the yield of oxidation should thus be independent of the hydrogen concentration in solution.

If reactions (4) and (5) were not effective, the inevitable result would be a diminution of the efficiency with increasing H_2 concentration. Actually, the fraction of the OH radicals which react with H_2 according to reaction (3) is given by:

$$\frac{k_3[H_2]}{k_3[H_2] + k_1[Fe^{2+}]} = \frac{1}{1 + k_1[Fe^{2+}]/k_3[H_2]}$$

The value of k_3/k_1 is known [2] to be equal to 0.15. This fraction was 0.94 for saturation with a 180 atm pressure of hydrogen above the solution. The H atoms which are thereby formed might be consumed according to one of the following reactions:

$$H + OH \xrightarrow{k_6} H_2O, \qquad (6)$$

$$Fe^{3+} + H \xrightarrow{k_7} Fe^{2+} + H^+, \qquad (7)$$

$$2H \xrightarrow{k_8} H_2. \qquad (8)$$

The result would be that the yield would diminish to $G_{H_2O_2}$, or possibly, even lower, as a consequence of (7) and the reaction:

$$H_2O_2 + H \xrightarrow{k_9} H_2O + OH. \qquad (9)$$

The experimentally observed independence of the yield of oxidation and the hydrogen concentration over a wide interval of values is in full agreement with the above-adduced scheme in which the atomic hydrogen functions as an oxidizing agent. This scheme also opens up the possibility of interpreting the data of the literature [3] on the relation between the oxidation efficiency and the concentration of divalent iron, and of evaluatin the velocity constant for the reaction of formation of the molecular ion H_2^+. According to calculations, the value of this latter constant is $k_4 = 2 \cdot 10^4$ 1/mole·sec.

Several experiments were carried out in the presence of O_2 (without preliminary saturation of the solution with H_2, or evacuation of the system). The oxidation yield was 41.6 mole/100 ev with a H_2 pressure of 30 atm above the solution; 71.2 mole/100 ev at a pressure of 75 atm; and 108.5 mole/100 ev at a pressure of 130 atm. It is clear that the reaction proceeds according to a chain mechanism, under these conditions, and that the chain includes the reactions: $H + O_2^+ \rightarrow HO_2$, $Fe^{2+} + HO_2 + H^+ \rightarrow Fe^{3+} + H_2O_2$.(2); and (3). Chain rupture is through reaction (1). Starting from this scheme for the development of the chain, calculation led to $k_3/k_1 = 0.135$. This value is in good agreement with the above cited 0.15.

LITERATURE CITED

[1] L. M. Kantorovich and F. M. Rappoport, Reports, State Ins. for the Nitrogen Industry, vol. 1, 1953, p. 202.

[2] F. Dainton and T. Hardwick, Trans. Farad. Soc. 53, 333 (1957).

[3] F. Dainton and H. Sutton, Trans. Farad. Soc. 49, 1011 (1953).

Received January 19, 1959

THE EFFECT OF OXIDATION PRODUCTS ON THE OXIDATION KINETICS OF HEXADECANE

V. M. Yur'ev, A. N. Pravednikov and Academician S. S. Medvedev

L. Ya. Karpov Physicochemical Scientific Research Institute

Hexadecane was oxidized at 140° in a closed system with the oxygen circulating under pressure. The rate of oxygen absorption was determined volumetrically while concentration of peroxides,iodometrically.

In its initial stage the absorption of oxygen by hexadecane (Fig. 1, 1) is an autocatalytic reaction (up to 25-30% of completion), but under further oxidation the reaction rate rapidly declines; after the reaction attains 40-50% of completion the rate becomes practically constant. The peroxide-accumulation curve (Fig. 1, 2) goes through a maximum at 25-30% of completion and then rapidly declines; after 40-50% of completion the concentration of peroxides in the system remains practically constant.

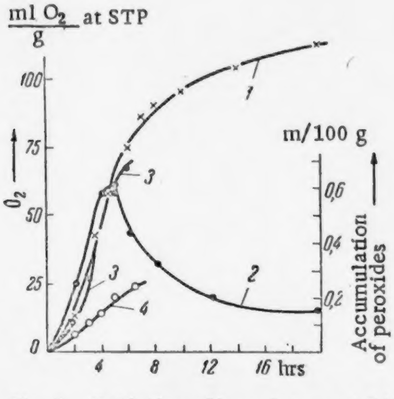

Fig. 1. Oxidation of hexadecane at 140°. 1) Hexadecane oxidation; 2) accumulation of peroxides; 3) oxidation of hexadecane + 6% of the upper (hydrocarbon) layer; 4) oxidation of hexadecane + 4% of the lower (acid) layer.

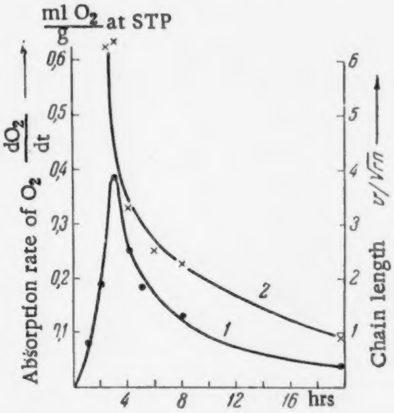

Fig. 2. Oxidation of hexadecane at 140°. 1) Change in O_2 absorption rate with time; change in the kinetic chain length.

The decline in the absorption rate of oxygen at 25-30% of completion evidently is not connected with the exhaustion of the hydrocarbon; the fact that the peroxide accumulation and the oxygen absorption rate dO_2/dt (Fig. 2, 1) have their maxima on the nonstationary segment of the curve (as one can see in these figures,the stationary state is attained after 40-50% of completion) indicate that the oxidation is accompanied by processes which decrease the oxidation rate and become increasingly important after 25-30% of completion, and that the stationary state depends not only on the concentration of the hydrocarbon and the rates of formation and decomposition of peroxides, but also on the rates of these oxidation-retarding processes.

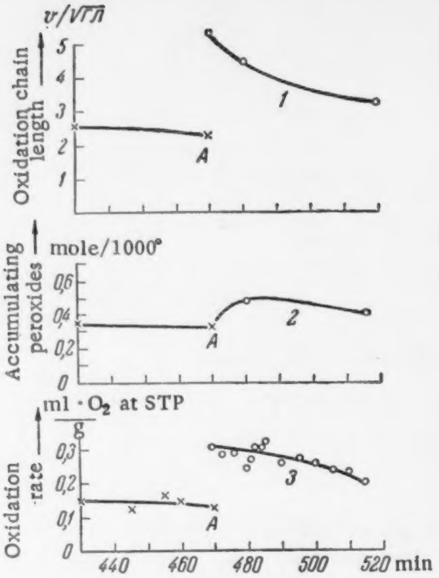

Fig. 3. The effect of removing the lower (acid) layer on the oxidation of hexadecane; the lower layer was removed at point A. 1) Change in the kinetic chain length; 2) change in the concentration of peroxides; 3) change in the oxygen absorption rate.

In order to discover the true nature of the reactions which retarded the oxidation of hexadecane we determined the length of the kinetic reaction chain (to be more precise a function proportional to it, $v/\sqrt{rn}$, where $\underline{v}$ is the rate of O_2 absorption, rn the concentration of peroxides). As one can see in Fig. 2, $v/\sqrt{rn}$ decreases in the course of oxidation. The decreased kinetic chain length, accompanied by diminished concentration of peroxides ($>$ 25-30% of completion) indicates unequivocally that compounds capable of breaking reaction chains are formed in the course of reaction.

It is known that when the oxidation of hydrocarbons is allowed to proceed far enough, the reacting system will become subdivided into two layers: an upper (hydrocarbon) layer and a lower one containing alcohols, ketones, aldehydes, acids, and some water. When the upper layer was added to pure unoxidized hexadecane the oxidation rate remained practically unchanged and even somewhat increased (Fig. 1, 3); however, addition of the lower layer decreased the oxidation rate quite markedly (Fig. 1, 4). When the lower layer was removed from the reaction vessel at the stationary stage the oxidation rate abruptly increased and was accompanied by increased concentration of peroxides and increased kinetic chain length. With further oxidation, as the lower layer accumulated, the reaction rate and the kinetic chain length declined, while the concentration of peroxides again passed through a maximum (Fig. 3). If the lower layer was removed again the same sequence of events followed.

Therefore, the results obtained indicate that the decreased oxidation rate is connected with the accumulation of products which disrupt the reaction chains.

Received February 11, 1959